AD-A037 735 ARMY MISSILE RESEARCH AND DEVELOPMENT COMMAND REDSTO--ETC F/G 20/4
AN EXPERIMENTAL INVESTIGATION USING A NORMAL JET PLUME SIMULATO--ETC(U)
FEB 77 J H HENDERSON, C W DAHLKE, G BATIUK

UNCLASSIFIED DRDMI-TD-77-2 NL

1 OF 2
AD
A037 735

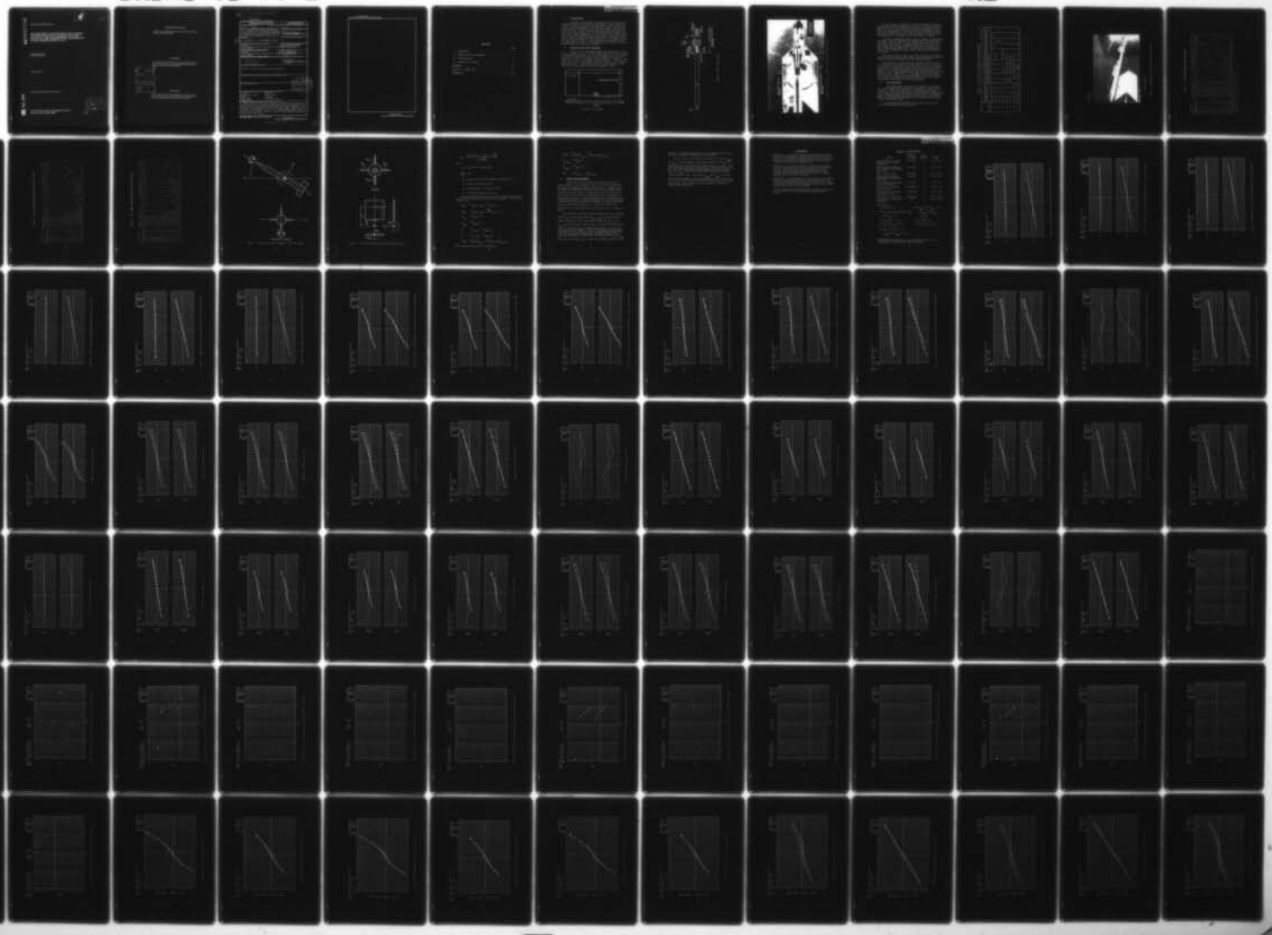

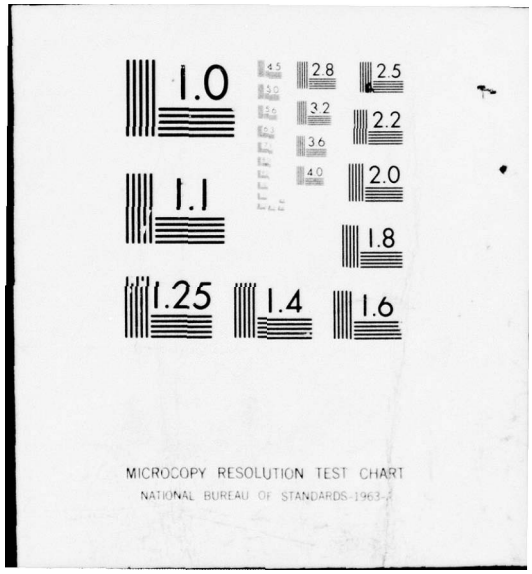
1.0
1.1
1.25
1.4
1.6
1.8
2.0
2.2
2.5
2.8
3.2
3.6
4.0
4.5
5.0
5.6
6.3
MICROCOPY RESOLUTION TEST CHART
NATIONAL BUREAU OF STANDARDS-1963-A

TECHNICAL REPORT TD-77-2

AN EXPERIMENTAL INVESTIGATION USING A NORMAL JET PLUME SIMULATOR TO DETERMINE JET PLUME EFFECTS ON A LONG SLENDER ROCKET CONFIGURATION AT MACH NUMBERS FROM 0.2 TO 1.5

Aeroballistics Directorate
Technology Laboratory

4 February 1977

US Army Missile Research and Development Command
Redstone Arsenal, Alabama 35809

DISPOSITION INSTRUCTIONS

DESTROY THIS REPORT WHEN IT IS NO LONGER NEEDED. DO NOT RETURN IT TO THE ORIGINATOR.

DISCLAIMER

THE FINDINGS IN THIS REPORT ARE NOT TO BE CONSTRUED AS AN OFFICIAL DEPARTMENT OF THE ARMY POSITION UNLESS SO DESIGNATED BY OTHER AUTHORIZED DOCUMENTS.

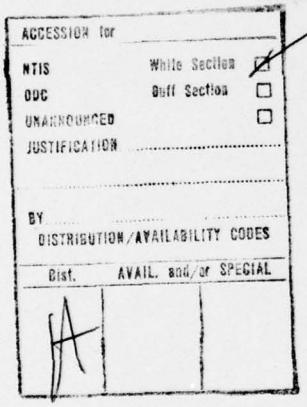

TRADE NAMES

USE OF TRADE NAMES OR MANUFACTURERS IN THIS REPORT DOES NOT CONSTITUTE AN OFFICIAL INDORSEMENT OR APPROVAL OF THE USE OF SUCH COMMERCIAL HARDWARE OR SOFTWARE.

(14) DRDMI-TD-77-2

UNCLASSIFIED

SECURITY CLASSIFICATION OF THIS PAGE *(When Data Entered)*

REPORT DOCUMENTATION PAGE

READ INSTRUCTIONS BEFORE COMPLETING FORM

1. REPORT NUMBER (6) TD-77-2	2. GOVT ACCESSION NO.
3. RECIPIENT'S CATALOG NUMBER (9)	
4. TITLE *(and Subtitle)* AN EXPERIMENTAL INVESTIGATION USING A NORMAL JET PLUME SIMULATOR TO DETERMINE JET PLUME EFFECTS ON A LONG SLENDER ROCKET CONFIGURATION AT MACH NUMBERS FROM 0.2 TO 1.5,	5. TYPE OF REPORT & PERIOD COVERED (9) Technical Report
	6. PERFORMING ORG. REPORT NUMBER
7. AUTHOR(s) (10) J. H. Henderson, C. W. Dahlke, and G. Batiuk	8. CONTRACT OR GRANT NUMBER(s)
9. PERFORMING ORGANIZATION NAME AND ADDRESS Commander US Army Missile Research and Development Command Attn: DRDMI-TD Redstone Arsenal, Alabama 35809	10. PROGRAM ELEMENT, PROJECT, TASK AREA & WORK UNIT NUMBERS (6) (DA) 1W362303A214
11. CONTROLLING OFFICE NAME AND ADDRESS Commander US Army Missile Research and Development Command Attn: DRDMI-TI Redstone Arsenal, Alabama 35809	12. REPORT DATE (11) 4 February 1977
	13. NUMBER OF PAGES 145
14. MONITORING AGENCY NAME & ADDRESS *(If different from Controlling Office)* (12) 143p.	15. SECURITY CLASS. *(of this report)* Unclassified
	15a. DECLASSIFICATION/DOWNGRADING SCHEDULE

16. DISTRIBUTION STATEMENT *(of this Report)*

Approved for public release; distribution unlimited.

17. DISTRIBUTION STATEMENT *(of the abstract entered in Block 20, if different from Report)*

18. SUPPLEMENTARY NOTES

19. KEY WORDS *(Continue on reverse side if necessary and identify by block number)*

Jet plume	Supersonic
Longitudinal stability	Thrust effects
Missiles	Transonic
Plume effects	Wind tunnel tests
Slender body	

20. ABSTRACT *(Continue on reverse side if necessary and identify by block number)*

Experimental aerodynamic investigations were conducted at the AEDC 16-foot Transonic Wind Tunnel to determine longitudinal stability characteristics of a long slender rocket configuration with simulated jet plume. The effect of jet plume on rocket aerodynamics is given over an angle of attack range from -11 to 11 degrees at Mach numbers from 0.2 to 1.5. Plume simulator chamber pressure varied from 0 to 600 psia. Individual cruciform fin aerodynamic loads are also shown over the same ranges.

DD FORM 1 JAN 73 1473 EDITION OF 1 NOV 65 IS OBSOLETE

UNCLASSIFIED

SECURITY CLASSIFICATION OF THIS PAGE *(When Data Entered)*

410126

LB

CONTENTS

I. INTRODUCTION

One of the major thrusts of the US Army Missile Research and Development Command is technological improvement of indirect-fire free rockets. Studies to date point favorably toward rockets characterized by long slender configurations with short boost times. Because of the short boost times, jet plume effects on missile longitudinal stability will be critical. Plume effects have been investigated previously on short rocket configurations [1,2,3]. The purpose of the present investigation was to obtain longitudinal stability data on long configurations and to determine if plume effects on aerodynamics are affected by body length. Test Mach number was varied from 0.2 to 1.5 and angle of attack was varied from -11° to 11°. Plume simulation was accomplished with the same normal jet simulator used in previous tests [1,2,3]. Simulator chamber pressure was varied up to 600 psi.

II. APPARATUS AND TEST CONDITIONS

The model is a sting-mounted body of revolution having a diameter of 5 inches. It has a 3-caliber tangent ogive nose with a cylindrical afterbody which can be tested in total lengths of 18 and 24 calibers. A cruciform fin configuration was tested in combination with the 24-caliber body. Fins are rectangular and have chords of 5 inches and semispans of 2.5 inches. Fin geometry is shown in Figure 1. The fins were tested only in the forward location with fin trailing edge 7.5 inches ahead of the base. A sketch of the model is shown in Figure 2. The model base area and plume simulator is presented in Figure 3.

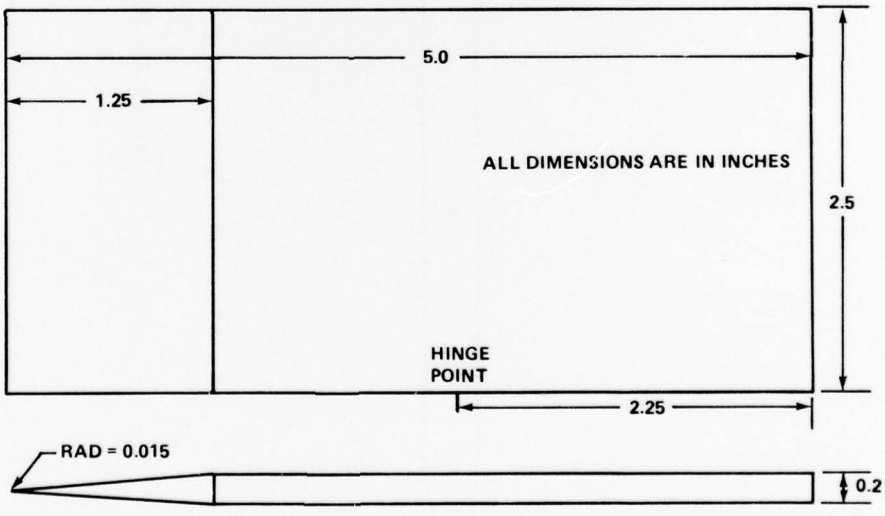

(a) FIN F1

Figure 1. Fin geometry.

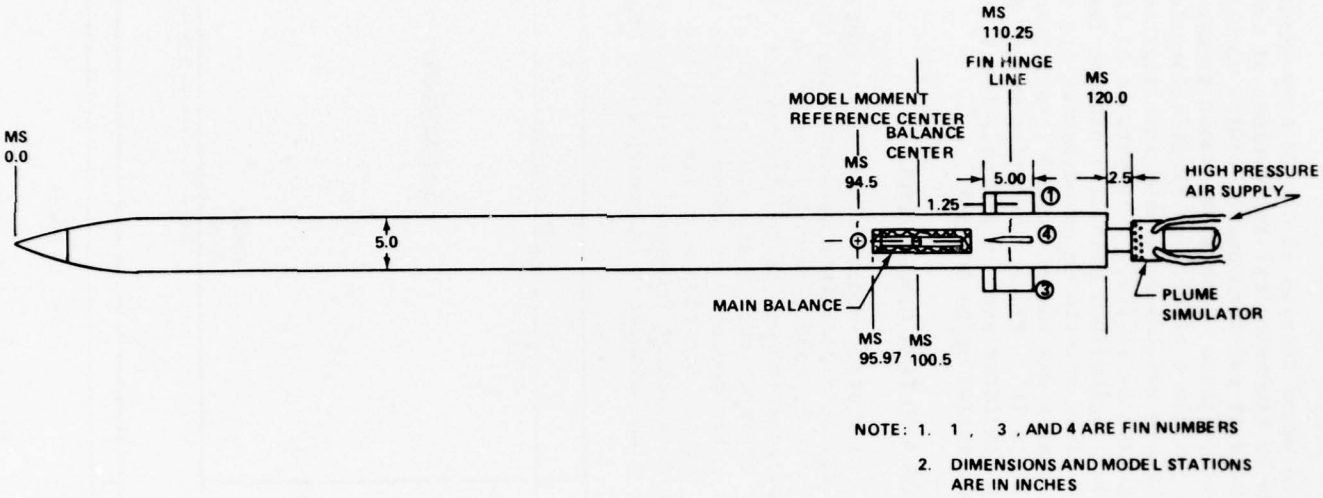

Figure 2. Model details, B24F1.

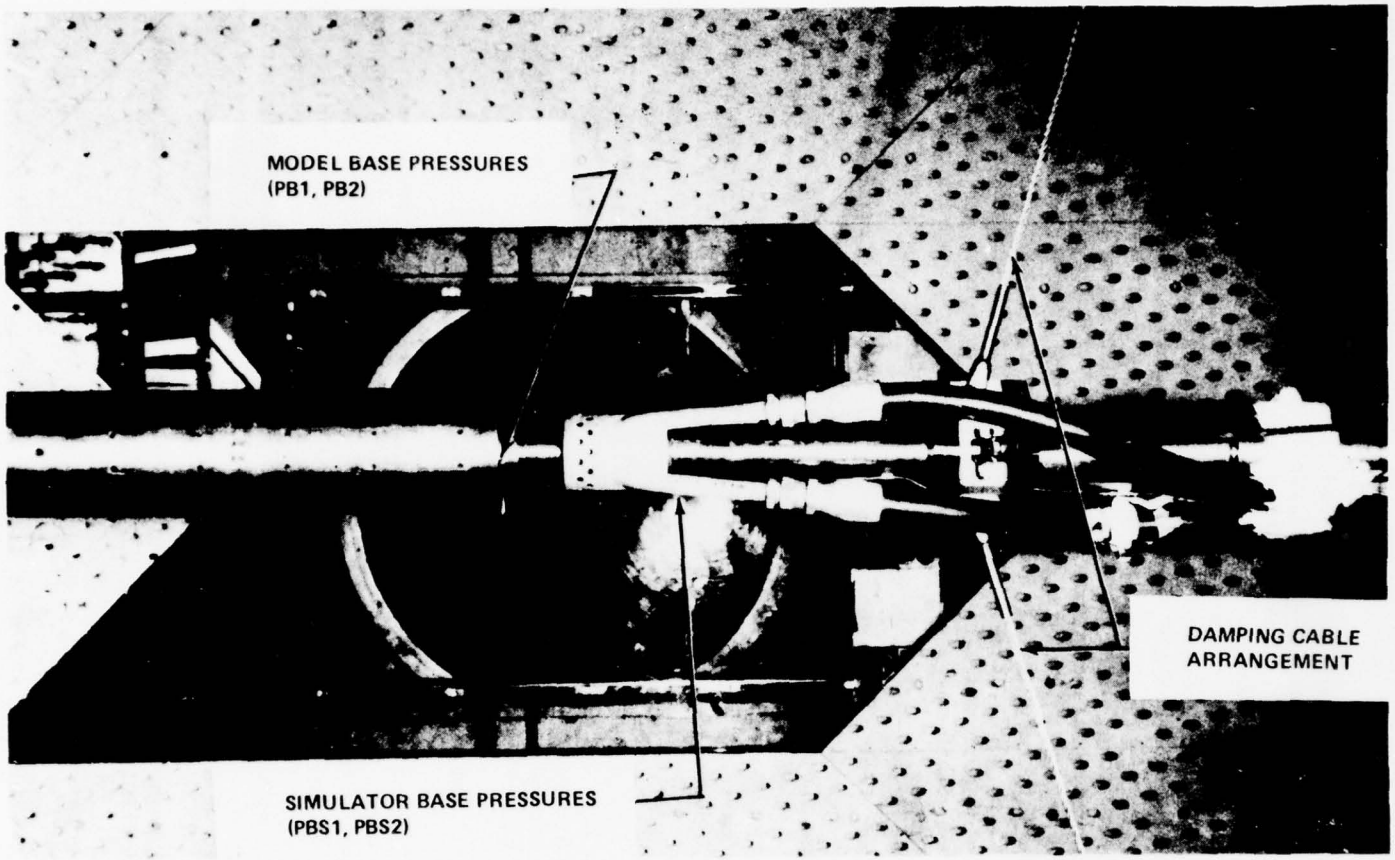

Figure 3. Model base, simulator, and damping cable details (B24).

The plume simulator consisted of 24 sonic jets normal to the sting centerline and arranged circumferentially in two rows with a common air chamber (Figure 3). The simulator was located 0.5 caliber aft of the model base. The combined exit area of the 24 jets represents 6% of the model base (reference) area. The level of plume simulation was established by varying pressures in the simulator chamber as shown in Table 1. The maximum rate of air supplied to the simulator was 15 lbs/sec.

A 2.0-inch, 6-component balance was used to measure the model forces and moments. Balance capacities were 1500-lbf normal force and 800-lbf side force, while the axial force and rolling moment were 200 lbf and 2000 in-lbf, respectively. To achieve better data resolution in the model pitch plane, the balance 800-lbf capacity side-force gages were used to measure model normal force. The fin forces and moments were measured with 5-component (no axial force) balances rated at 60 pounds normal force.

Model angle of attack, which varied from -11° to 11°, was measured using a pendulum-type angle sensor, with a back-up measurement determined from the indicated sting angle and balance sting deflections.

AEDC Tunnel 16T is a closed-circuit, continuous-flow tunnel that can be operated at Mach numbers from 0.20 to 1.60. The test section is 16 × 16 feet in cross section and 40 feet long. Details of the tunnel's capabilities and supporting equipment can be found in the Test Facility Handbook [4]. The model installed in the test section is shown in Figure 4. Table 2 gives the specific conditions under which data were taken during this test. Tables 3, 4, 5, and 6 present normal force slopes at zero angle of attack, pitching normal slopes at zero angle of attack, Fin 2 normal force slopes at zero angle of attack, and Fin 4 normal force slopes at zero angle of attack, respectively.

III. DATA REDUCTION

Model aerodynamic coefficients were calculated in the body-axis system (Figure 5) and referenced to a point 25.5 inches forward of the model base (missile station 94.5). Hinge moments for the tail balances were taken about the centerline of the attachment points; the root bending moments were taken about the body surface at the attachment point. Reference lengths and areas for fins and total configurations (Figure 6) are based on model diameter of 5 inches and cross-sectional area of 19.635 square inches.

A parameter used in setting the level of plume effects is the radial thrust coefficient, C_{RT}, defined as:

TABLE 1. AEDC TF-416 PLUME SIMULATOR CHAMBER PRESSURES

Mach No.	C_{RT}														
	0.01	1.0	1.5	2.0	2.5	3.0	4.0	6.0	9.0	12.0	18.0	25.0	37.5	50.0	75.0
	Simulator Chamber Pressure (psi)														
0.2	0.0											135		259	
0.4	0.0									184			557		
0.4	0.0												241		479
0.7	0.0						113			330	492				
0.9	0.0				96		151	224	334	445					
1.0	0.0				105		166	247	368	490					
1.25	0.0	49		95		141	188	280	419	558					
1.5	0.0	45		88		131		260							

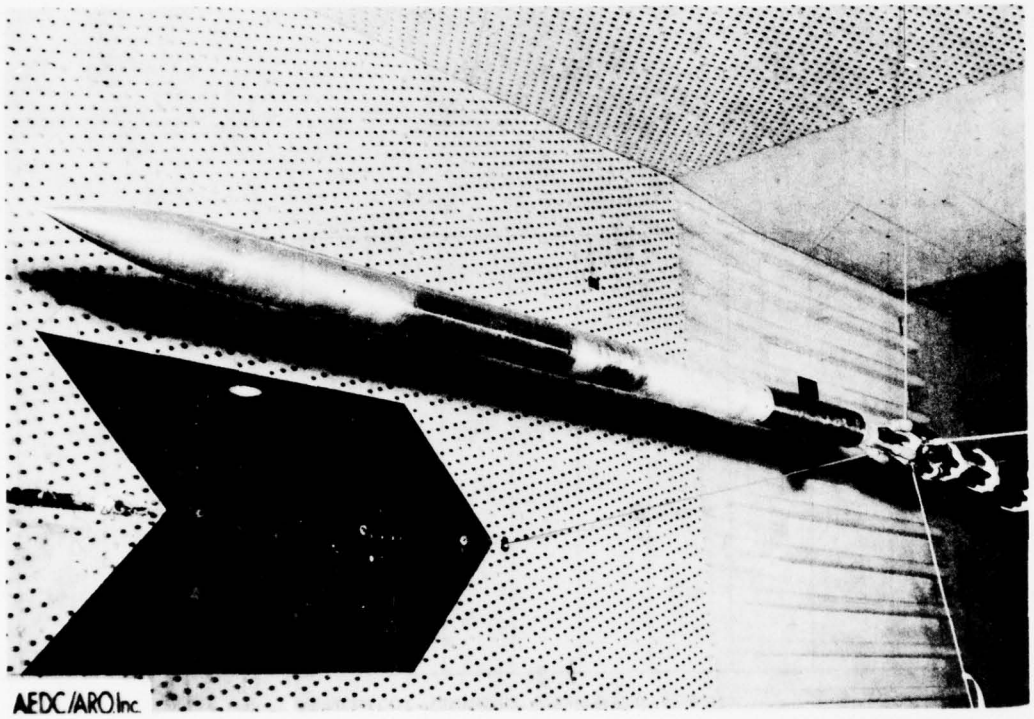

3868 (6-23-76) PWIT-F1A ARMY SIMULATED PLUME MODEL
IN THE PROPULSION WIND TUNNEL (16T)

Figure 4. Photograph of model (B24F1) installed in tunnel.

TABLE 2. DATA SET/RUN NUMBER COLLATION SUMMARY

TEST: AEDC TF-416 DATE: 8/2/76

Data Set Identifier	Configuration	Schedule		Parameters		Radial Thrust Coefficient, C_{RT}													
		α	β	P_T	Mach No.	0.01	1.0	2.0	2.5	3.0	4.0	6.0	9.0	12.0	18.0	25.0	37.5	50.0	75.0
RXI*01	B24	A	0	2000	0.2	251												252	
RXI*02	B24	A	0	1600	0.4	240											241		
RXI*03	B24	A	0	693	0.4	253											254		
RXI*04	B24	A	0	1200	0.7	255									256				
RXI*05	B24	A	0	1200	0.9	257													
RXI*06	B24	A	0	1200	1.0	242						243							
RXI*07	B24	A	0	1200	1.25	258					260		259						
RXI*08	B24	A	0	1100	1.5	244						261							
RXI*09	B24F1	B	0	2000	0.2	201										202		203	
RXI*10	B24F1	B	0	1600	0.4	205								206			207		
RXI*11	B24F1	B	0	693	0.4	208											209		210
RXI*12	B24F1	A	0	1200	0.7	211					212			213	214				
RXI*13	B24F1	A	0	1200	0.9	215			216			217		218					
RXI*14	B24F1	A	0	1200	1.0	219			220		221	222	223	224					
RXI*15	B24F1	A	0	1200	1.25	225	226	227		228		230	231	232					
RXI*16	B24F1	A	0	1100	1.5	233	234	235		236		237							

For *=0: CN, CLM, CY, CYN, CBL, CA, PB P1 For *=1: CNF1, CNF2, CNF3, CNF4, XCPF1, XCPF2, XCPF3, XCPF4, YCPF1, YCPF3

For *=2: CLMH1, CLMH2, CLMH3, CLMH4, CLMR1, CLMR2, CLMR3, CLMR4, YCPF2, YCPF4

α or β ΔA: -4, -3, -2, -1.5, -1, -0.5, 0, 0.5, 1, 1.5, 2, 3, 4
Schedules ΔB: -11, -9, -7, -5, -4, -3, -2, -1, -0.5, 0, 0.5, 1, 1.5, 2, 3, 4, 5, 7, 9, 11

TABLE 3. NORMAL FORCE SLOPES AT ZERO ANGLE OF ATTACK

TEST: AEDC TF-416 DATE: 8/2/76

Data Set Identifier	Configuration	Schedule		Parameters		Radial Thrust Coefficient, C_{RT}													
		α	β	P_T	Mach No.	0.01	1.0	2.0	2.5	3.0	4.0	6.0	9.0	12.0	18.0	25.0	37.5	50.0	75.0
RXI*01	B24	A	0	2000	0.2	0.064												0.036	
RXI*02	B24	A	0	1600	0.4	0.052											0.028		
RXI*03	B24	A	0	693	0.4	0.054											0.017		
RXI*04	B24	A	0	1200	0.7	0.049									-0.011				
RXI*05	B24	A	0	1200	0.9	0.047													
RXI*06	B24	A	0	1200	1.0	0.052						-0.007							
RXI*07	B24	A	0	1200	1.25	0.056					-0.057		-0.080						
RXI*08	B24	A	0	1100	1.5	0.054						-0.066							
RXI*09	B24F1	B	0	2000	0.2	0.141										0.093		0.104	
RXI*10	B24F1	B	0	1600	0.4	0.120								0.088			0.038		
RXI*11	B24F1	B	0	693	0.4	0.114											0.026		0.062
RXI*12	B24F1	A	0	1200	0.7	0.122					0.096			0.028	0.023				
RXI*13	B24F1	A	0	1200	0.9	0.127			0.101			-0.039		0.007					
RXI*14	B24F1	A	0	1200	1.0	0.147			0.099		0.066	-0.040	0.020	0.005					
RXI*15	B24F1	A	0	1200	1.25	0.148	0.129	0.094		0.078		-0.039	-0.051	-0.209					
RXI*16	B24F1	A	0	1100	1.5	0.143	0.126	0.095		0.073		0.051							

TABLE 4. PITCHING MOMENT SLOPES AT ZERO ANGLE OF ATTACK

TEST: AEDC TF-416 DATE: 8/2/76

Data Set Identifier	Configuration	Schedule		Parameters		Radial Thrust Coefficient, C_{RT}													
		α	β	P_T	Mach No.	0.01	1.0	2.0	2.5	3.0	4.0	6.0	9.0	12.0	18.0	25.0	37.5	50.0	75.0
RXI*01	B24	A	0	2000	0.2	0.63												0.62	
RXI*02	B24	A	0	1600	0.4	0.66											0.68		
RXI*03	B24	A	0	693	0.4	0.65											0.70		
RXI*04	B24	A	0	1200	0.7	0.64									0.82				
RXI*05	B24	A	0	1200	0.9	0.65													
RXI*06	B24	A	0	1200	1.0	0.66						0.91							
RXI*07	B24	A	0	1200	1.25	0.70					1.18		1.16						
RXI*08	B24	A	0	1100	1.5	0.79						1.29							
RXI*09	B24F1	B	0	2000	0.2	0.44										0.49		0.49	
RXI*10	B24F1	B	0	1600	0.4	0.44								0.57			0.61		
RXI*11	B24F1	B	0	693	0.4	0.47											0.67		0.50
RXI*12	B24F1	A	0	1200	0.7	0.44					0.55			0.71	0.70				
RXI*13	B24F1	A	0	1200	0.9	0.43			0.53			0.73		0.75					
RXI*14	B24F1	A	0	1200	1.0	0.41			0.57		0.66	0.74	0.77	0.77					
RXI*15	B24F1	A	0	1200	1.25	0.45	0.53	0.68		0.74		0.80	0.108	1.50					
RXI*16	B24F1	A	0	1100	1.5	0.52	0.61	0.75		0.84		0.87							

TABLE 5. FIN 2 NORMAL FORCE SLOPES AT ZERO ANGLE OF ATTACK

TEST: AEDC TF-416 DATE: 8/2/76

Data Set Identifier	Configuration	Schedule		Parameters		Radial Thrust Coefficient, C_{RT}													
		α	β	P_T	Mach No.	0.01	1.0	2.0	2.5	3.0	4.0	6.0	9.0	0.12	0.18	0.25	37.5	50.0	75.0
RXI*01	B24	A	0	2000	0.2														
RXI*02	B24	A	0	1600	0.4														
RXI*03	B24	A	0	693	0.4														
RXI*04	B24	A	0	1200	0.7														
RXI*05	B24	A	0	1200	0.9														
RXI*06	B24	A	0	1200	1.0														
RXI*07	B24	A	0	1200	1.25														
RXI*08	B24	A	0	1100	1.5														
RXI*09	B24F1	B	0	2000	0.2	0.023										0.016		0.013	
RXI*10	B24F1	B	0	1600	0.4	0.023								0.018			0.005		
RXI*11	B24F1	B	0	693	0.4	0.022											0.003		0.004
RXI*12	B24F1	A	0	1200	0.7	0.025					0.023			0.011	0.007				
RXI*13	B24F1	A	0	1200	0.9	0.025			0.023			0.016		0.005					
RXI*14	B24F1	A	0	1200	1.0	0.028			0.023		0.020	0.016	0.010	0.003					
RXI*15	B24F1	A	0	1200	1.25	0.029	0.029	0.029		0.029		0.022	0.002	-0.035					
RXI*16	B24F1	A	0	1100	1.5	0.027	0.026	0.027		0.026		0.027							

TABLE 6. FIN 4 NORMAL FORCE SLOPES AT ZERO ANGLE OF ATTACK

TEST: AEDC TF-416 DATE: 8/2/76

Data Set Identifier	Configuration	Schedule		Parameters		Radial Thrust Coefficient, C_{RT}													
		α	β	P_T	Mach No.	0.01	1.0	2.0	2.5	3.0	4.0	6.0	9.0	12.0	18.0	25.0	37.5	50.0	75.0
RXI*01	B24	A	0	2000	0.2														
RXI*02	B24	A	0	1600	0.4														
RXI*03	B24	A	0	693	0.4														
RXI*04	B24	A	0	1200	0.7														
RXI*05	B24	A	0	1200	0.9														
RXI*06	B24	A	0	1200	1.0														
RXI*07	B24	A	0	1200	1.25														
RXI*08	B24	A	0	1100	1.5														
RXI*09	B24F1	B	0	2000	0.2	0.020										0.018		0.013	
RXI*10	B24F1	B	0	1600	0.4	0.023								0.017			0.005		
RXI*11	B24F1	B	0	693	0.4	0.022											0		0.004
RXI*12	B24F1	A	0	1200	0.7	0.023					0.021			0.010	0.007				
RXI*13	B24F1	A	0	1200	0.9	0.024			0.022			0.016		0.005					
RXI*14	B24F1	A	0	1200	1.0	0.027			0.022		0.019	0.015	0.009	0.003					
RXI*15	B24F1	A	0	1200	1.25	0.027	0.027	0.028		0.028		0.020	0.002	-0.041					
RXI*16	B24F1	A	0	1100	1.5	0.027	0.026	0.026		0.026		0.026							

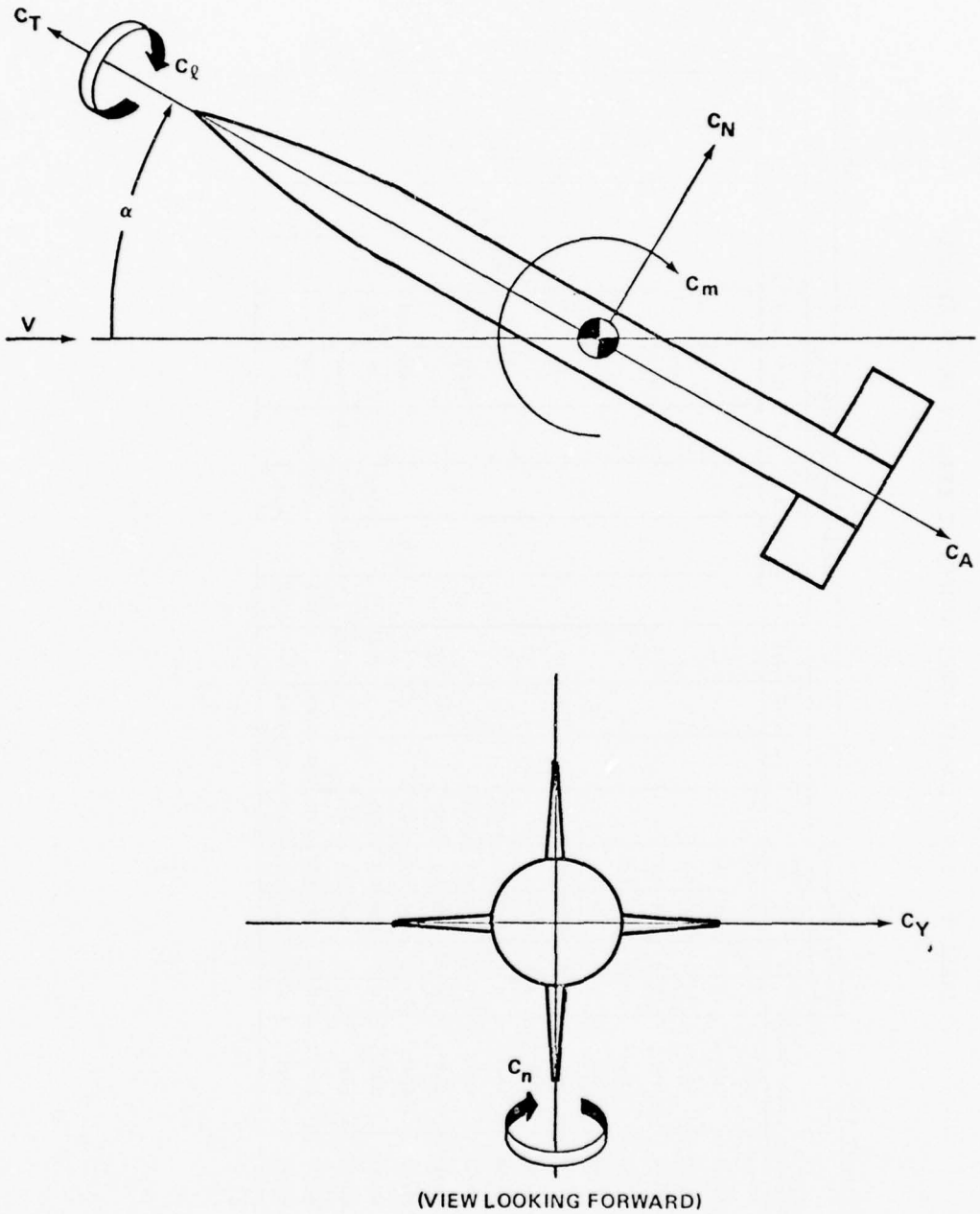

Figure 5. Axis system and sign convention - body axis system.

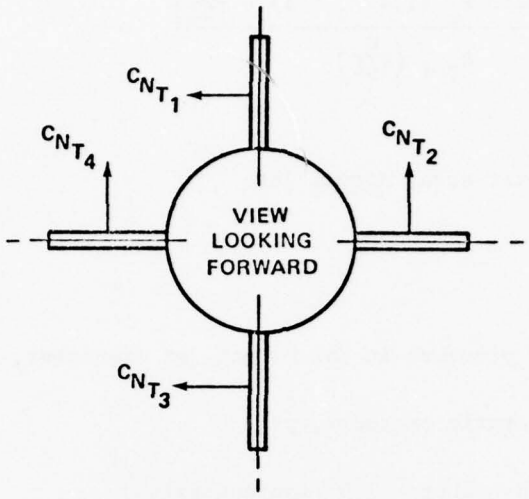

TAIL FINS

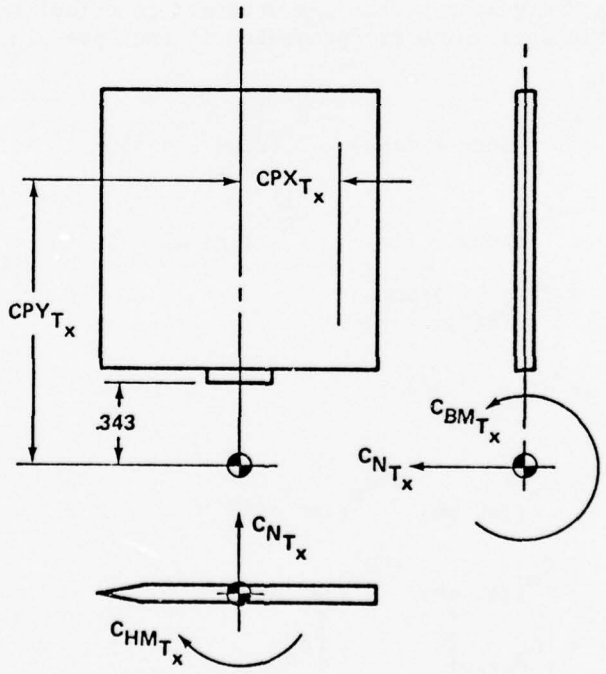

Figure 6. Axis system and positive sign convention for fins.

$$C_{RT} = \frac{A_{NJ}\left[0.5283\ P_c\ (1.4\ M_J^2 + 1) - \frac{P_s}{144}\right]}{A_{ref}\left(\frac{Q}{144}\right)}$$

where

A_{NJ} = total exit area, normal jet

$\frac{A_{NJ}}{A_{ref}} = 0.06$

P_c = chamber pressure in the normal jet simulator, psi

P_s = tunnel static pressure, psf

M_J = jet Mach number = 1.0 (sonic nozzles)

Q = free-stream dynamic pressure, psf

The Data Management System was utilized to calculate various interference coefficients which are presented in the Appendix. The equations utilized were:

$$C_{N_{B(F)}} = C_{N_{(body + fins)}} - C_{N_{(fins\ 2 + 4)}}$$

$$C_{m_{B(F)}} = C_{m_{(body + fins)}} - C_{HM_{(fins\ 2 + 4)}}\ ①$$

$$C_{N_{\alpha_{B(F)}}} = d(C_{N_{B(F)}})/d\alpha$$

$$C_{m_{\alpha_{B(F)}}} = d(C_{m_{B(F)}})/d\alpha$$

$$\Delta C_N = C_{N_{(jet\ on)}} - C_{N_{(jet\ off)}}$$

$$\Delta C_m = C_{m_{(jet\ on)}} - C_{m_{(jet\ off)}}$$

$$\Delta C_{N_{B(F)}} = \left[C_{N_{B(F)}}\right]_{jet\ on} - \left[C_{N_{(body\ alone)}}\right]_{jet\ off}$$

① fin hinge moment was moved to station 94.5.

$$\Delta C_{m_{B(F)}} = \left[C_{m_{B(F)}}\right]_{\text{jet on}} - \left[C_{m_{(\text{body alone})}}\right]_{\text{jet off}}$$

$$\Delta C_{N_{\alpha_{B(F)}}} = d(\Delta C_{N_{B(F)}})/d\alpha$$

$$\Delta C_{m_{\alpha_{B(F)}}} = d(\Delta C_{m_{B(F)}})/d\alpha$$

$$\Delta C_{RT} = (C_{RT})_{\text{jet on}} - (C_{RT})_{\text{jet off}}$$

IV. RESULTS AND DISCUSSION

Plume effects on the variation of normal force, C_N, and pitching moment, C_m, with angle of attack, α, for the body alone (B24) are shown in the Appendix, Figures A-1 through A-8. In general, only one plume off and one value of C_{RT} was run at each Mach number because of lack of test time available. Plume effects on the variation of C_N and C_m with α for the body-fin configuration (B24F1) is presented in Figures A-9 through A-17. Fin balance data for the two horizontal fins (F2 and F4) are shown in Figures A-18 through A-44. These data consist of plume effects on the variation of fin normal force C_{NF}, hinge moment C_{HM_F}, and bending moment C_{BM_F} with α. Data for the vertical fins (F1 and F3) are not presented since the variations due to α and C_{RT} are small.

The variation of the initial slopes of normal force (C_{N_α}), pitching moment (C_{m_α}), and fin normal force ($C_{N_{\alpha F2}}$, $C_{N_{\alpha F4}}$) with C_{RT} is shown in Figures A-45 through A-62. Comparisons of plume effects on C_{N_α} and $C_{N_{\alpha F2}}$ between the present configurations (24 calibers long) and previous tests (10.4 calibers long) are shown in Figures A-49, A-53, A-57, and A-61 for several Mach numbers. The data on the short configuration are from References [1,2,3] with the same fin configuration as the present test. For the body-fin configurations, the longer configuration is affected by the plume at a lower thrust level (the loss in C_{N_α} and $C_{N_{\alpha F2}}$ occurs at a lower value of C_{RT}). This fact is probably due to the lower

momentum of the thicker boundary layer on the longer configuration and its lower resistance to plume-induced flow separation.

The plume effects on the body in the presence of the fins ($C_{N_{B(F)}}$ and $C_{m_{B(F)}}$) were determined by subtracting horizontal fin forces and moments from the total configuration (B24F1) forces and moments. These values and their derivatives are presented in Figures A-63 through A-84. Body alone coefficients with no plume effects were subtracted from $C_{N_{B(F)}}$ and $C_{m_{B(F)}}$ to obtain the plume effects on the model afterbody in the presence of fins. The values ($\Delta C_{N_{B(F)}}$ and $\Delta C_{m_{B(F)}}$) and their derivatives are presented in Figures A-85 through A-106. Plume effects on body alone (ΔC_N and ΔC_m) were obtained by subtracting plume-off from plume-on data. These values and their derivatives are presented in Figures A-107 through A-118.

REFERENCES

1. Henderson, J. H., Transonic Wind Tunnel Investigation of Thrust Effects on the Longitudinal Stability Characteristics of Several Body-Fin Configurations (Sting-Mounted Model with Normal-Jet Plume Simulator), US Army Missile Command, Redstone Arsenal, Alabama, Technical Report RD-75-14, 31 December 1974.

2. Henderson, J. H., An Investigation of Jet Plume Effects on the Stability Characteristics of a Body of Revolution in Conjunction with Fins of Various Geometry and Longitudinal Positions at Transonic Speeds (Sting-Mounted Model with Normal Jet Plume Simulator), US Army Missile Command, Redstone Arsenal, Alabama, Technical Report RD-75-37, 12 June 1975.

3. Henderson, J. H., Investigation of Jet Plume Effects on the Longitudinal Stability Characteristics of a Body of Revolution with Various Fin Configurations at Mach Numbers from 0.2 to 2.3 (Normal Jet Simulator), US Army Missile Command, Redstone Arsenal, Alabama, Technical Report RD-76-22, February 1976.

4. Test Facilities Handbook (Tenth Edition), "Propulsion Wind Tunnel Facility, Volume 4", Arnold Engineering Development Center, May 1974.

Appendix A. PLOTTED DATA*

Title	Conditions Varying	Plot Schedule	Figure
Thrust Effects on Stability Characteristics for Body Alone, B24	CRT, MACH	A	A-1 - A-8
Thrust Effects on Stability Characteristics for Body with Fins, B24F1	CRT, MACH	A	A-9 - A-17
Thrust Effects on Fins	CRT, MACH	B	A-18 - A-44
Effect on Radial Thrust Coefficient on Longitudinal Derivatives	PT, MACH	C	A-45 - A-58
Thrust Effects on Fin Normal Force Characteristics	PT, MACH	D	A-59 - A-62
Plume Effects on Body in Presence of Fins	CRT, MACH, PT	E	A-63 - A-84
Plume Effects on Afterbody in Presence of Fins	DCRT, MACH	F	A-85 - A-106
Plume Effects on Body Alone	DCRT, MACH	G	A-107 - A-114
Plume Effects on Body Alone Derivatives	MACH	H	A-115 - A-118

Plot Schedule:

(A) C_N and C_m vs. α

(B) $C_{N_{F2}}$, $C_{N_{F4}}$, $C_{HM_{F2}}$, $C_{HM_{F4}}$, $C_{BM_{F2}}$, and $C_{BM_{F4}}$ vs. α

(C) $C_{N\alpha}$ and $C_{m\alpha}$ vs. C_{RT}

(D) $C_{N_{\alpha F2}}$ and $C_{N_{\alpha F4}}$ vs. C_{RT}

(E) $C_{N_{B(F)}}$ and $C_{m_{B(F)}}$ vs. α, $C_{N_{\alpha B(F)}}$ and $C_{m_{\alpha B(F)}}$ vs. C_{RT}

(F) $\Delta C_{N_{B(F)}}$ and $\Delta C_{m_{B(F)}}$ vs. α, $\Delta C_{N_{\alpha B(F)}}$ and $\Delta C_{m_{\alpha B(F)}}$ vs. ΔC_{RT}

(G) ΔC_N and ΔC_m vs. α

(H) ΔC_{N_α} and ΔC_{m_α} vs. C_{RT}

*Tabulations of the plotted data and corresponding source data are available from Data Management Services Operations.

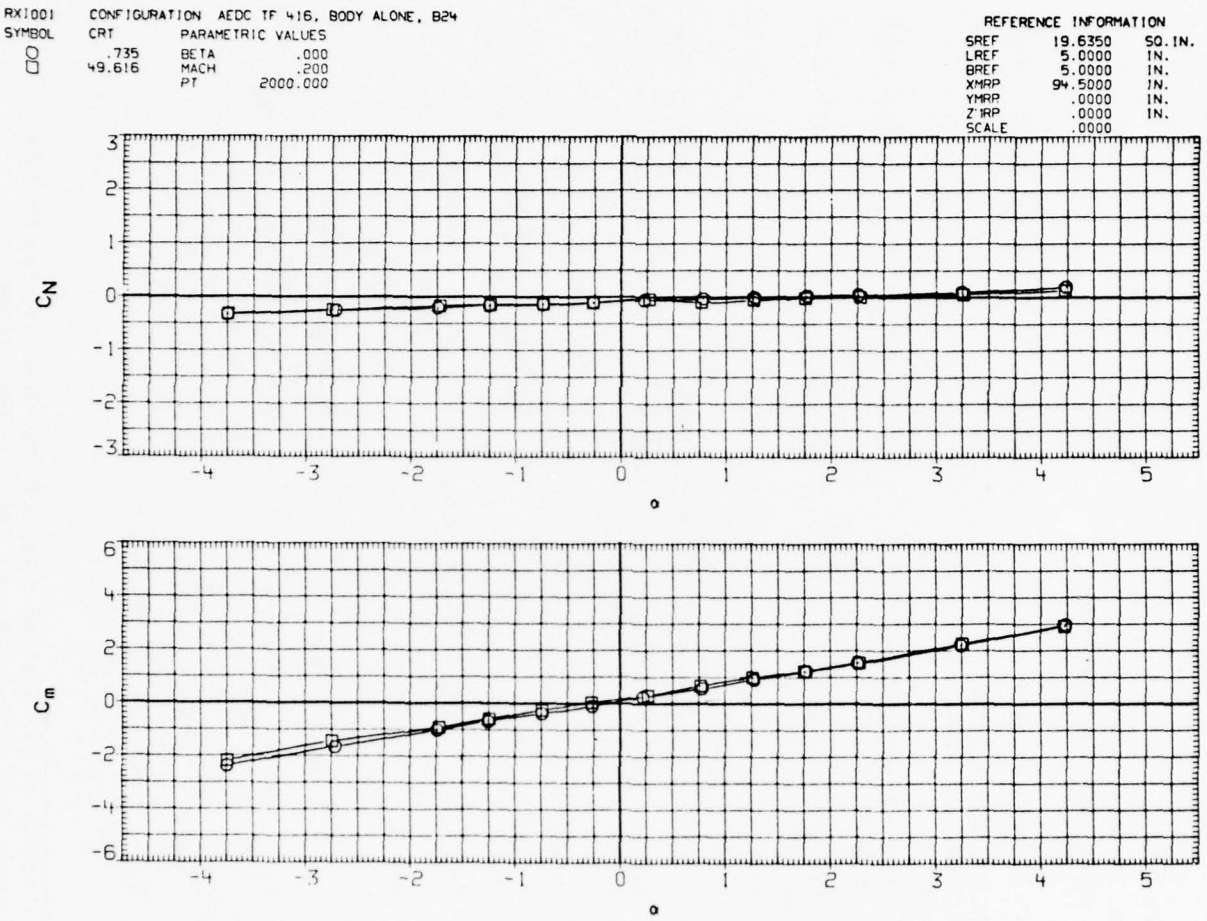

Figure A-1. Thrust effects on stability characteristics for body alone, B24.

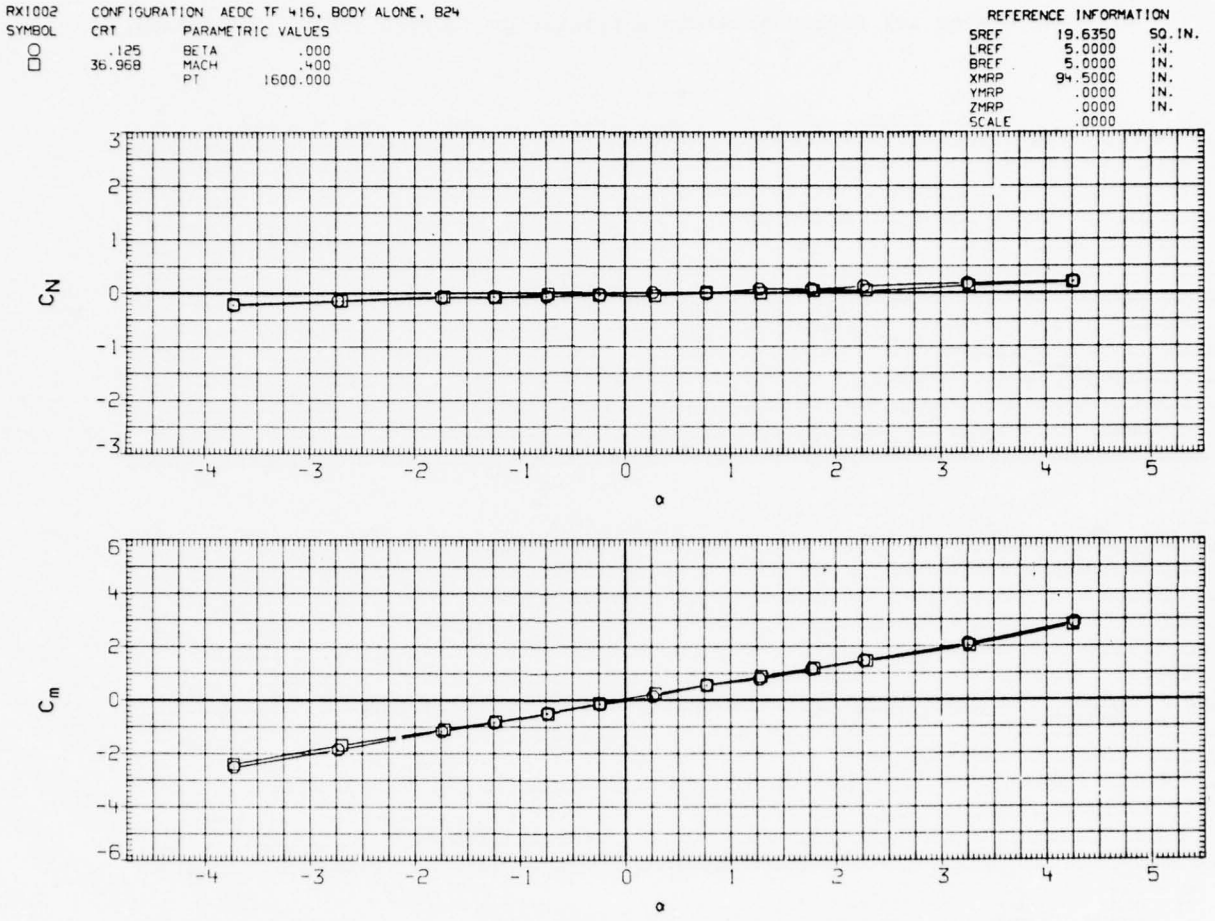

Figure A-2. Thrust effects on stability characteristics for body alone, B24.

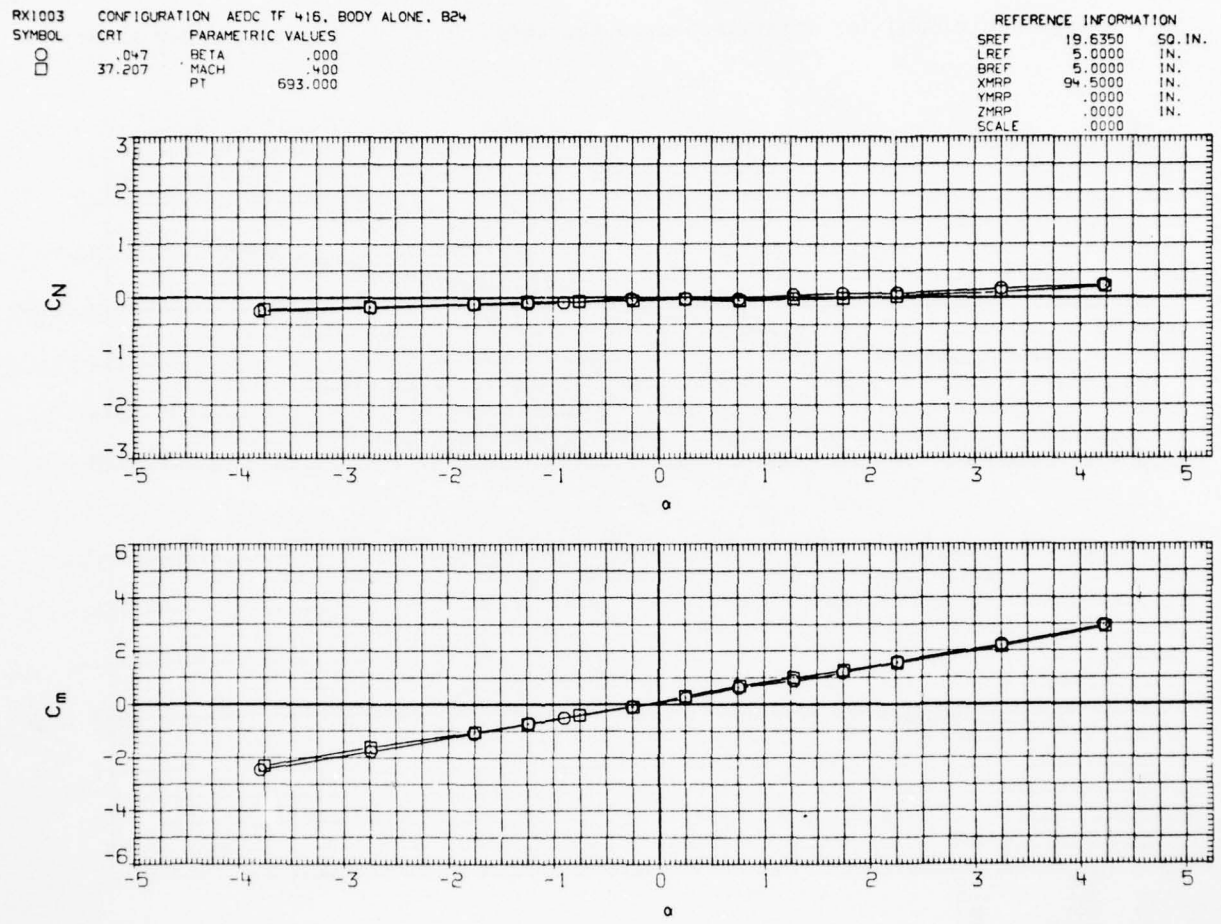

Figure A-3. Thrust effects on stability characteristics for body alone, B24.

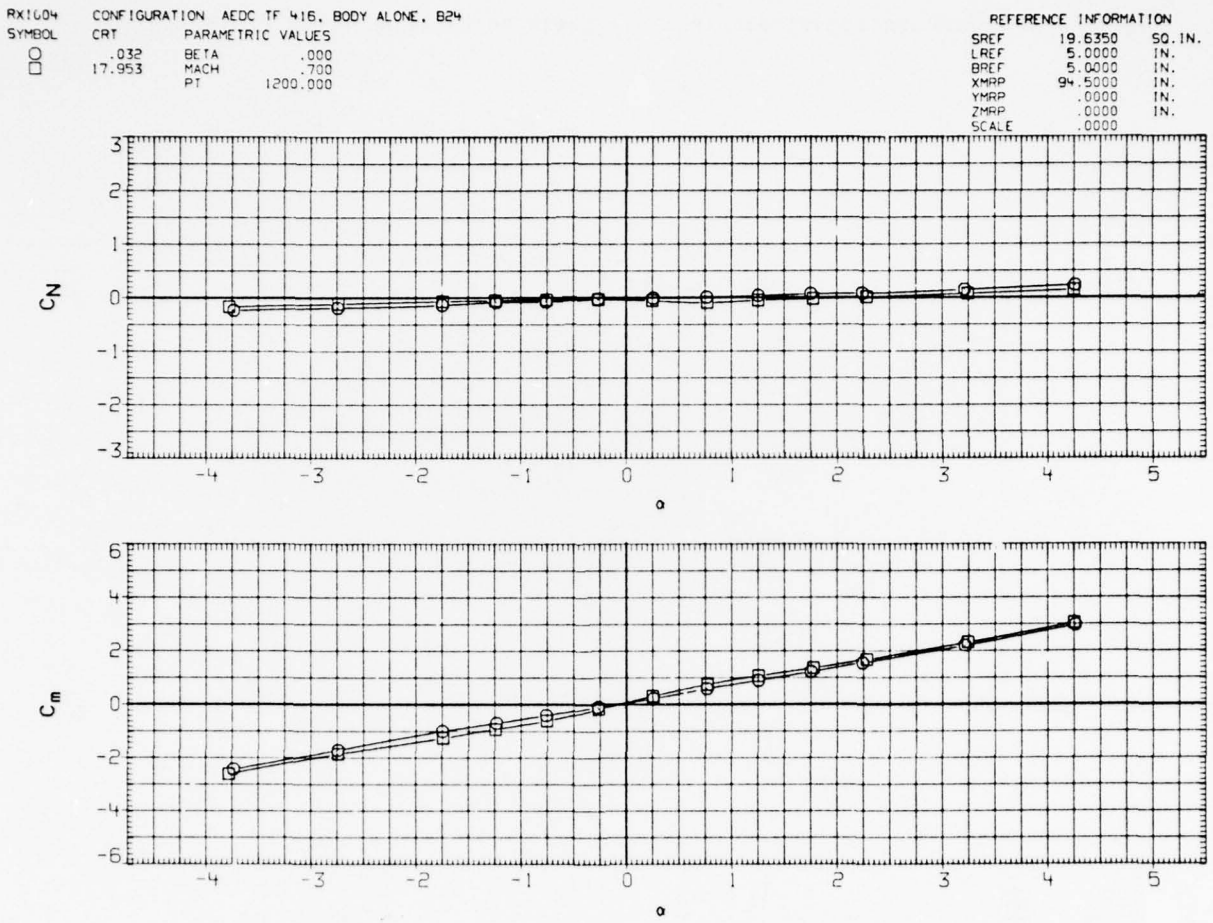

Figure A-4. Thrust effects on stability characteristics for body alone, B24.

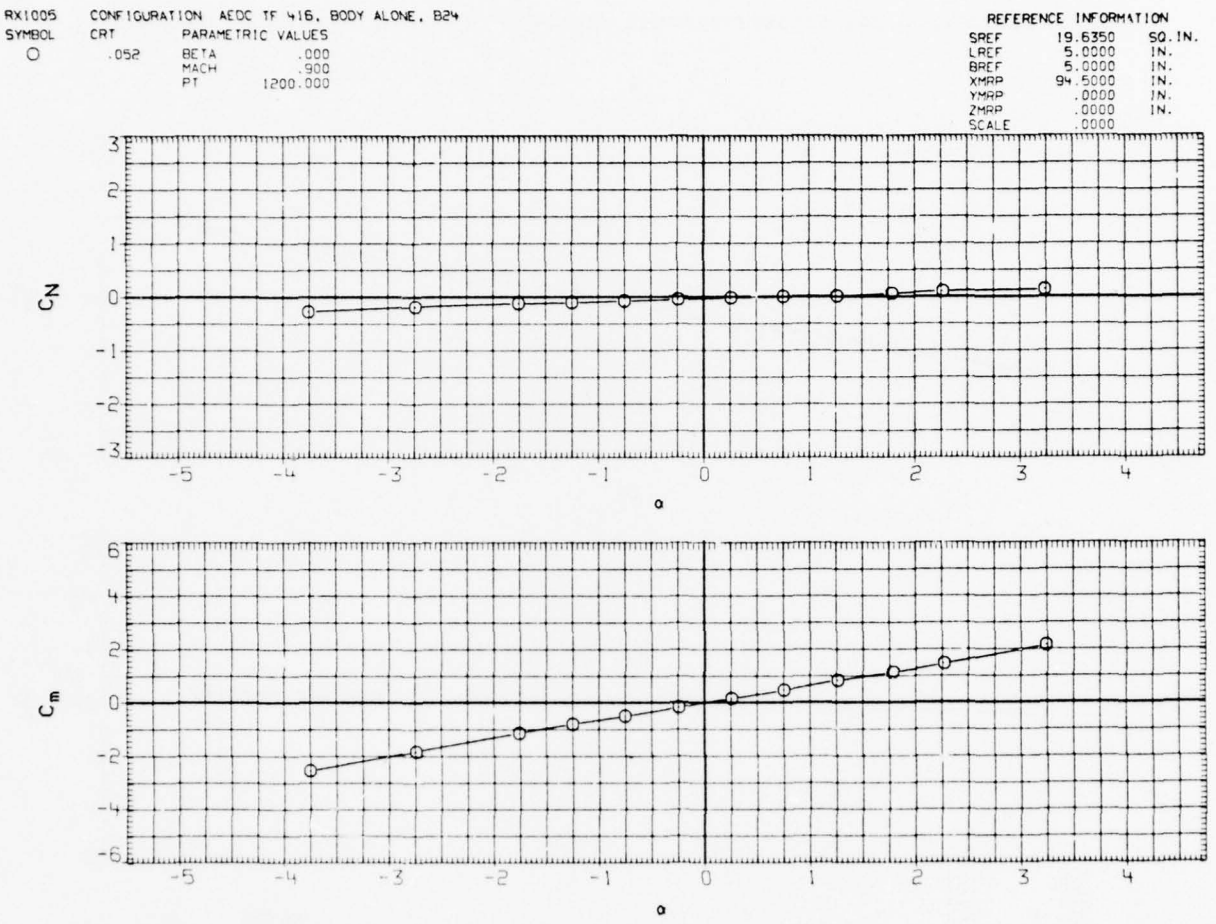

Figure A-5. Thrust effects on stability characteristics for body alone, B24.

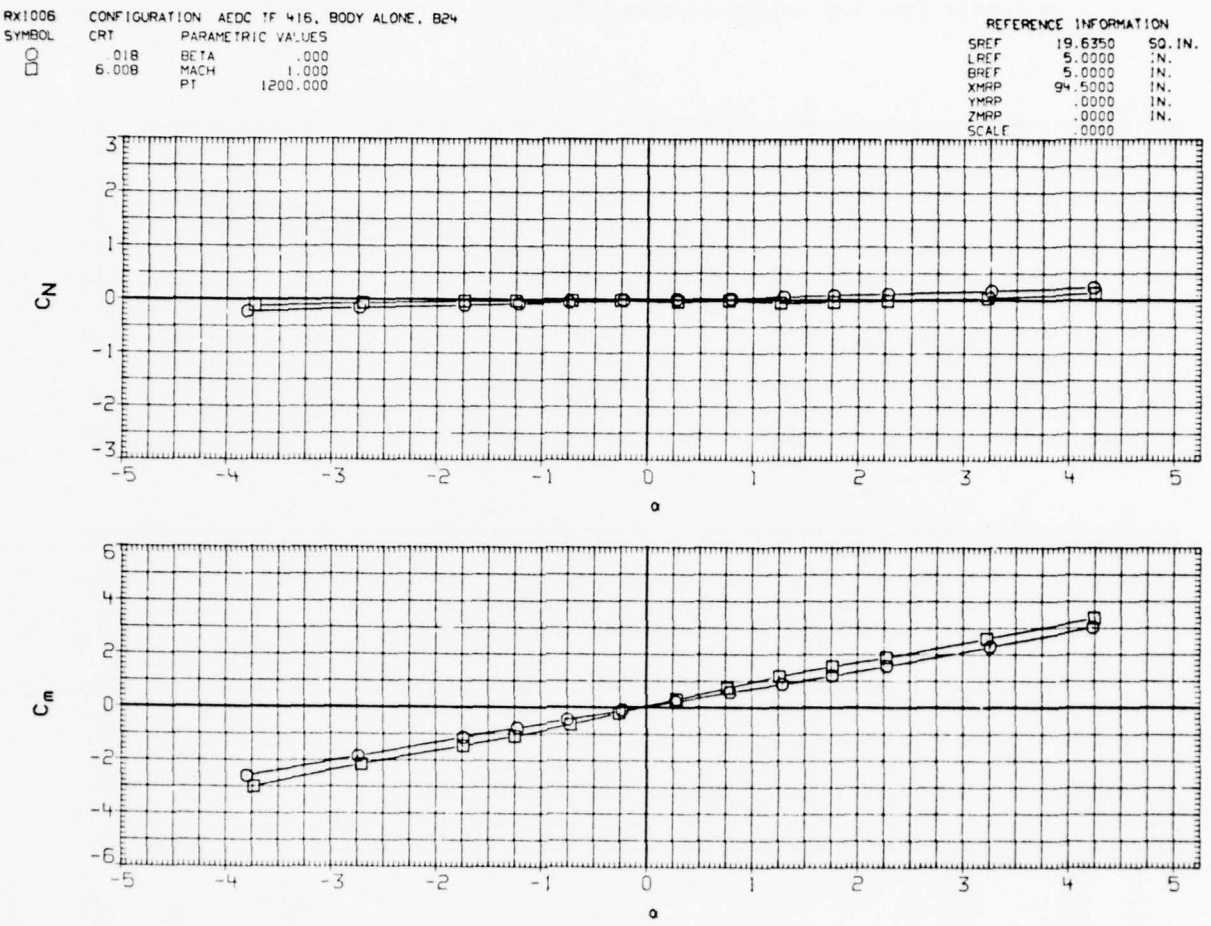

Figure A-6. Thrust effects on stability characteristics for body alone, B24.

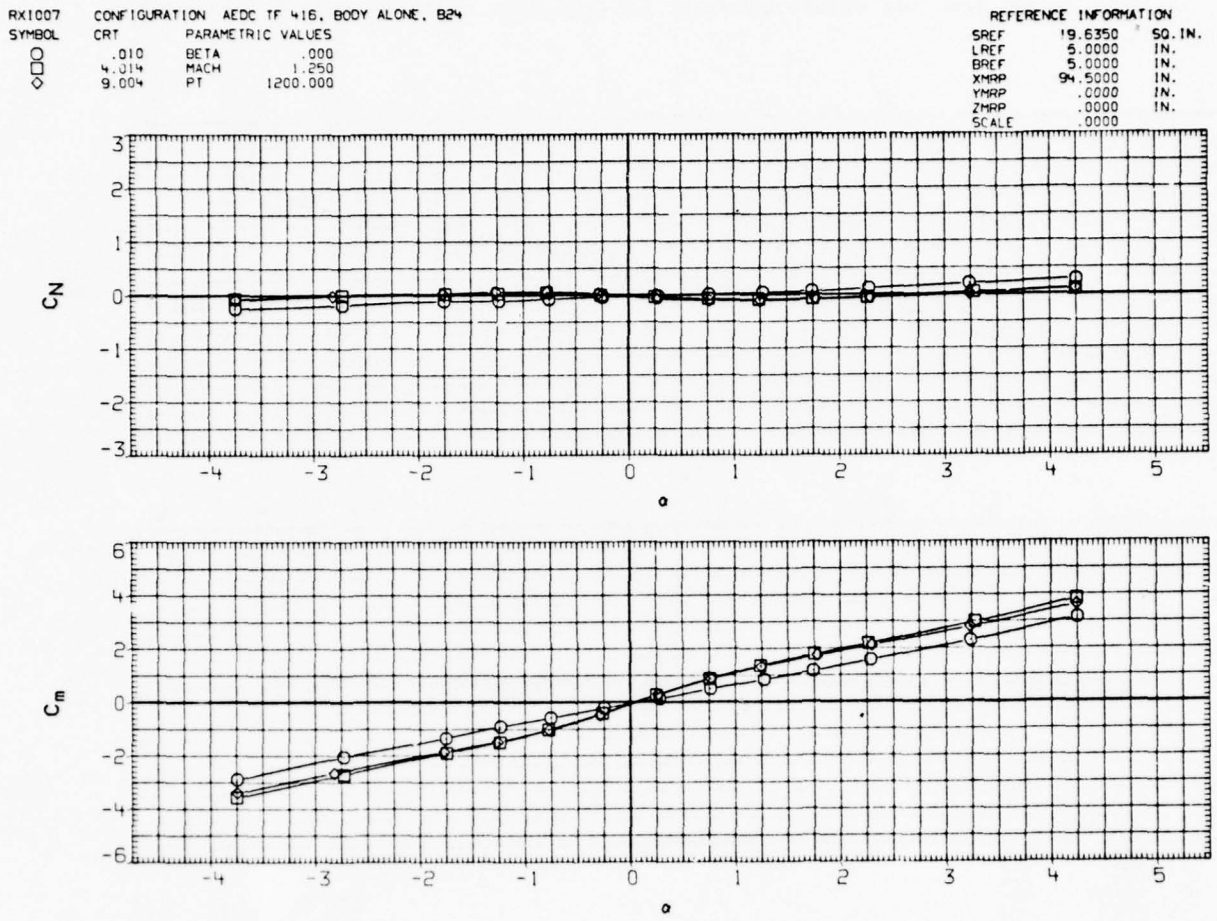

Figure A-7. Thrust effects on stability characteristics for body alone, B24.

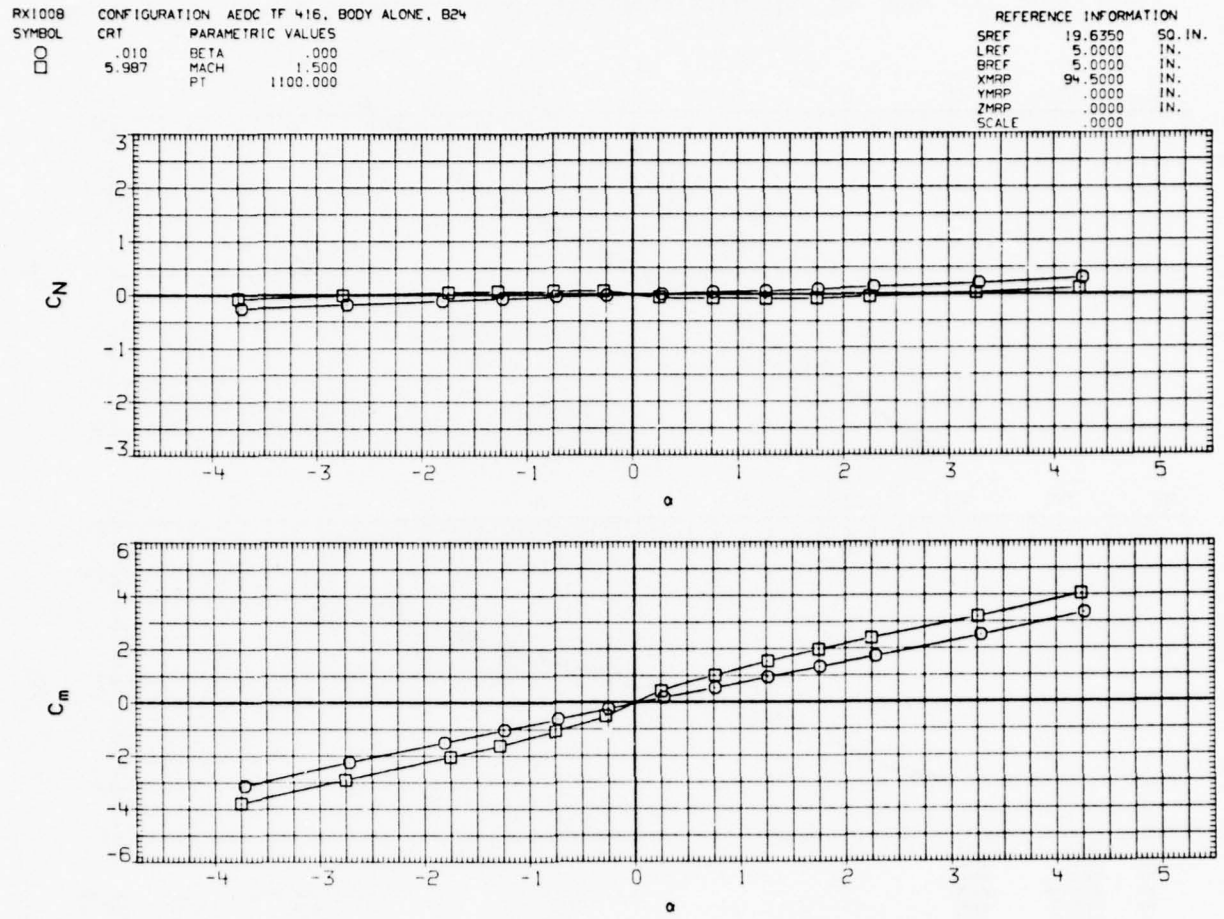

Figure A-8. Thrust effects on stability characteristics for body alone, B24.

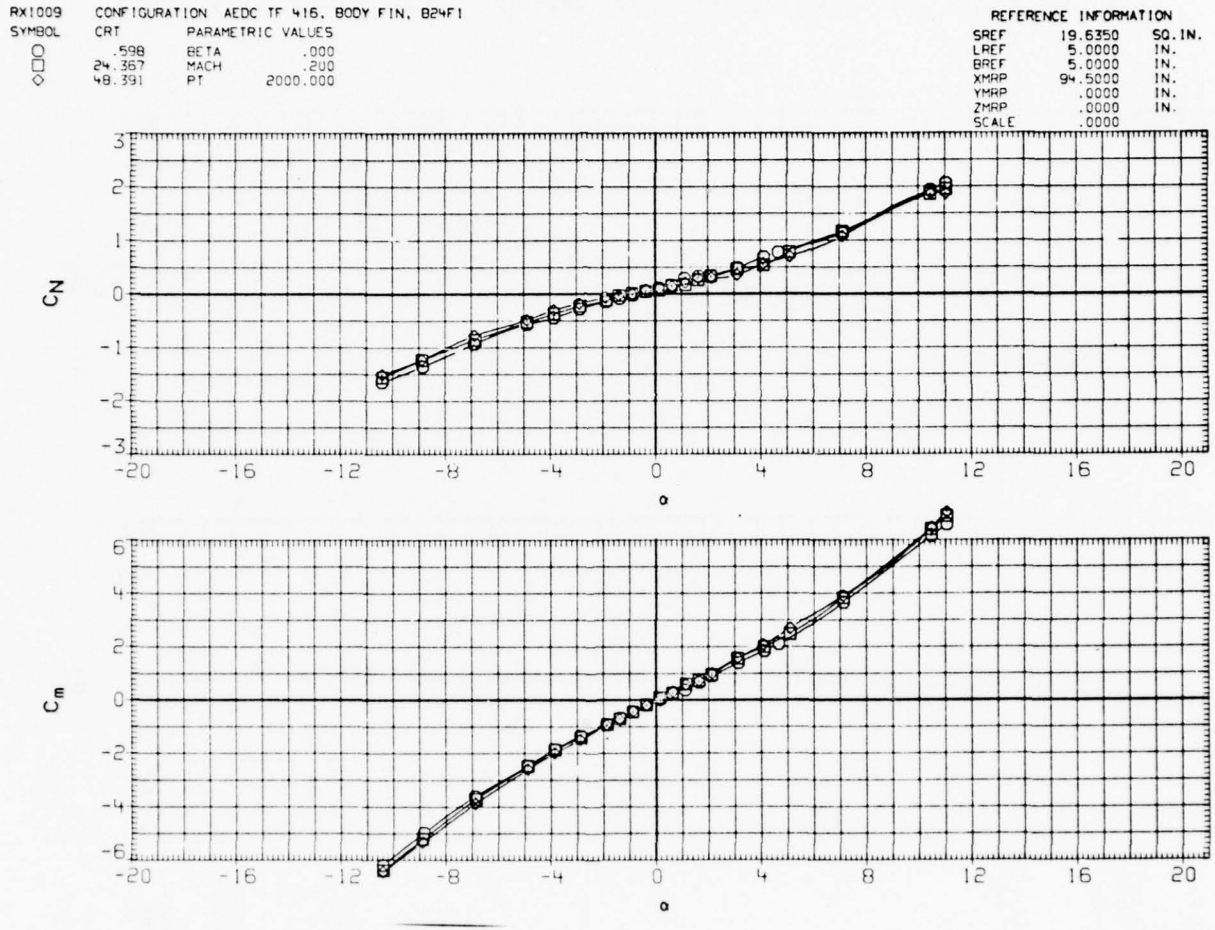

Figure A-9. Thrust effects on stability characteristics for body with fins, B24F1.

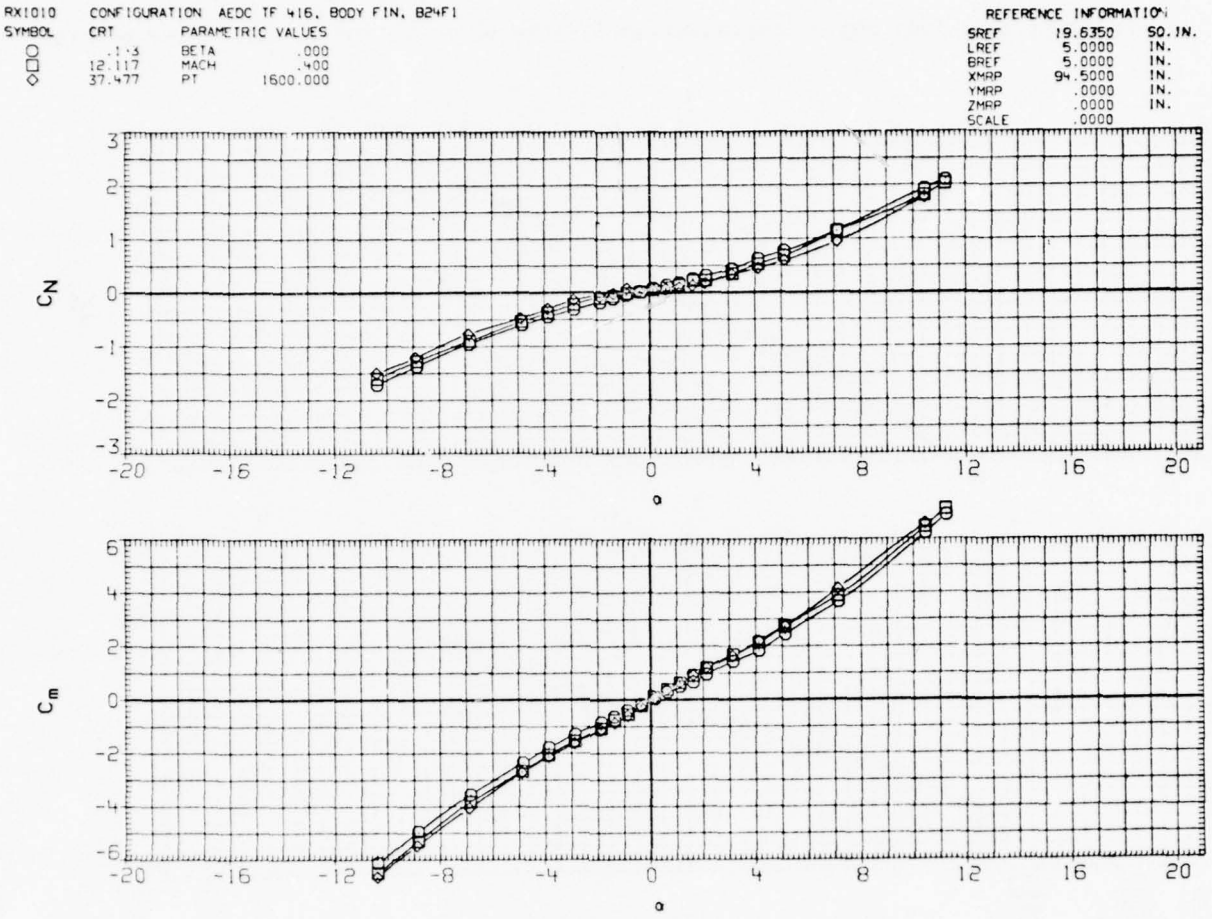

Figure A-10. Thrust effects on stability characteristics for body with fins, B24F1.

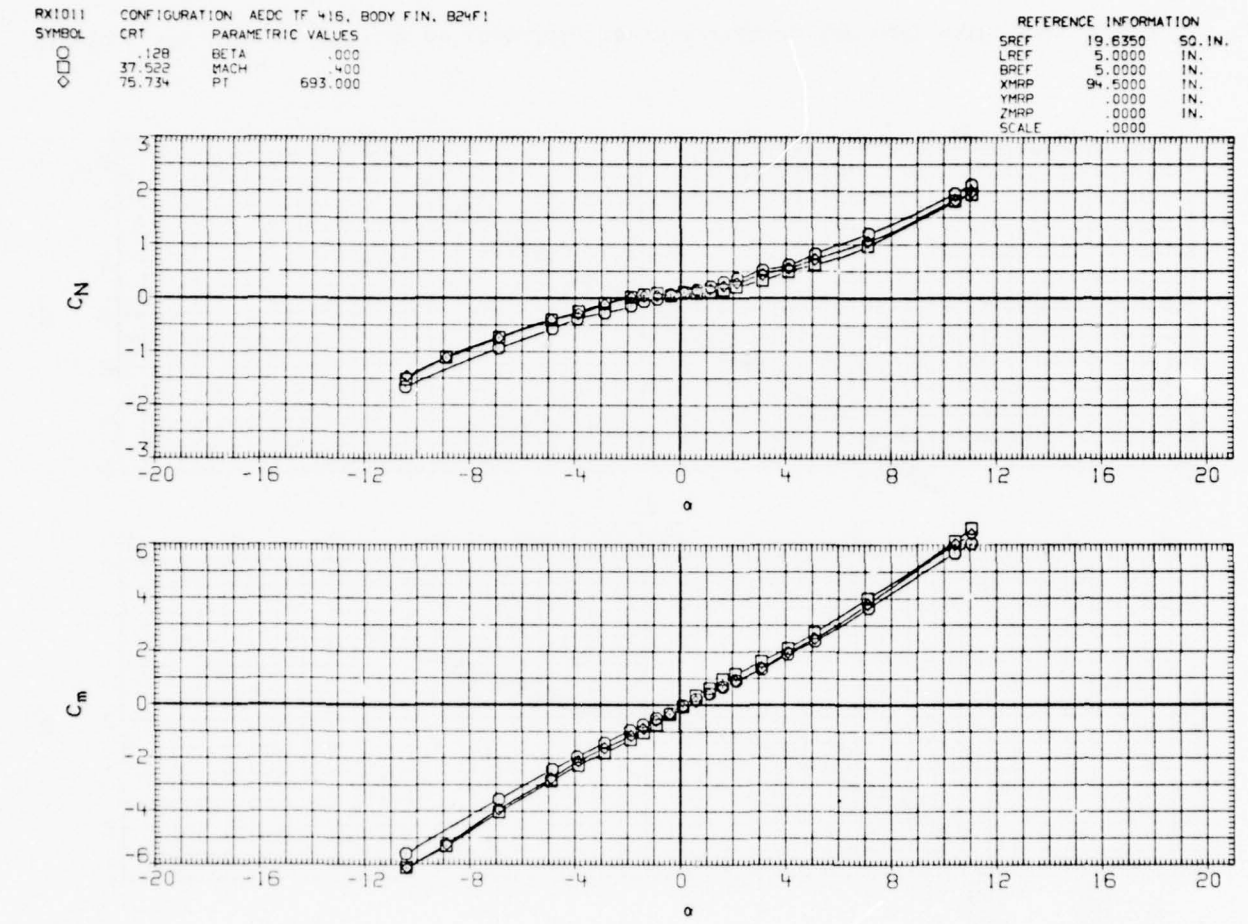

Figure A-11. Thrust effects on stability characteristics for body with fins, B24F1.

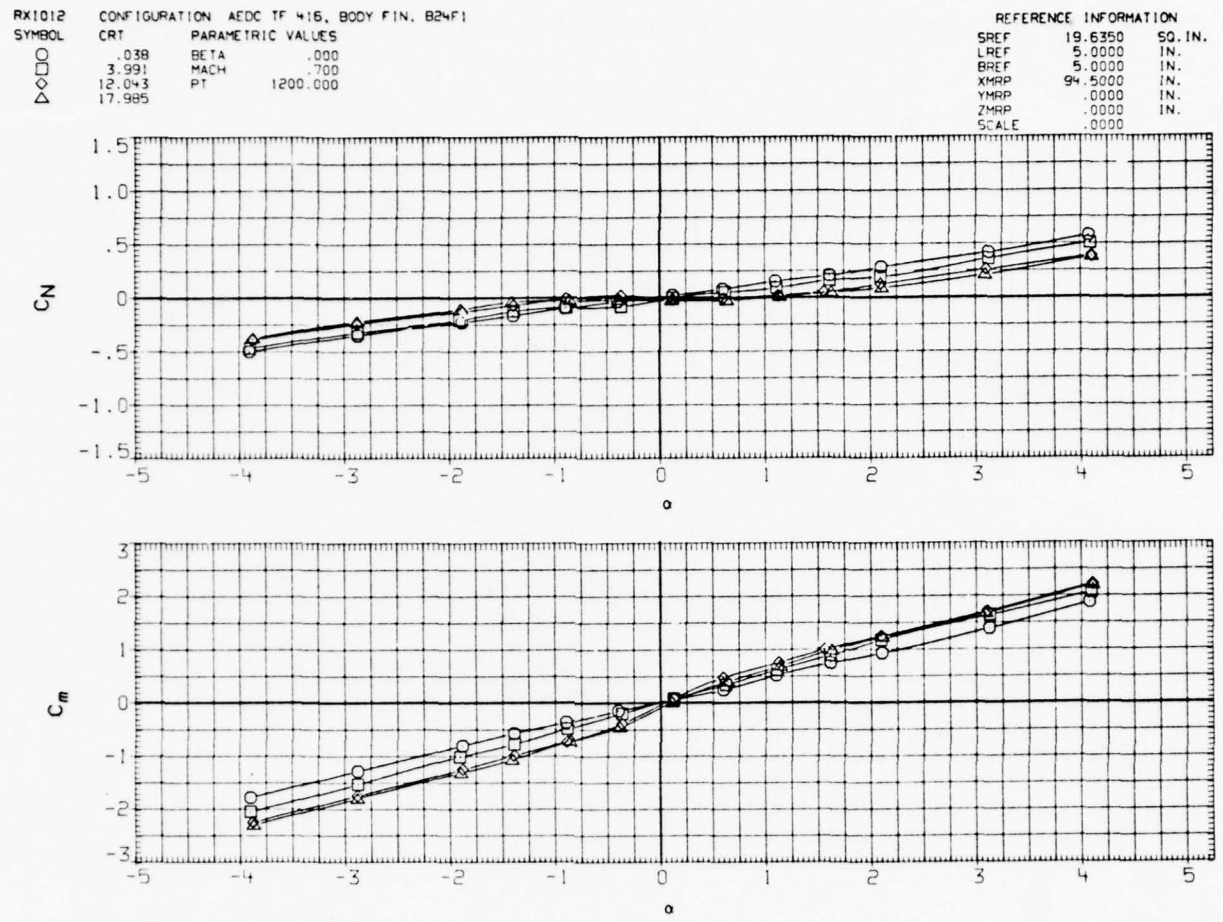

Figure A-12. Thrust effects on stability characteristics for body with fins, B24F1.

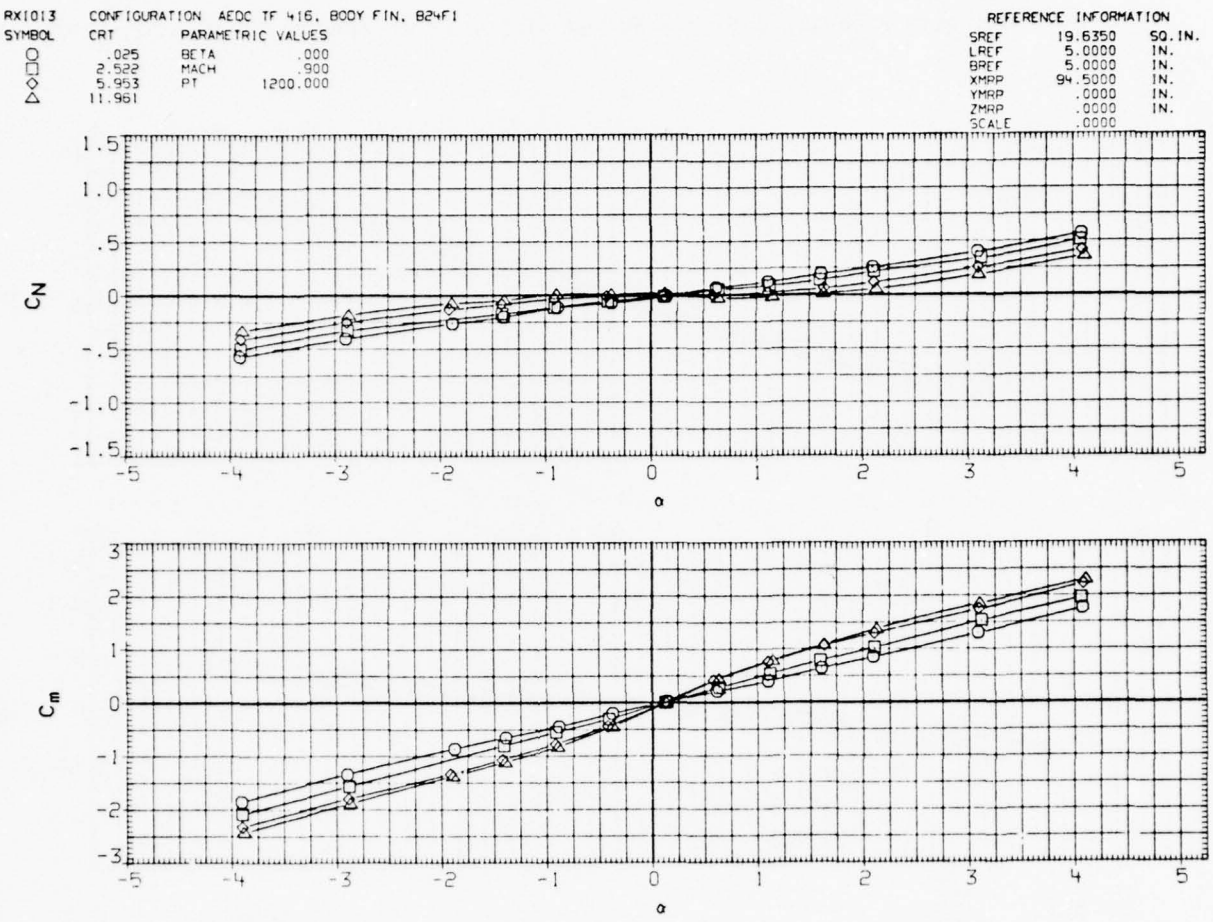

Figure A-13. Thrust effects on stability characteristics for body with fins, B24F1.

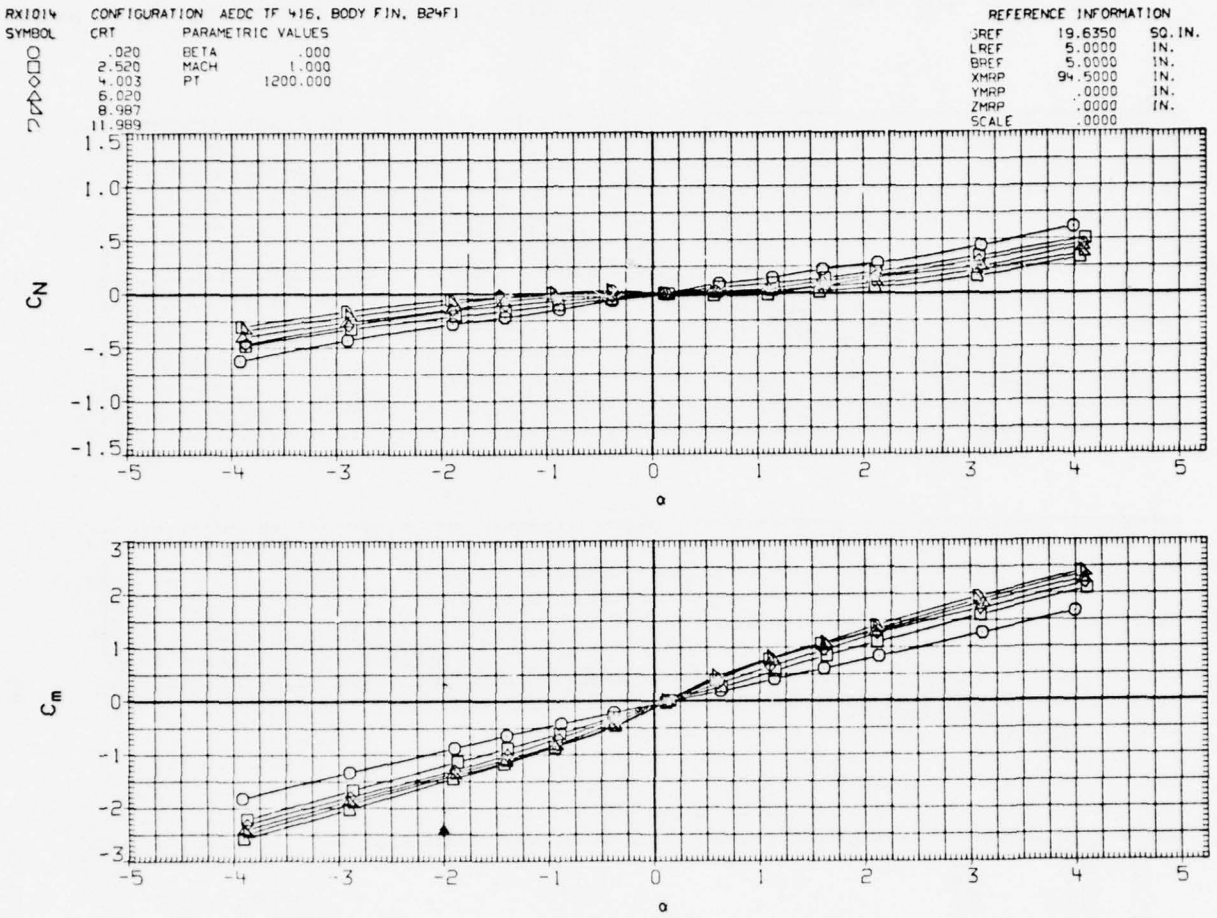

Figure A-14. Thrust effects on stability characteristics for body with fins, B24F1.

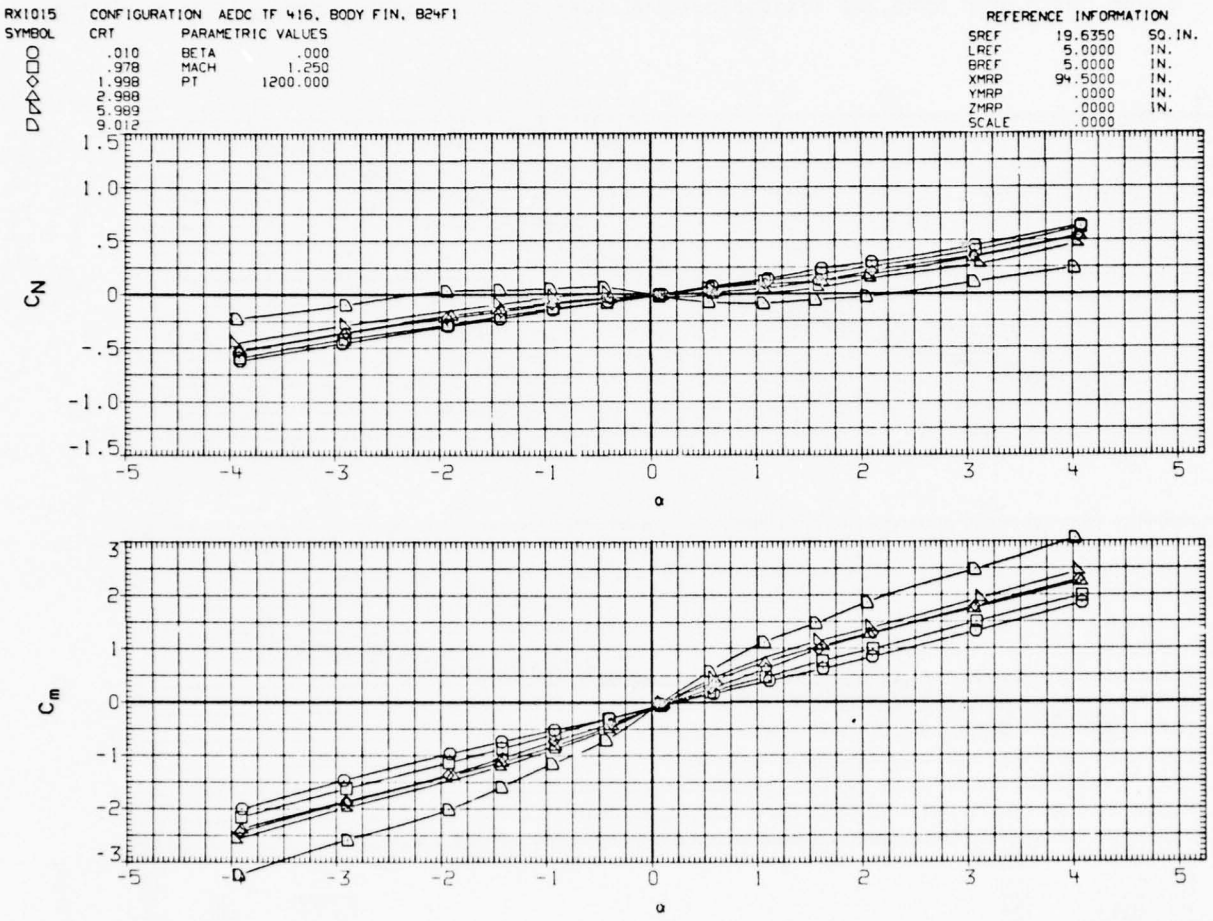

Figure A-15. Thrust effects on stability characteristics for body with fins, B24F1.

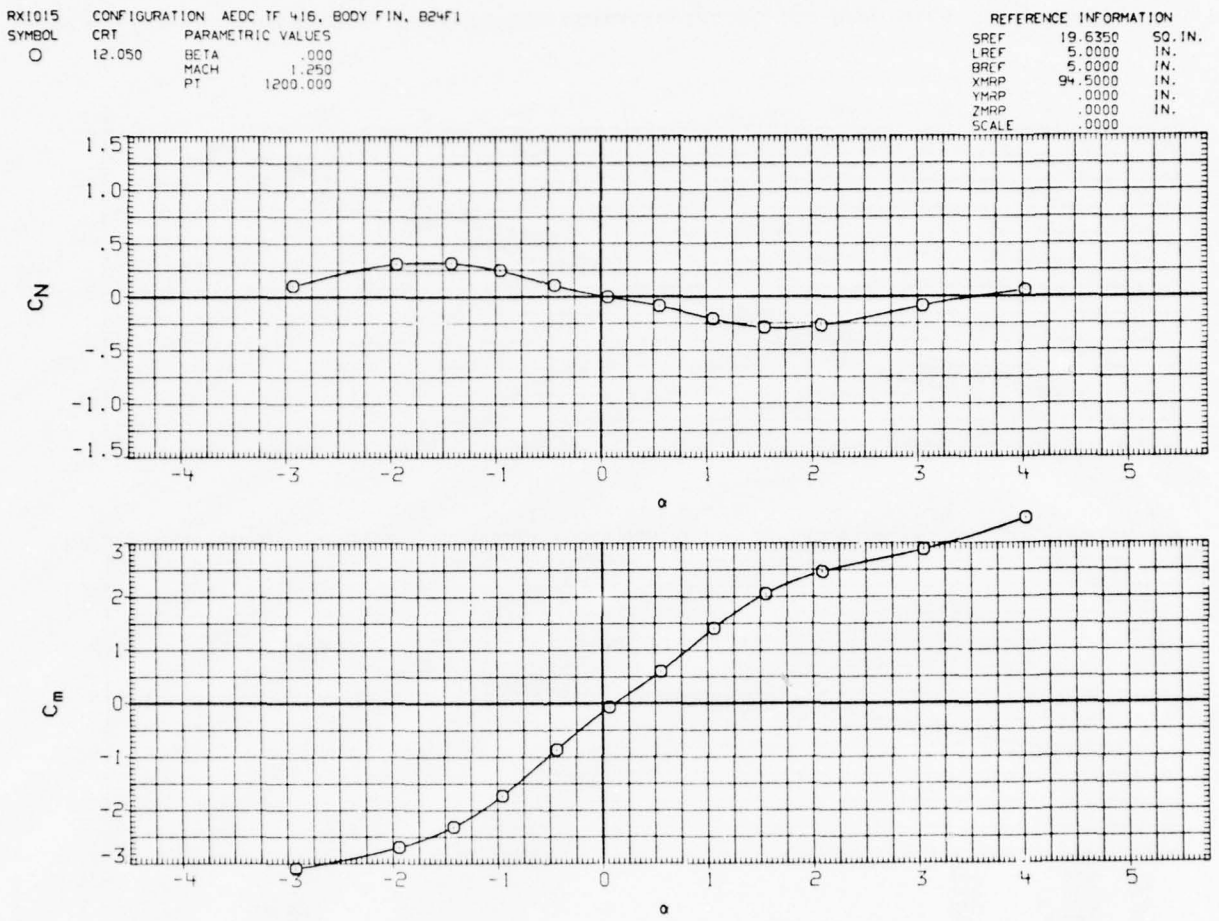

Figure A-16. Thrust effects on stability characteristics for body with fins, B24F1.

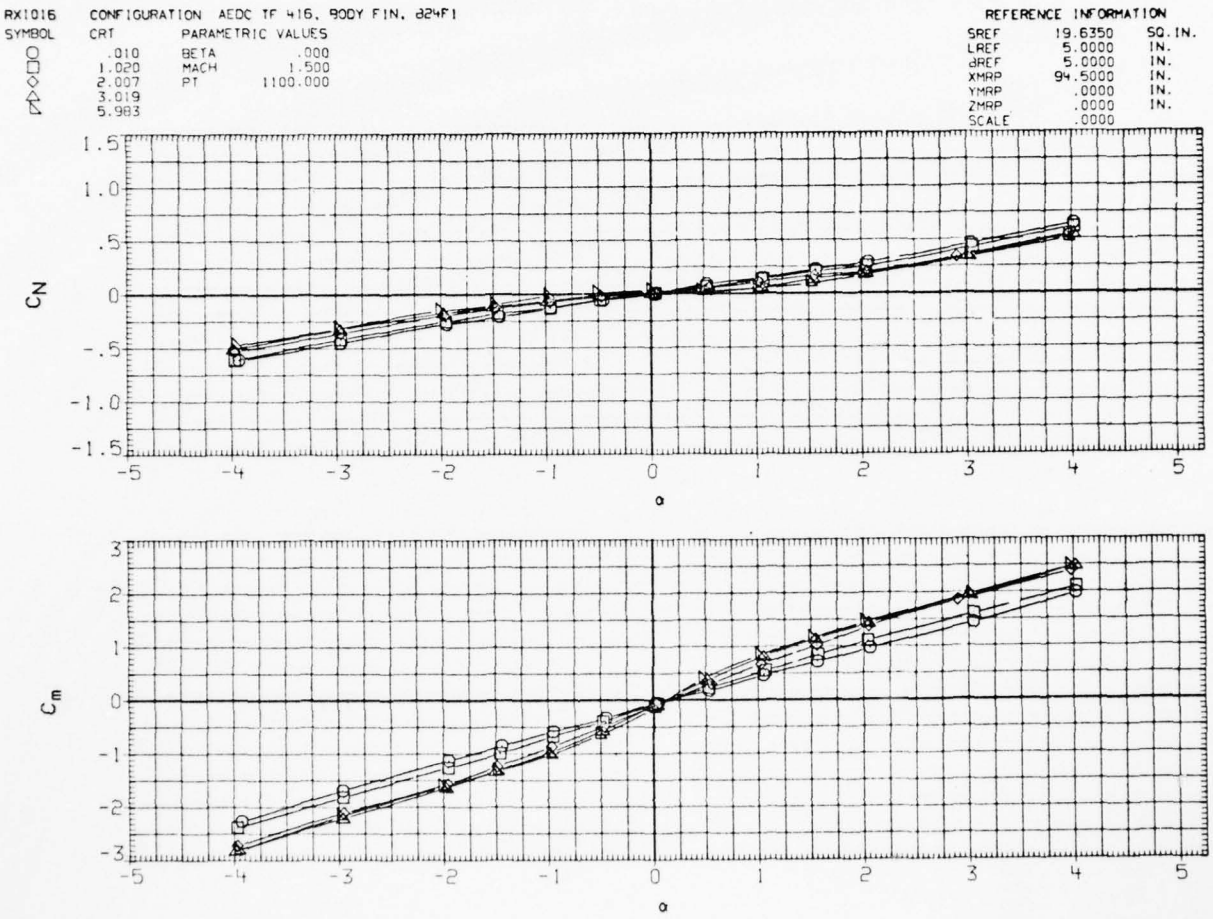

Figure A-17. Thrust effects on stability characteristics for body with fins, B24F1.

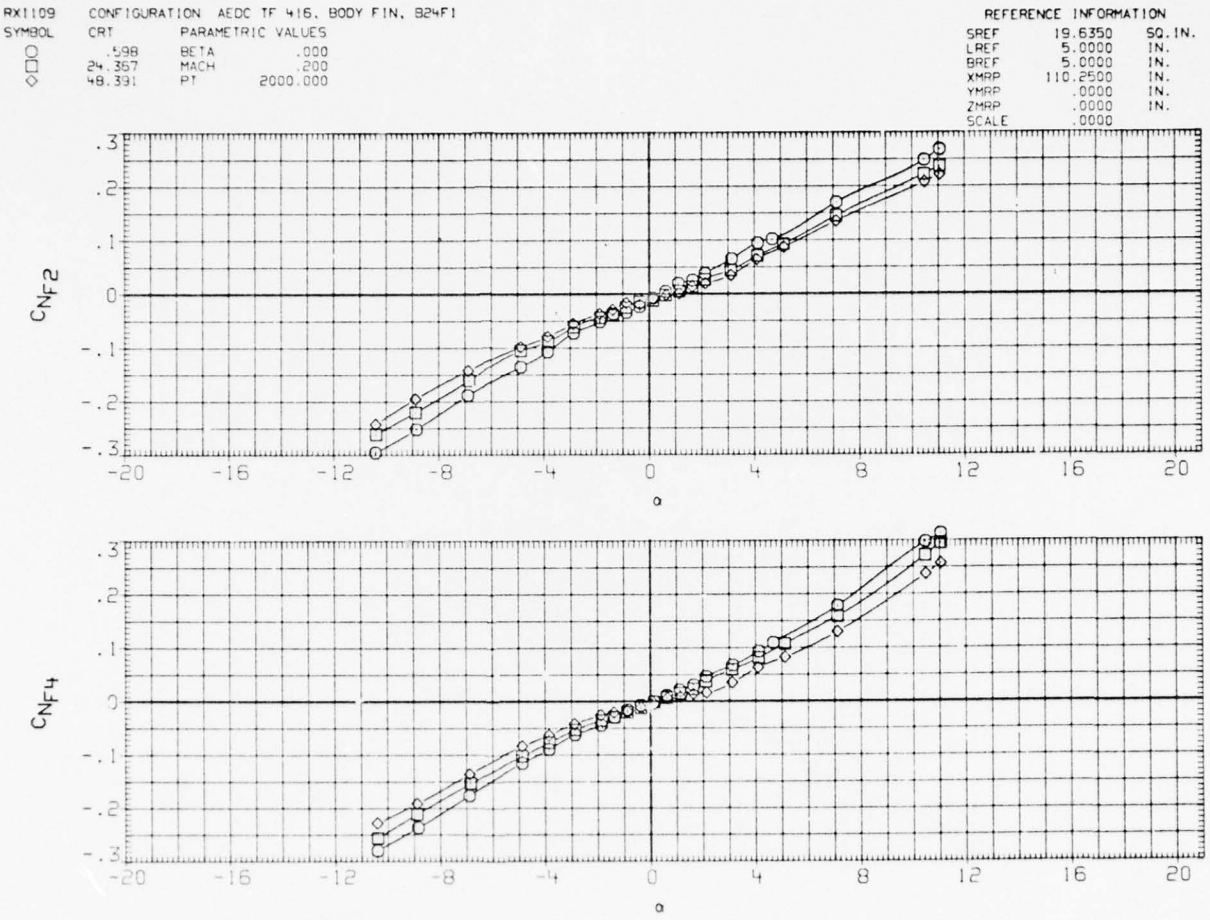

Figure A-18. Thrust effects on fins.

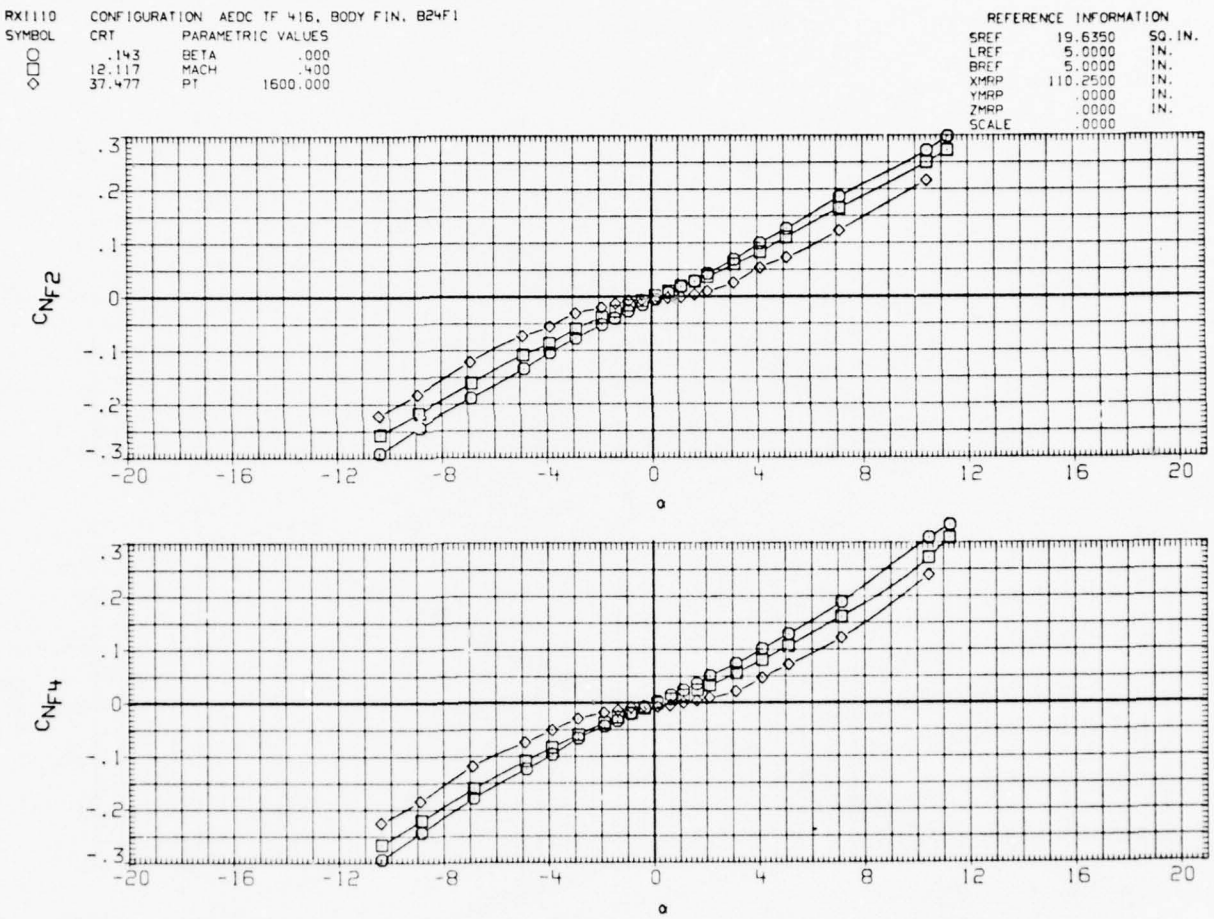

Figure A-19. Thrust effects on fins.

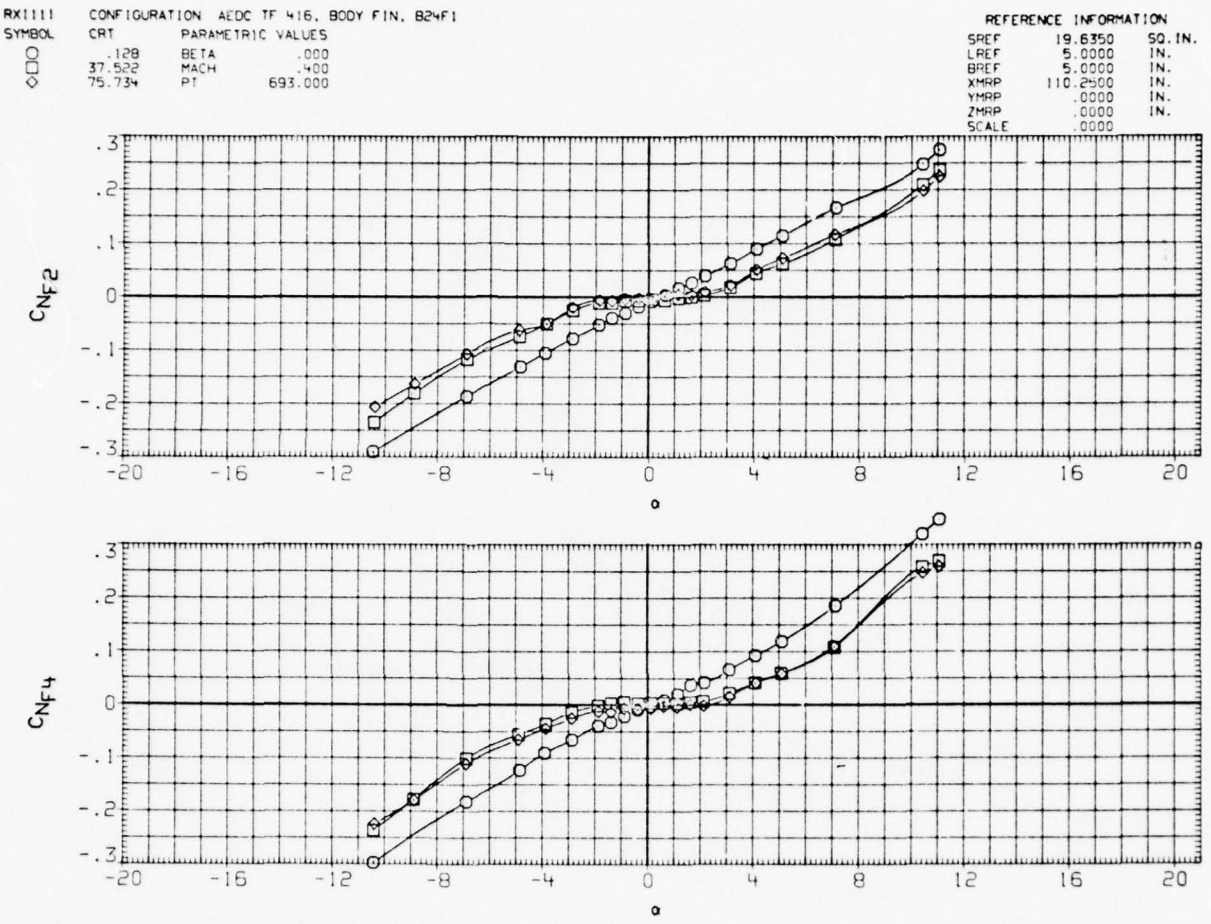

Figure A-20. Thrust effects on fins.

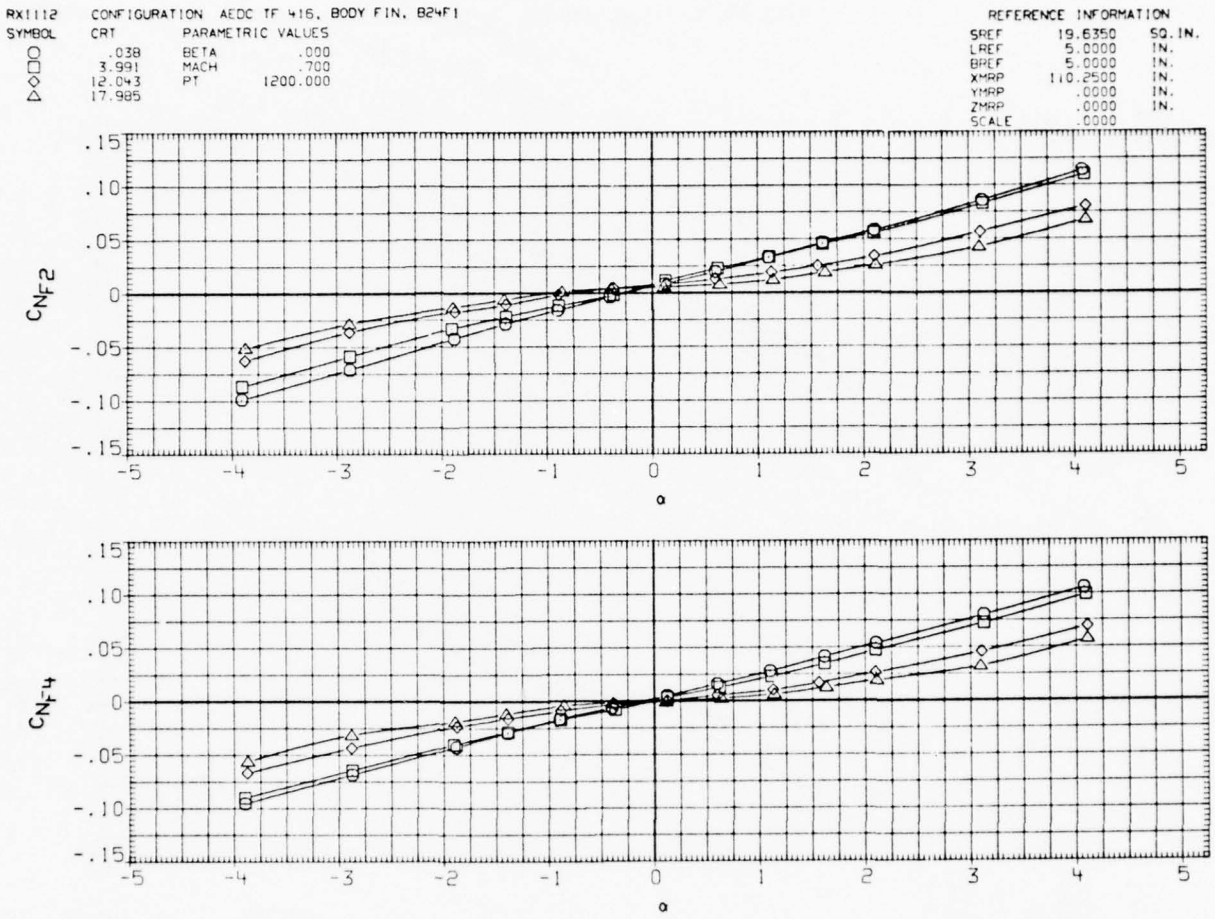

Figure A-21. Thrust effects on fins.

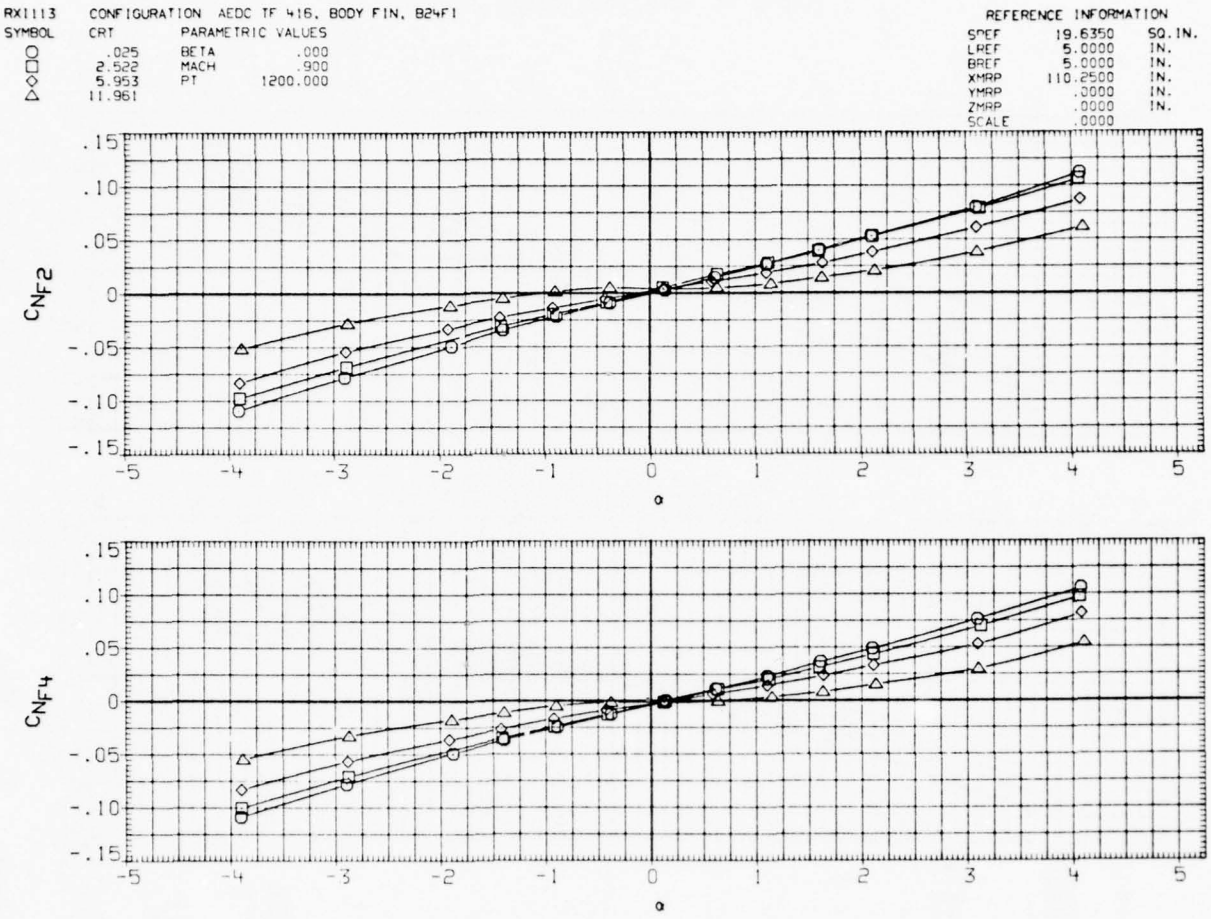

Figure A-22. Thrust effects on fins.

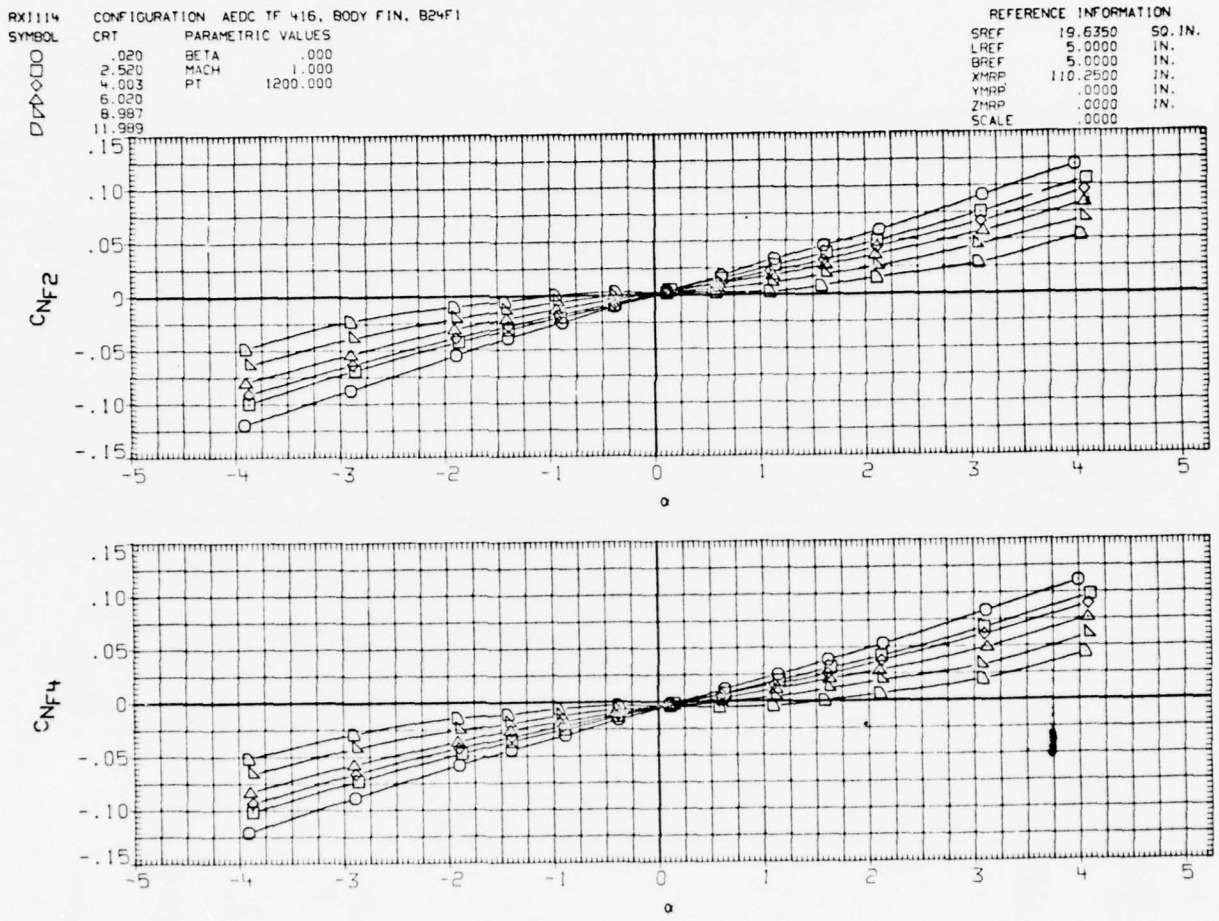

Figure A-23. Thrust effects on fins.

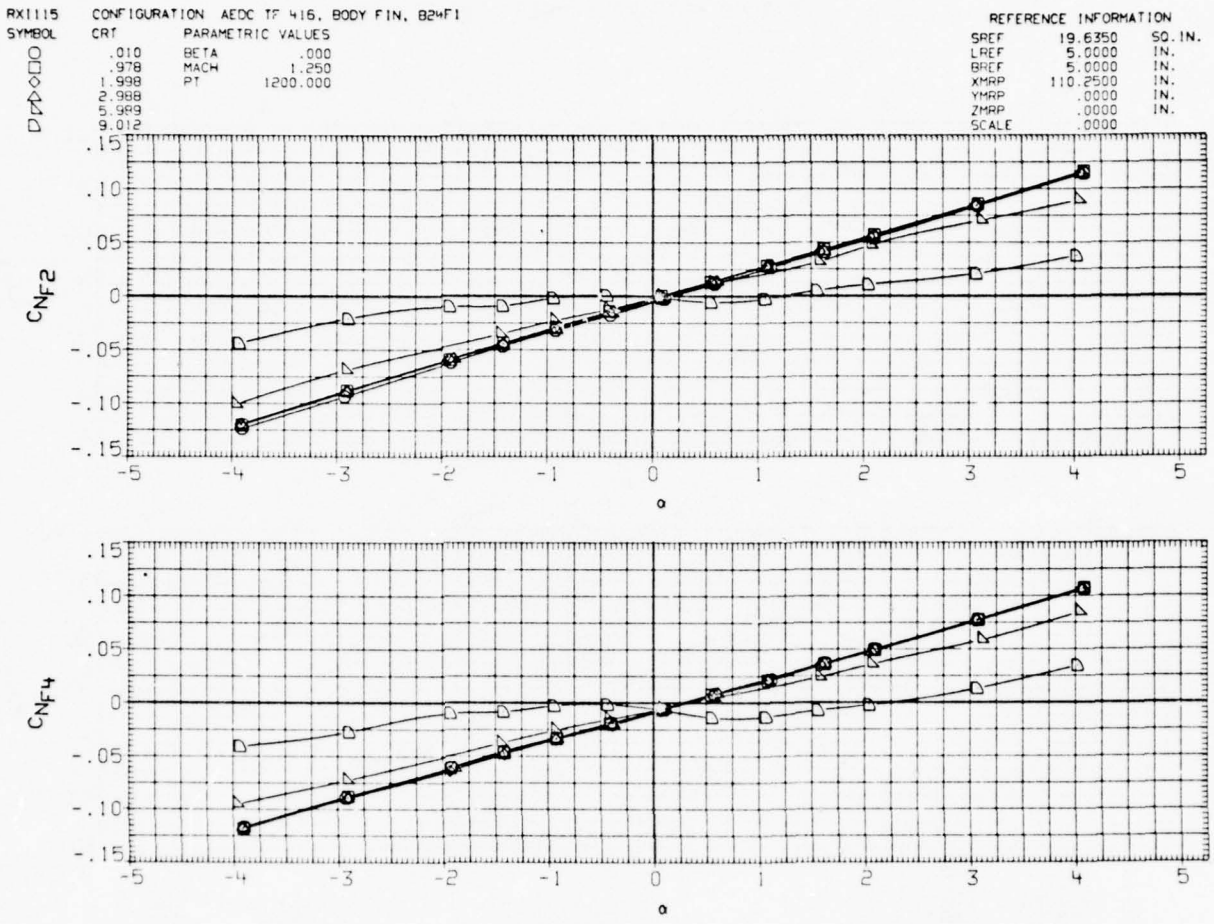

Figure A-24. Thrust effects on fins.

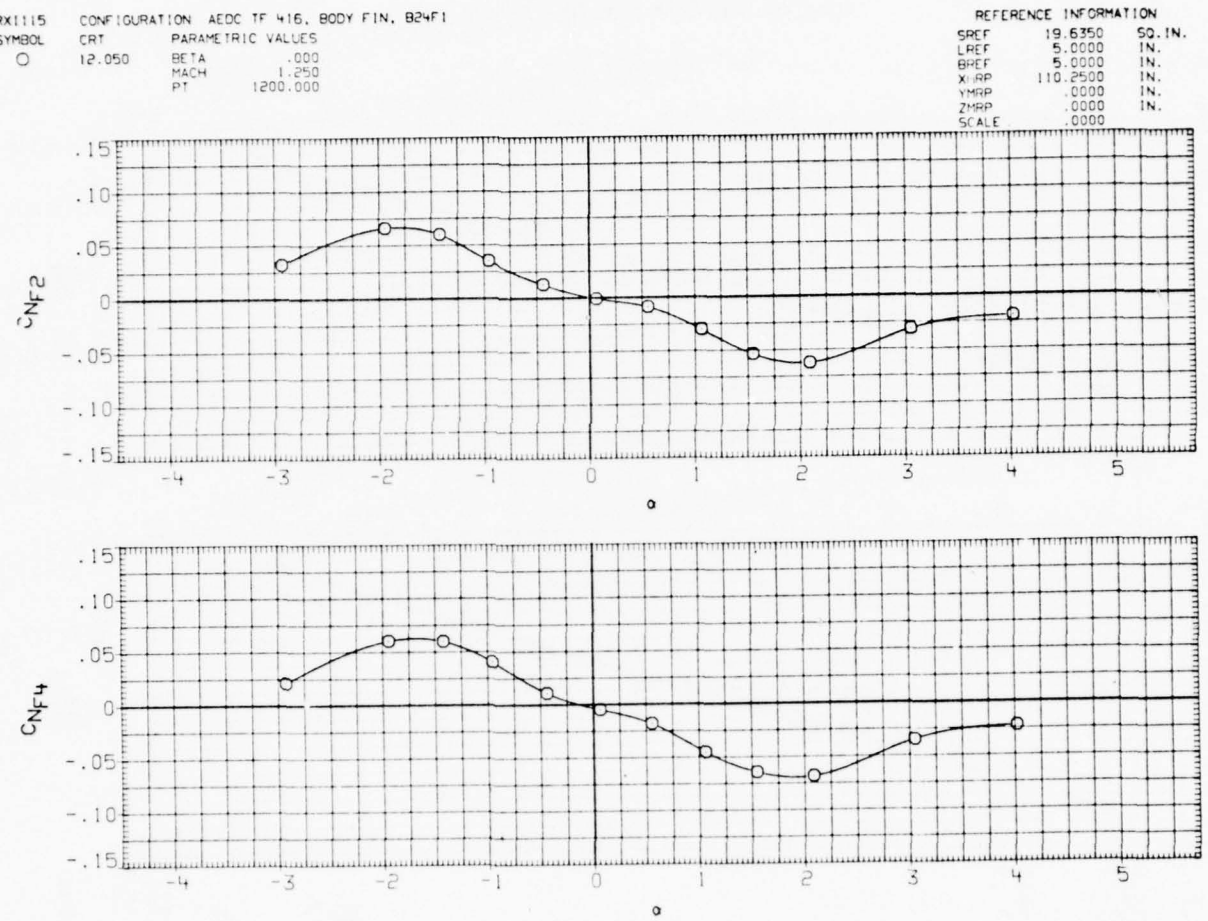

Figure A-25. Thrust effects on fins.

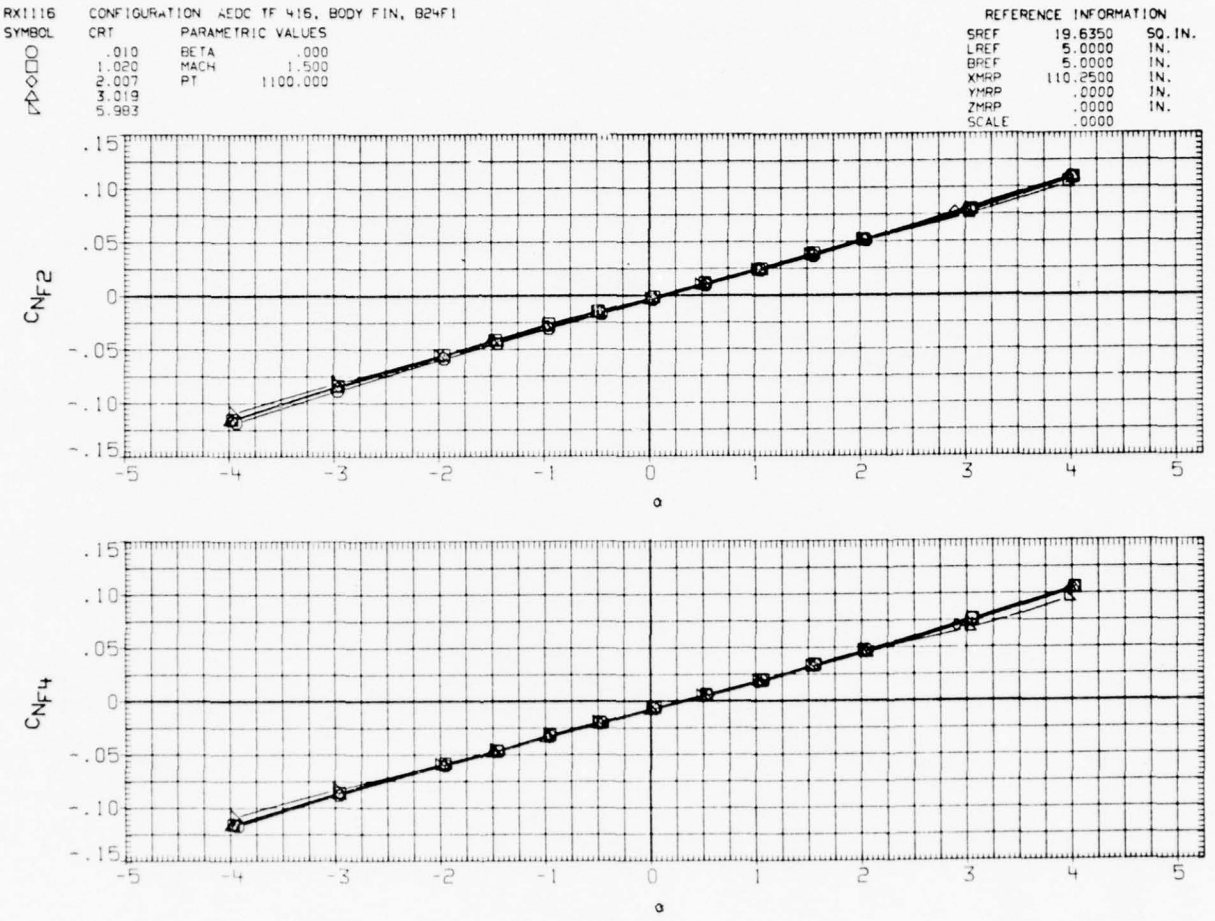

Figure A-26. Thrust effects on fins.

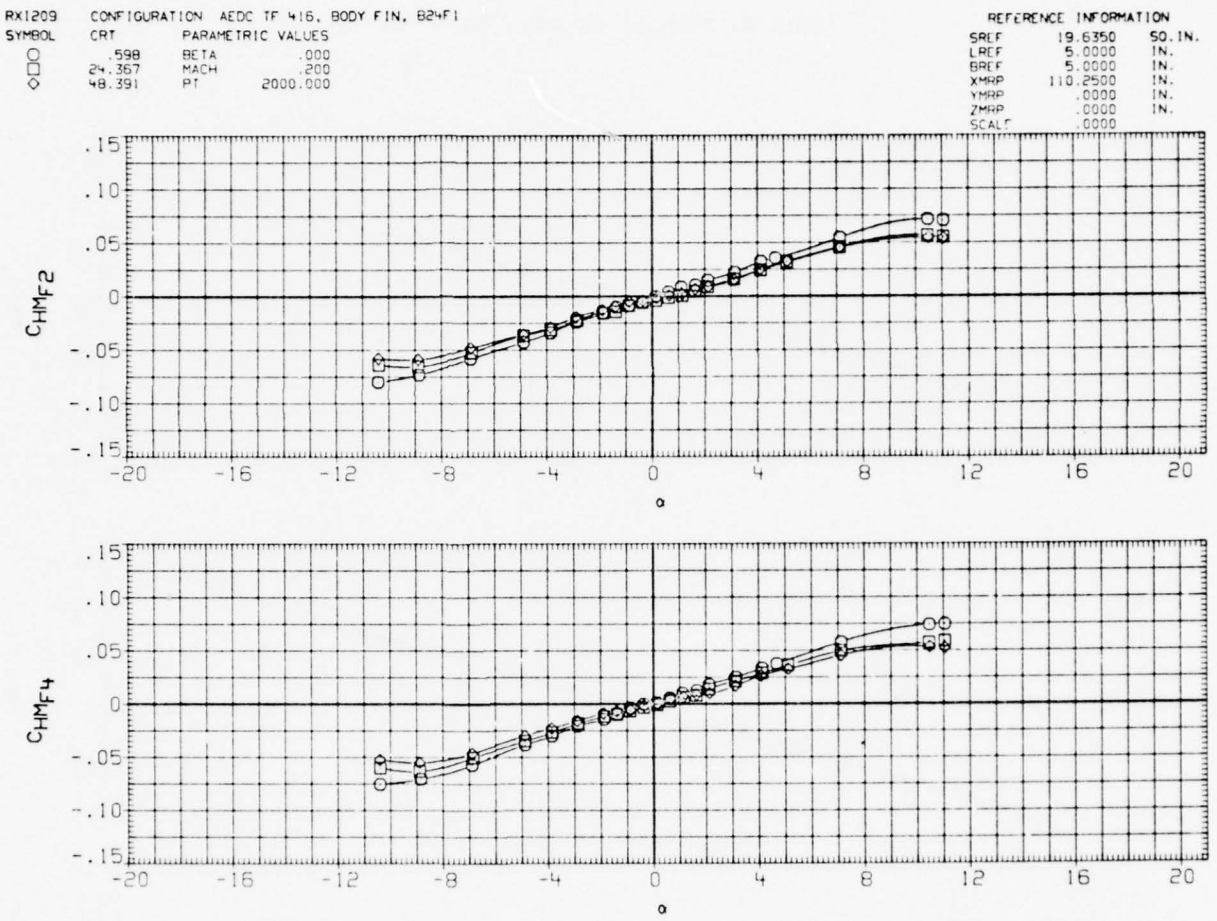

Figure A-27. Thrust effects on fins.

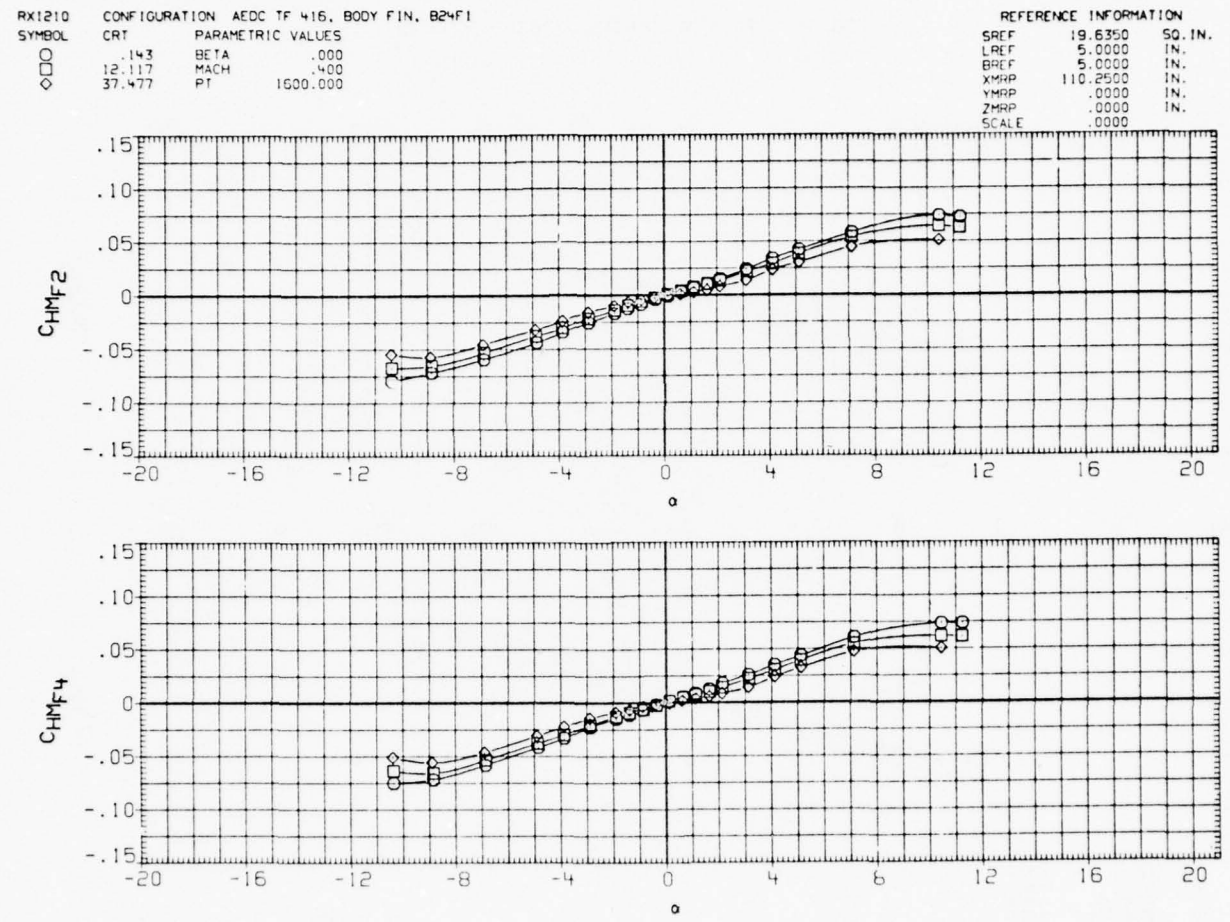

Figure A-28. Thrust effects on fins.

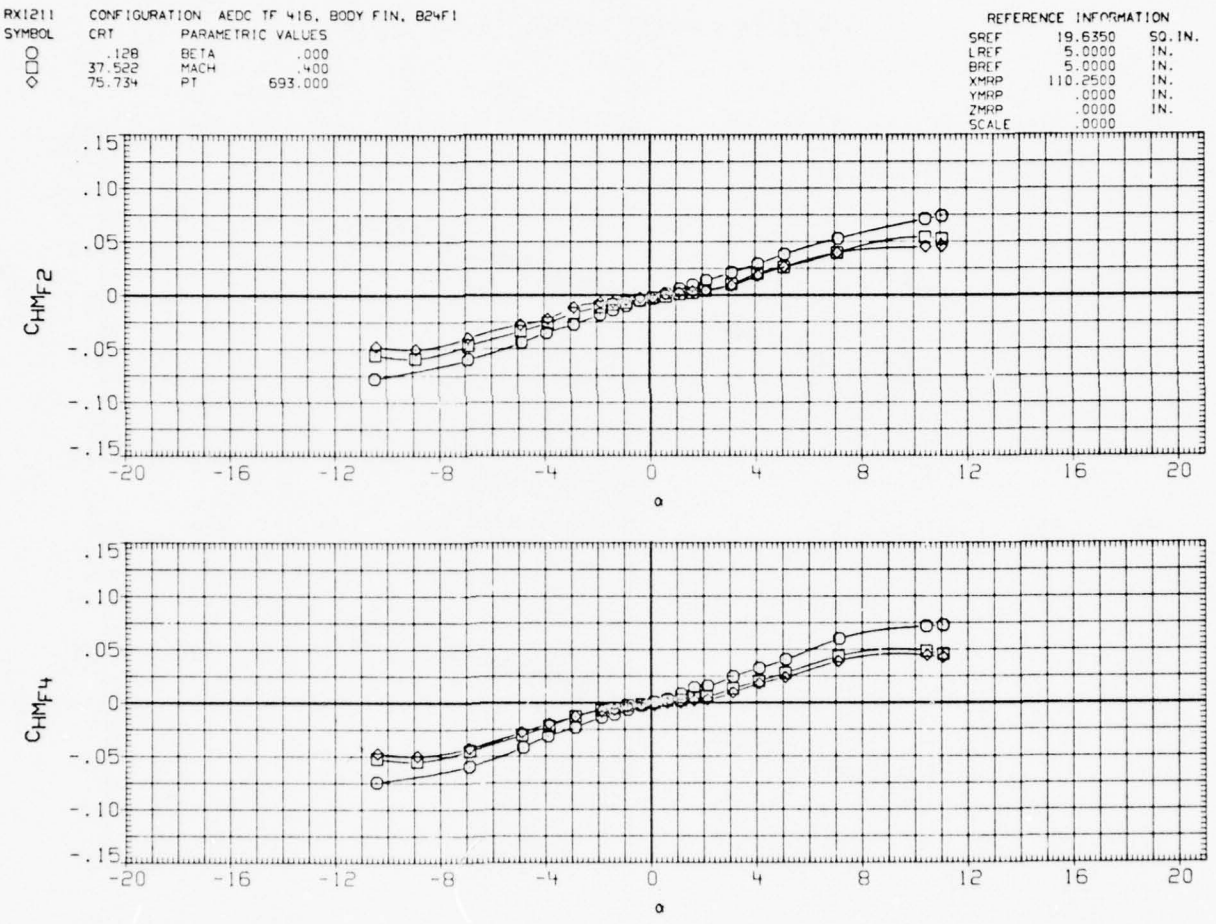

Figure A-29. Thrust effects on fins.

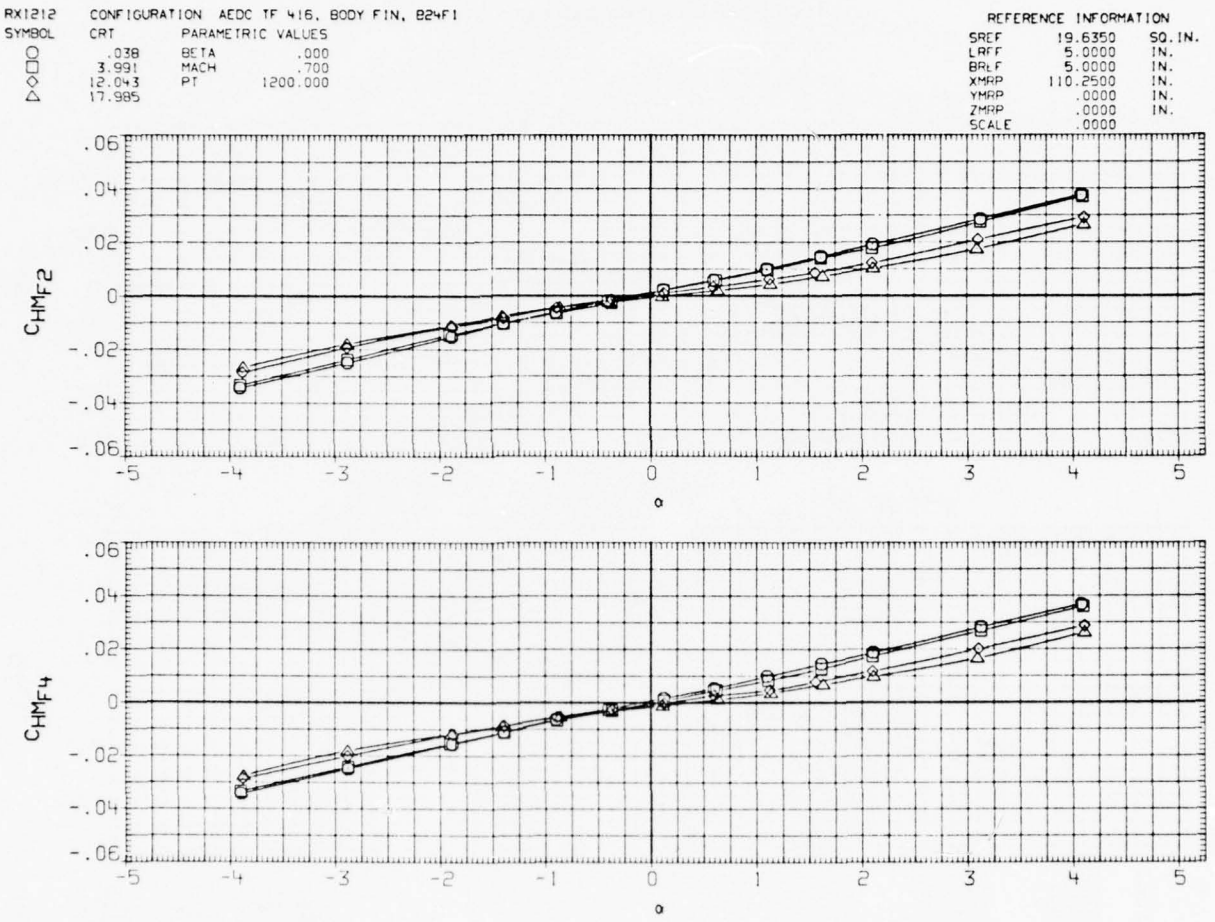

Figure A-30. Thrust effects on fins.

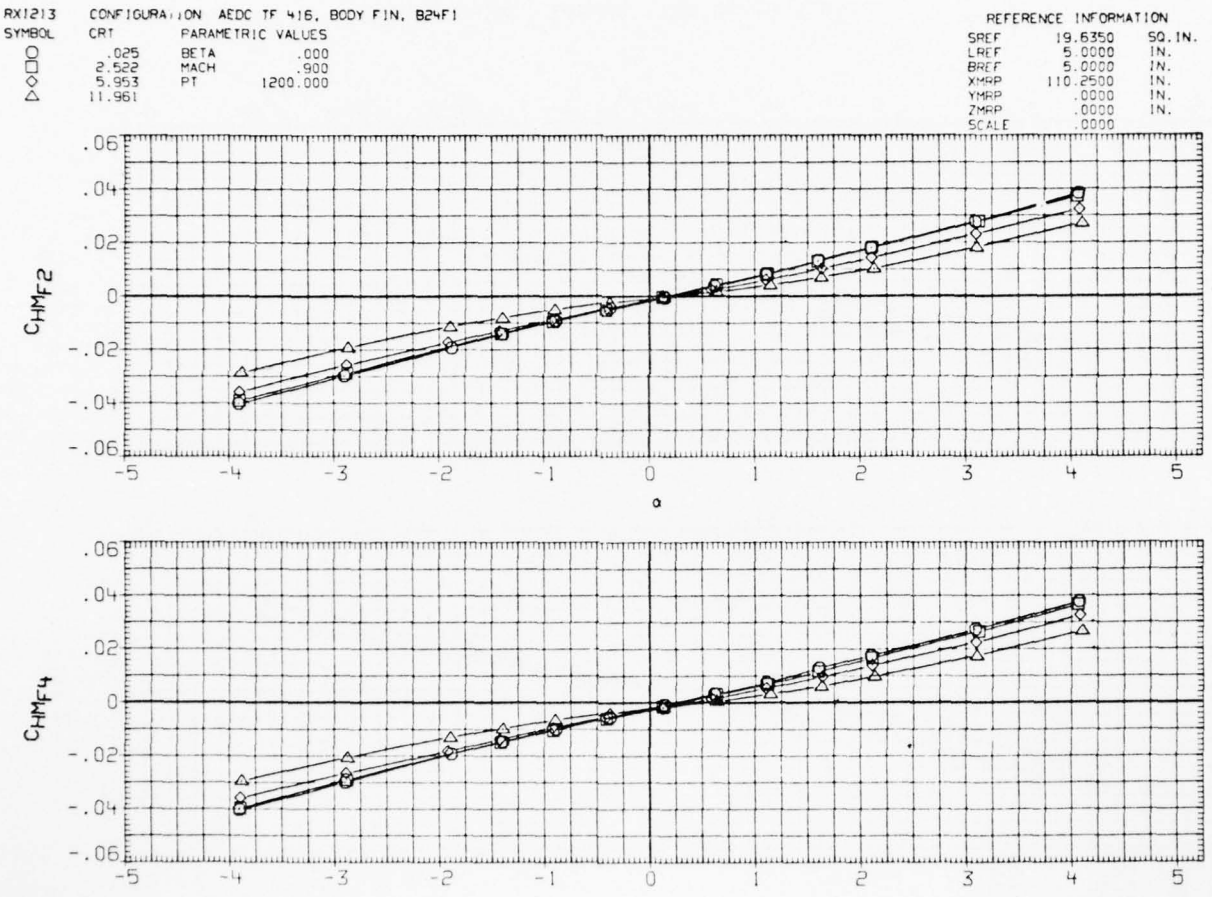

Figure A-31. Thrust effects on fins.

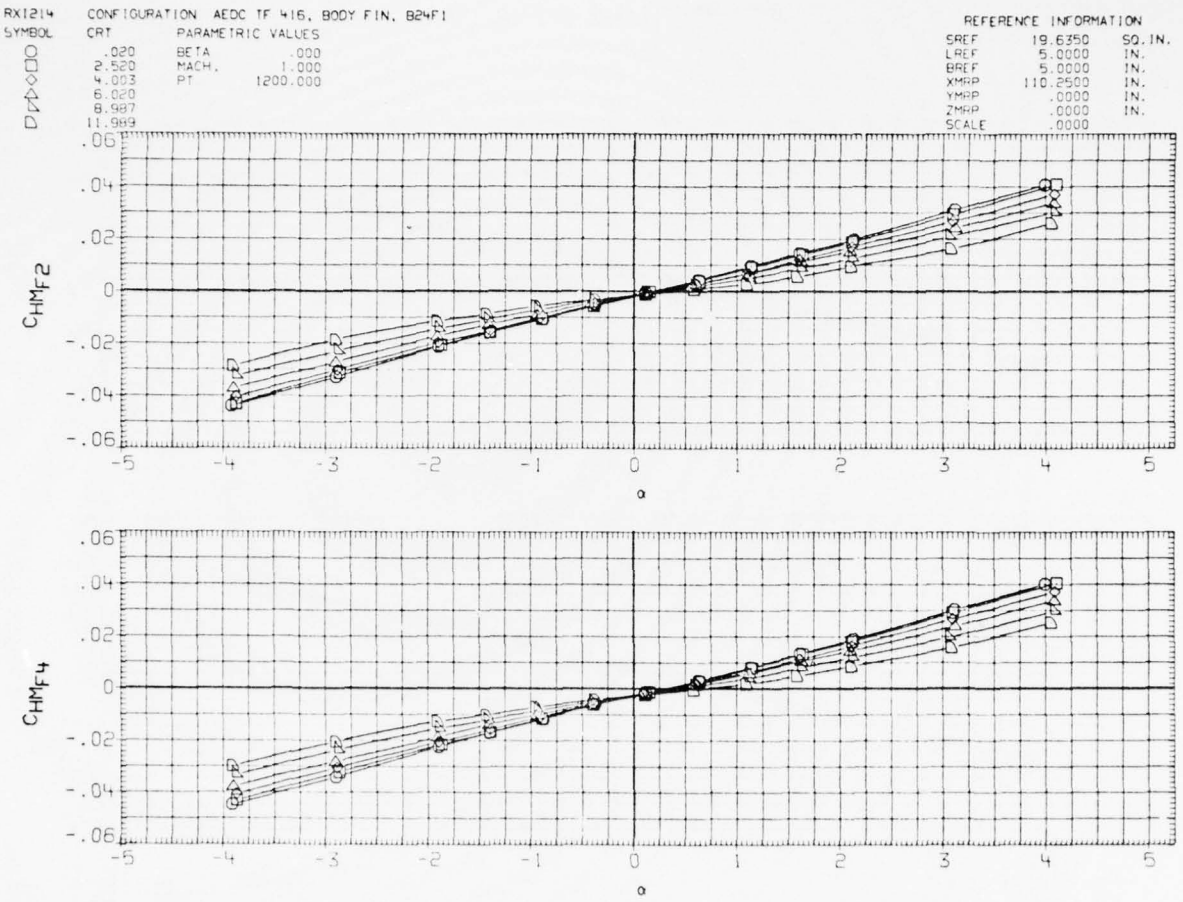

Figure A-32. Thrust effects on fins.

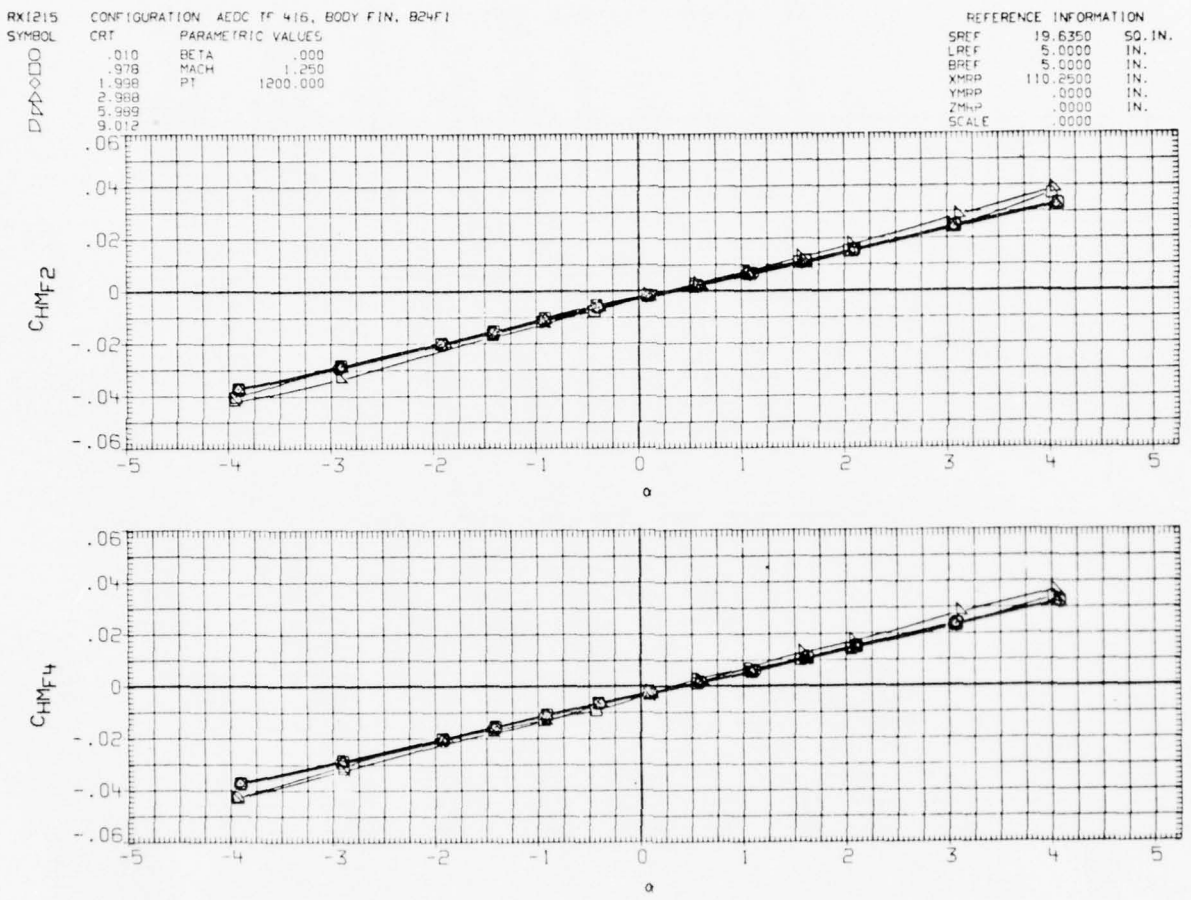

Figure A-33. Thrust effects on fins.

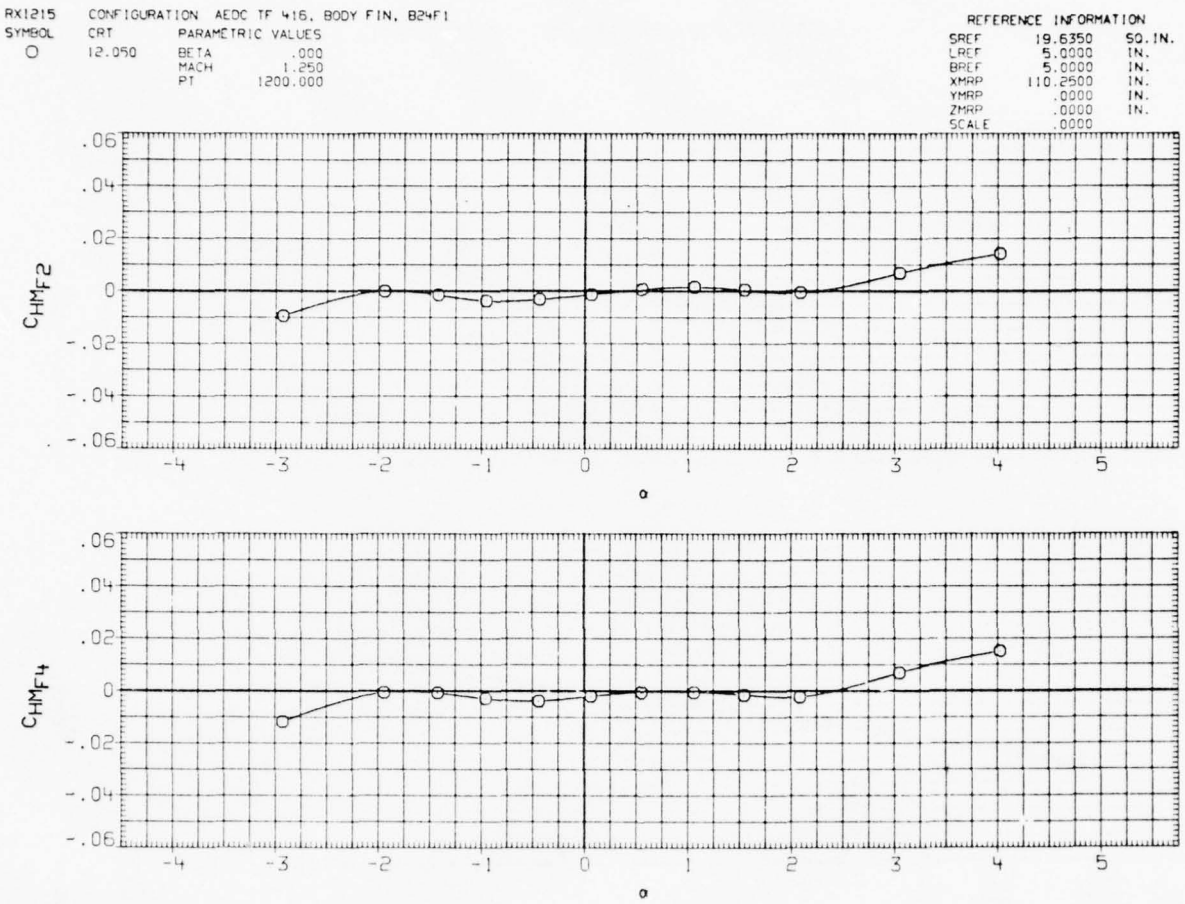

Figure A-34. Thrust effects on fins.

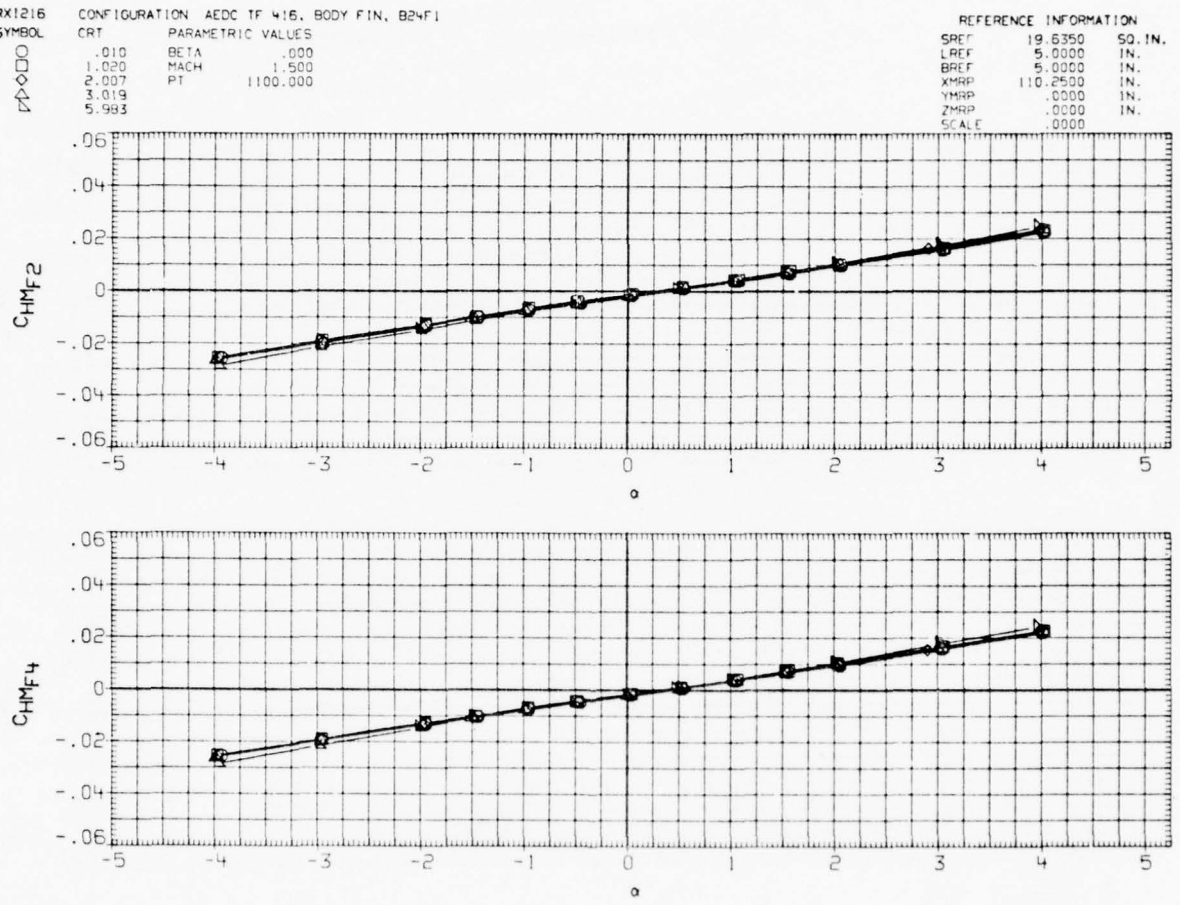

Figure A-35. Thrust effects on fins.

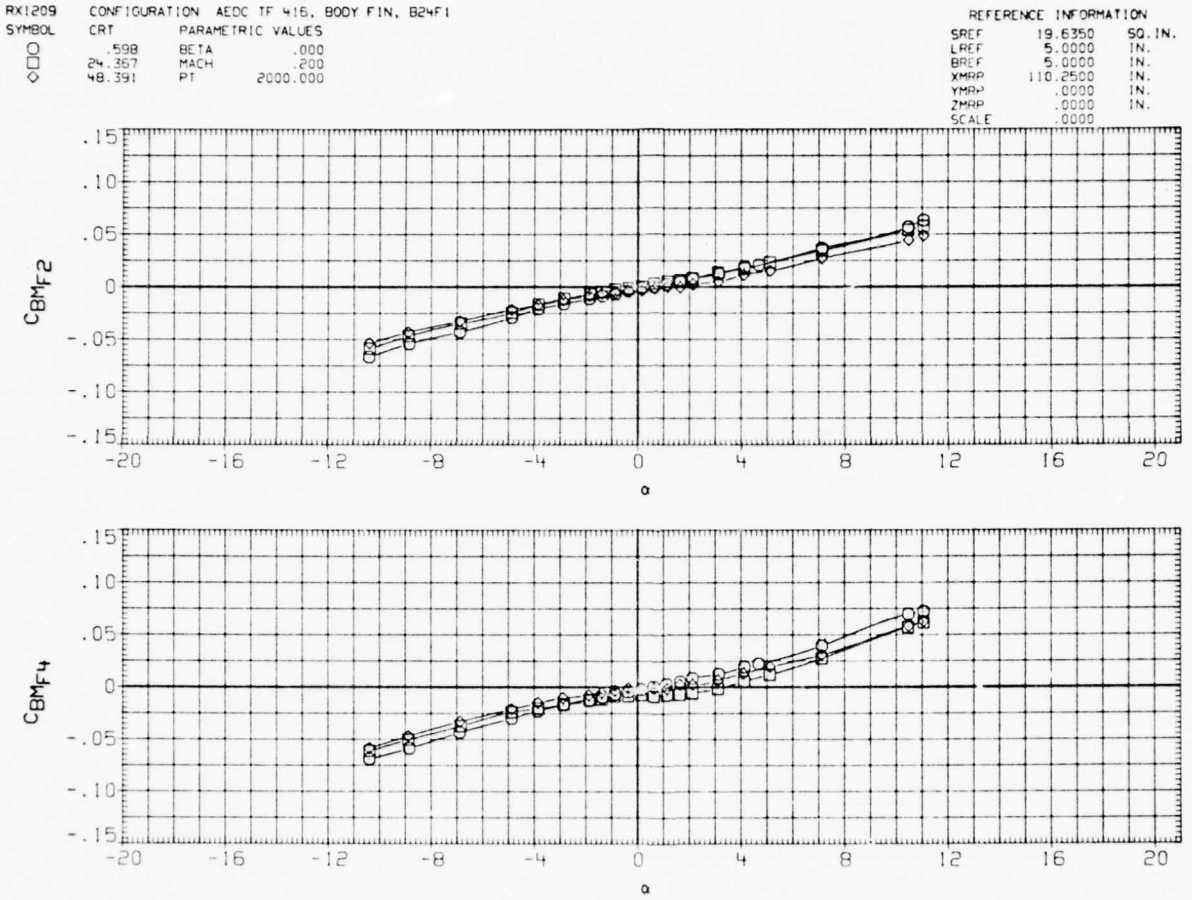

Figure A-36. Thrust effects on fins.

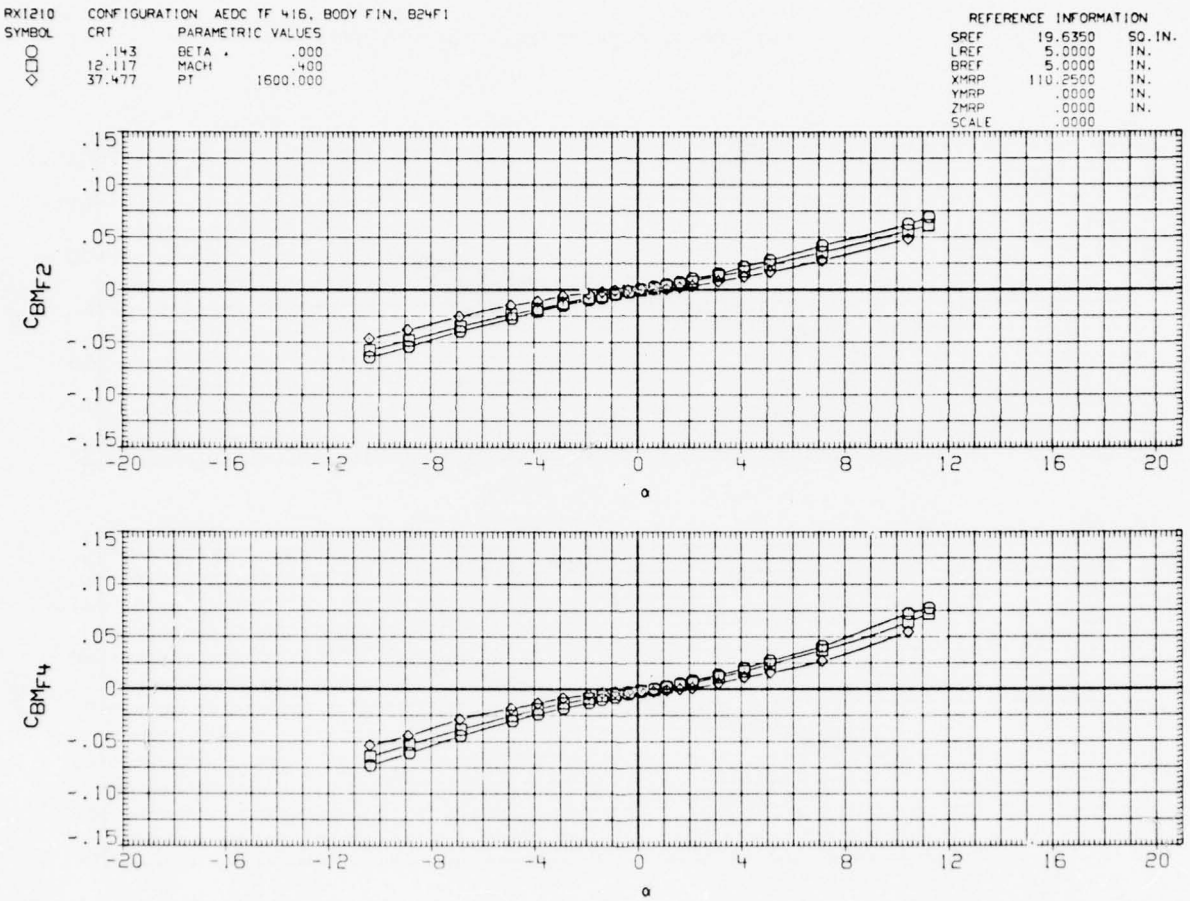

Figure A-37. Thrust effects on fins.

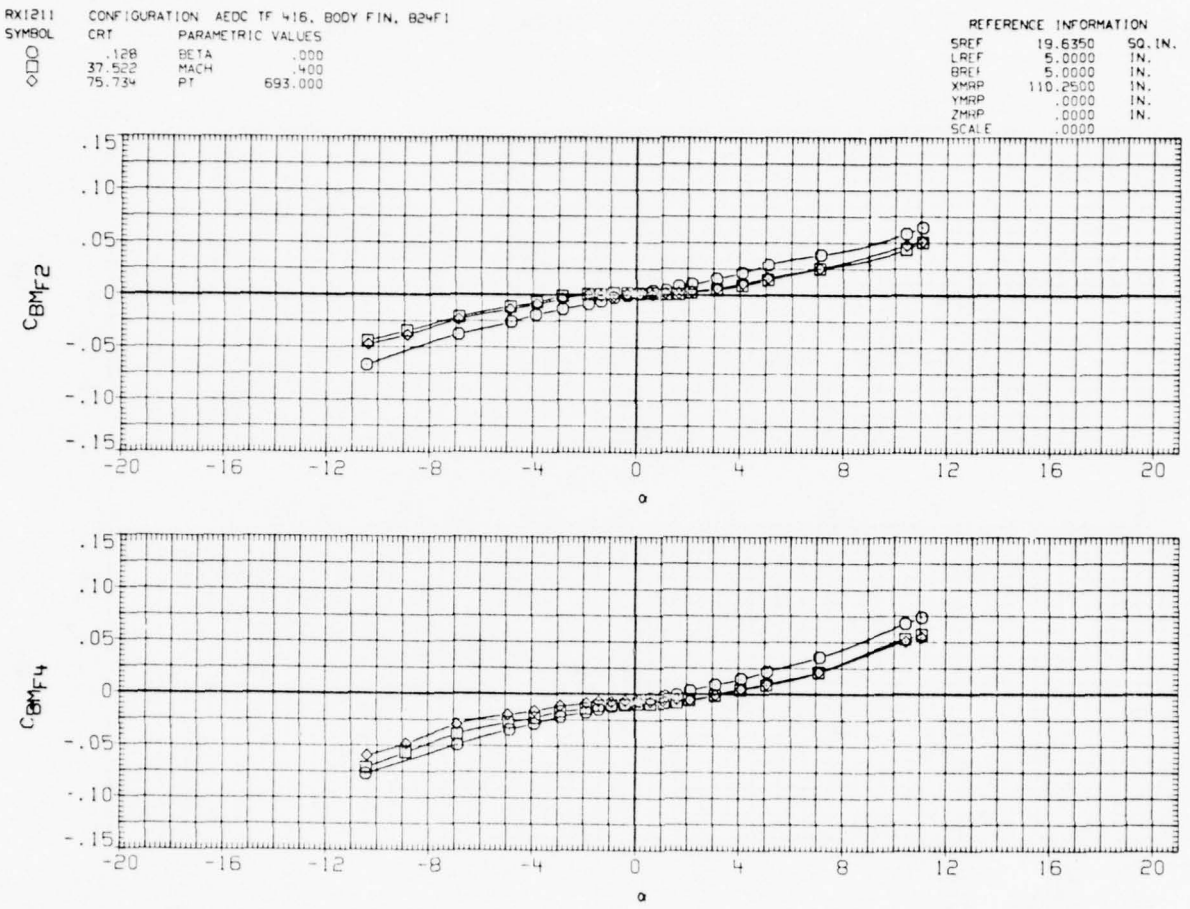

Figure A-38. Thrust effects on fins.

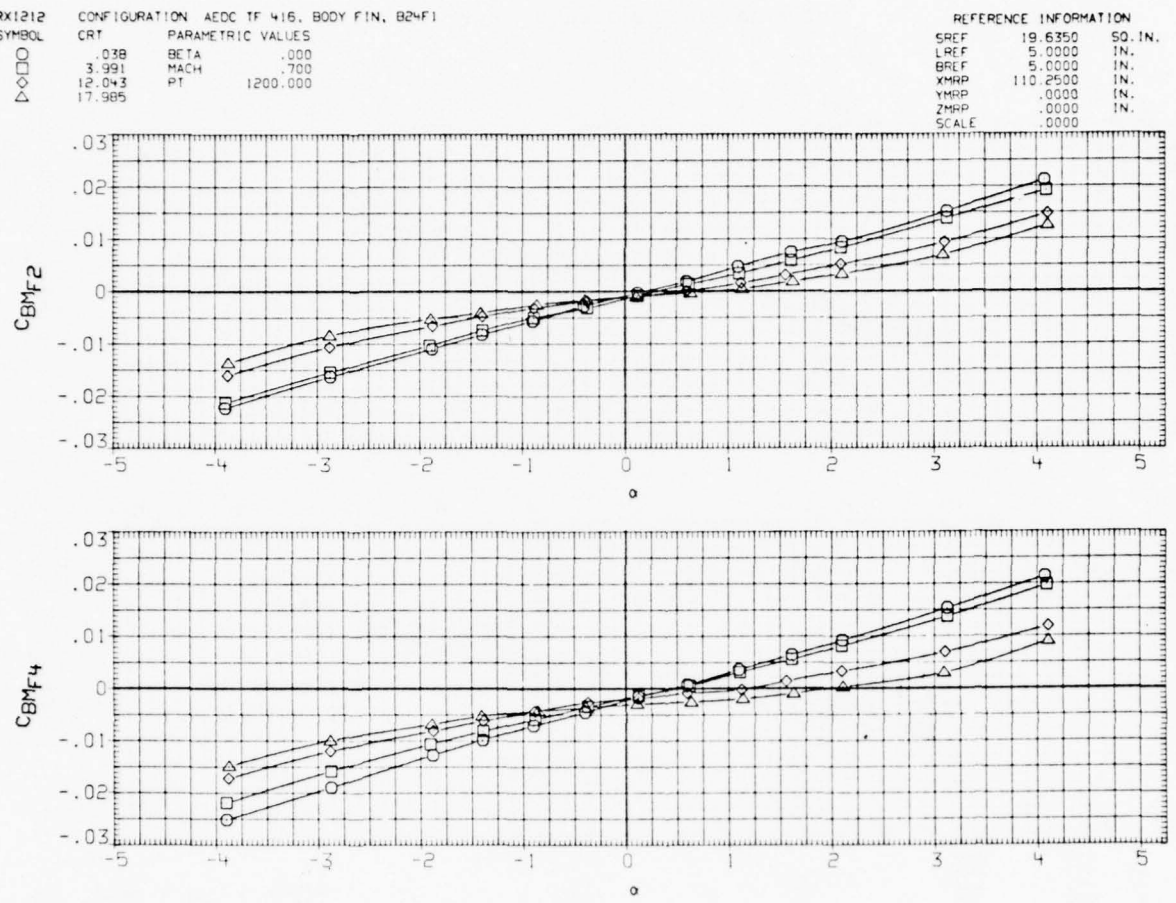

Figure A-39. Thrust effects on fins.

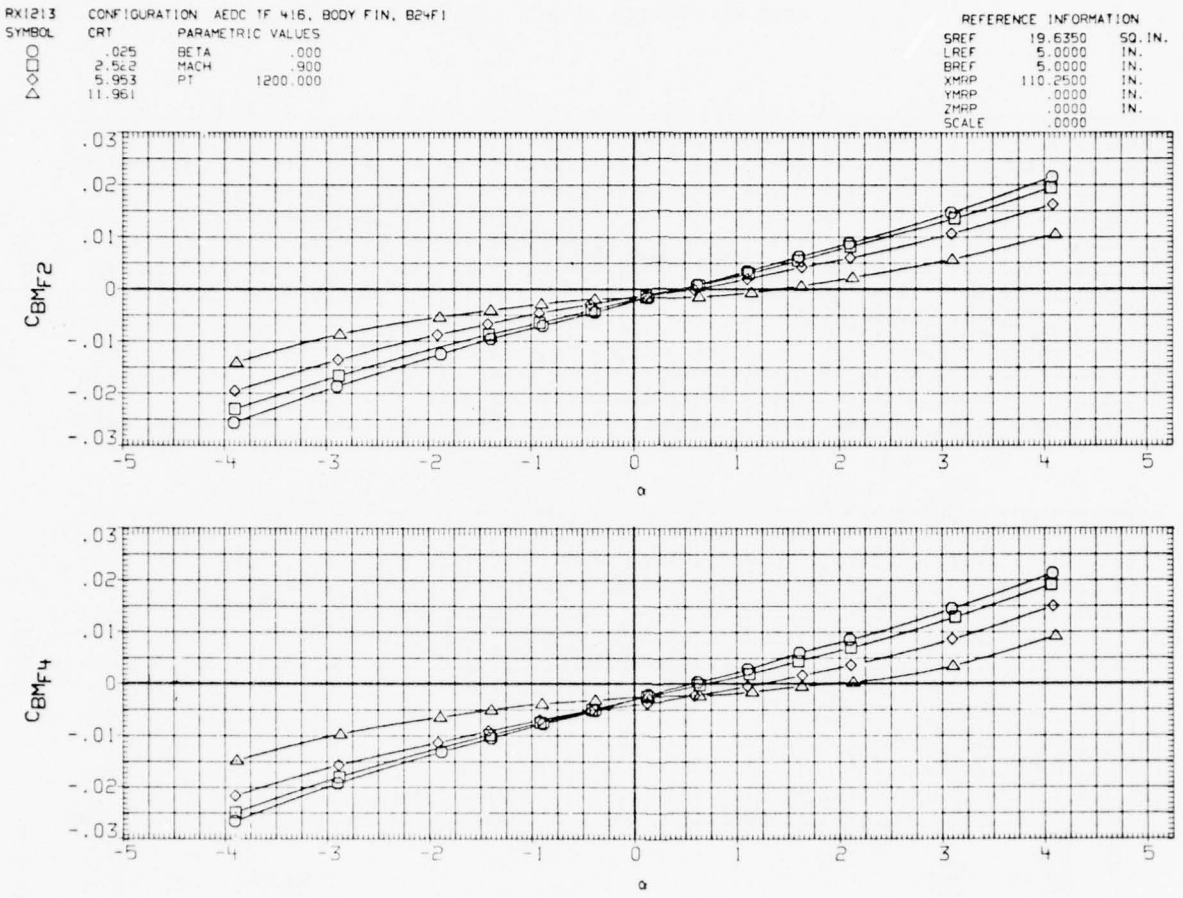

Figure A-40. Thrust effects on fins.

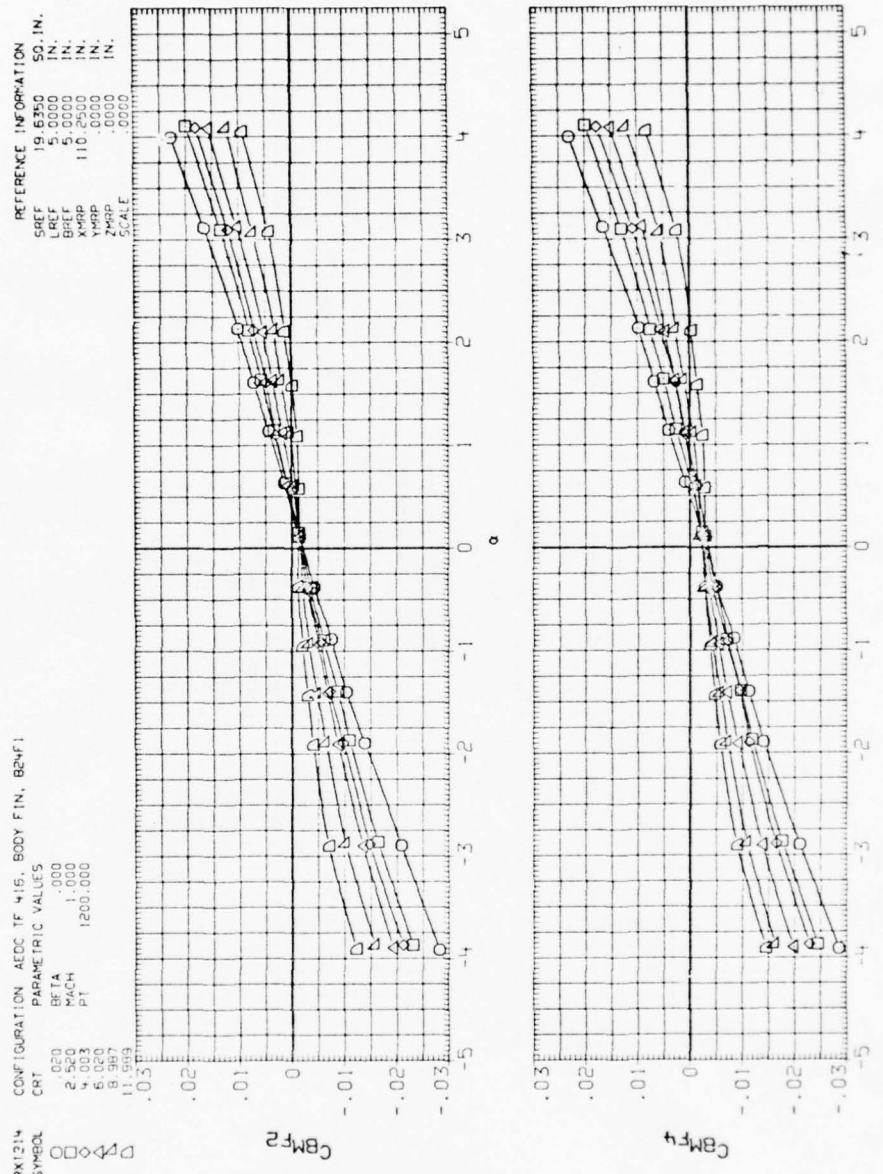

Figure A-41. Thrust effects on fins.

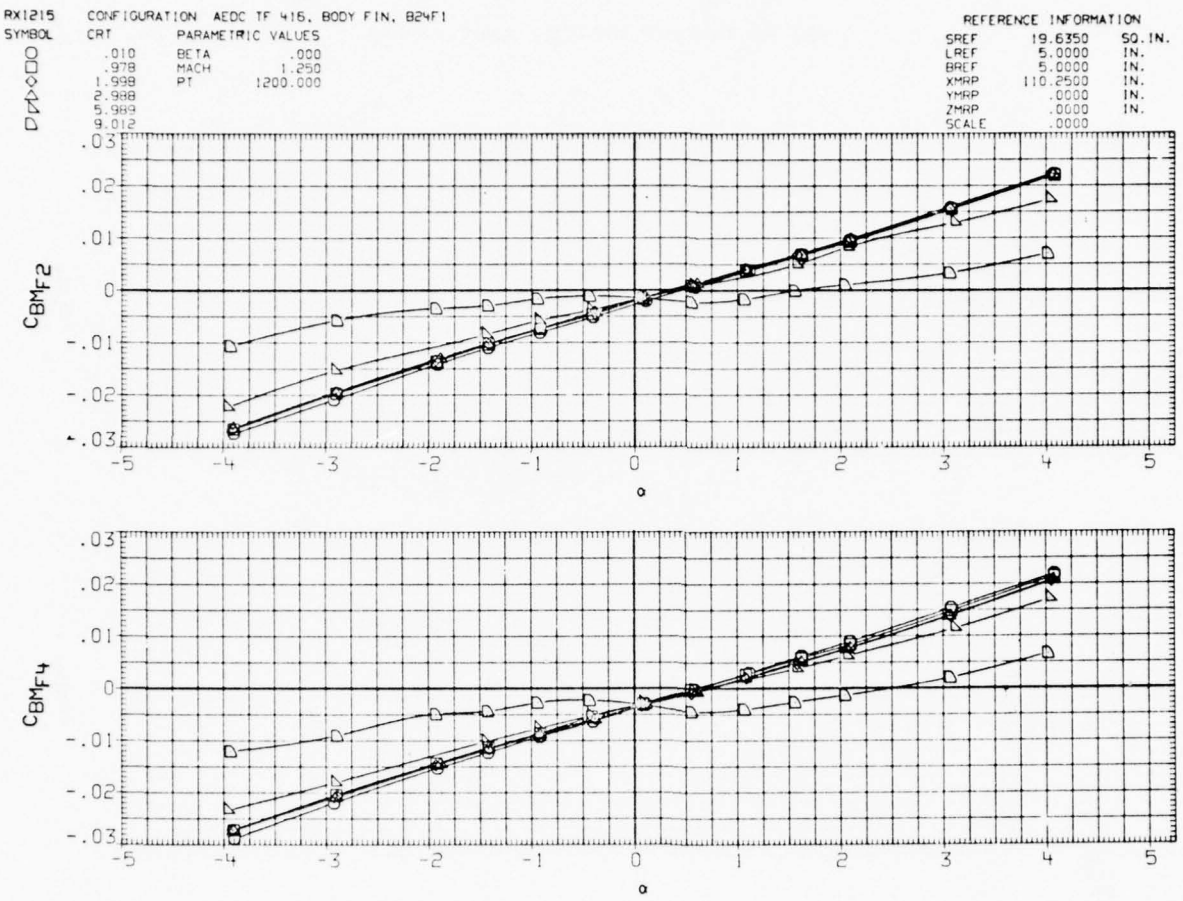

Figure A-42. Thrust effects on fins.

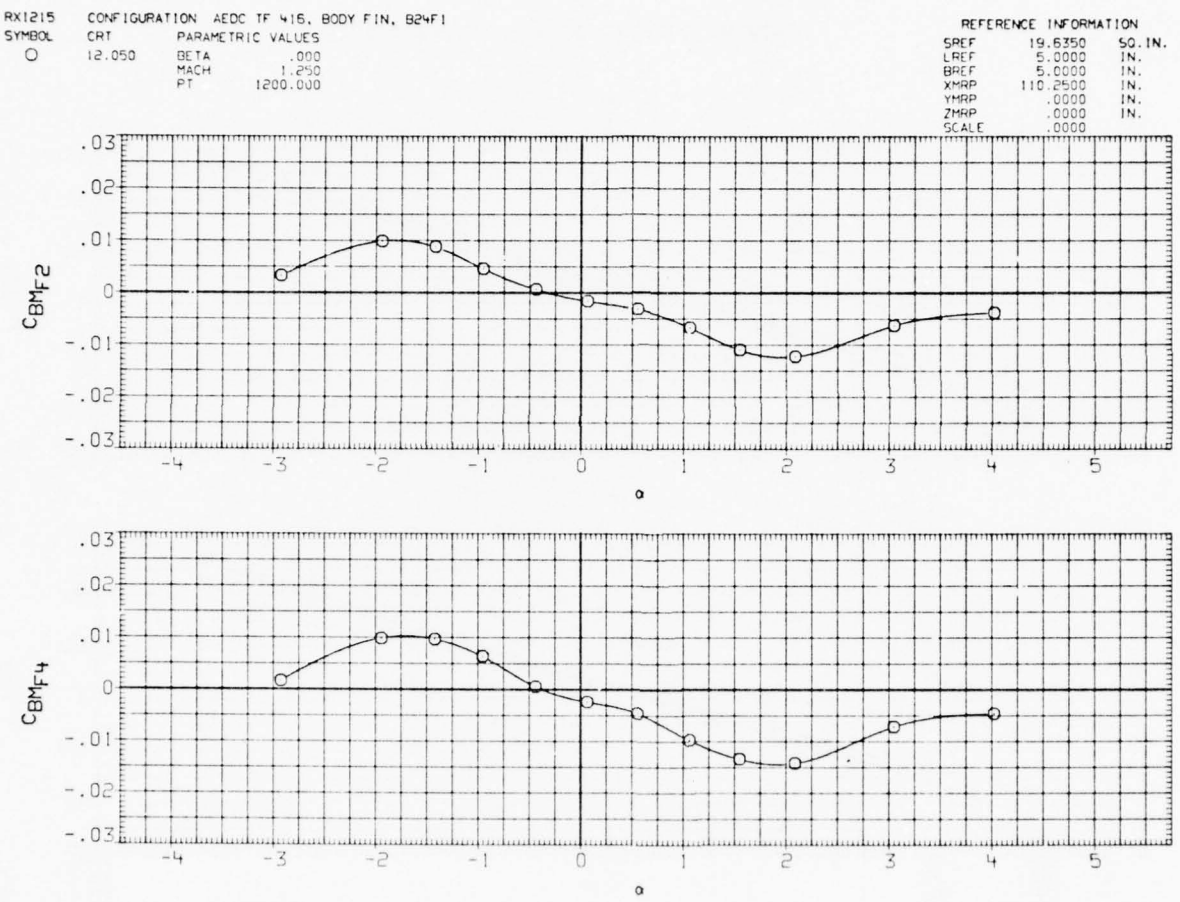

Figure A-43. Thrust effects on fins.

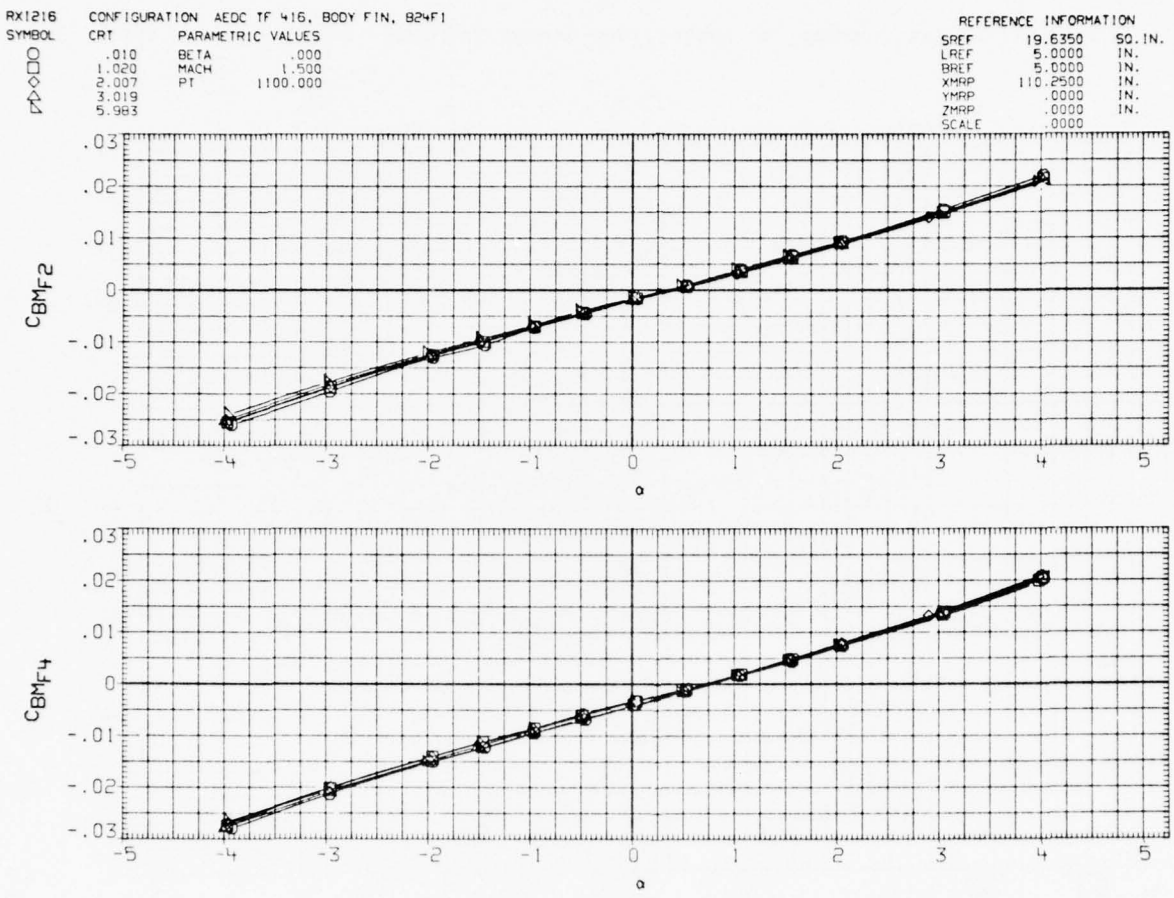

Figure A-44. Thrust effects on fins.

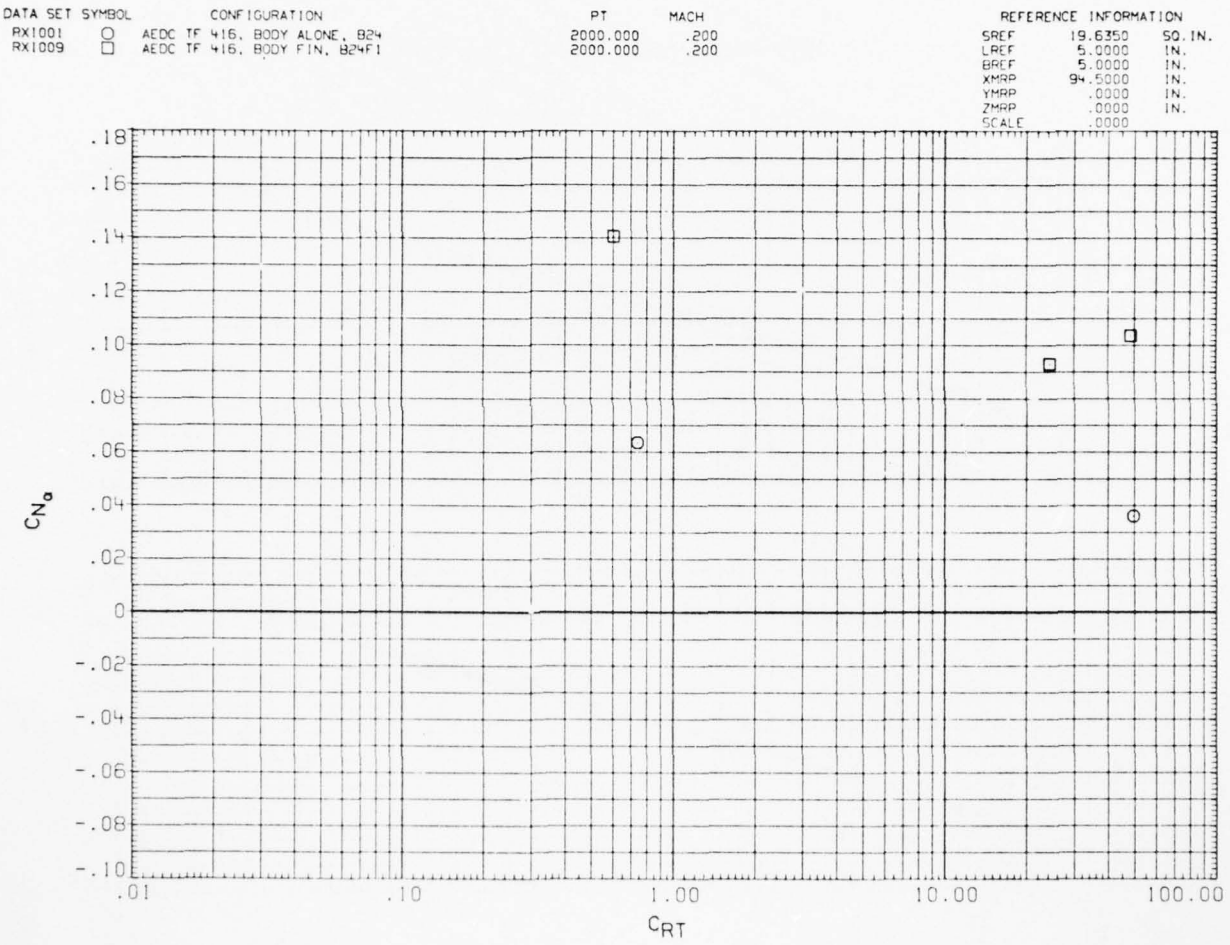

Figure A-45. Effect of radial thrust coefficient on longitudinal derivatives.

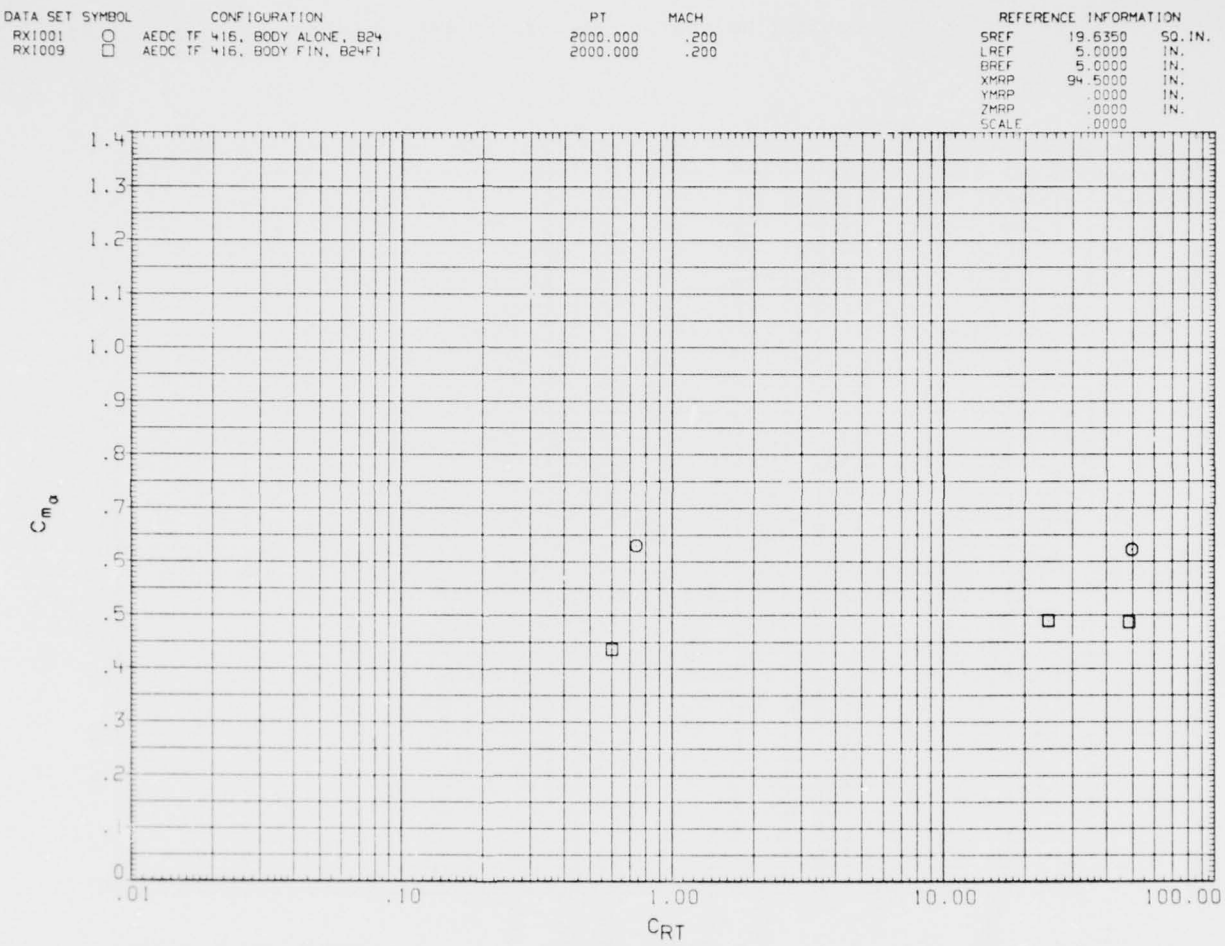

Figure A-46. Effect of radial thrust coefficient on longitudinal derivatives.

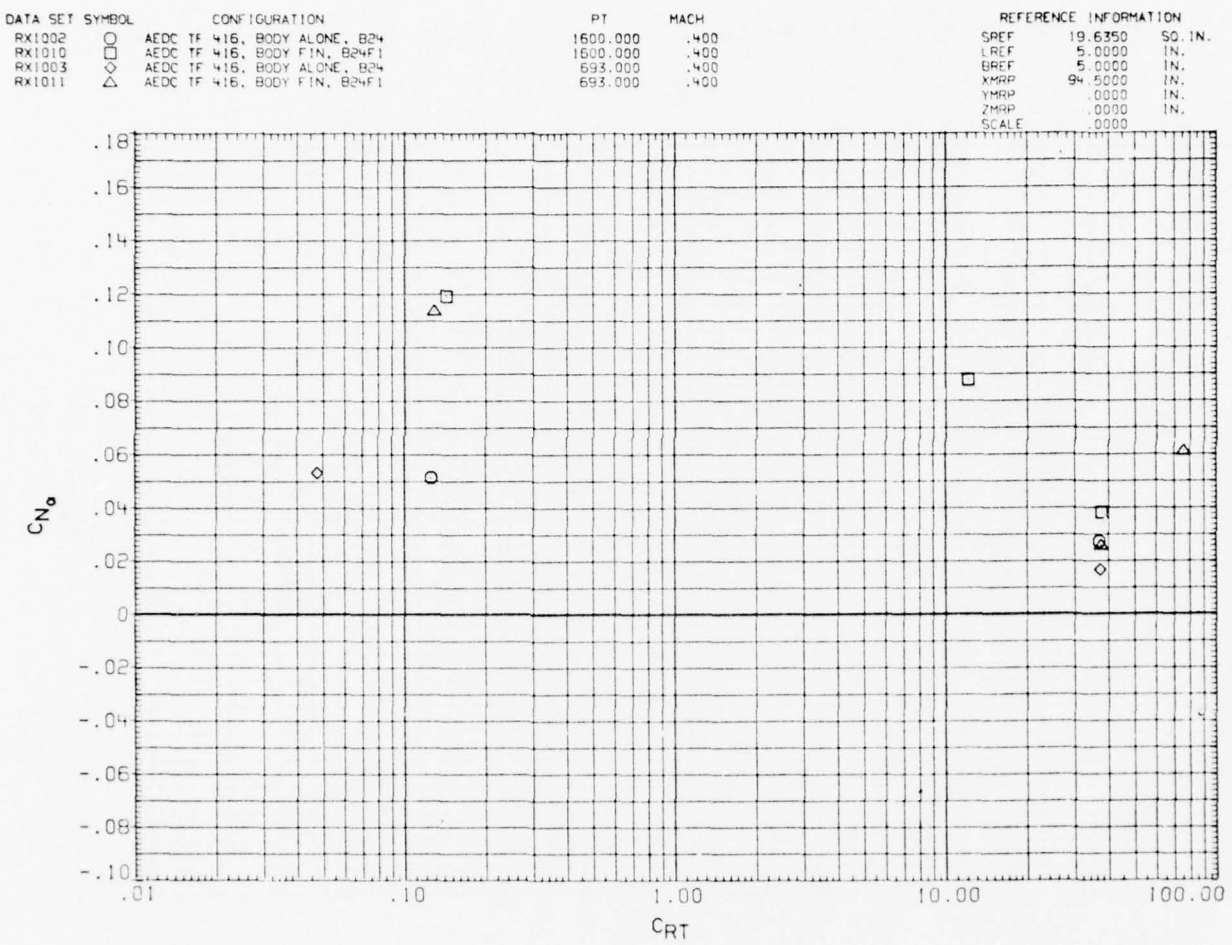

Figure A-47. Effect of radial thrust coefficient on longitudinal derivatives.

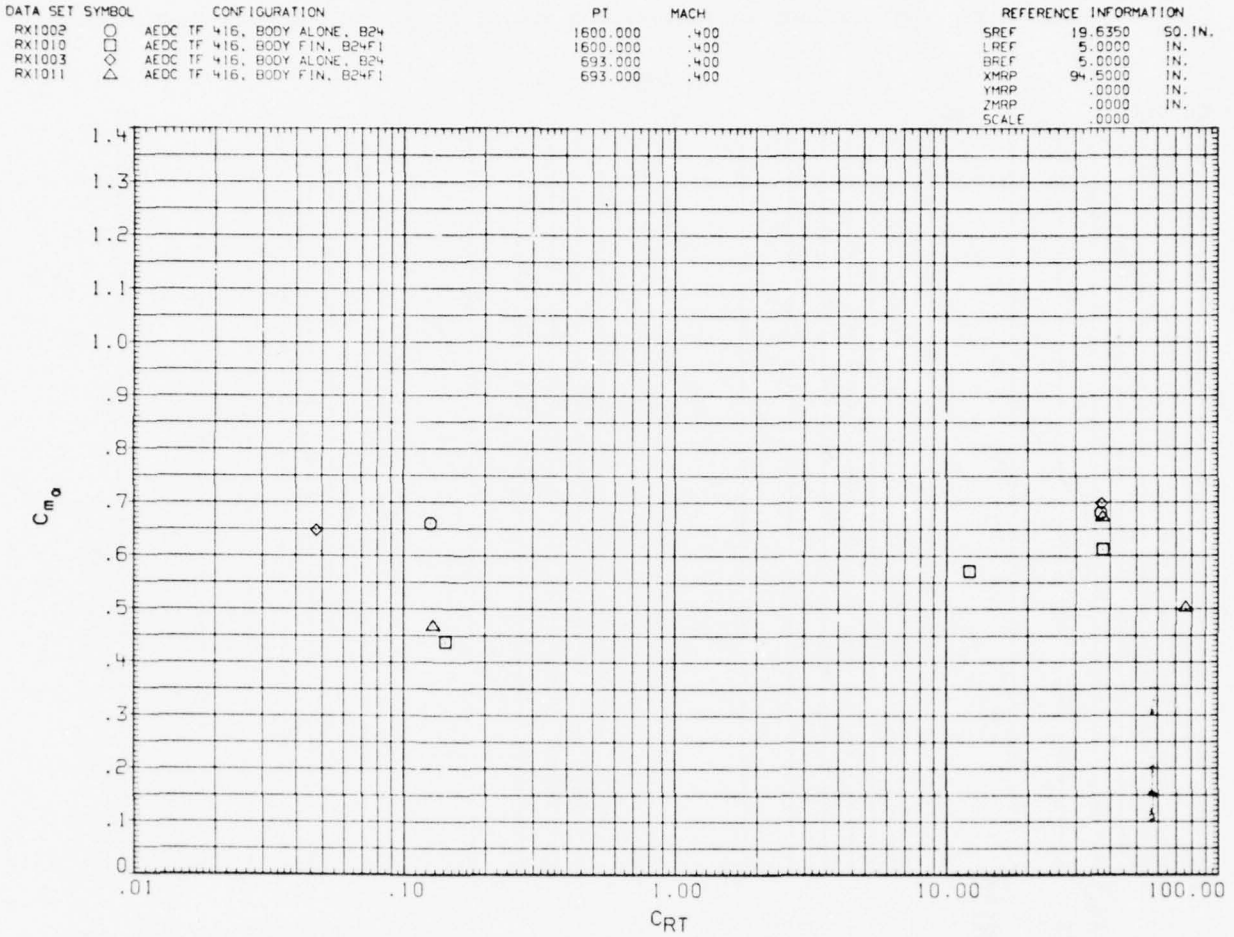

Figure A-48. Effect of radial thrust coefficient on longitudinal derivatives.

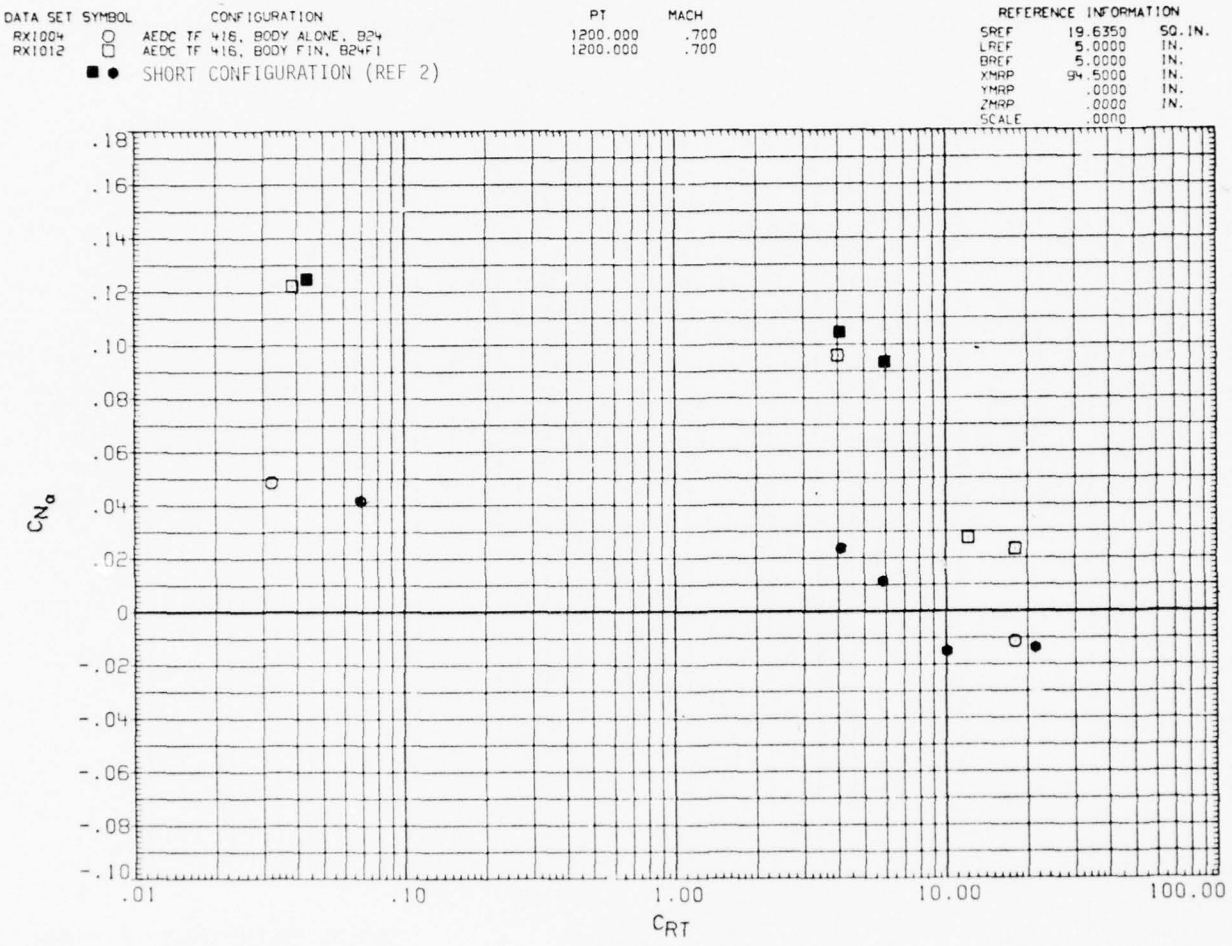

Figure A-49. Effect of radial thrust coefficient on longitudinal derivatives.

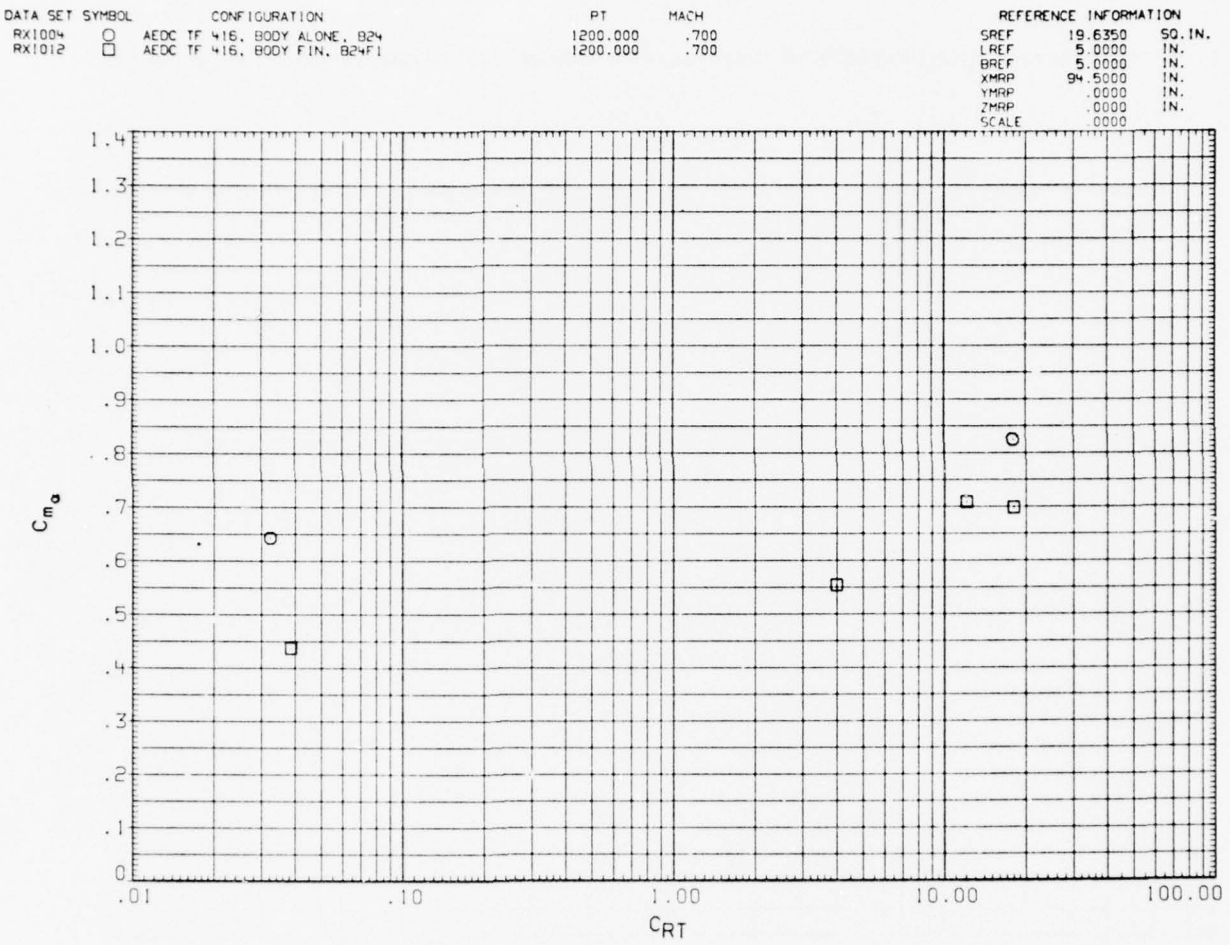

Figure A-50. Effect of radial thrust coefficient on longitudinal derivatives.

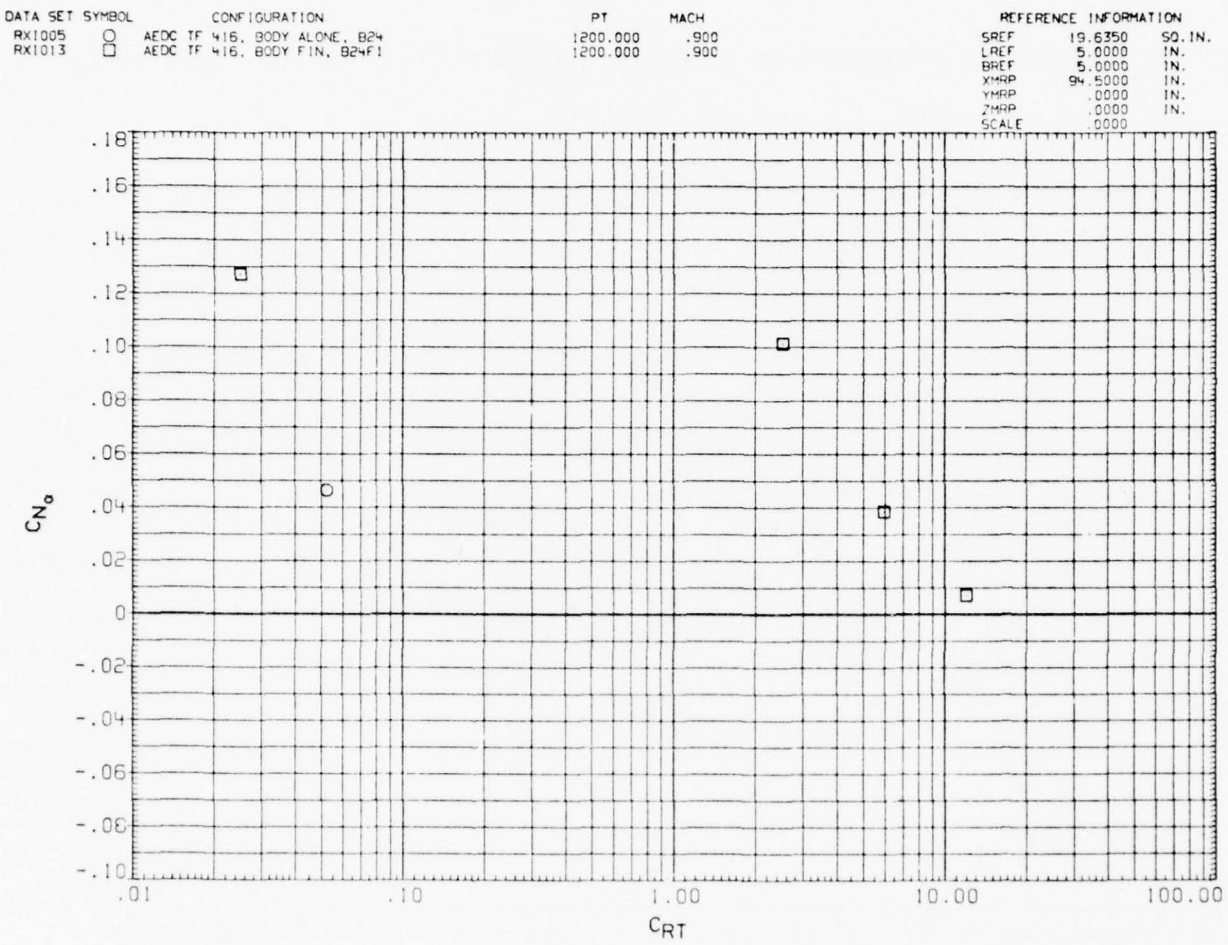

Figure A-51. Effect of radial thrust coefficient on longitudinal derivatives.

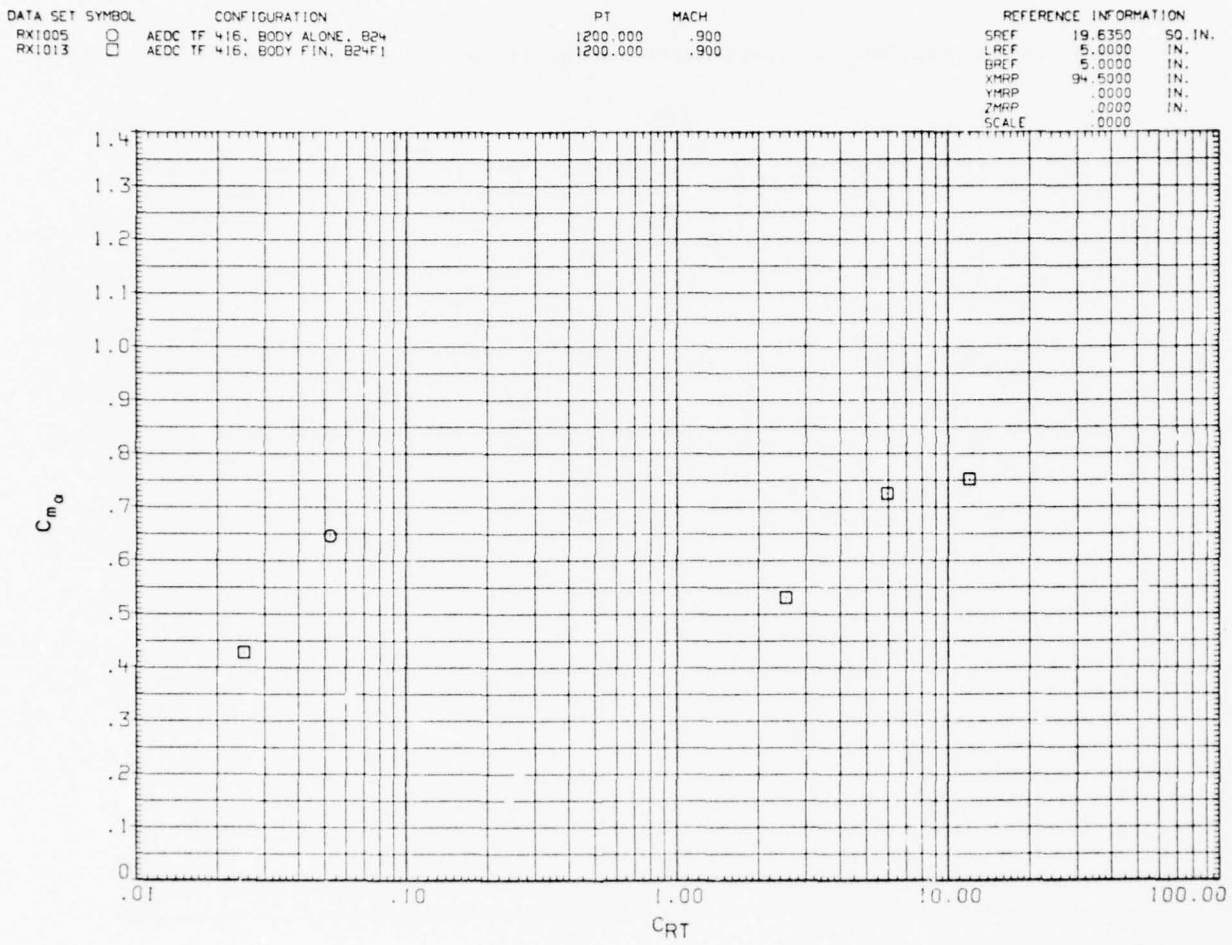

Figure A-52. Effect of radial thrust coefficient on longitudinal derivatives.

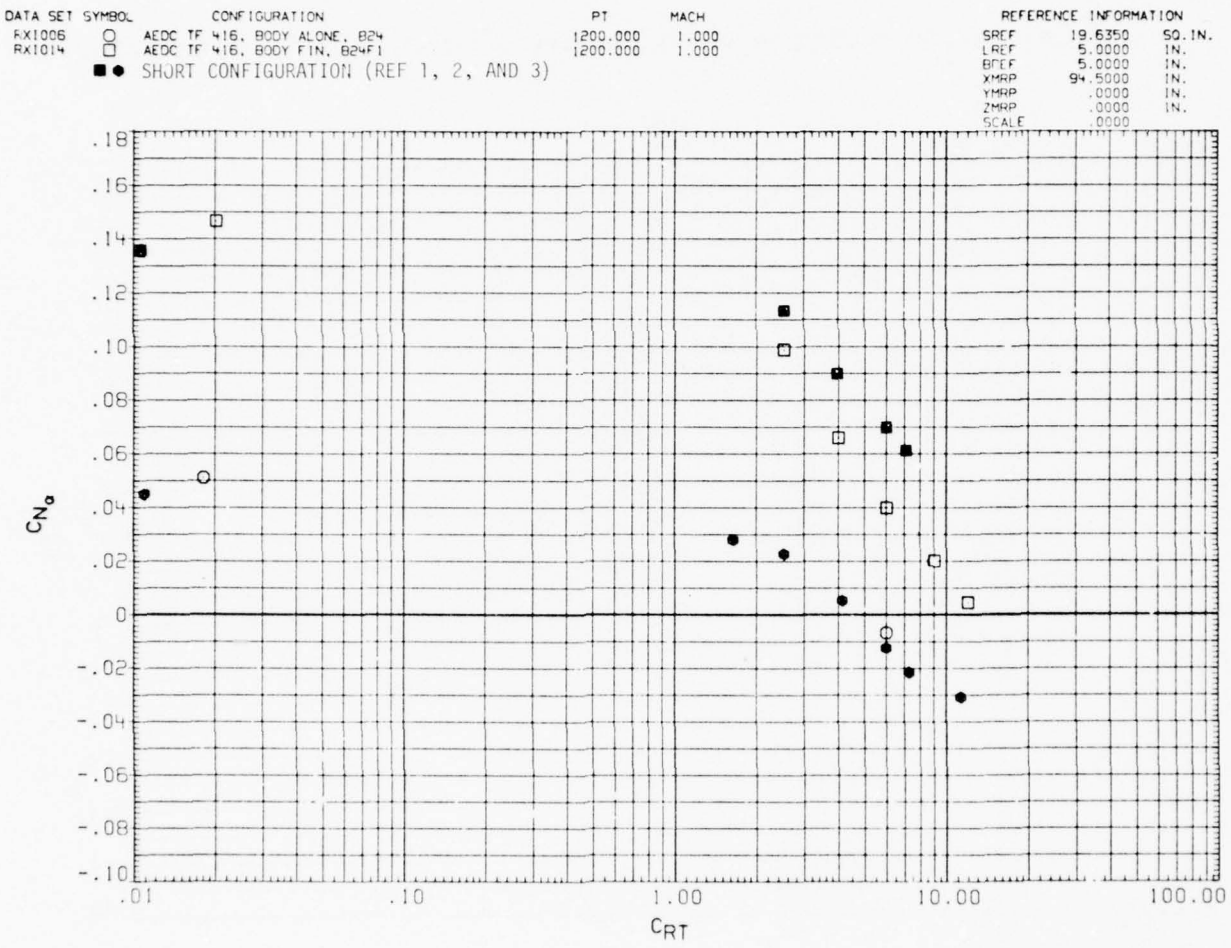

Figure A-53. Effect of radial thrust coefficient on longitudinal derivatives.

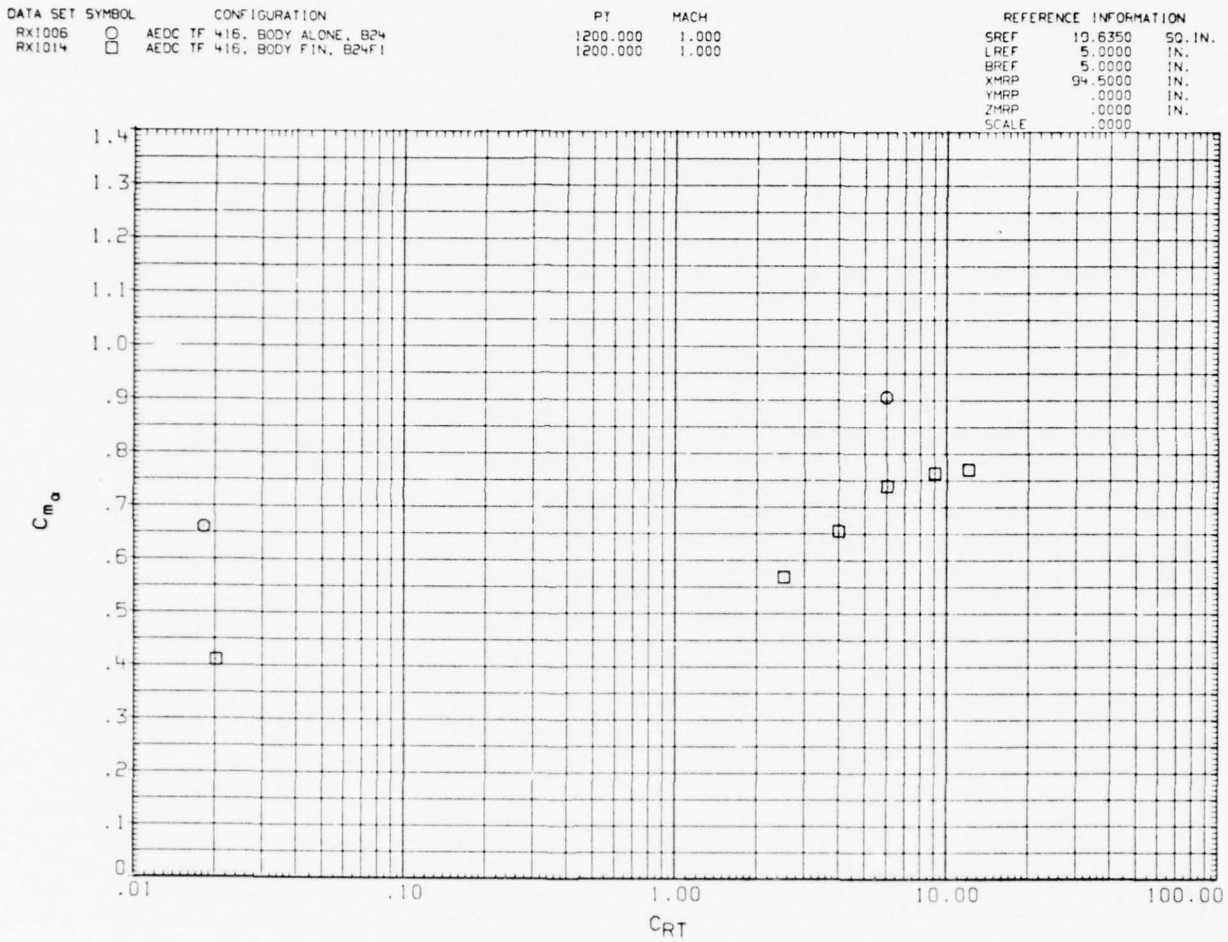

Figure A-54. Effect of radial thrust coefficient on longitudinal derivatives.

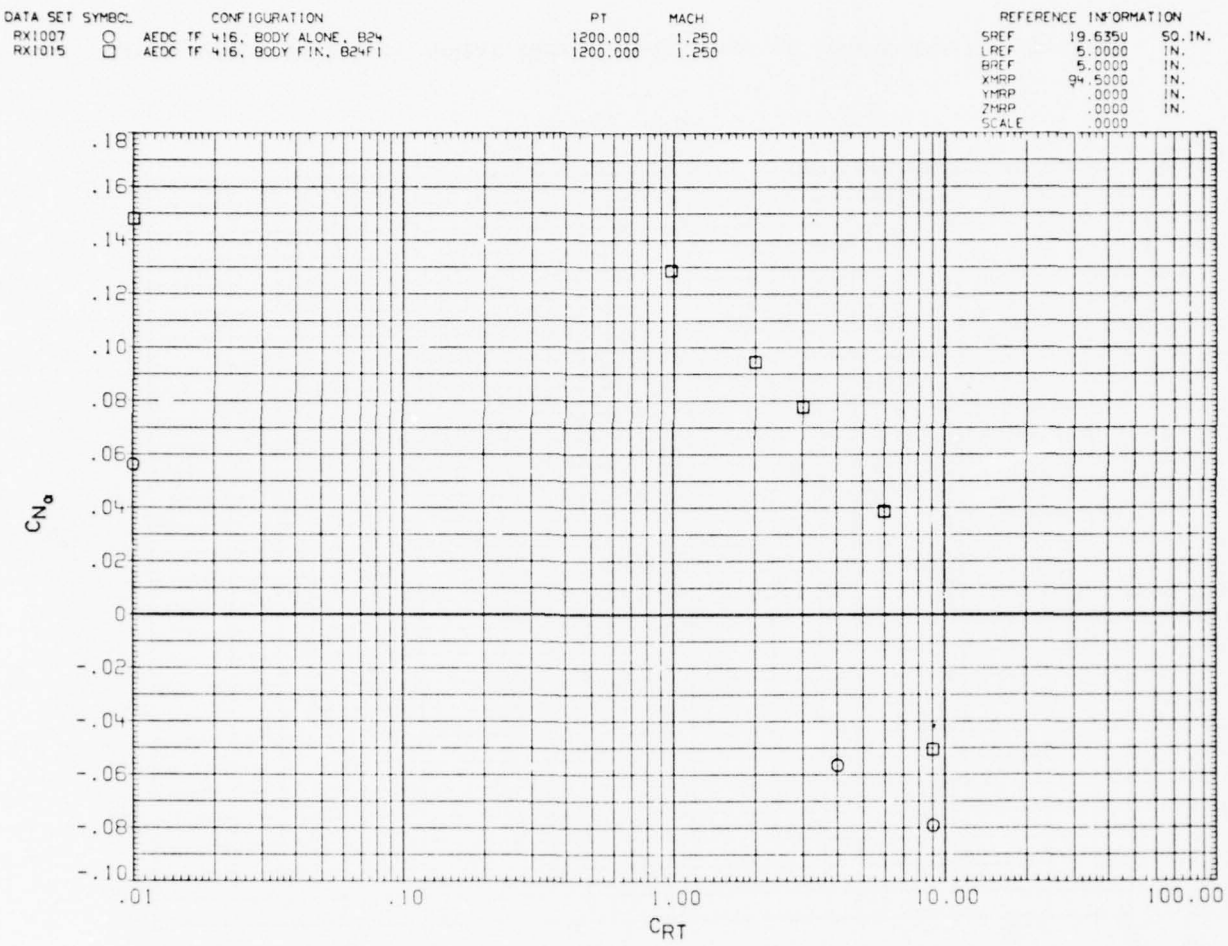

Figure A-55. Effect of radial thrust coefficient on longitudinal derivatives.

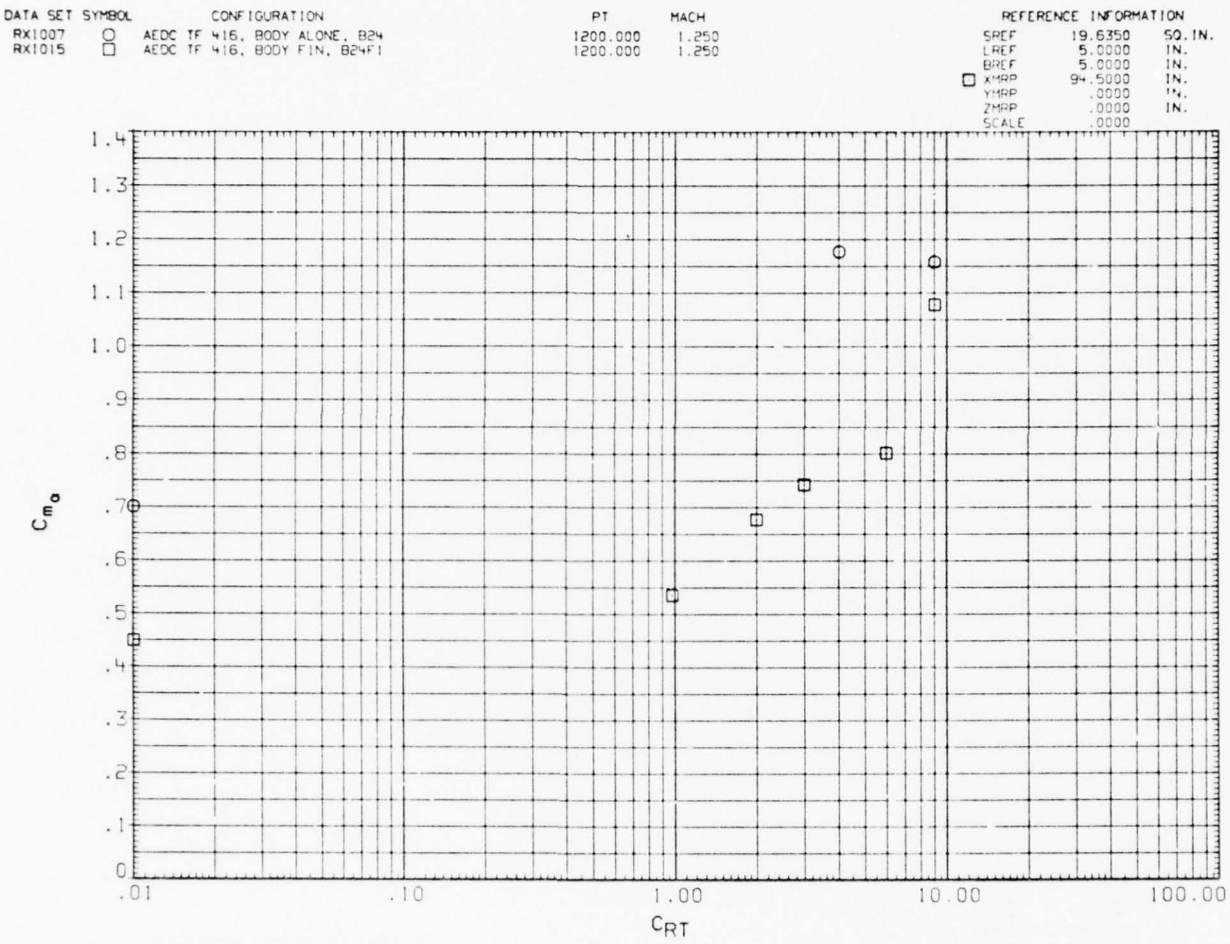

Figure A-56. Effect of radial thrust coefficient on longitudinal derivatives.

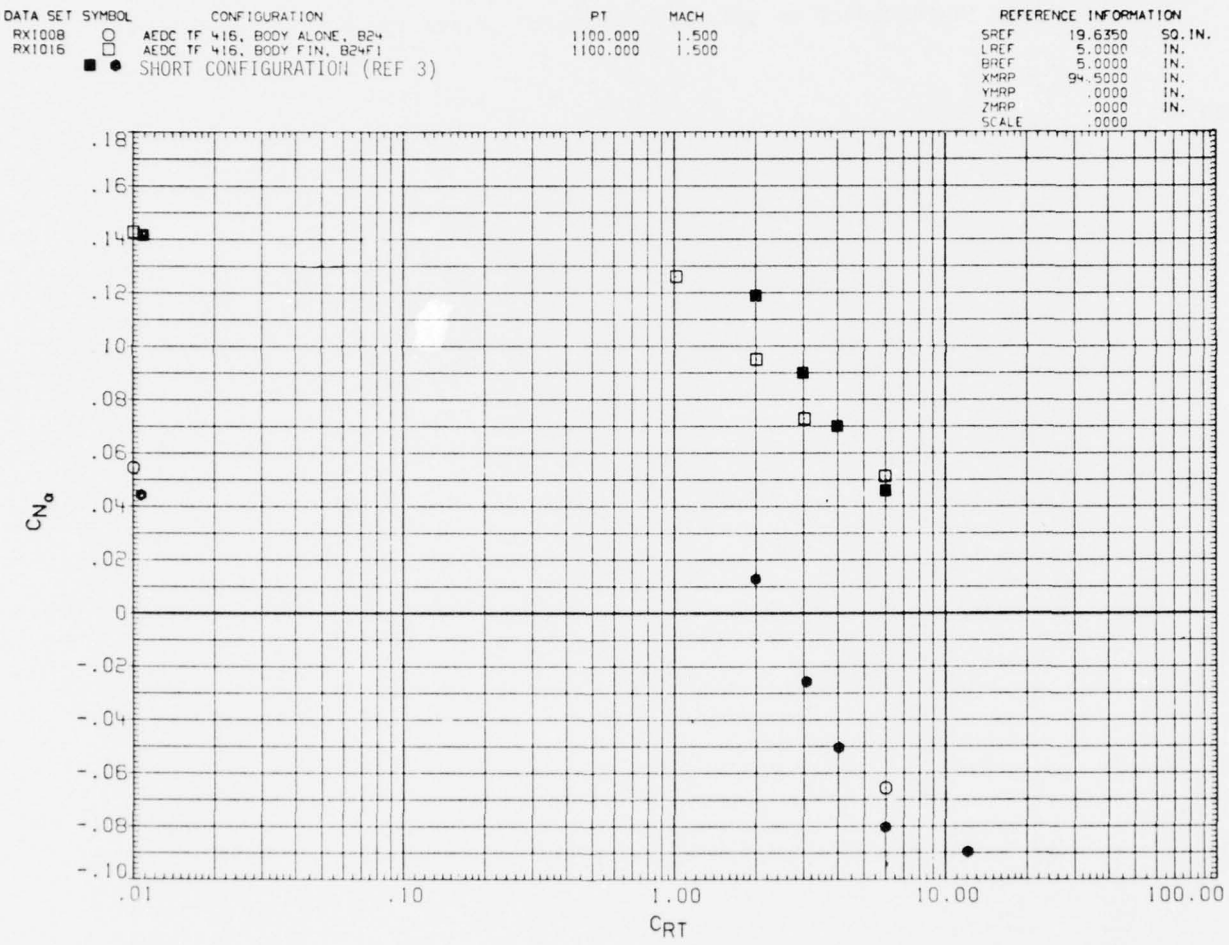

Figure A-57. Effect of radial thrust coefficient on longitudinal derivatives.

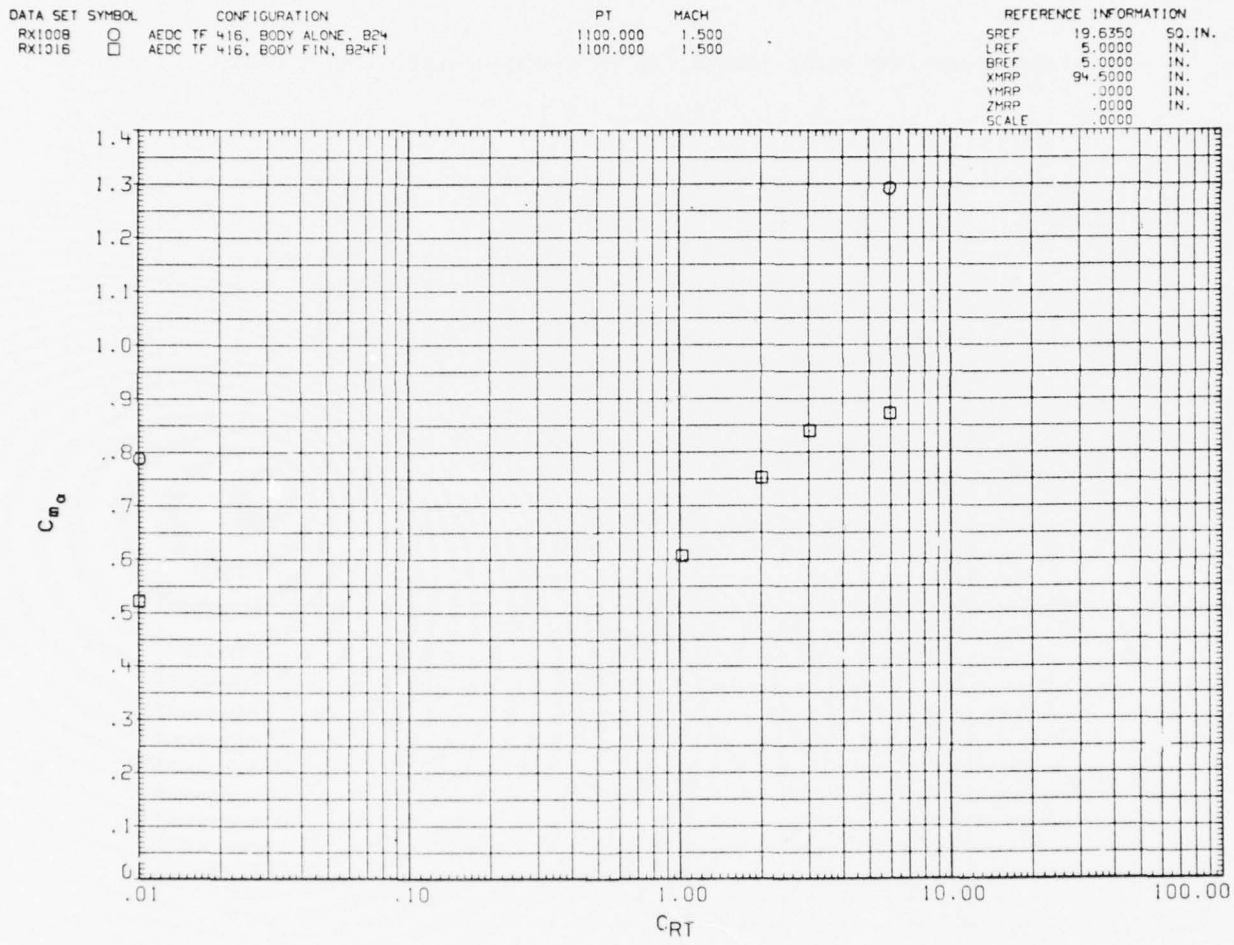

Figure A-58. Effect of radial thrust coefficient on longitudinal derivatives.

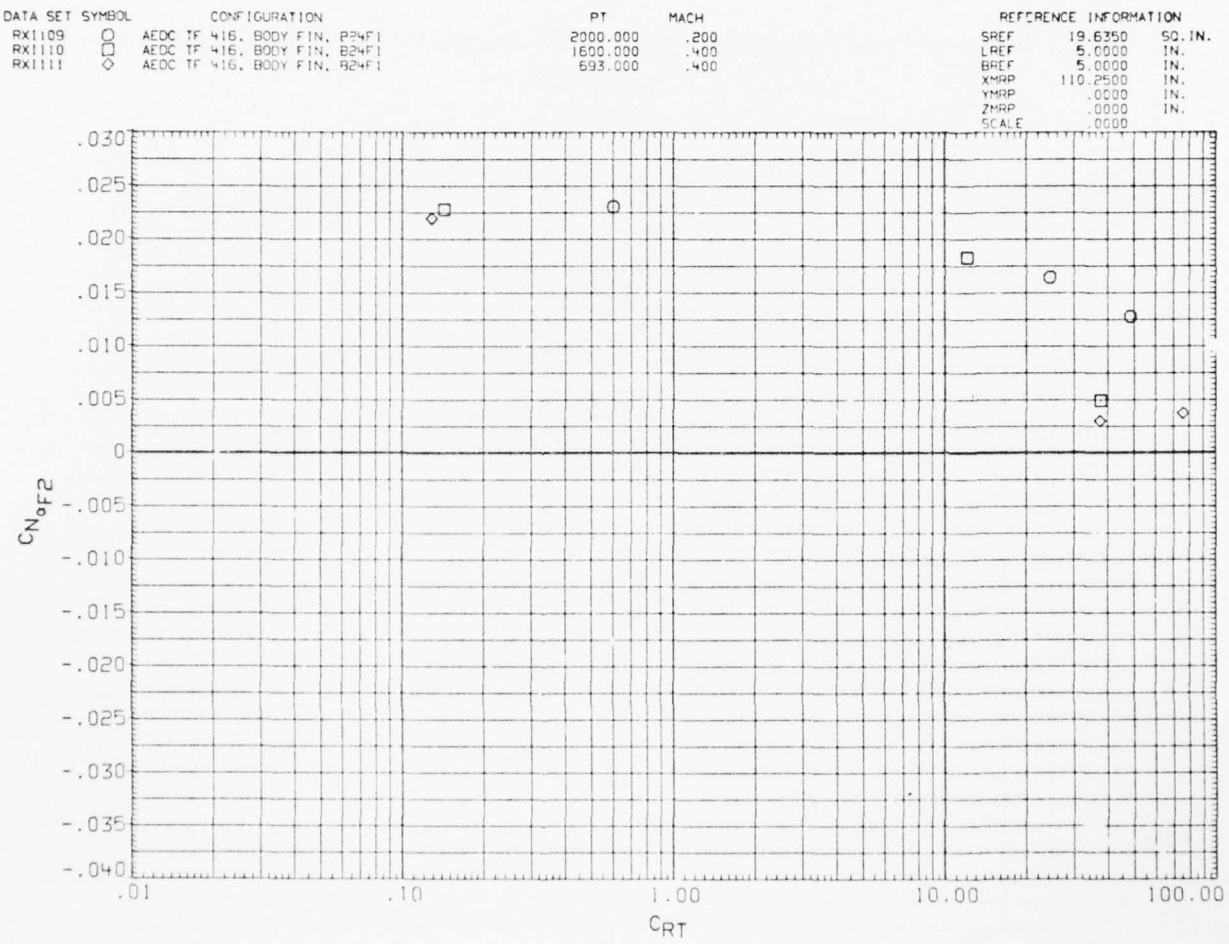

Figure A-59. Thrust effects on fin normal force characteristics.

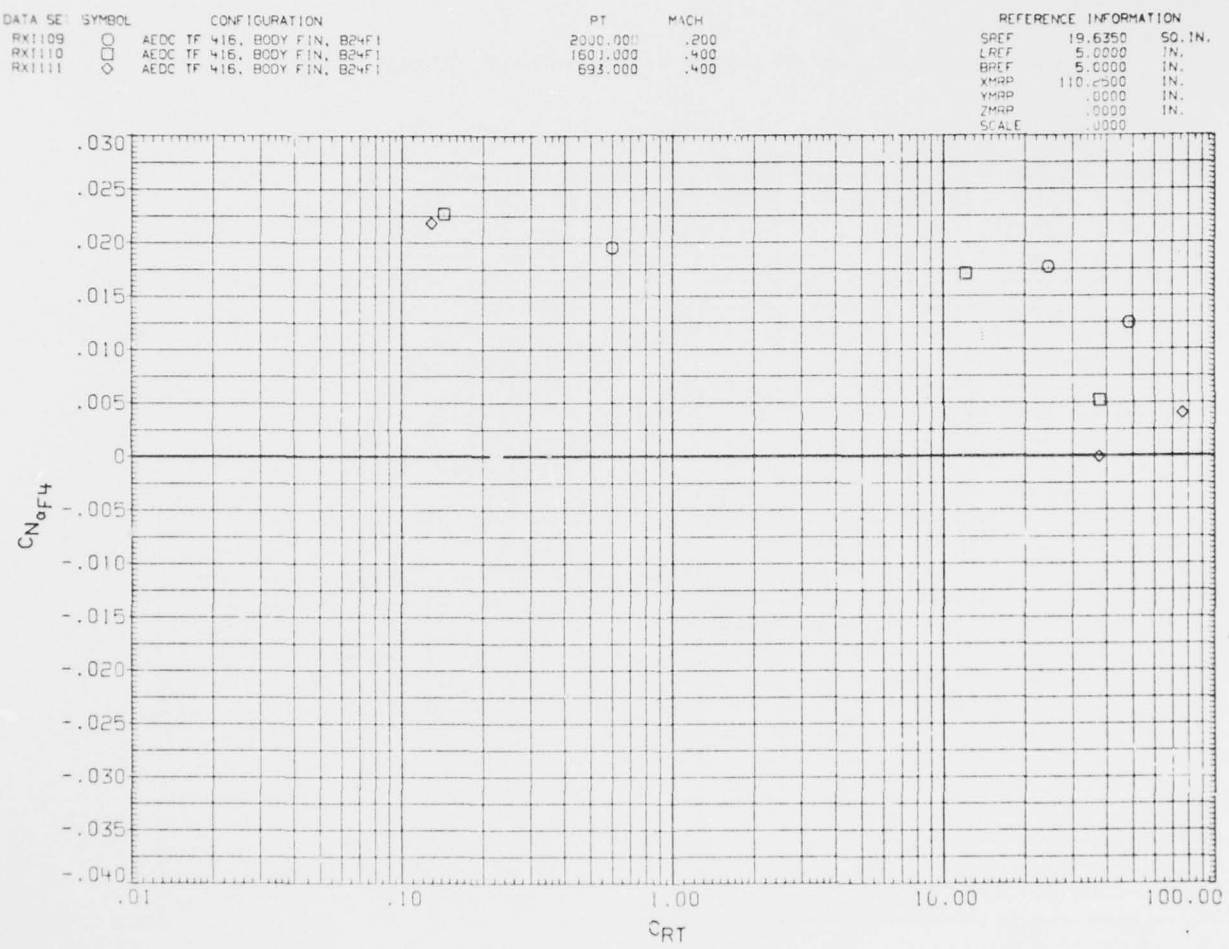

Figure A-60. Thrust effects on fin normal force characteristics.

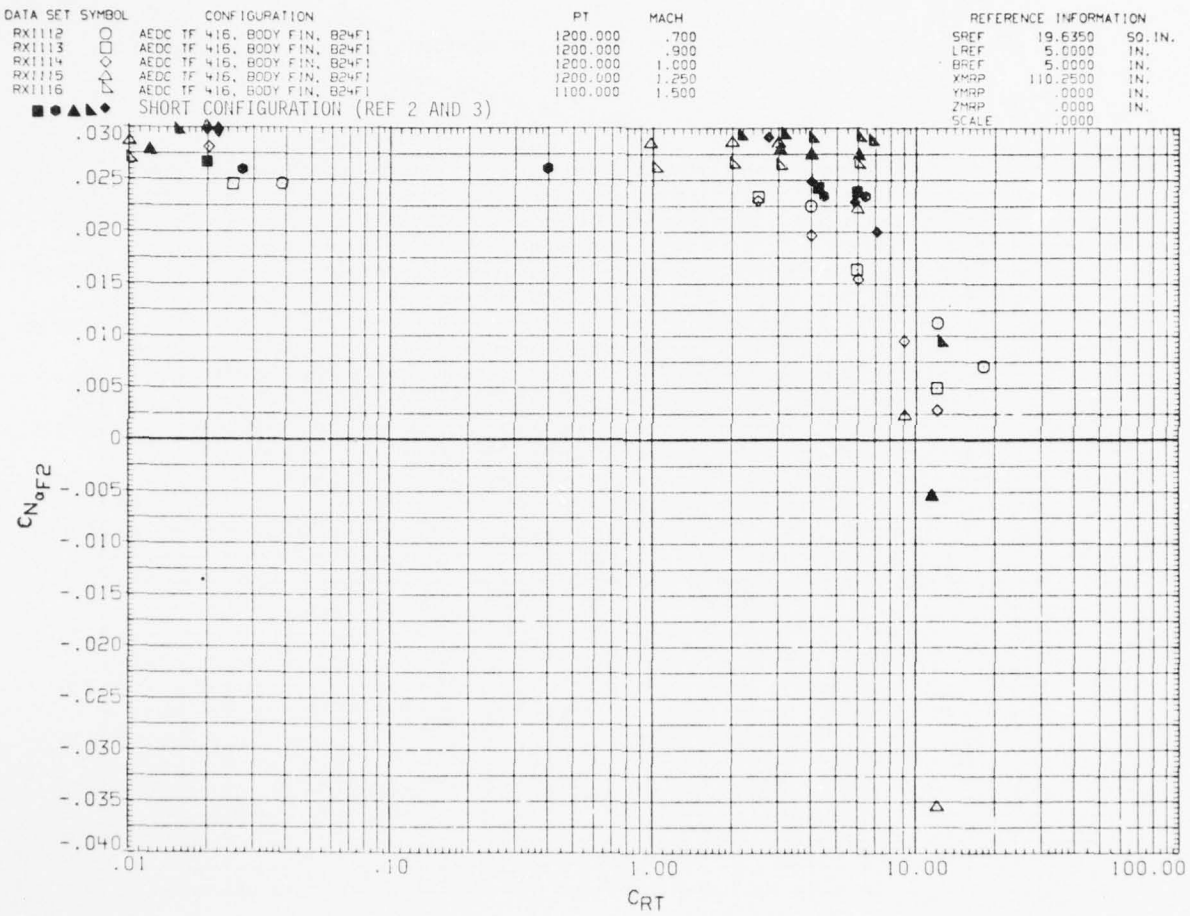

Figure A-61. Thrust effects on fin normal force characteristics.

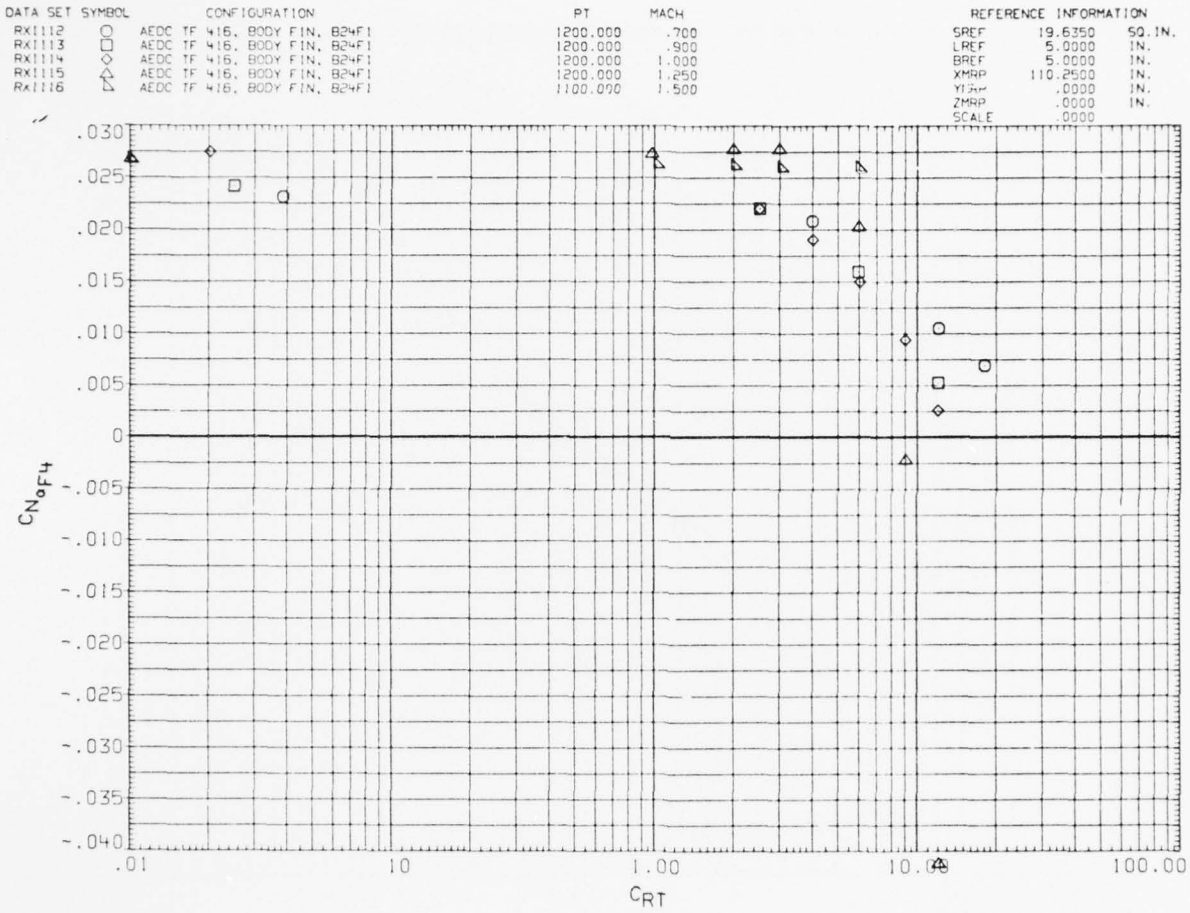

Figure A-62. Thrust effects on fin normal force characteristics.

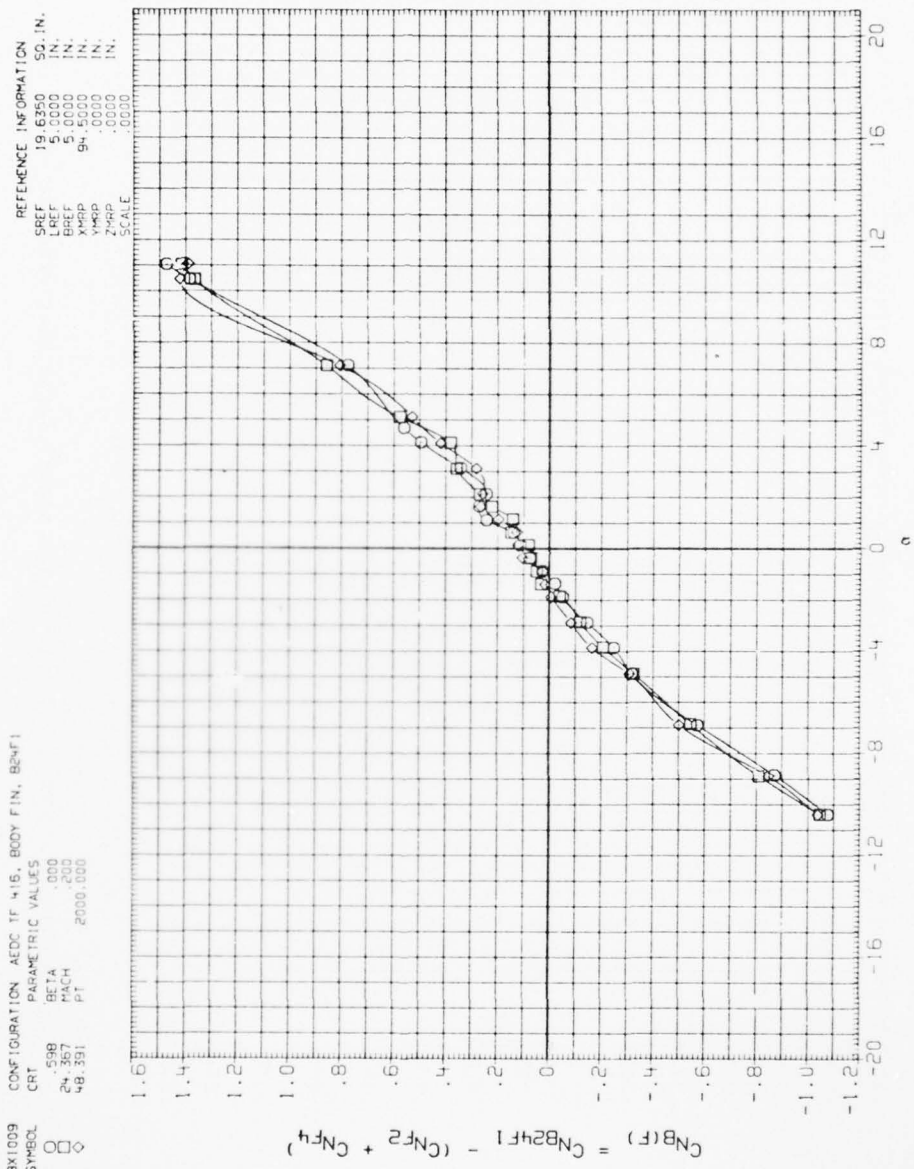

Figure A-63. Plume effects on body in presence of fins.

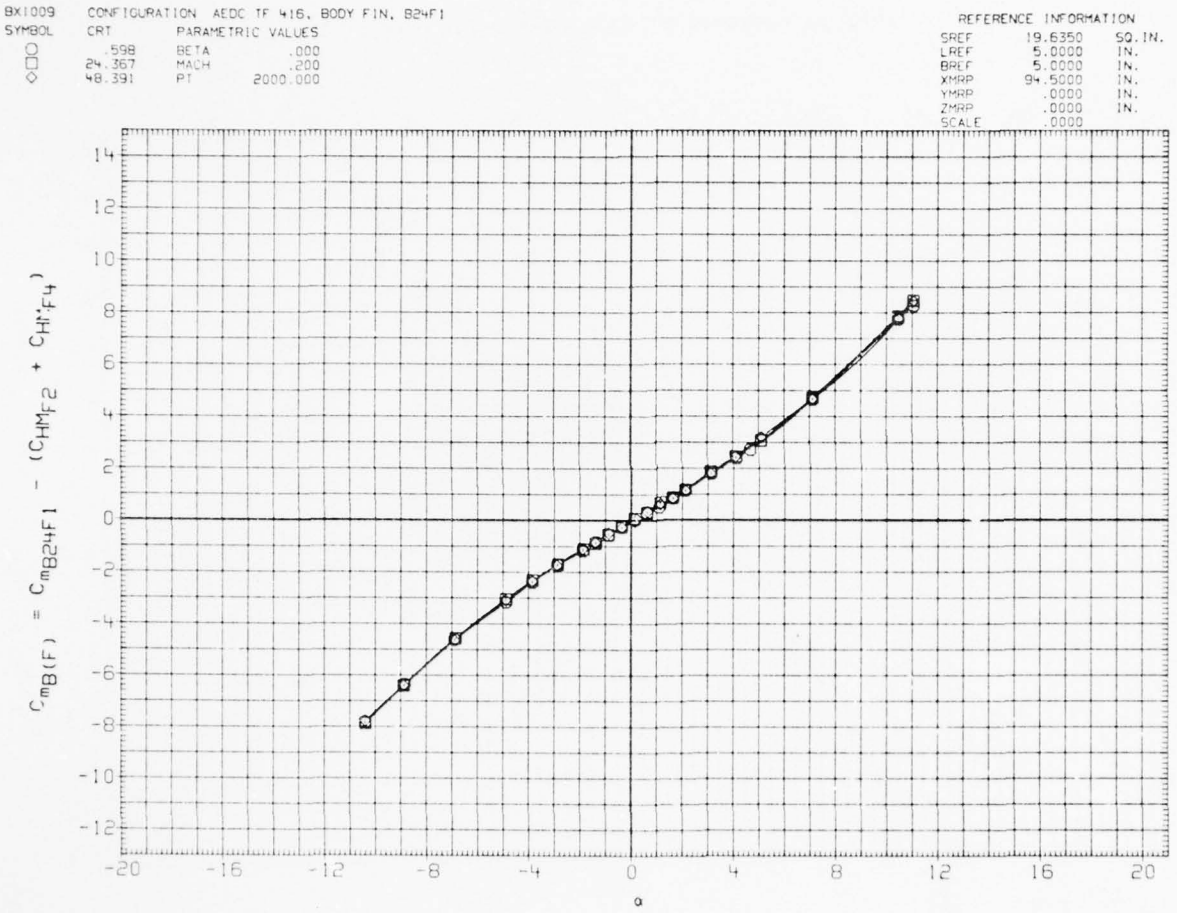

Figure A-64. Plume effects on body in presence of fins.

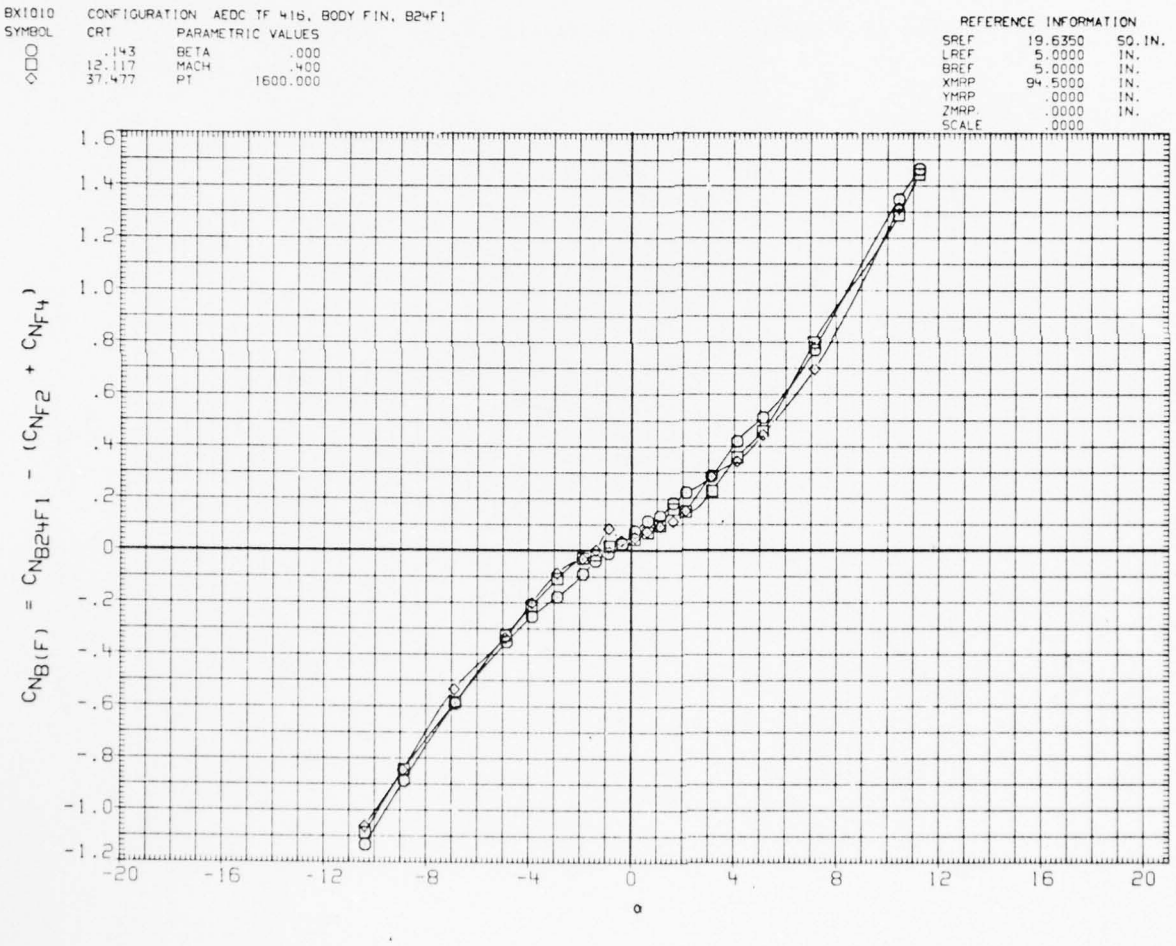

Figure A-65. Plume effects on body in presence of fins.

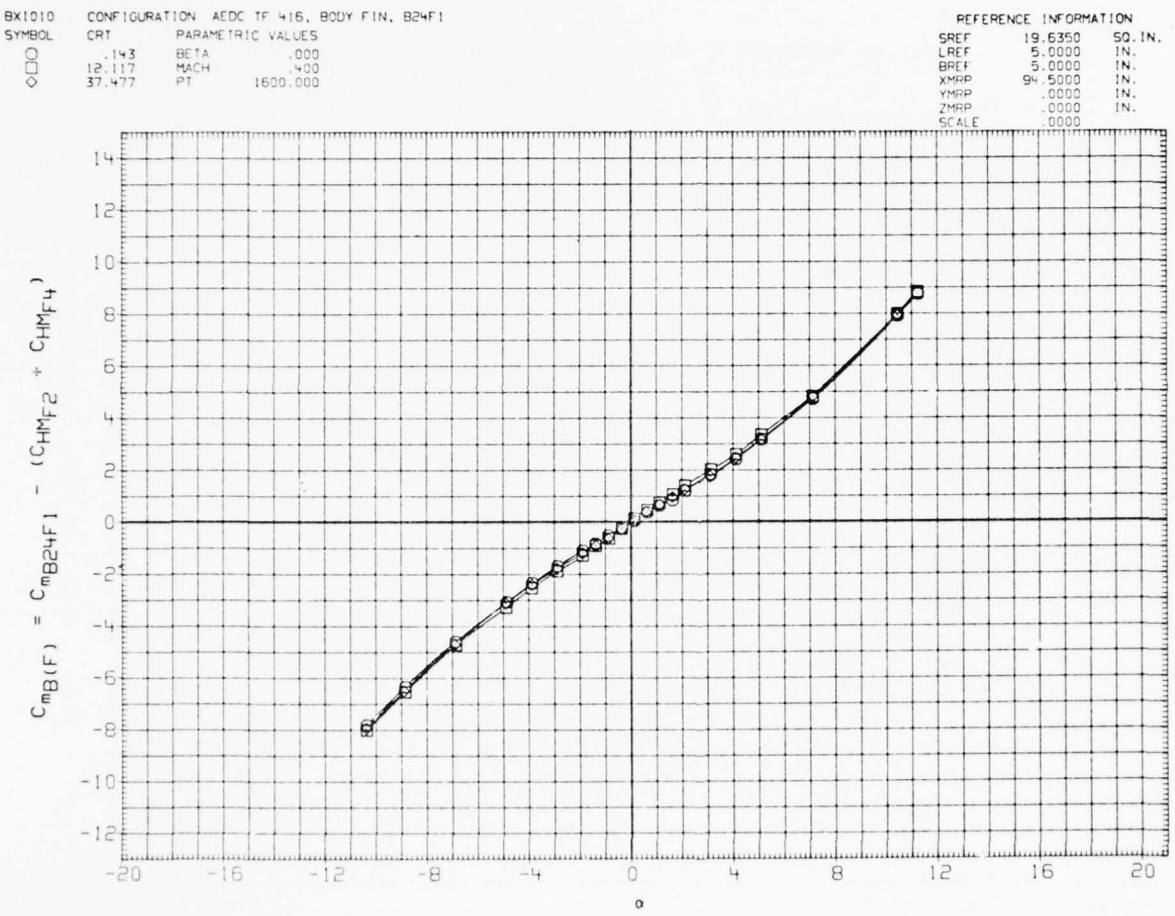

Figure A-66. Plume effects on body in presence of fins.

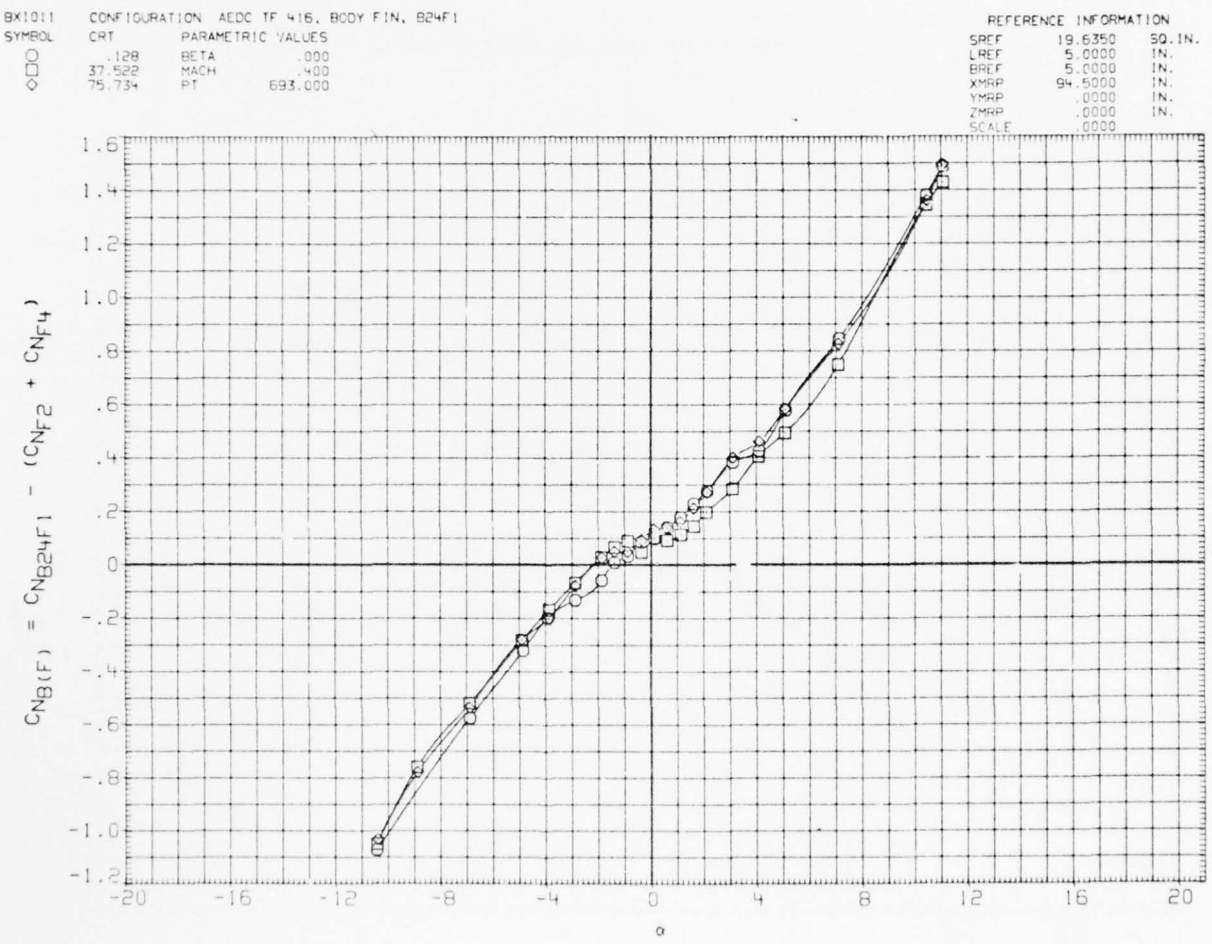

Figure A-67. Plume effects on body in presence of fins.

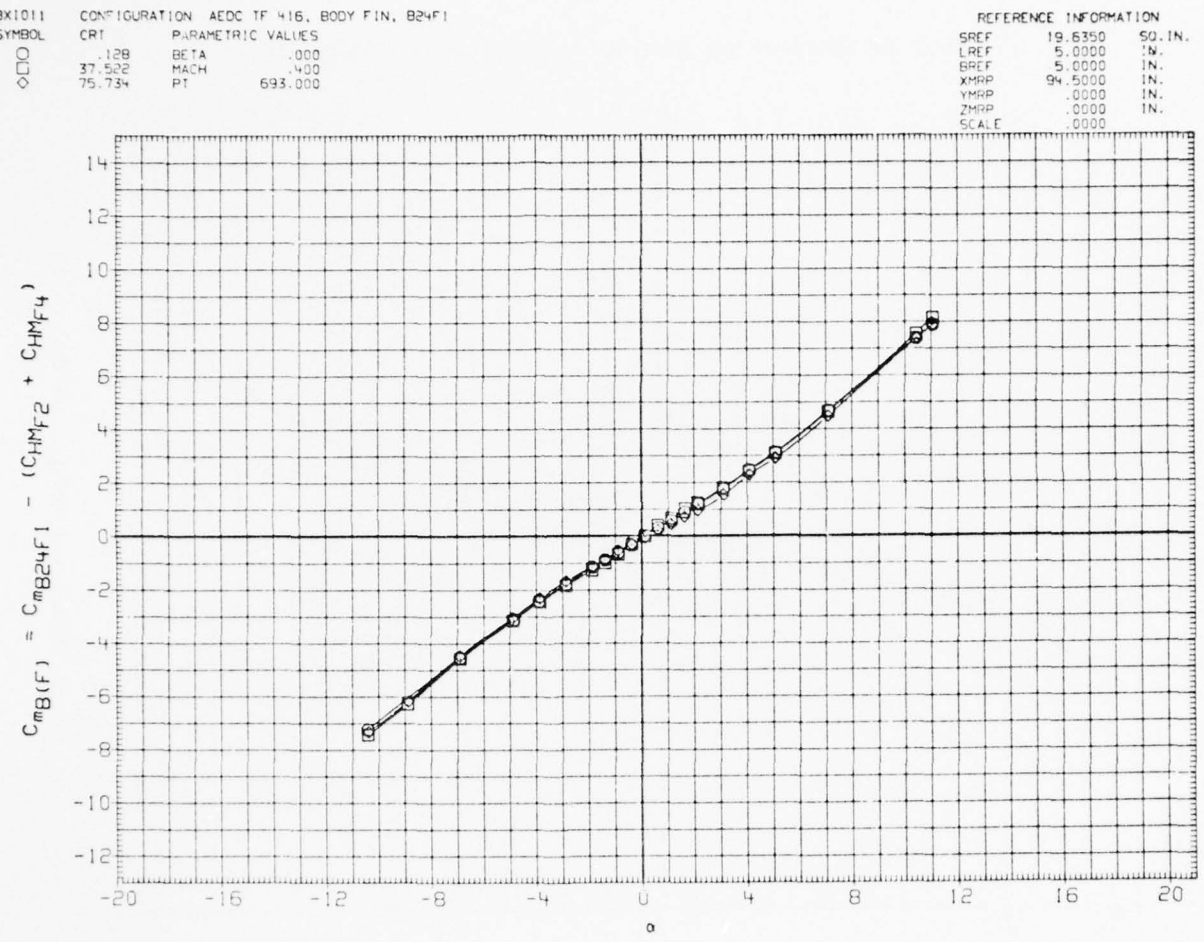

Figure A-68. Plume effects on body in presence of fins.

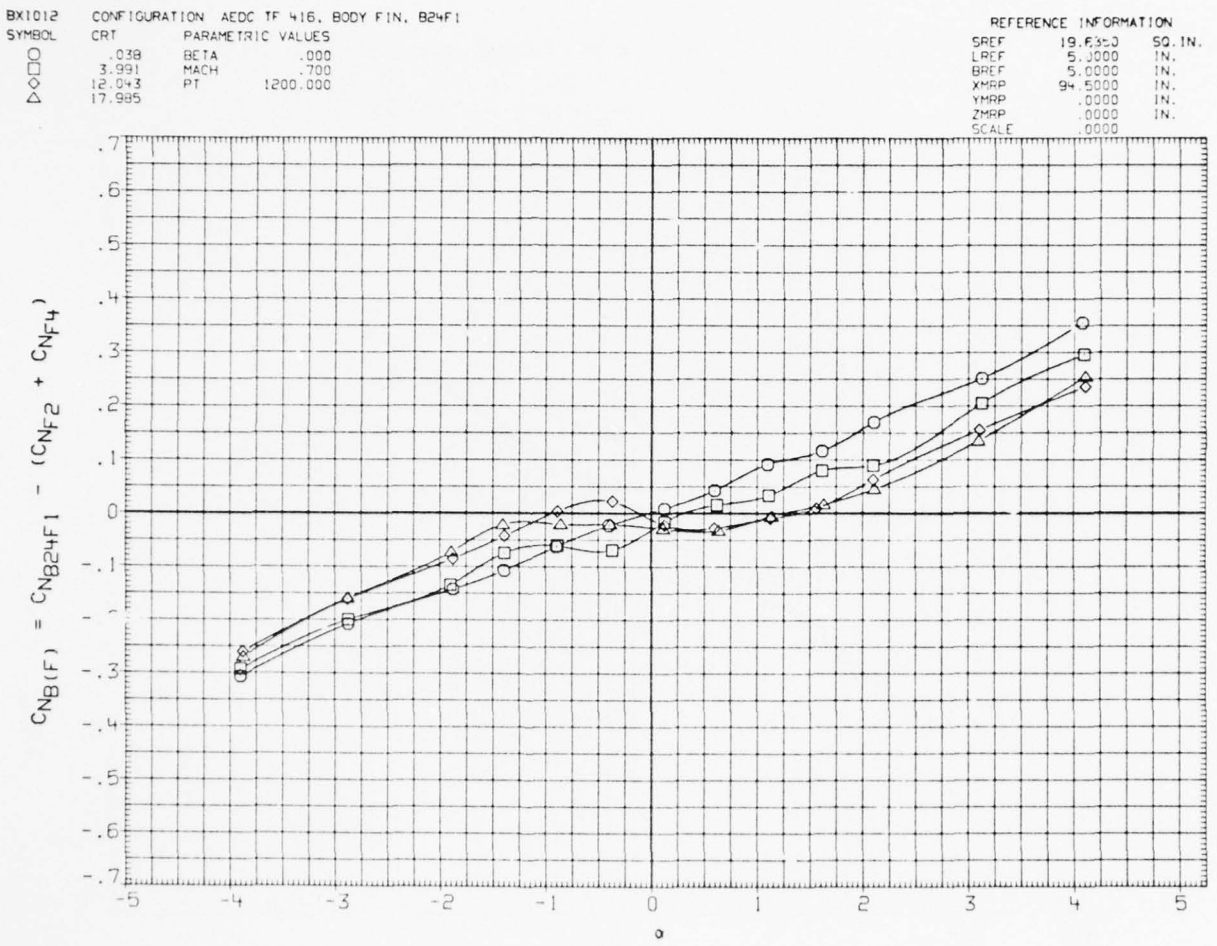

Figure A-69. Plume effects on body in presence of fins.

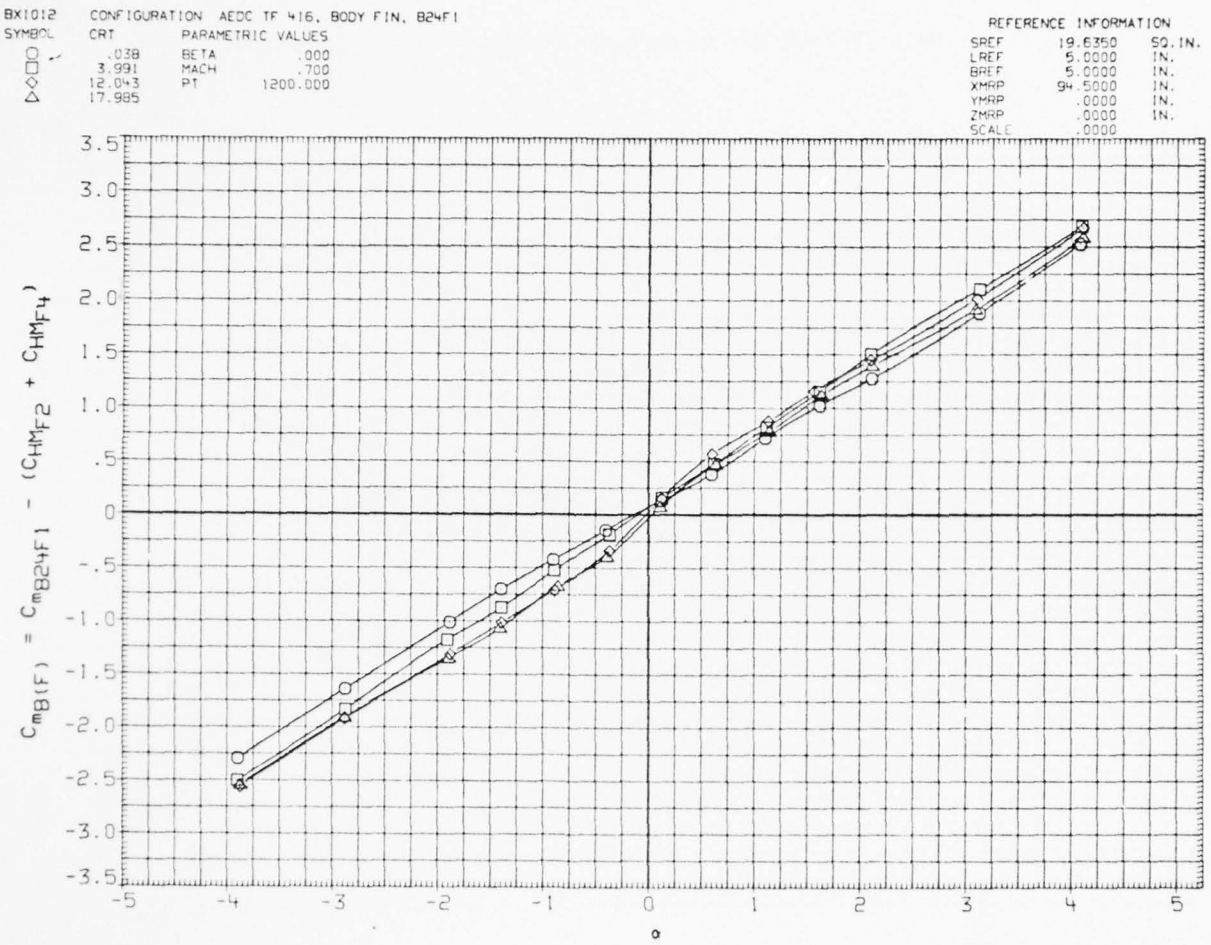

Figure A-70. Plume effects on body in presence of fins.

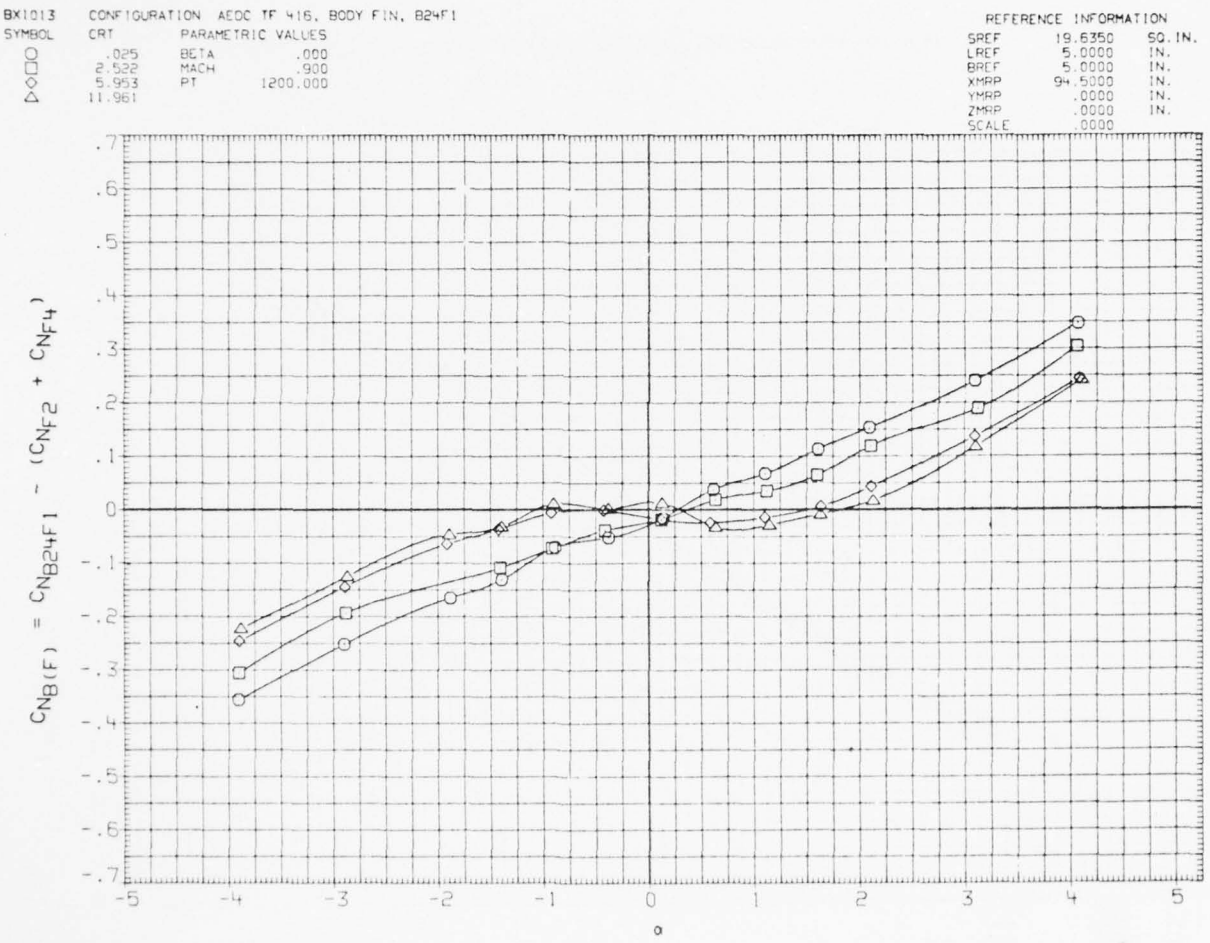

Figure A-71. Plume effects on body in presence of fins.

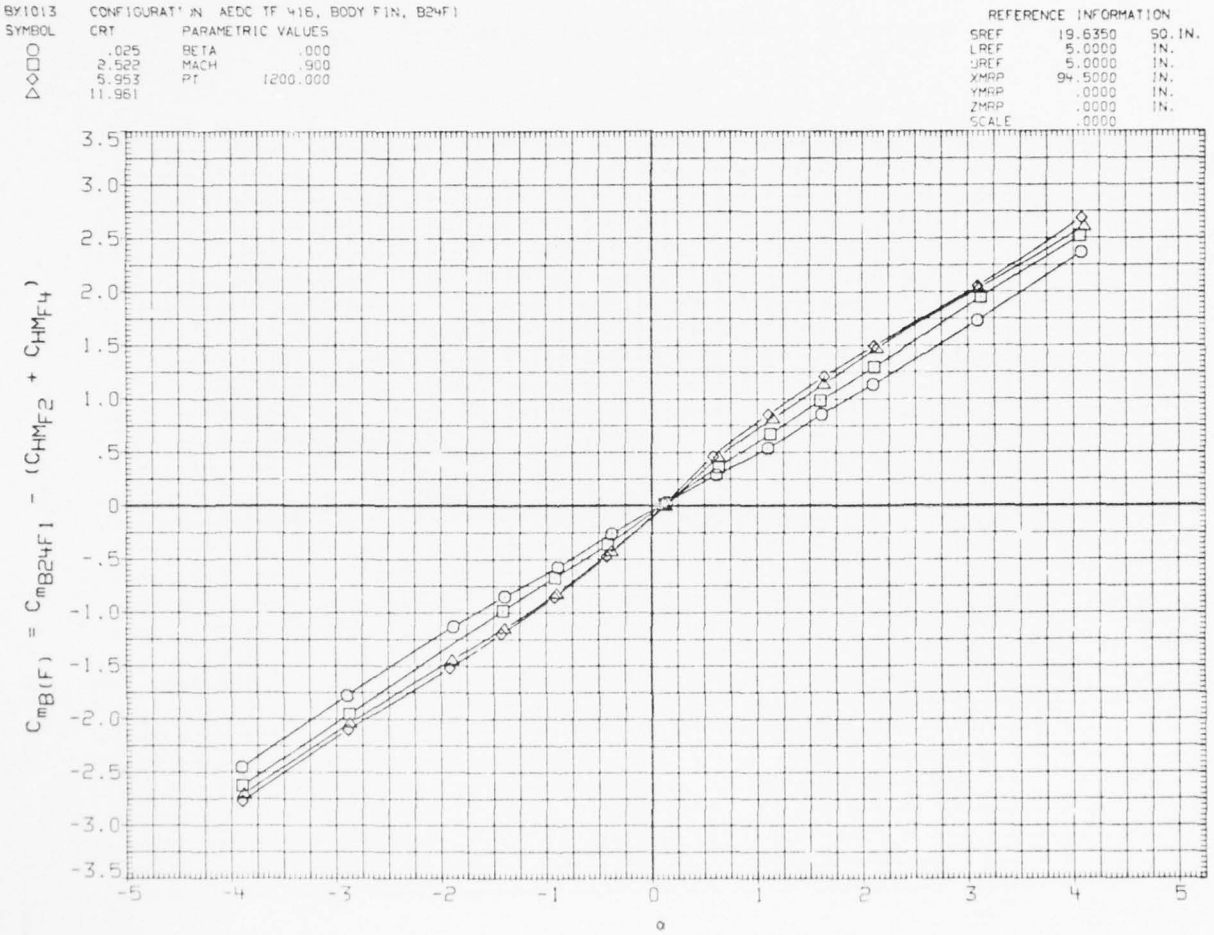

Figure A-72. Plume effects on body in presence of fins.

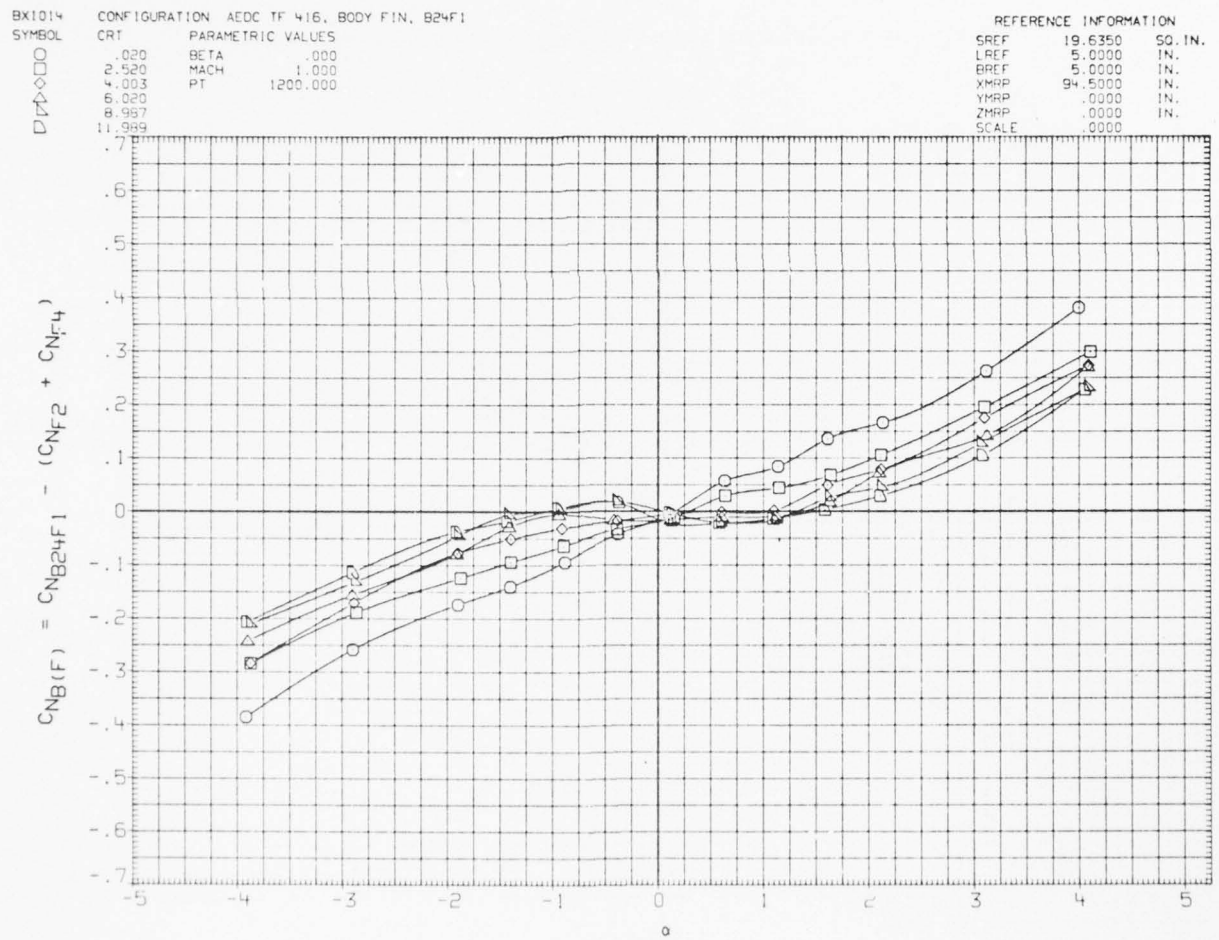

Figure A-73. Plume effects on body in presence of fins.

AD-A037 735 ARMY MISSILE RESEARCH AND DEVELOPMENT COMMAND REDSTO--ETC F/G 20/4
AN EXPERIMENTAL INVESTIGATION USING A NORMAL JET PLUME SIMULATO--ETC(U)
FEB 77 J H HENDERSON, C W DAHLKE, G BATIUK

UNCLASSIFIED DRDMI-TD-77-2 NL

2 OF 2
AD
A037 735

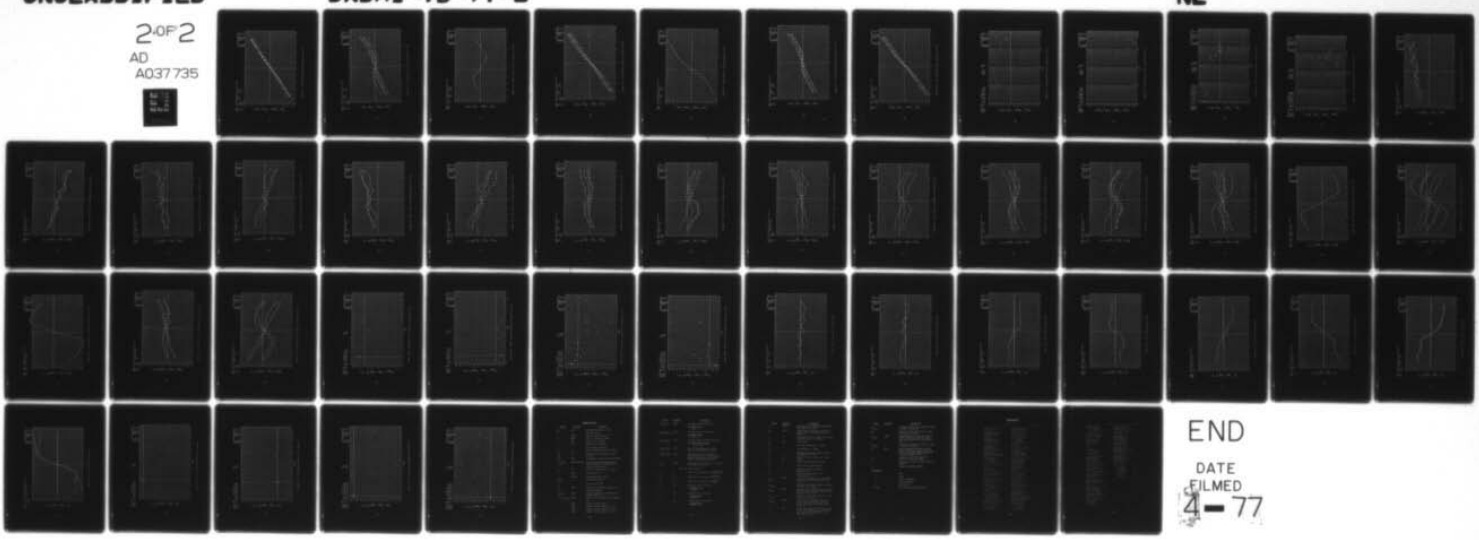

END
DATE FILMED
4-77

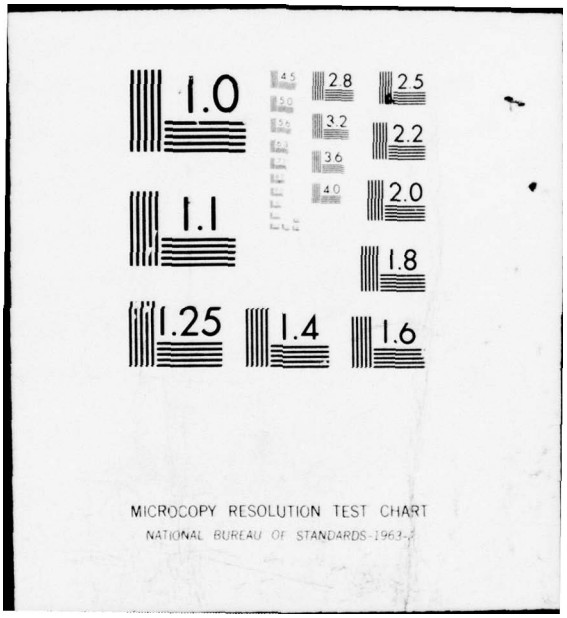
1.0
1.1
1.25
1.4
1.6
1.8
2.0
2.2
2.5
2.8
3.2
3.6
4.0
4.5
5.0
5.6
MICROCOPY RESOLUTION TEST CHART
NATIONAL BUREAU OF STANDARDS-1963-A

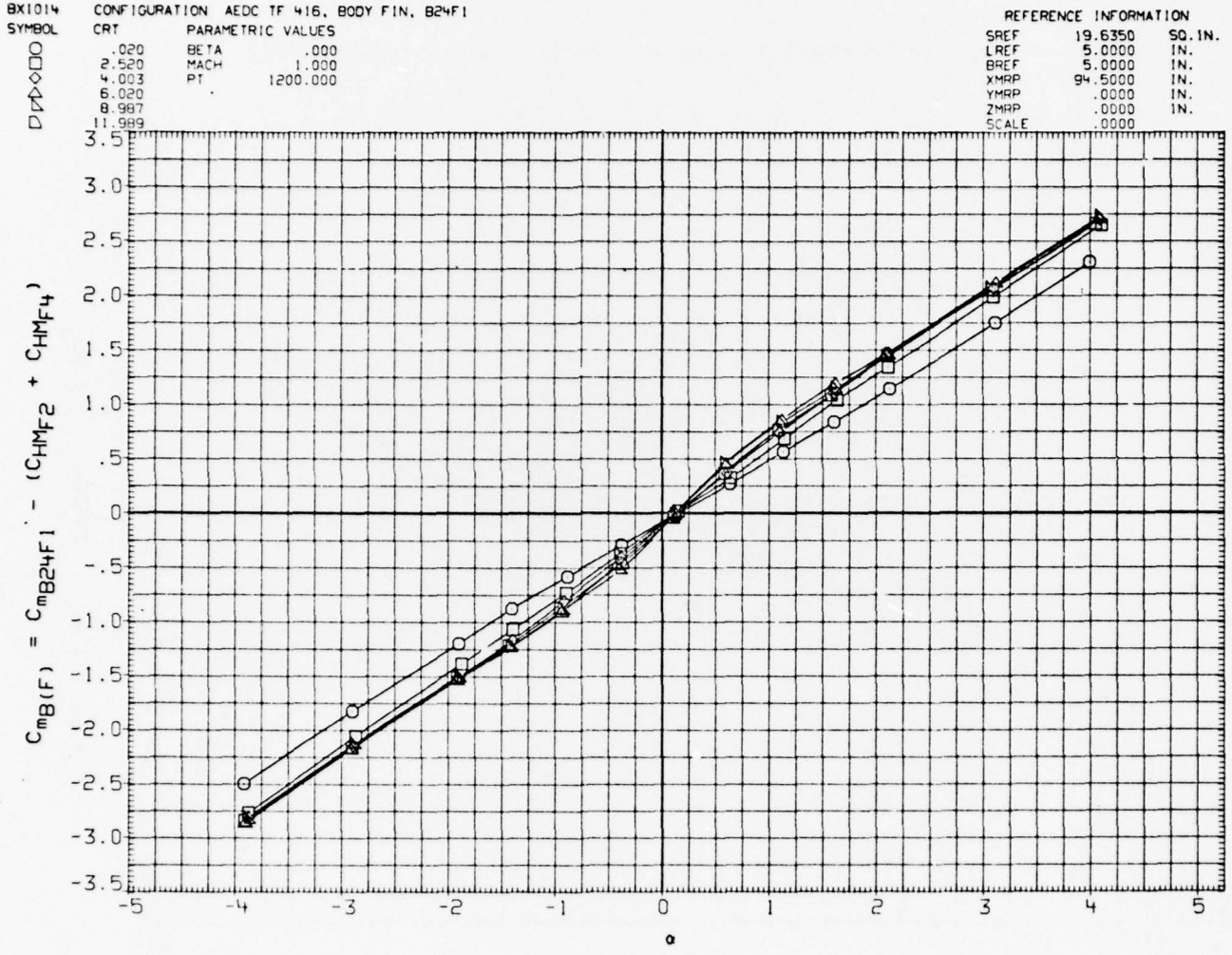

Figure A-74. Plume effects on body in presence of fins.

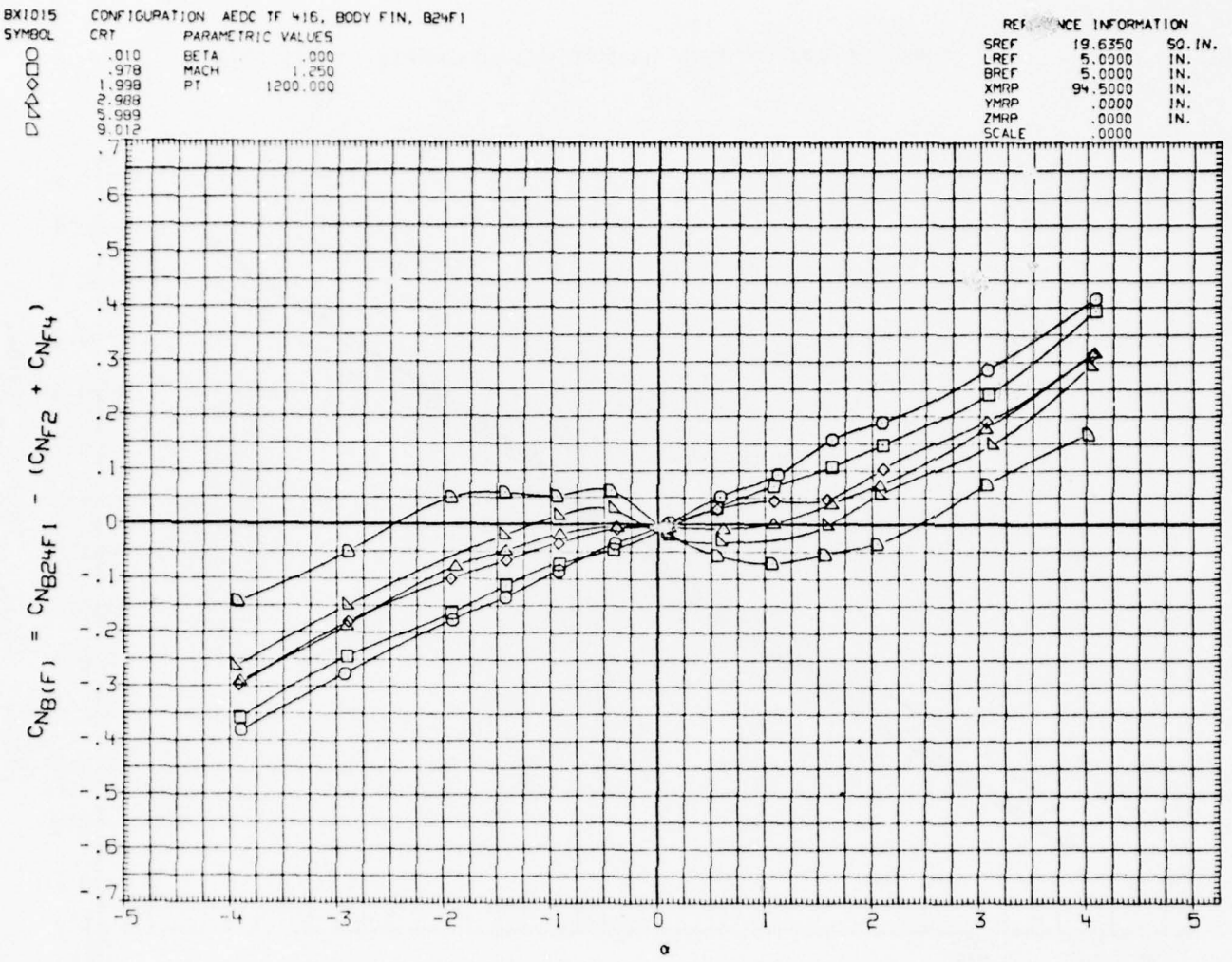

Figure A-75. Plume effects on body in presence of fins.

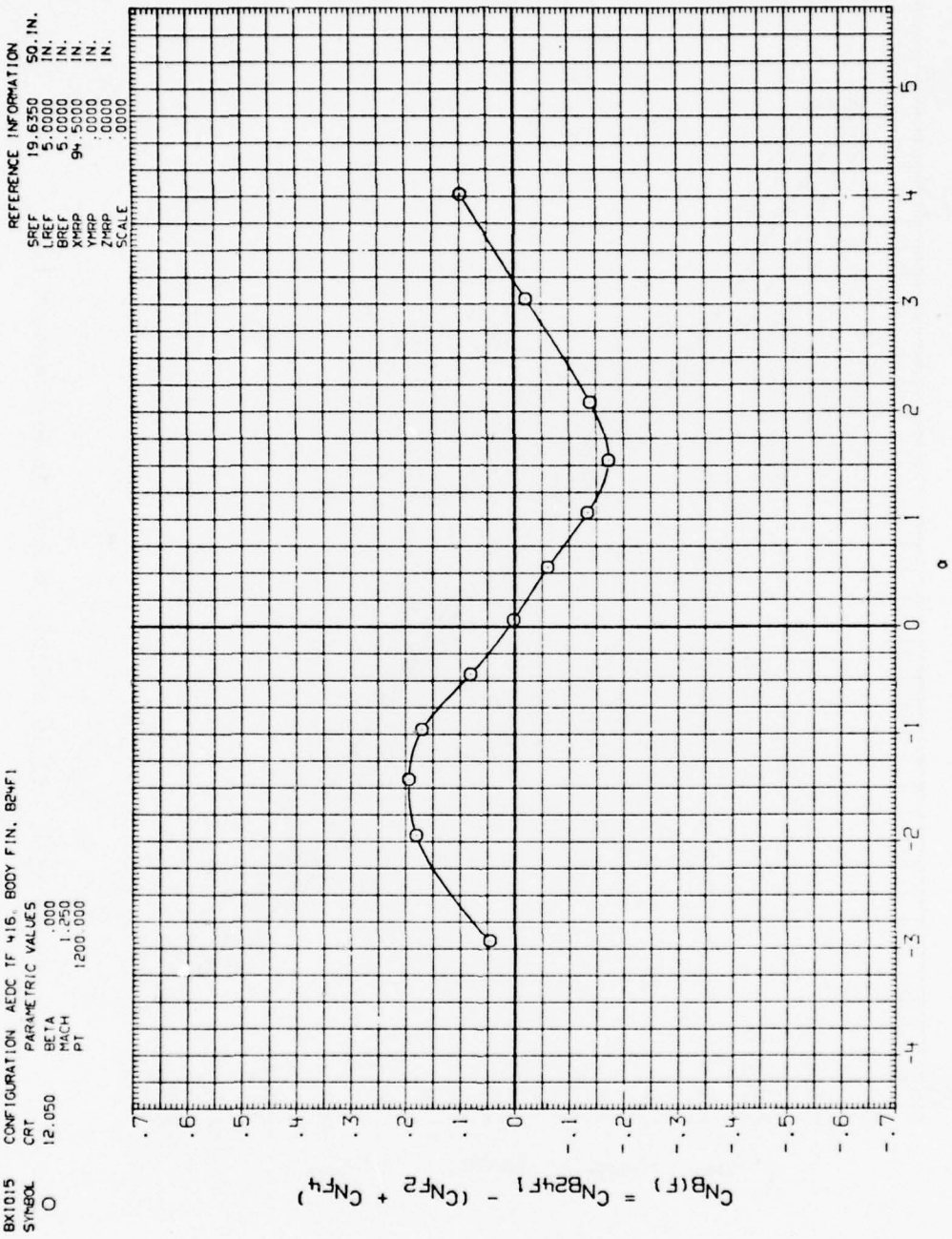

Figure A-76. Plume effects on body in presence of fins.

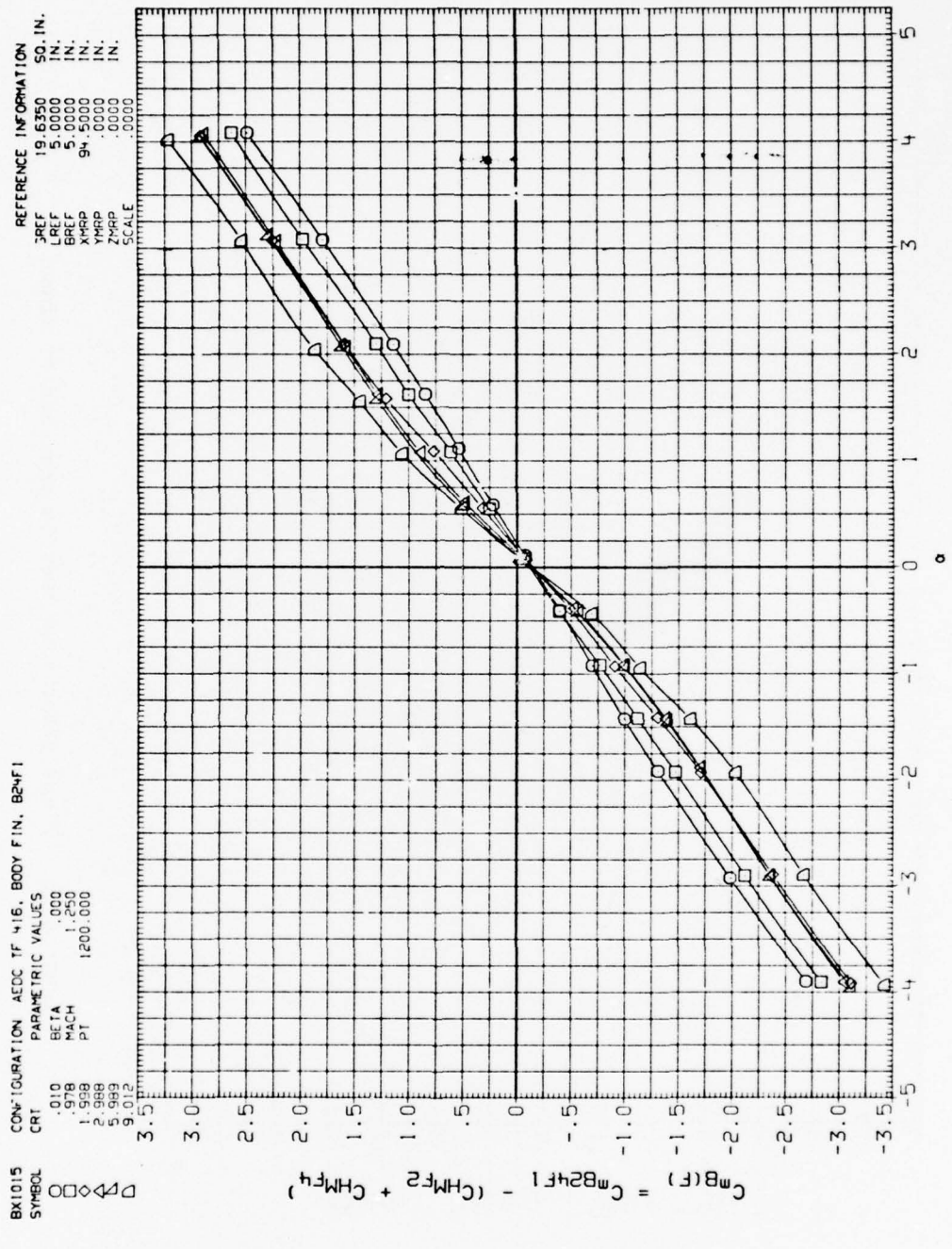

Figure A-77. Plume effects on body in presence of fins.

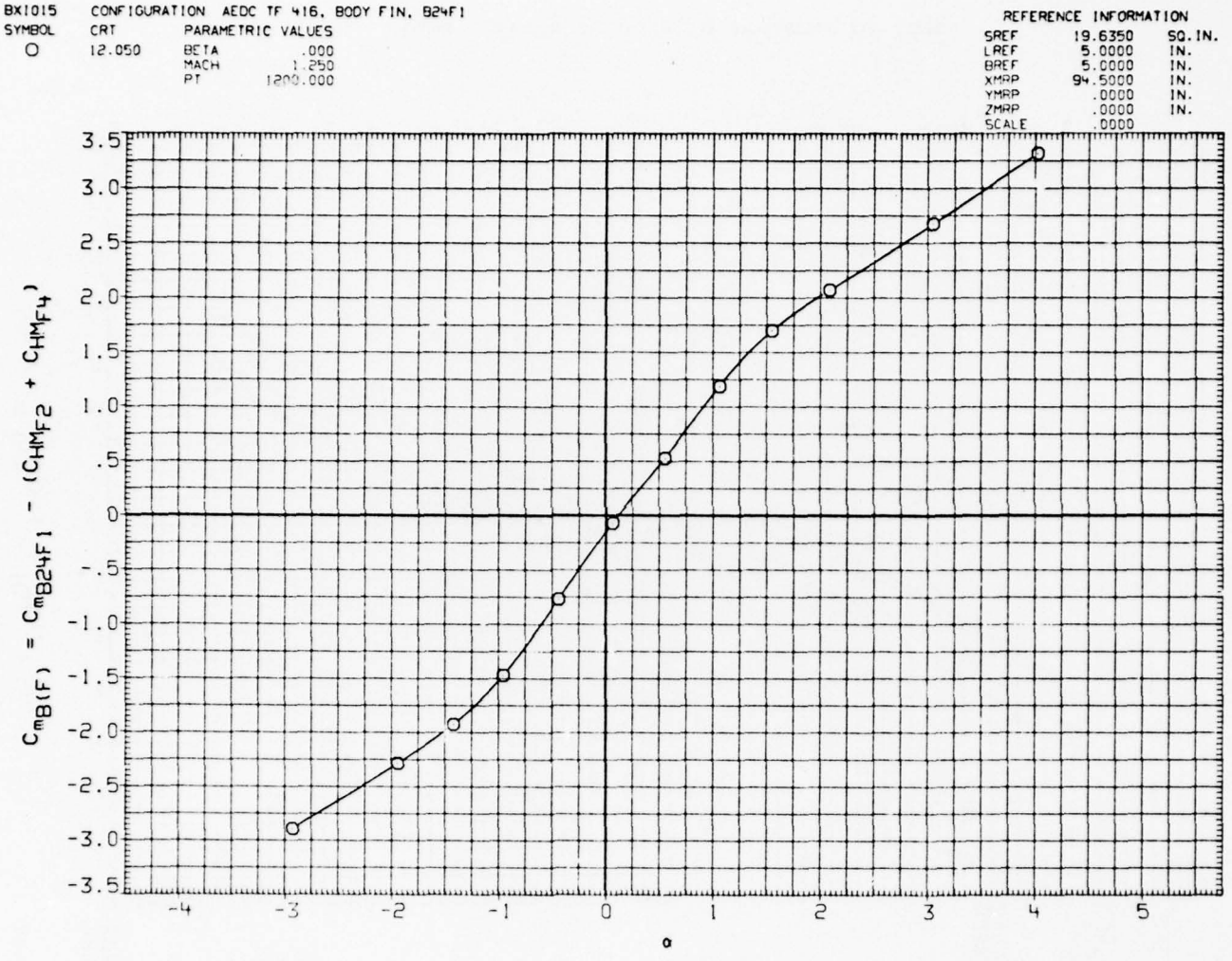

Figure A-78. Plume effects on body in presence of fins.

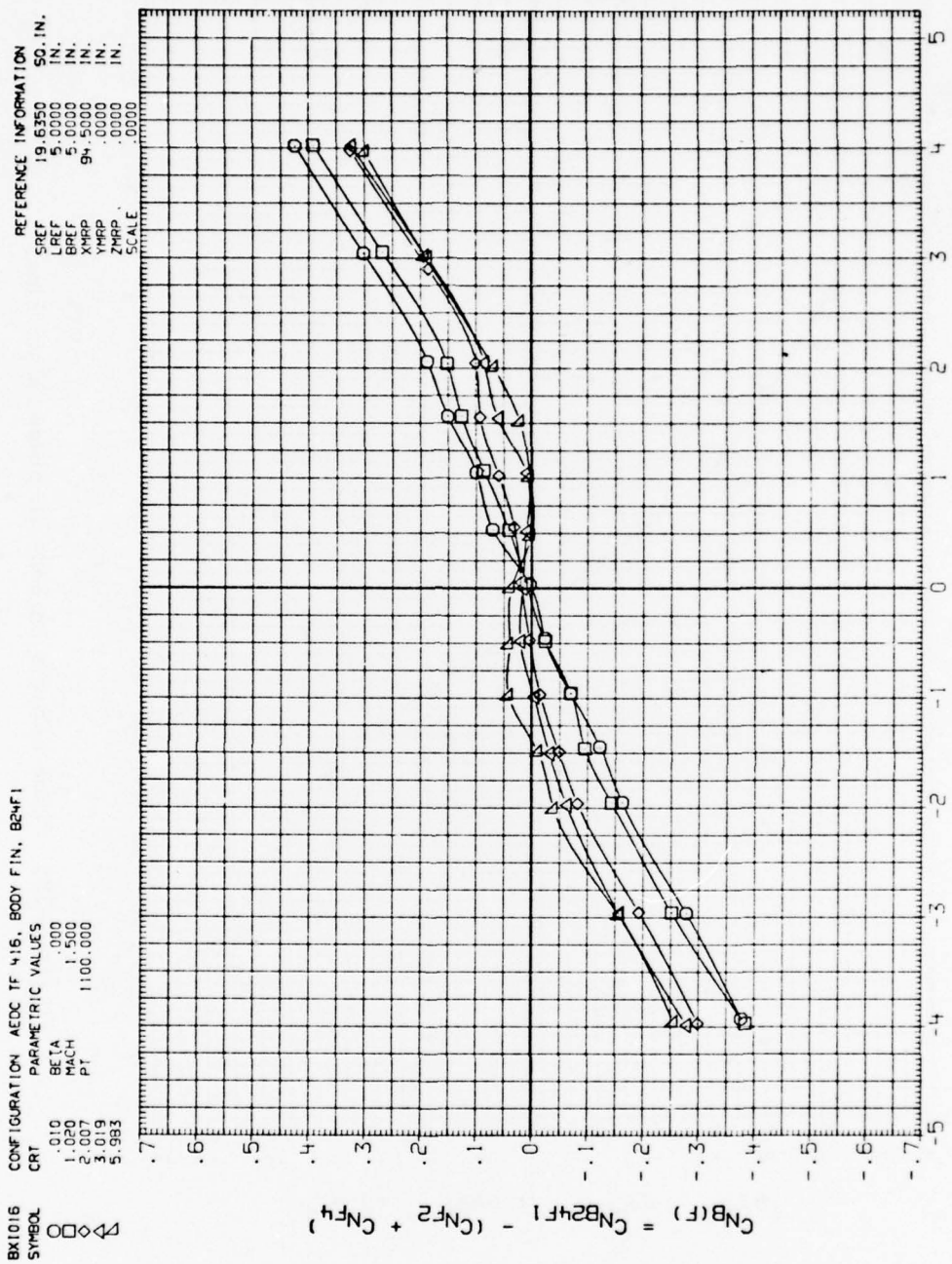

Figure A-79. Plume effects on body in presence of fins.

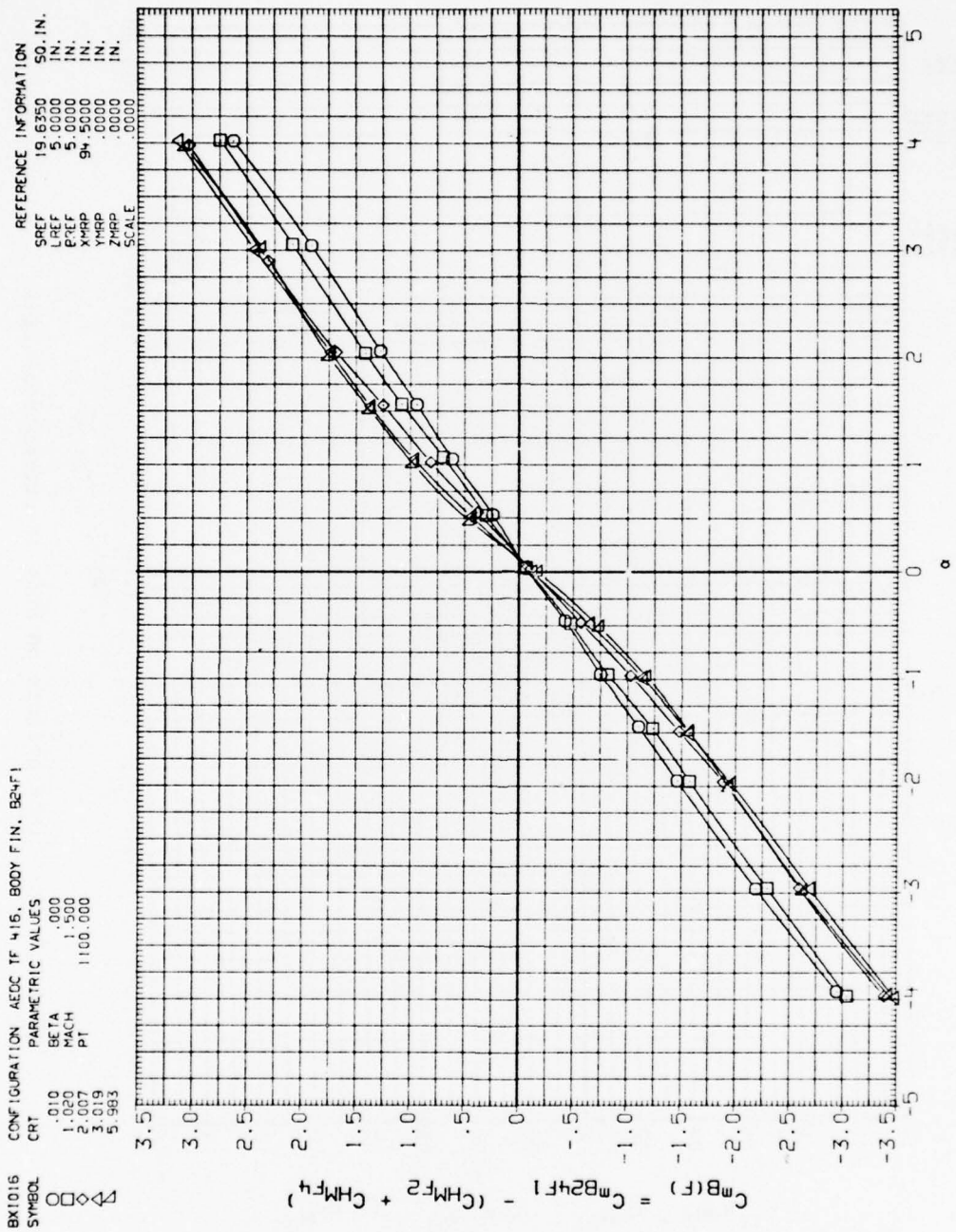

Figure A-80. Plume effects on body in presence of fins.

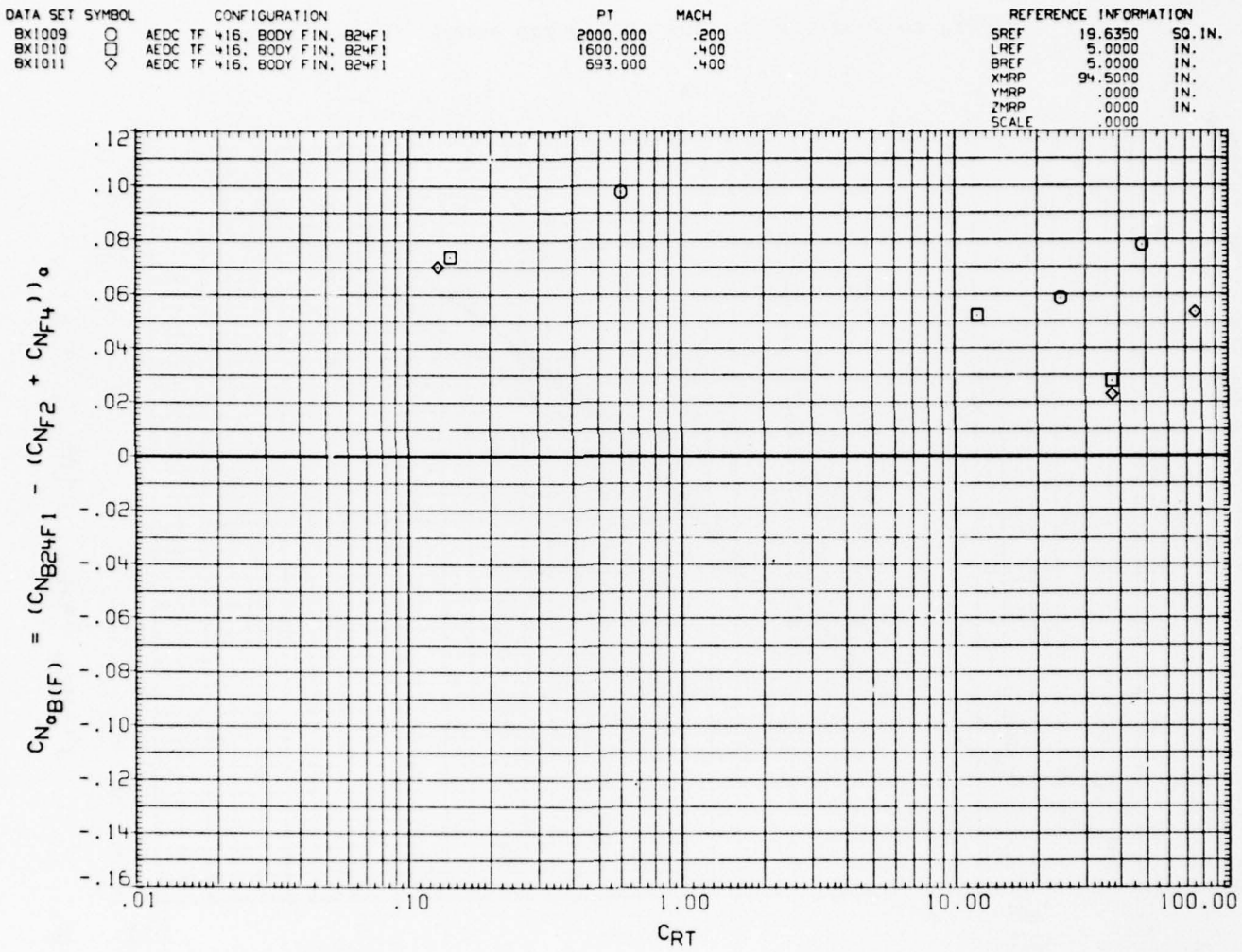

Figure A-81. Plume effects on body in presence of fins.

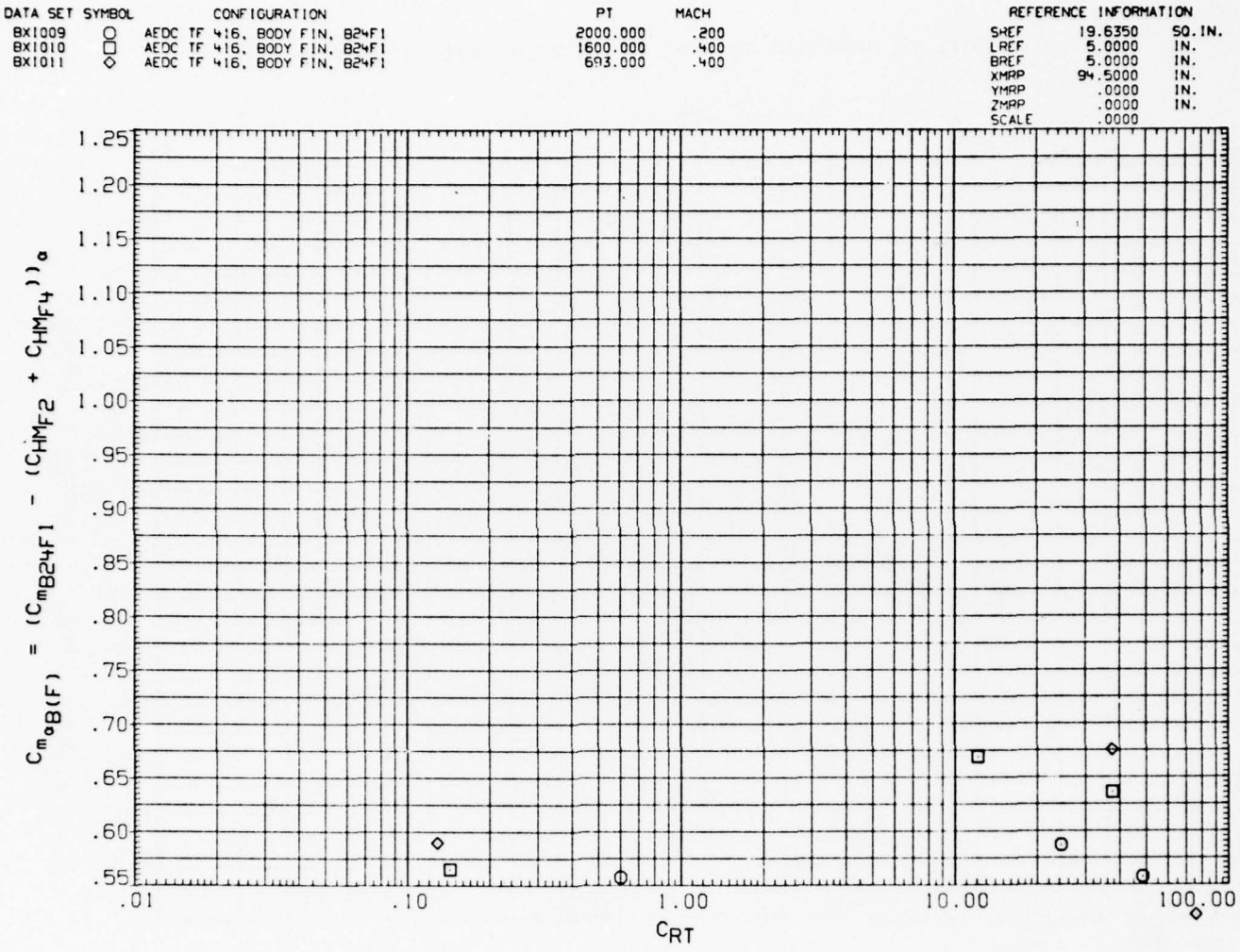

Figure A-82. Plume effects on body in presence of fins.

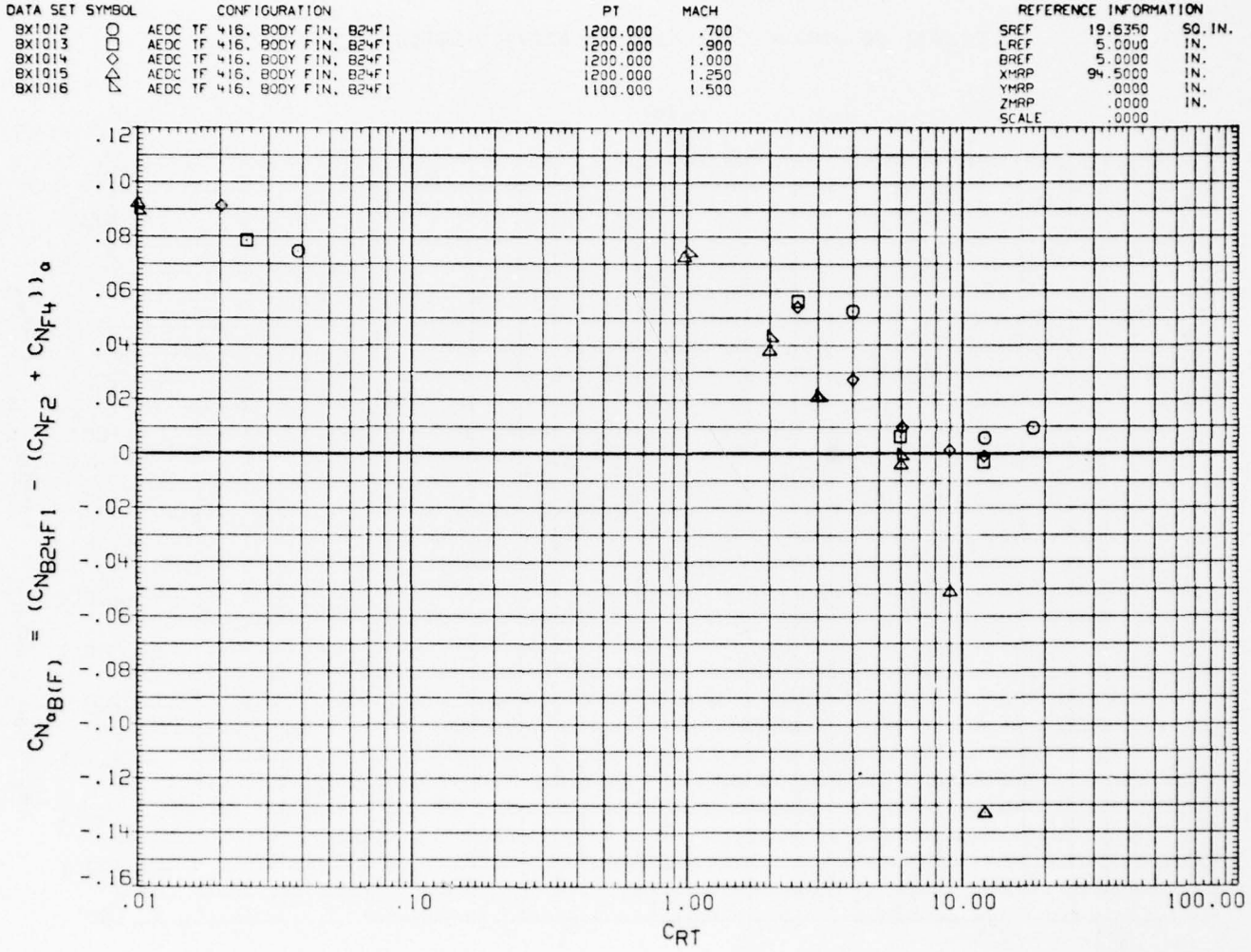

Figure A-83. Plume effects on body in presence of fins.

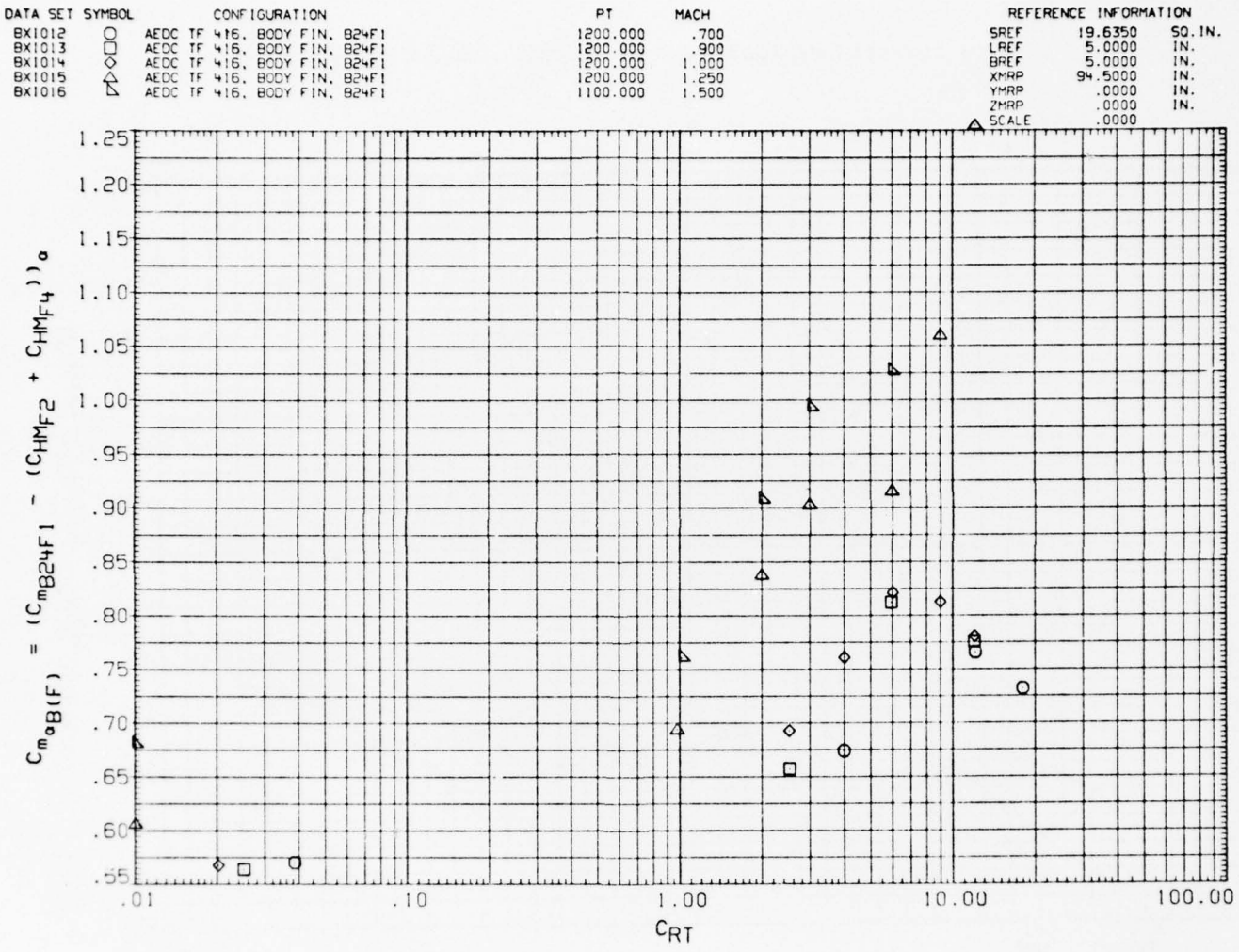

Figure A-84. Plume effects on body in presence of fins.

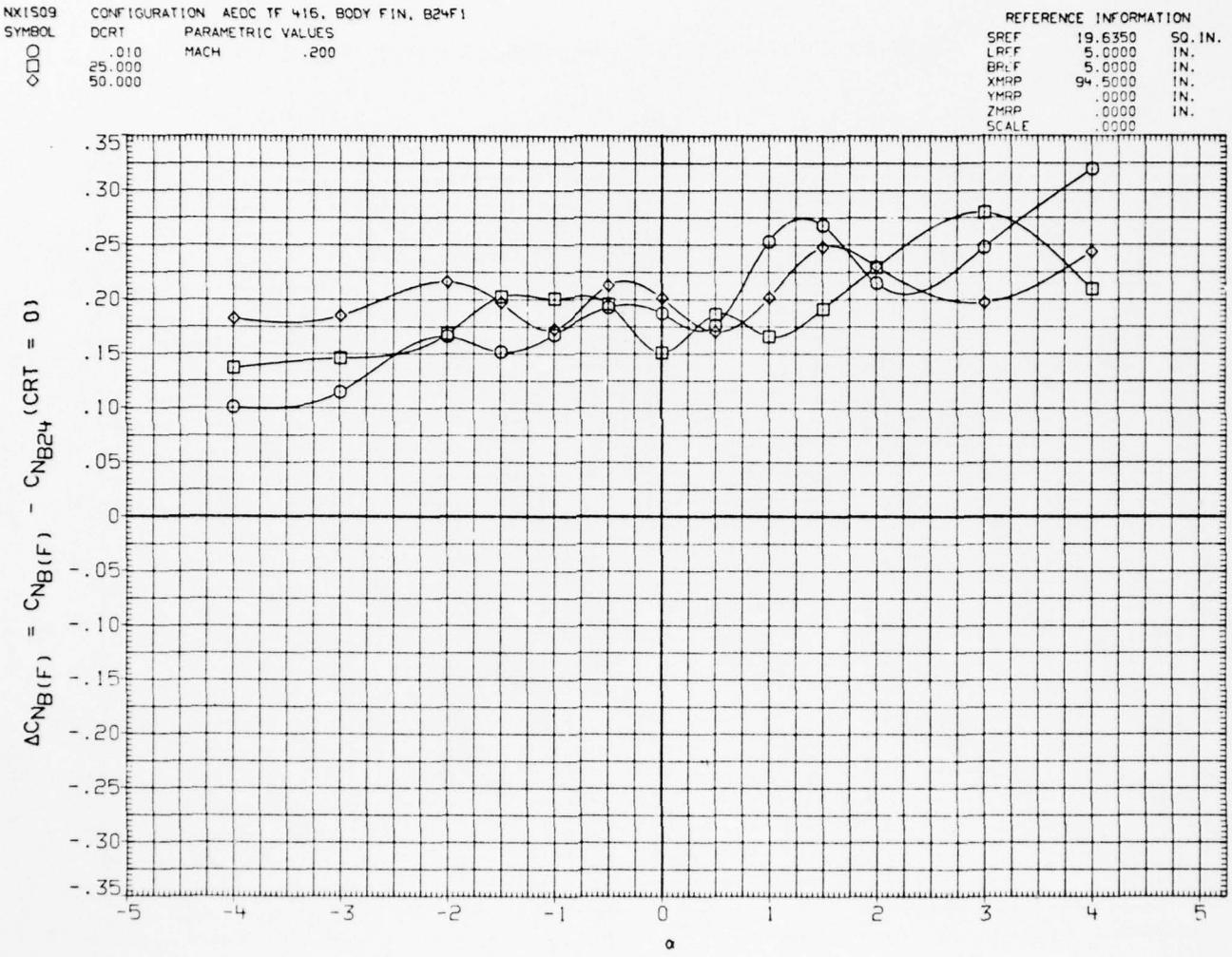

Figure A-85. Plume effects on afterbody in presence of fins.

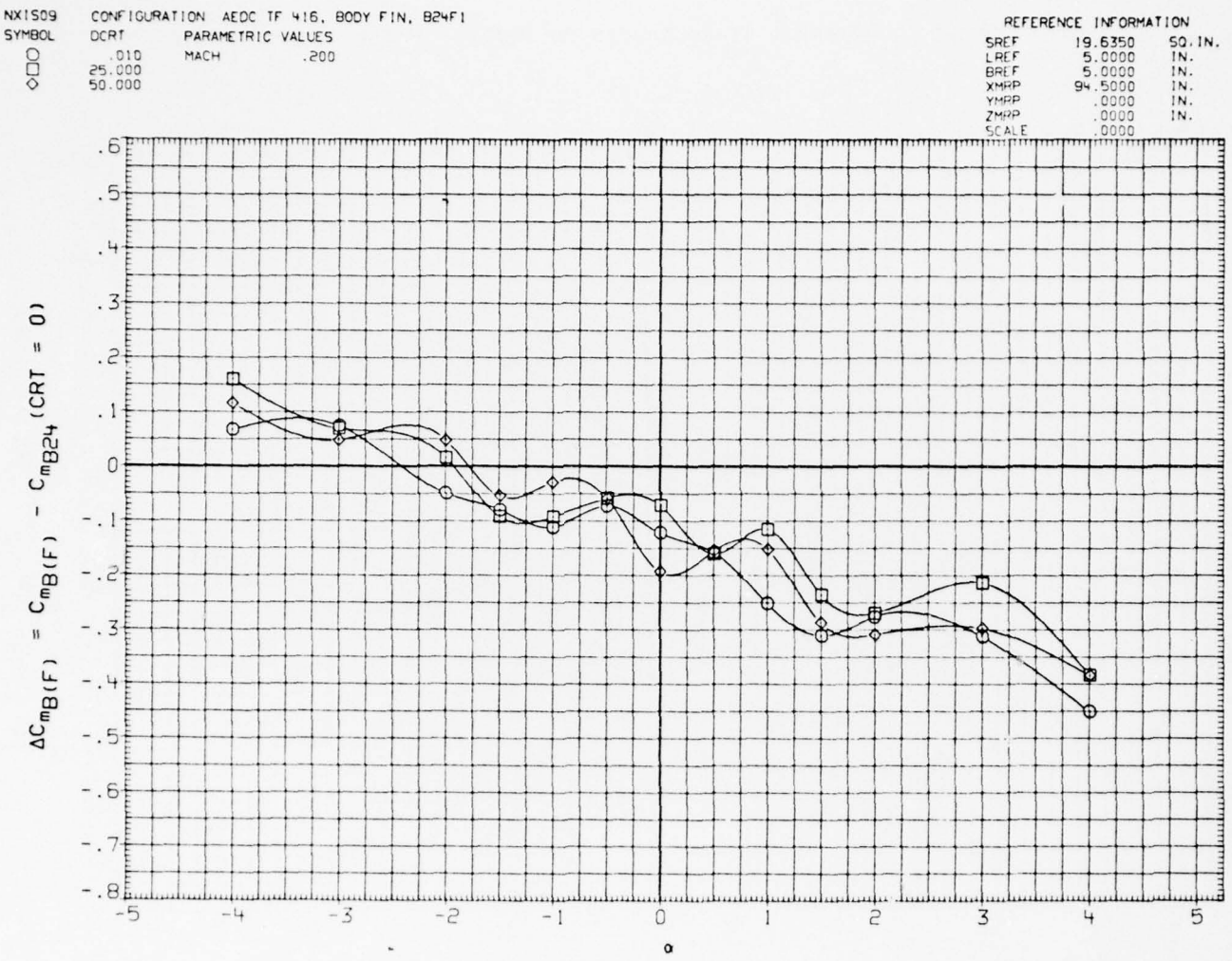

Figure A-86. Plume effects on afterbody in presence of fins.

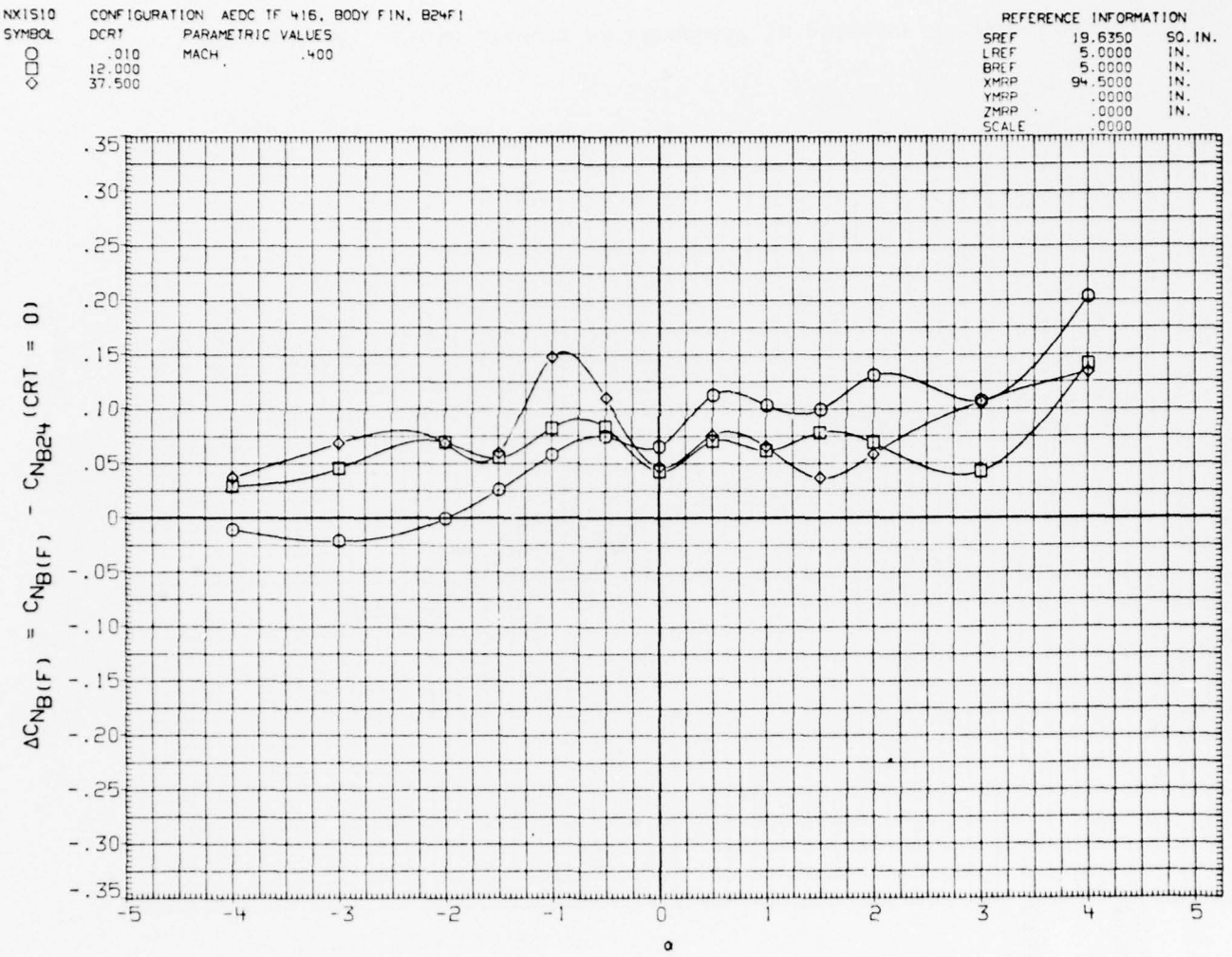

Figure A-87. Plume effects on afterbody in presence of fins.

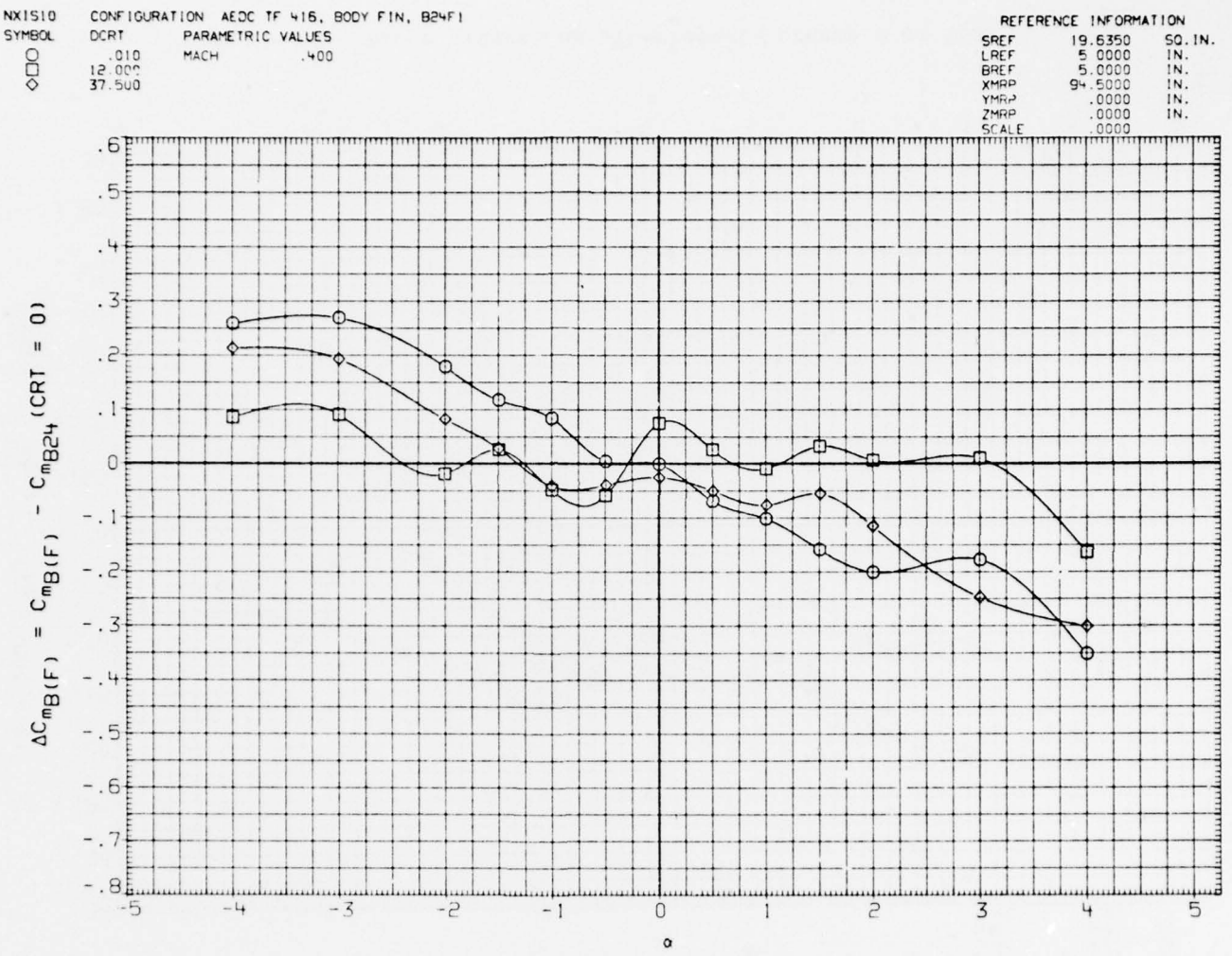

Figure A-88. Plume effects on afterbody in presence of fins.

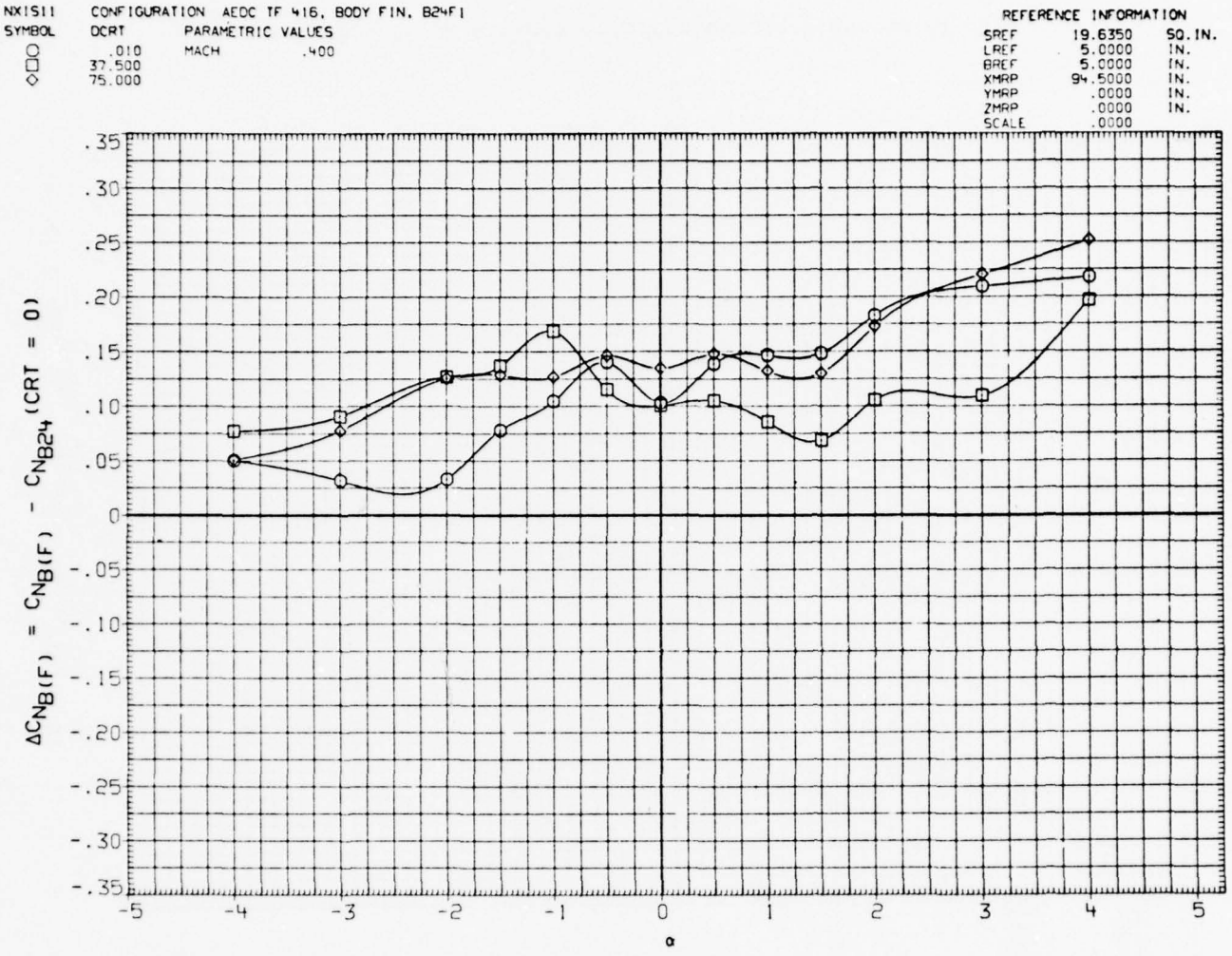

Figure A-89. Plume effects on afterbody in presence of fins.

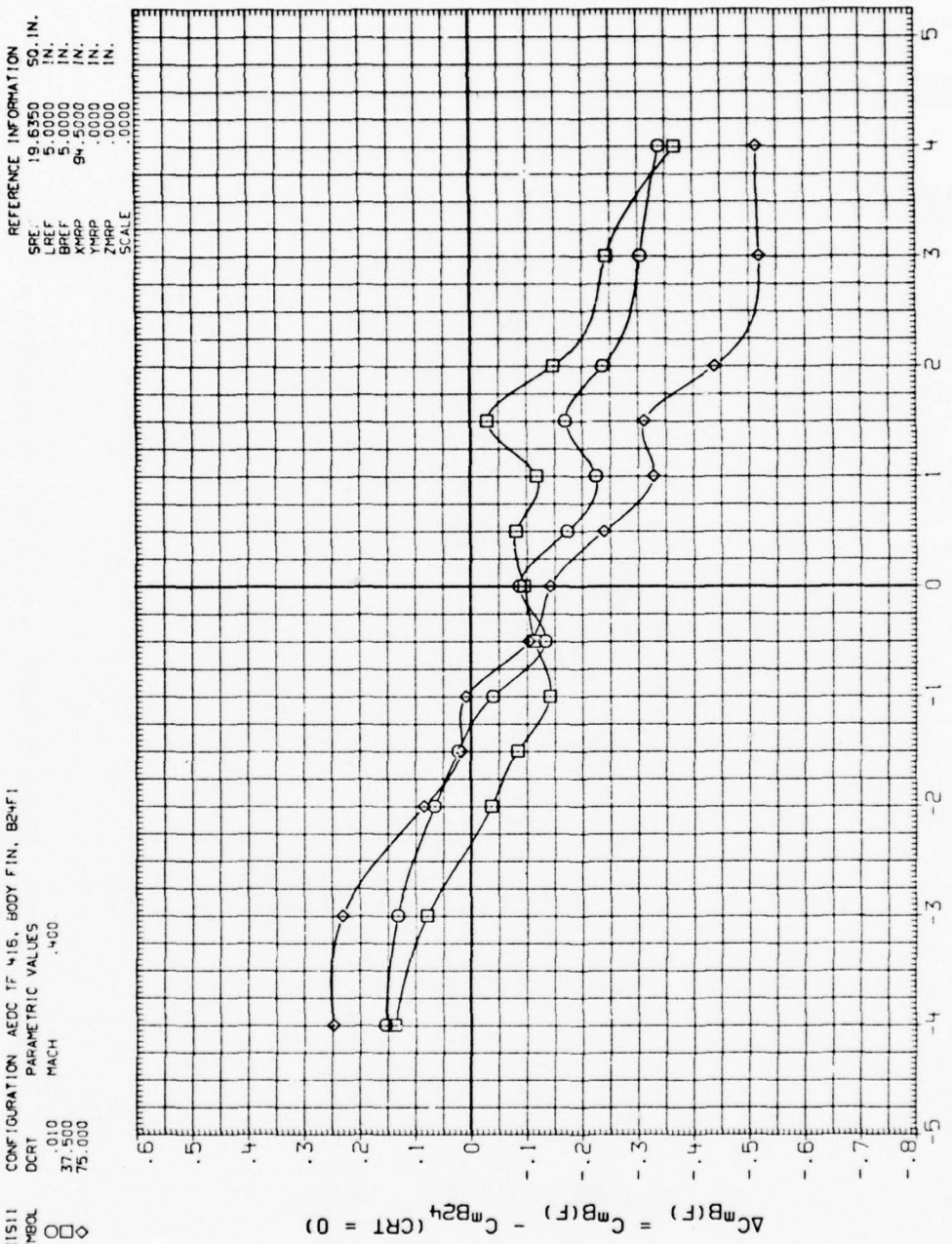

Figure A-90. Plume effects on afterbody in presence of fins.

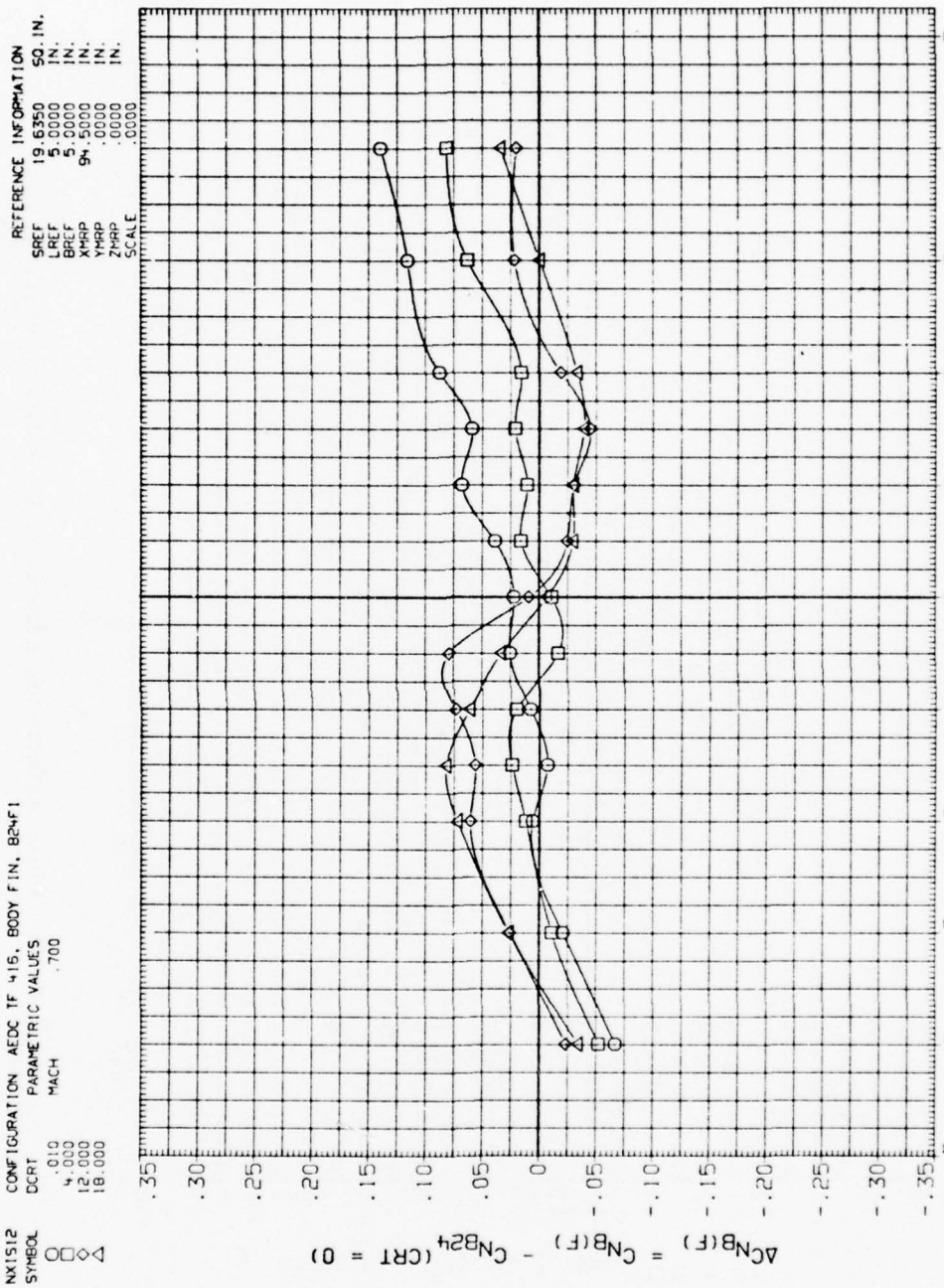

Figure A-91. Plume effects on afterbody in presence of fins.

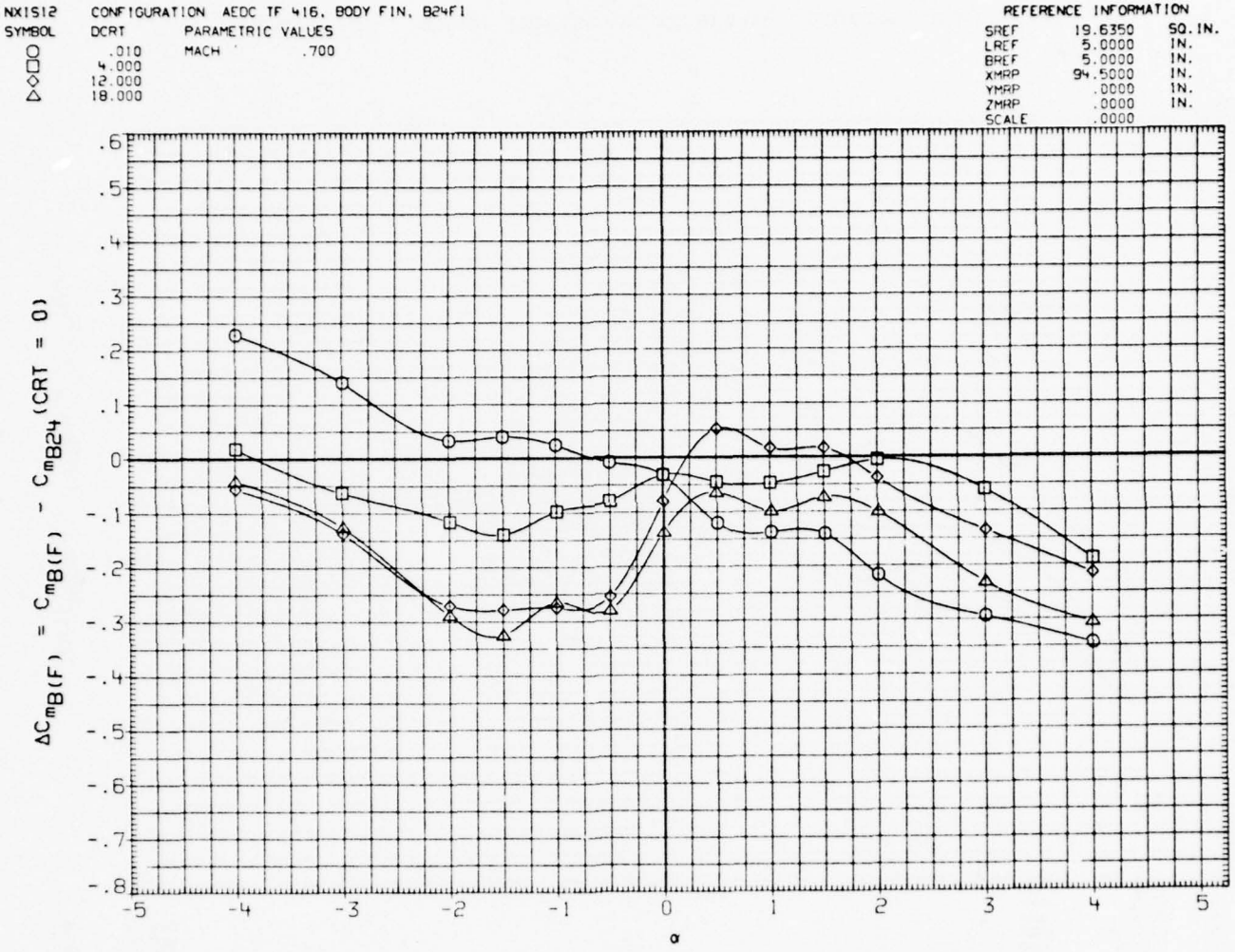

Figure A-92. Plume effects on afterbody in presence of fins.

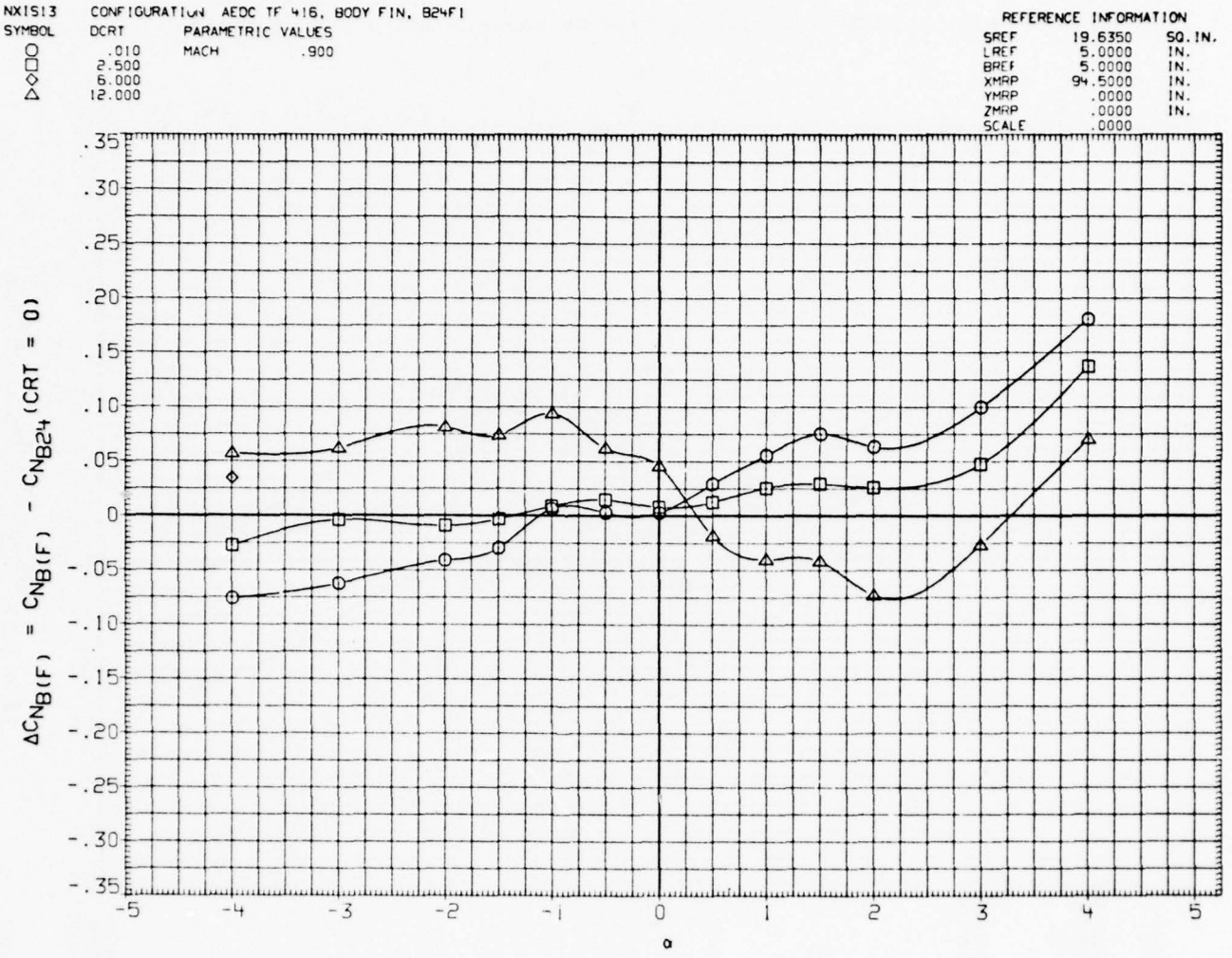

Figure A-93. Plume effects on afterbody in presence of fins.

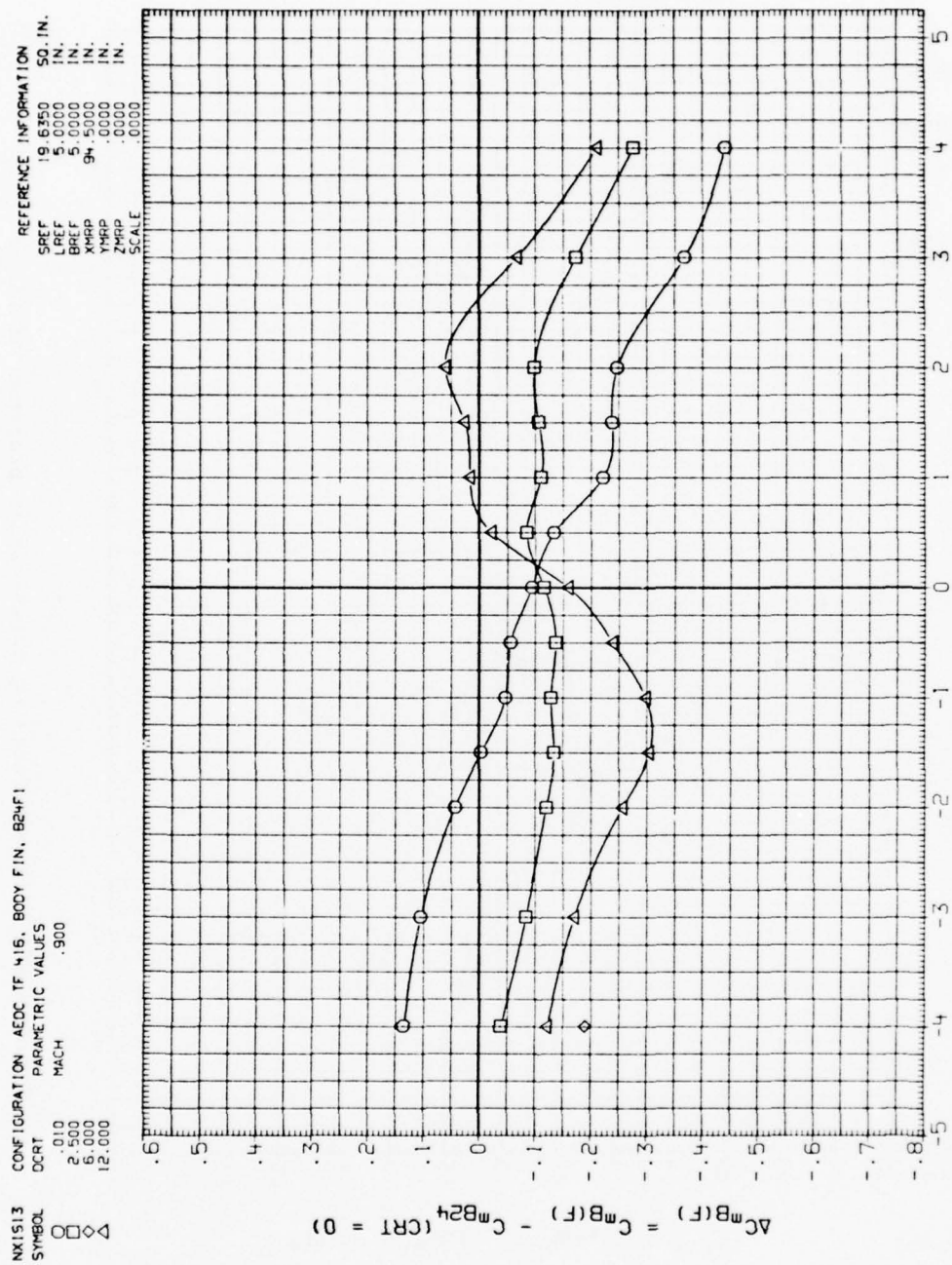

Figure A-94. Plume effects on afterbody in presence of fins.

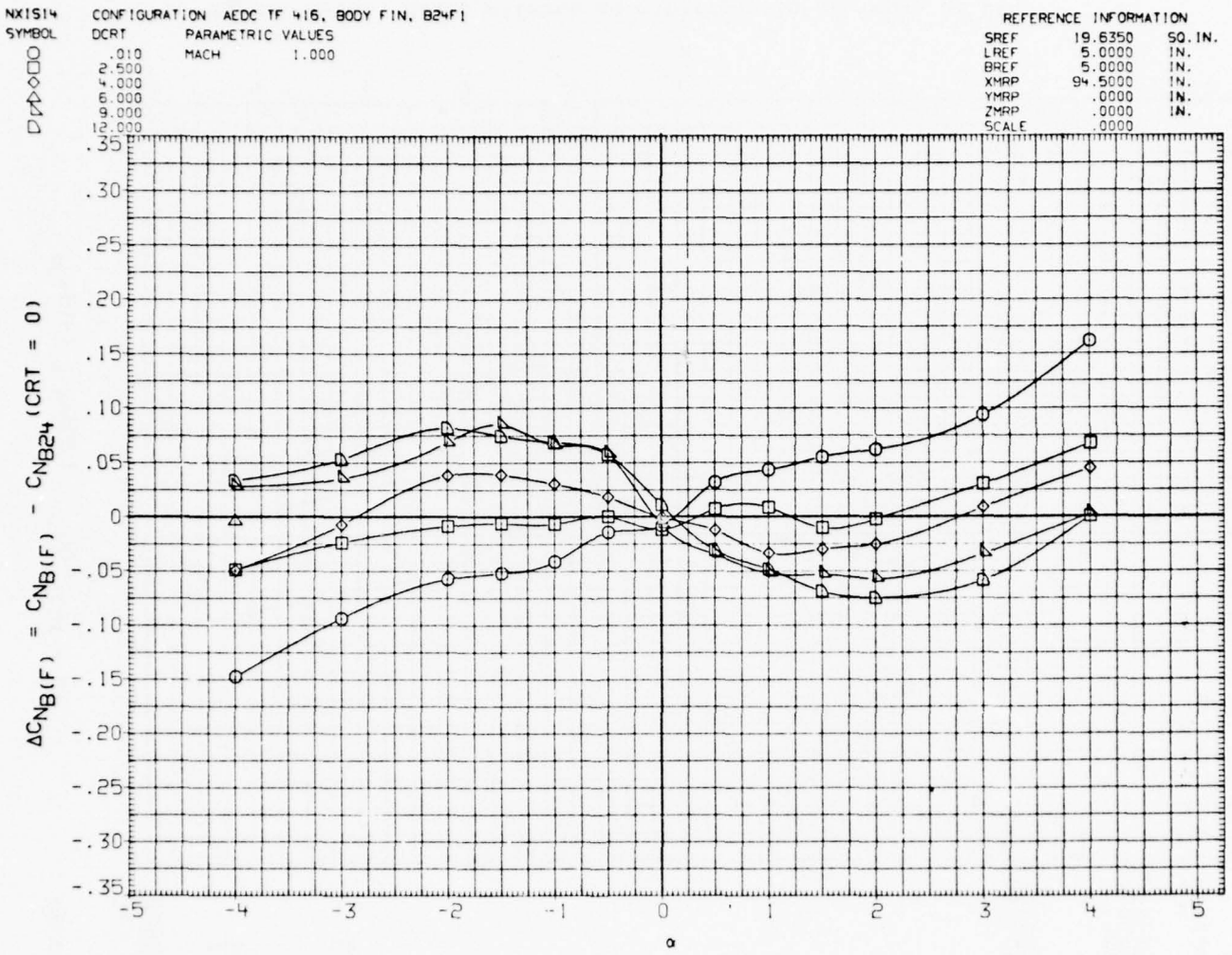

Figure A-95. Plume effects on afterbody in presence of fins.

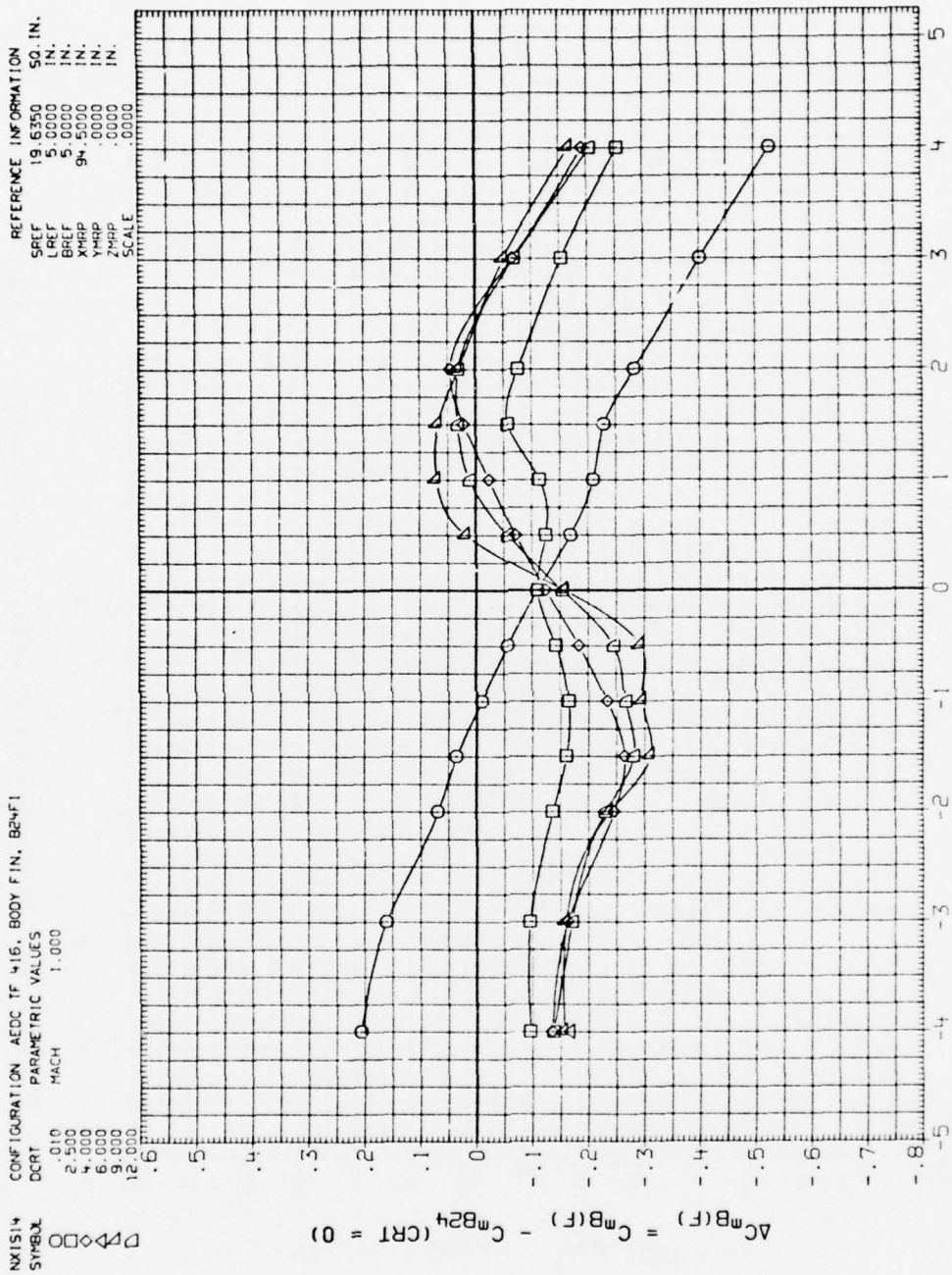

Figure A-96. Plume effects on afterbody in presence of fins.

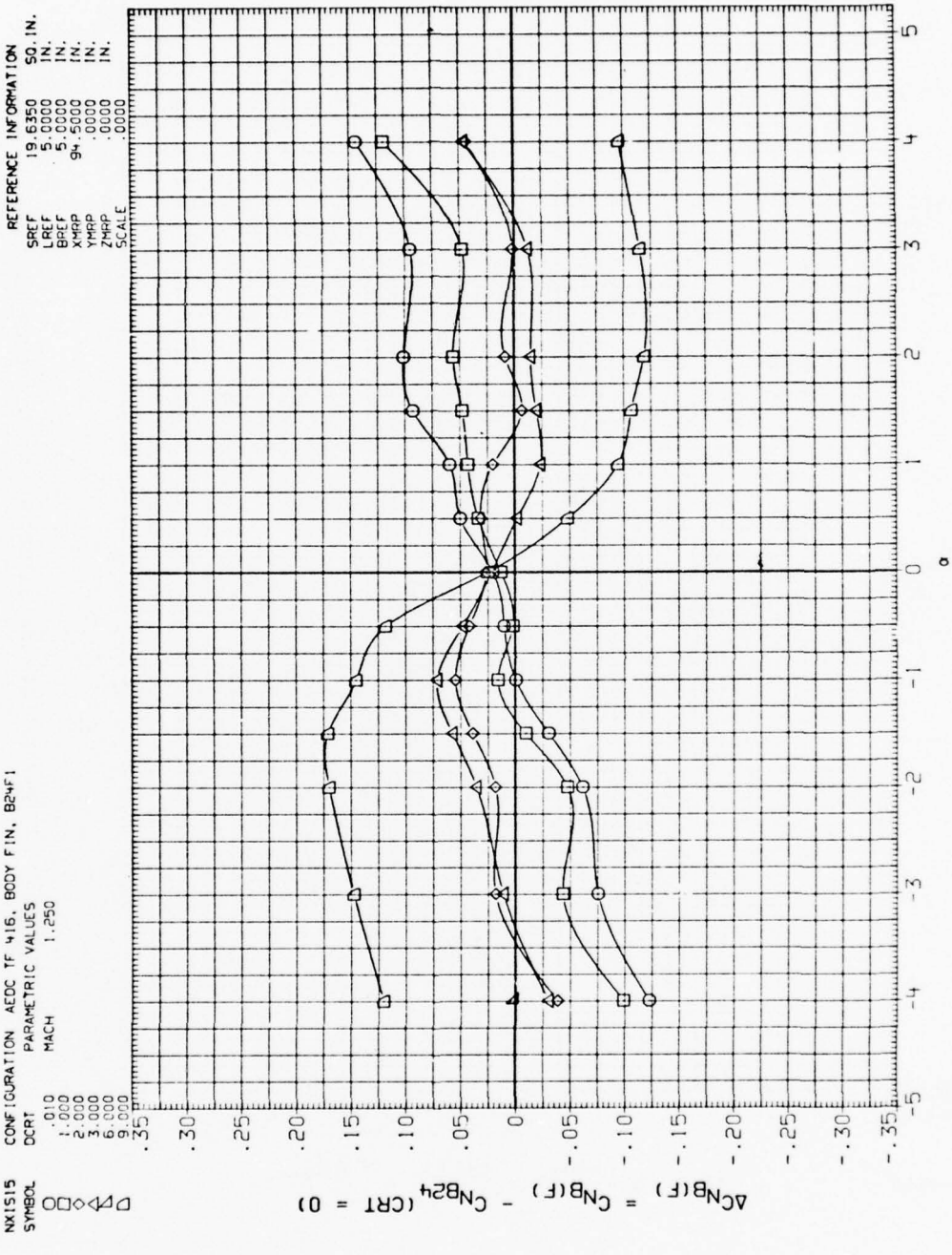

Figure A-97. Plume effects on afterbody in presence of fins.

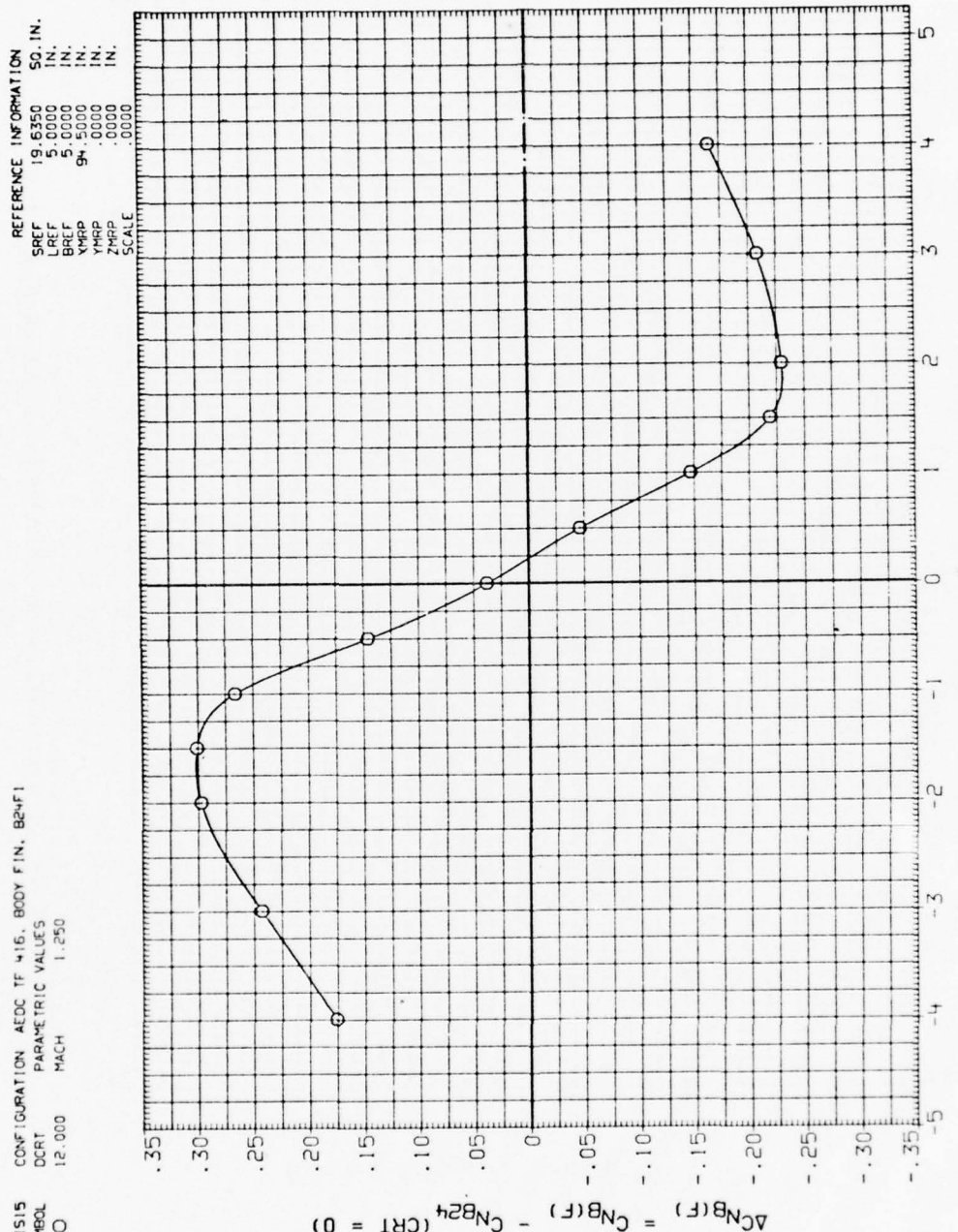

Figure A-98. Plume effects on afterbody in presence of fins.

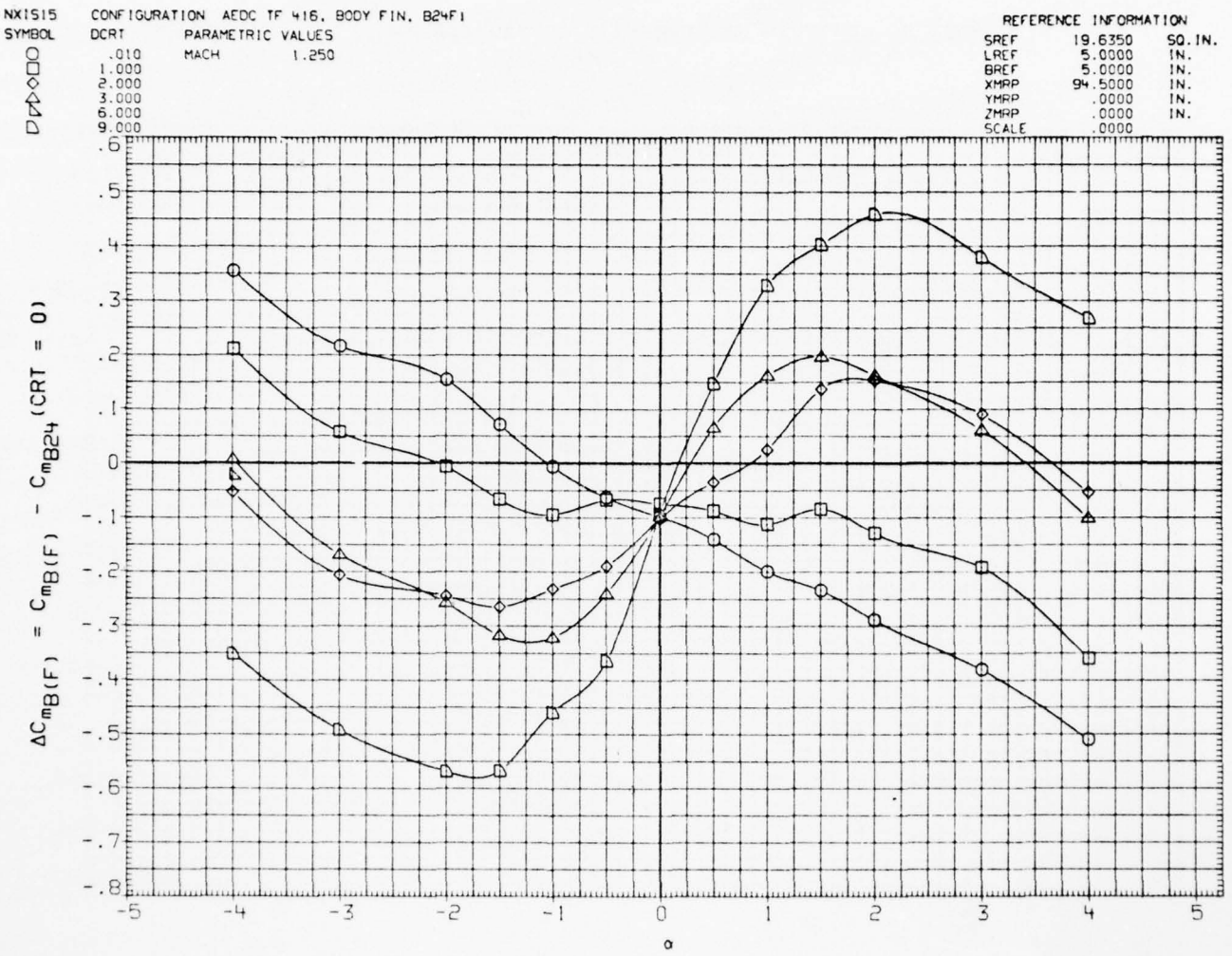

Figure A-99. Plume effects on afterbody in presence of fins.

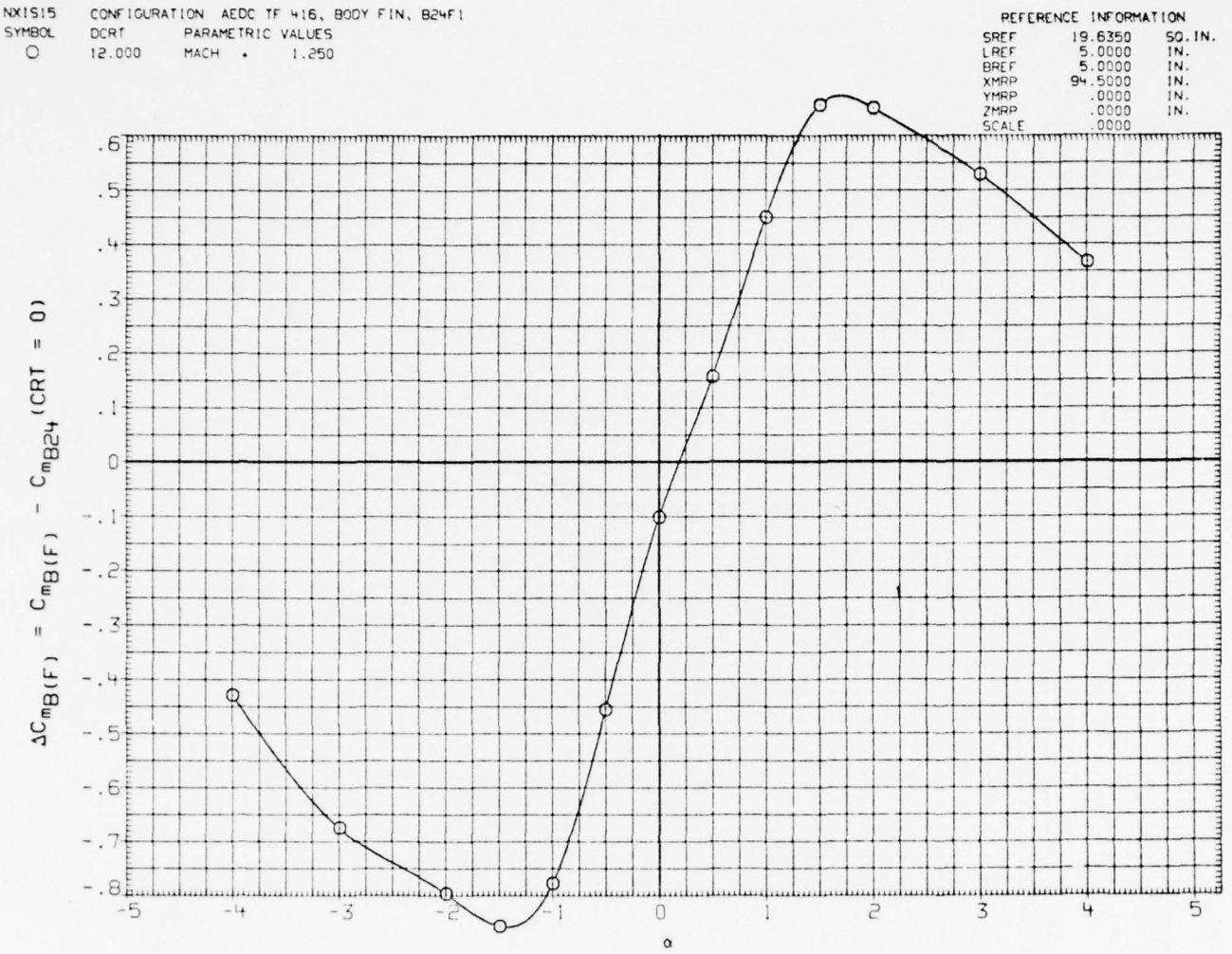

Figure A-100. Plume effects on afterbody in presence of fins.

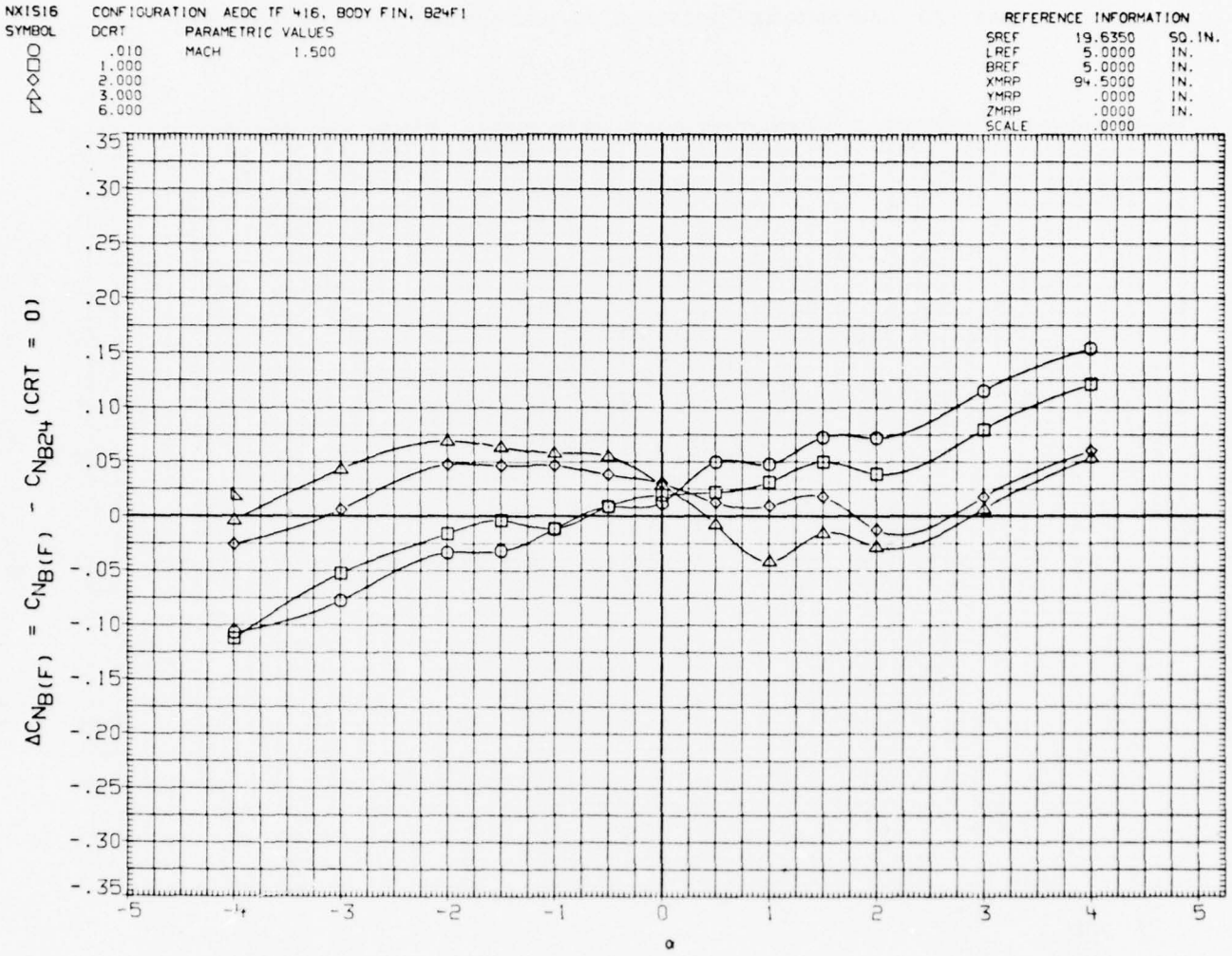

Figure A-101. Plume effects on afterbody in presence of fins.

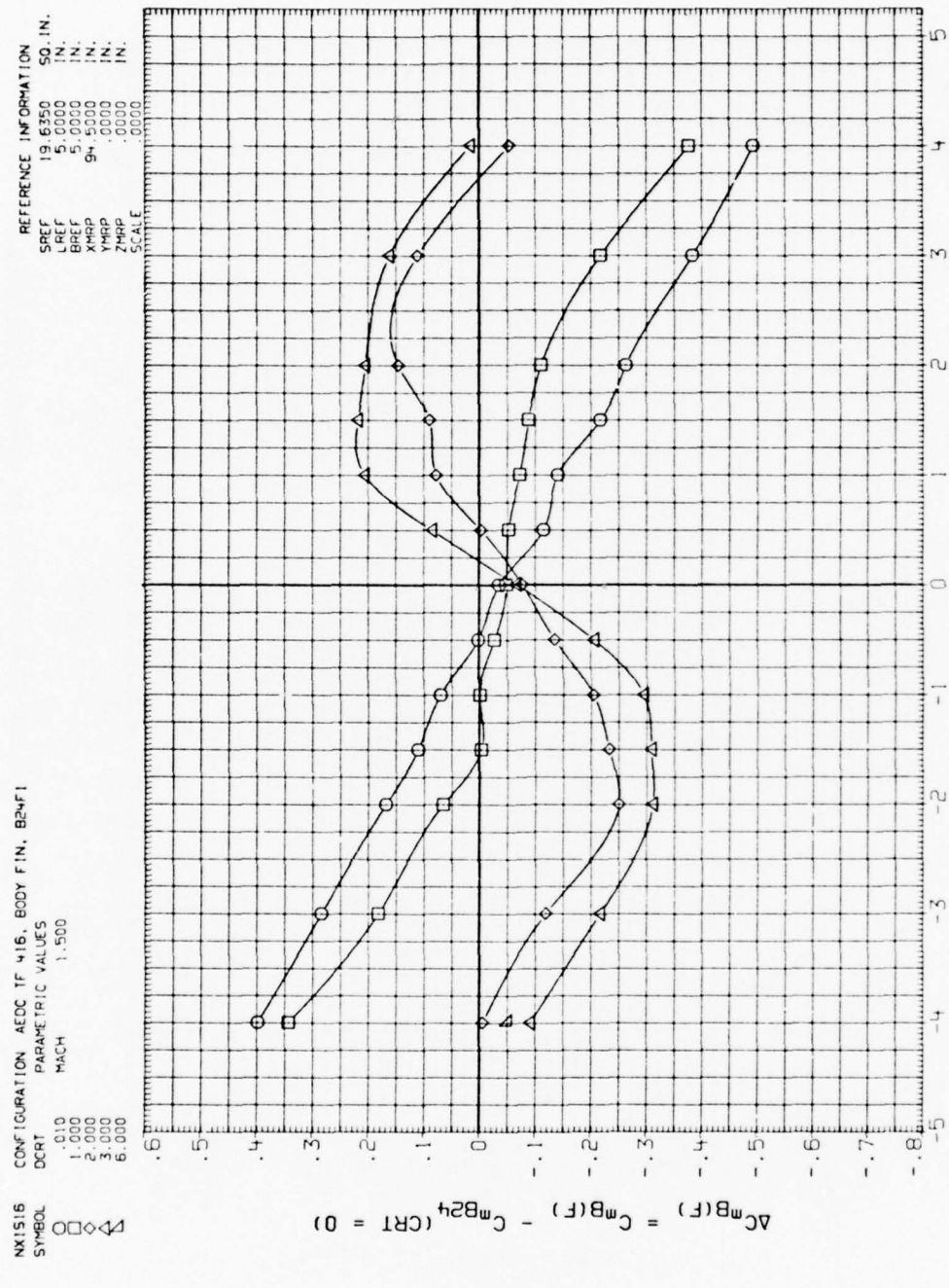

Figure A-102. Plume effects on afterbody in presence of fins.

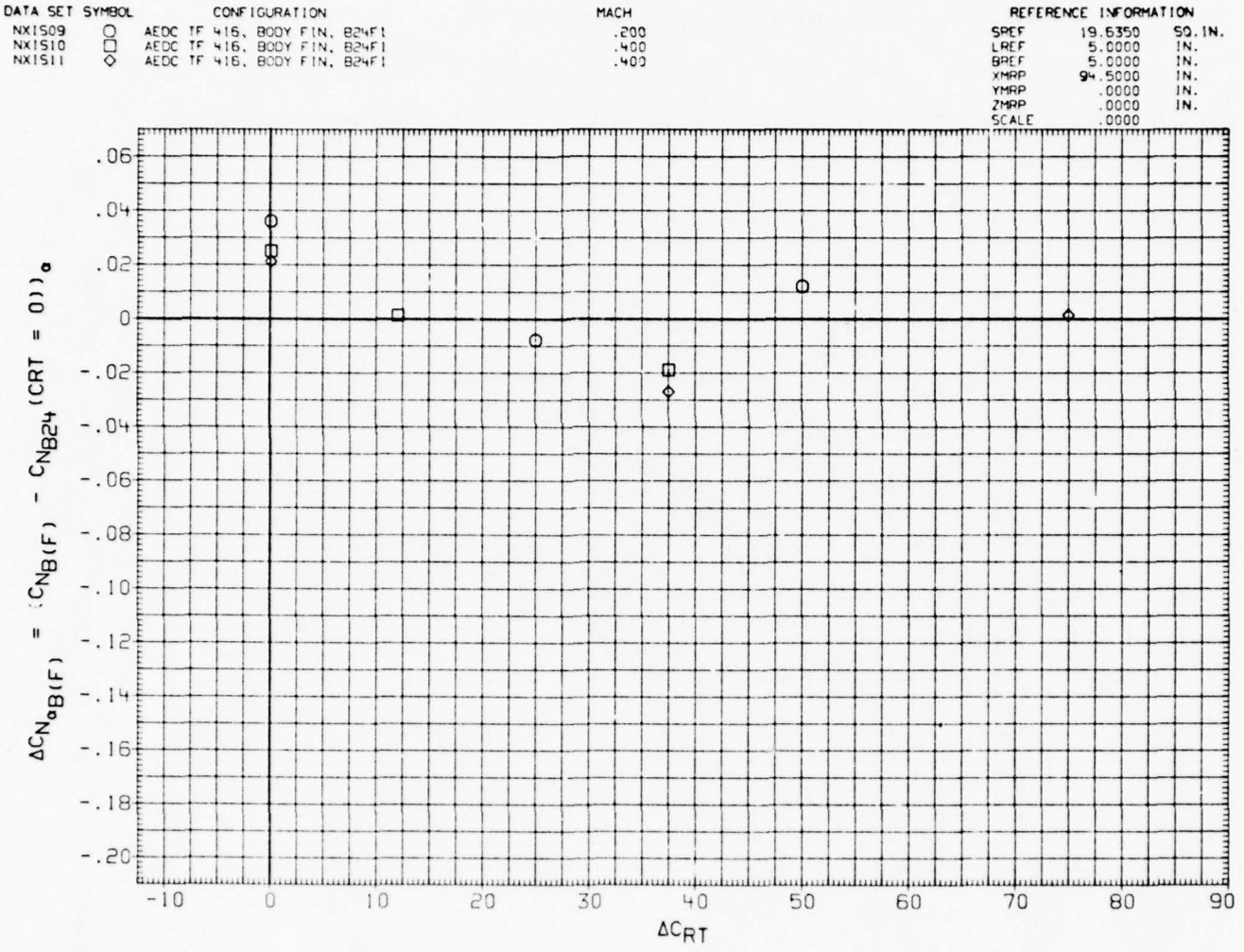

Figure A-103. Plume effects on afterbody in presence of fins.

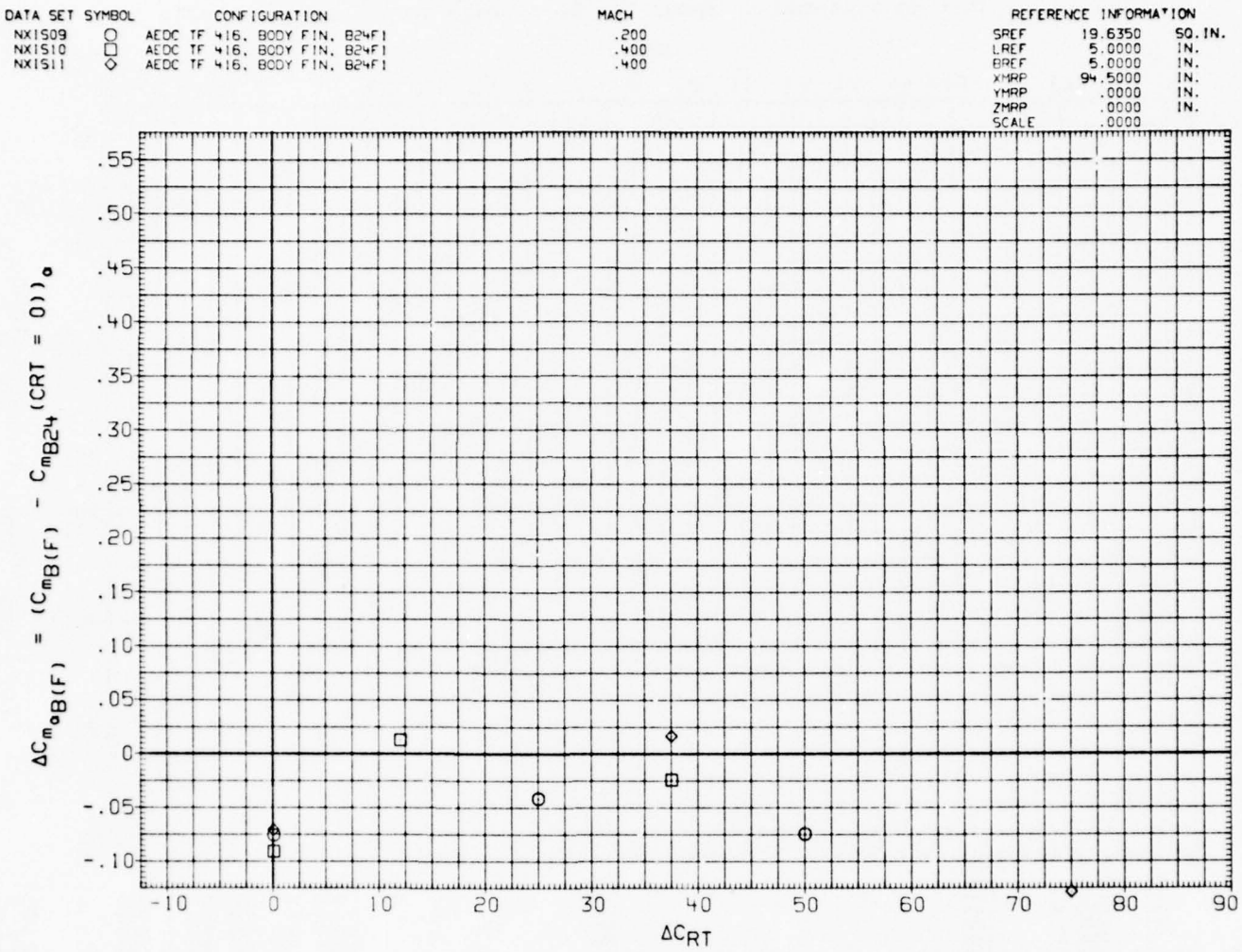

Figure A-104. Plume effects on afterbody in presence of fins.

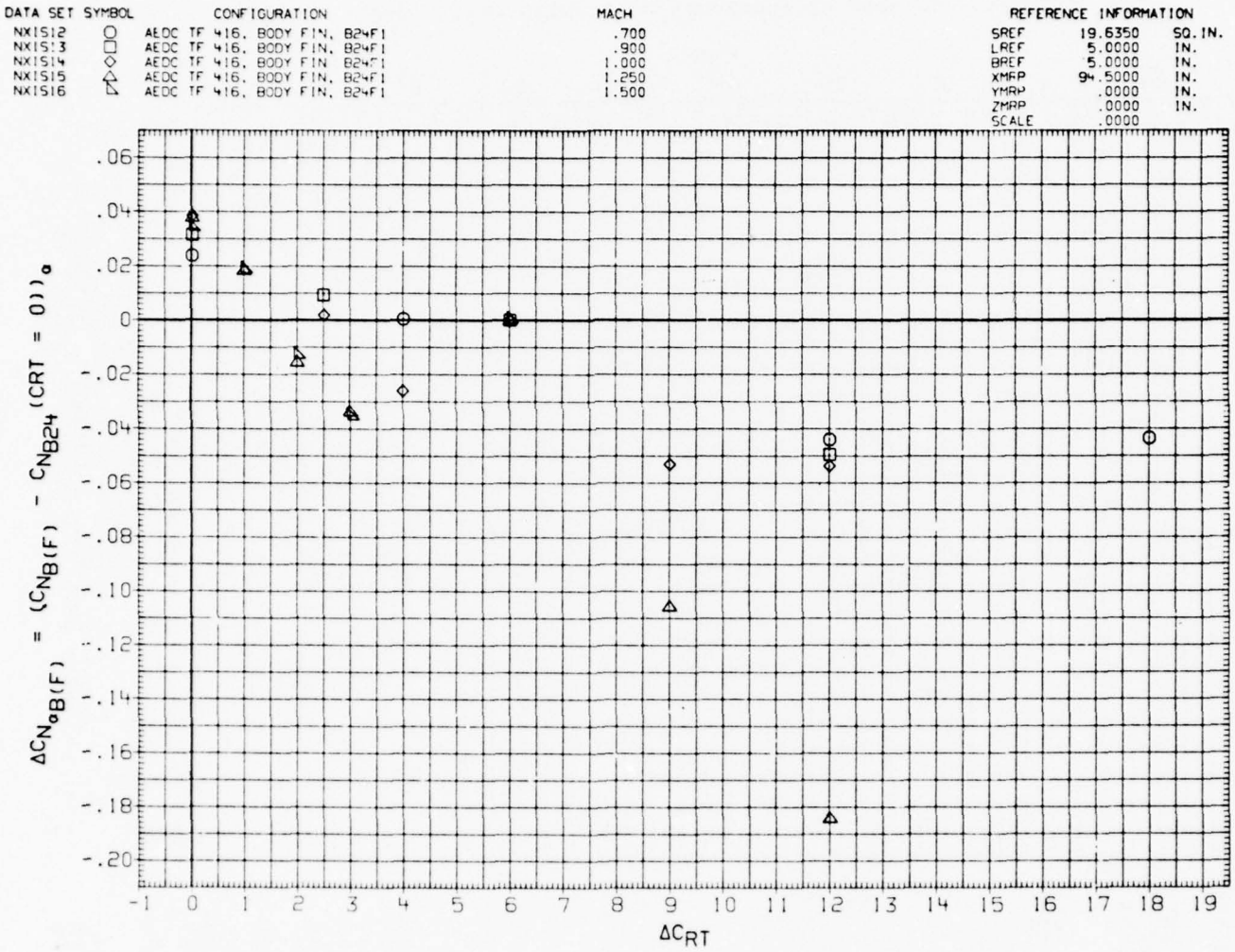

Figure A-105. Plume effects on afterbody in presence of fins.

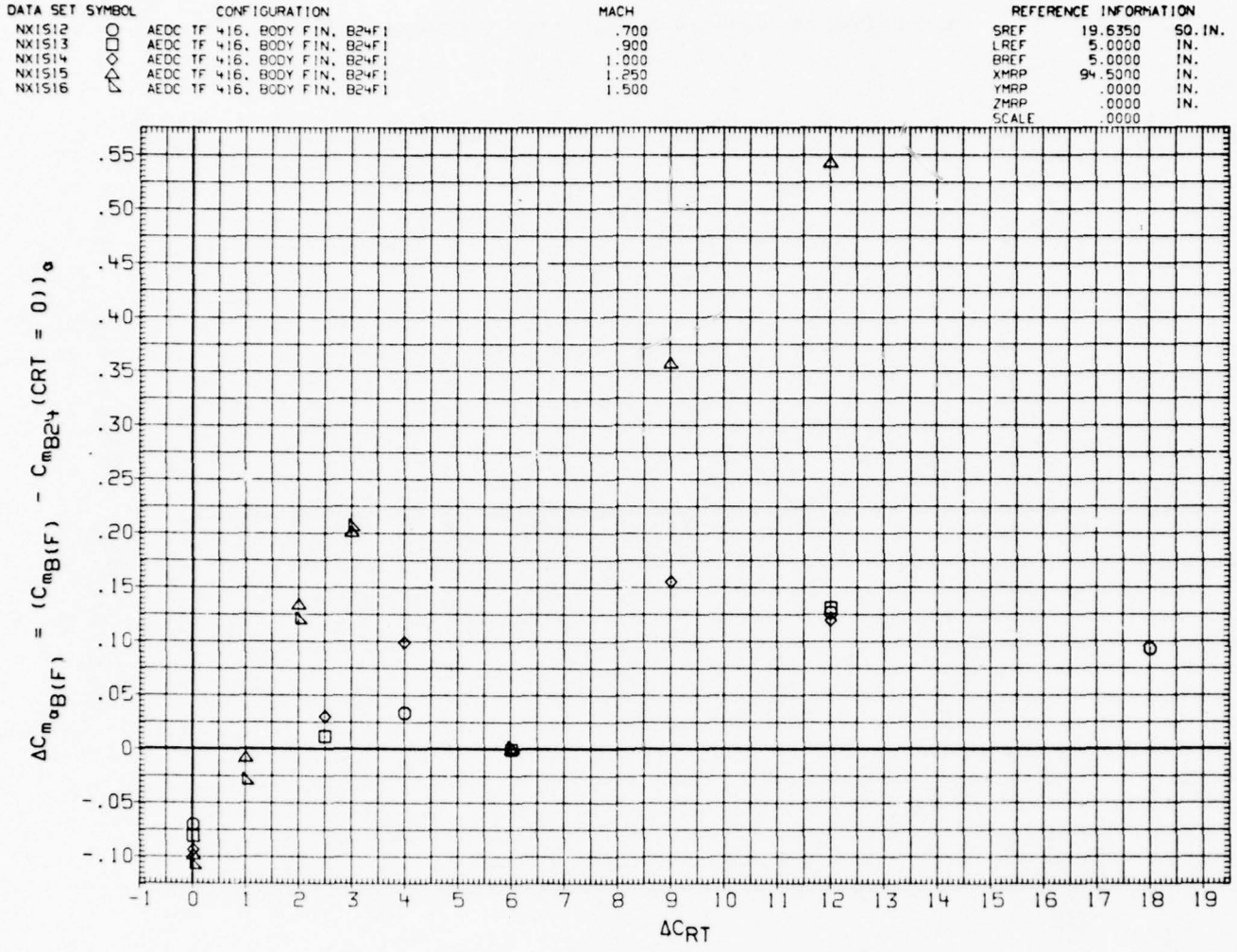

Figure A-106. - Plume effects on afterbody in presence of fins.

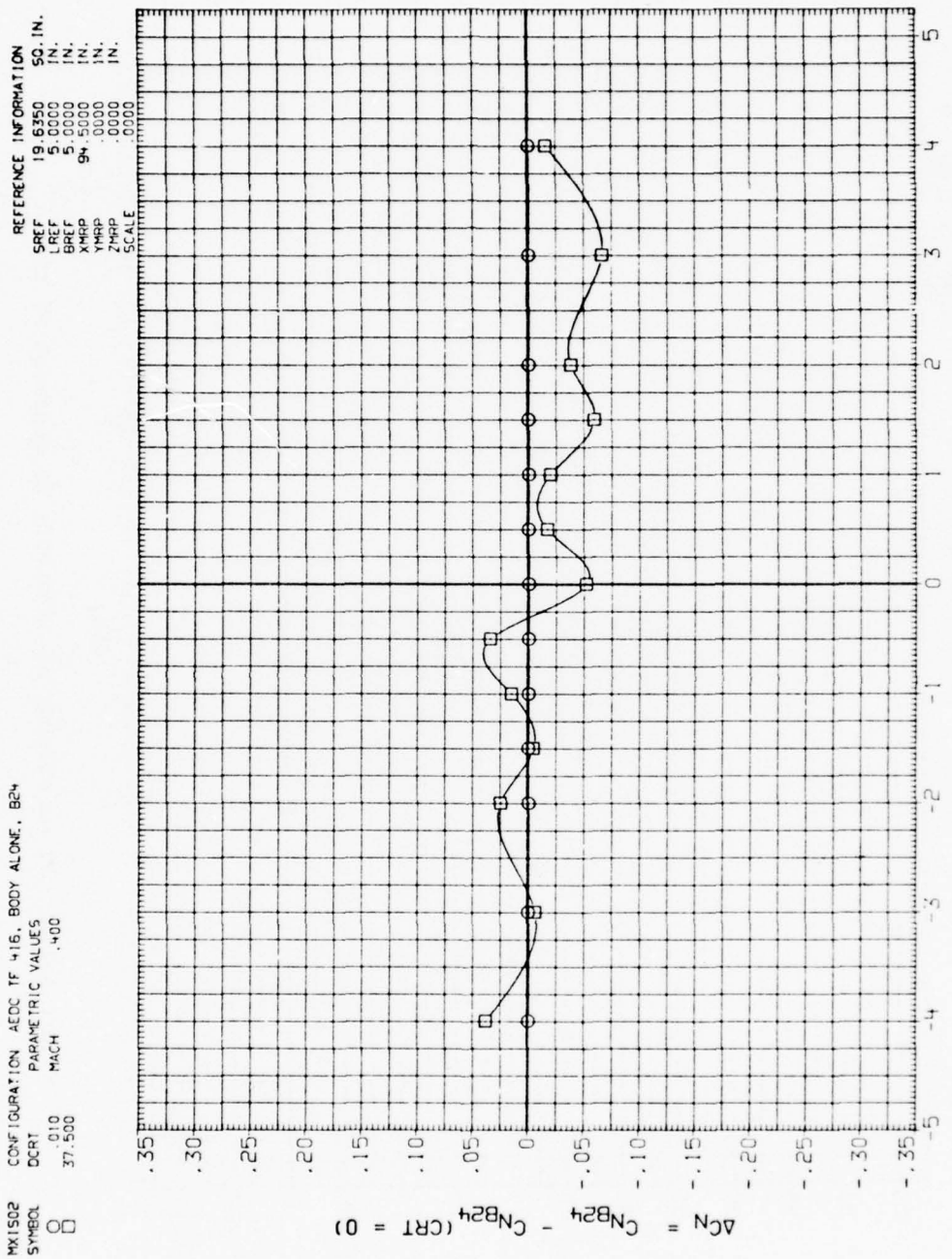

Figure A-107. Plume effects on body alone.

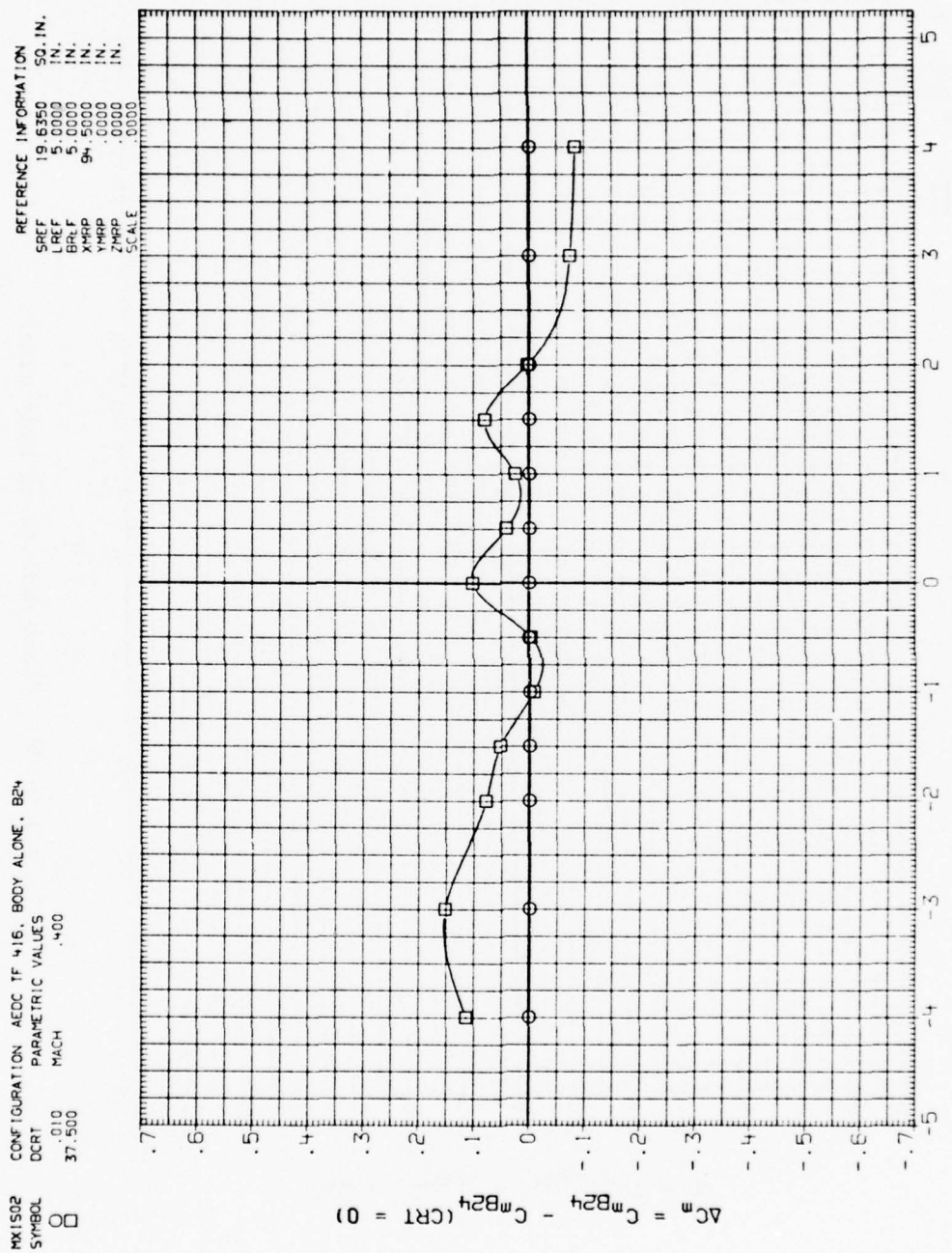

Figure A-108. Plume effects on body alone.

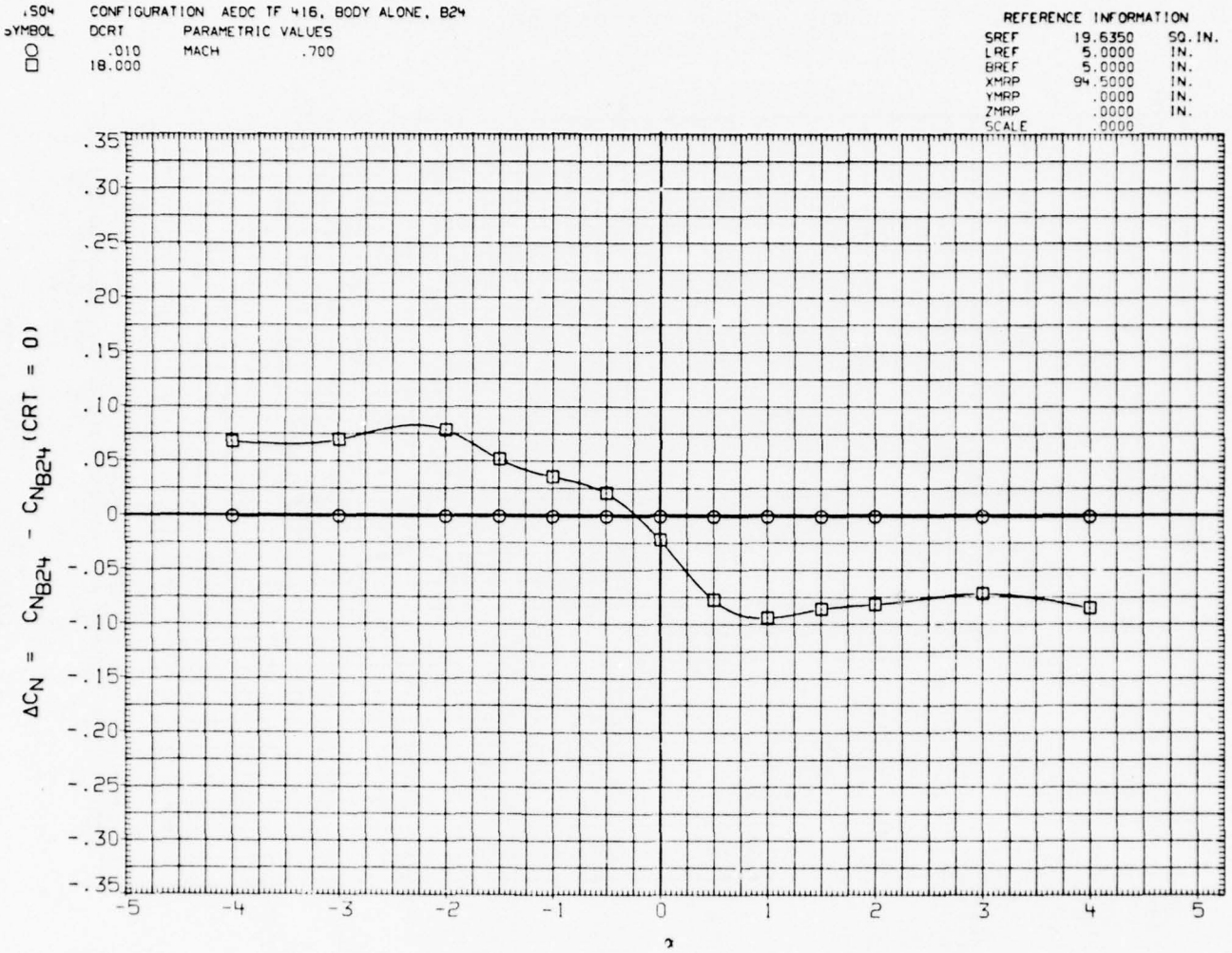

Figure A-109. Plume effects on body alone.

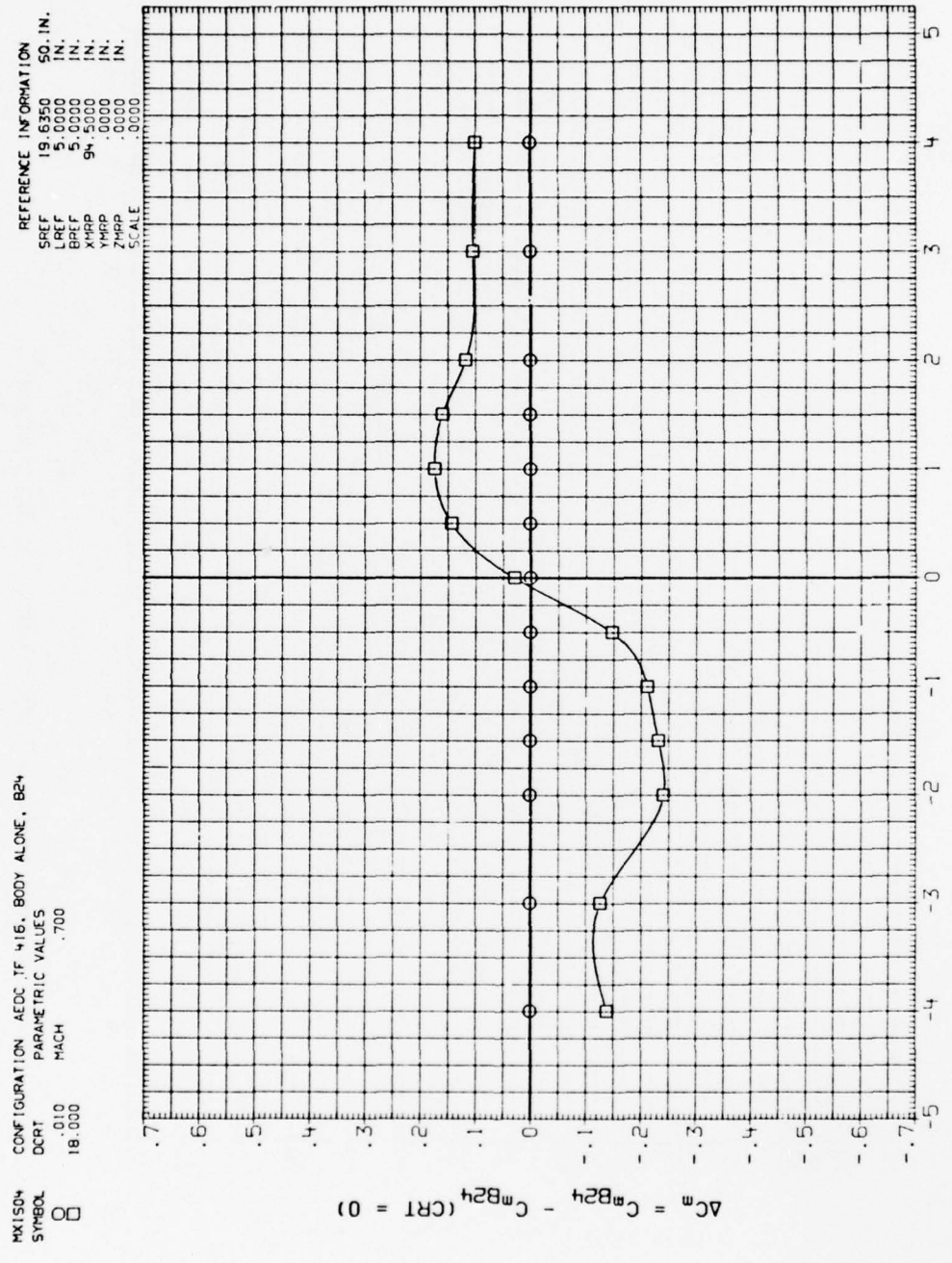

Figure A-110. Plume effects on body alone.

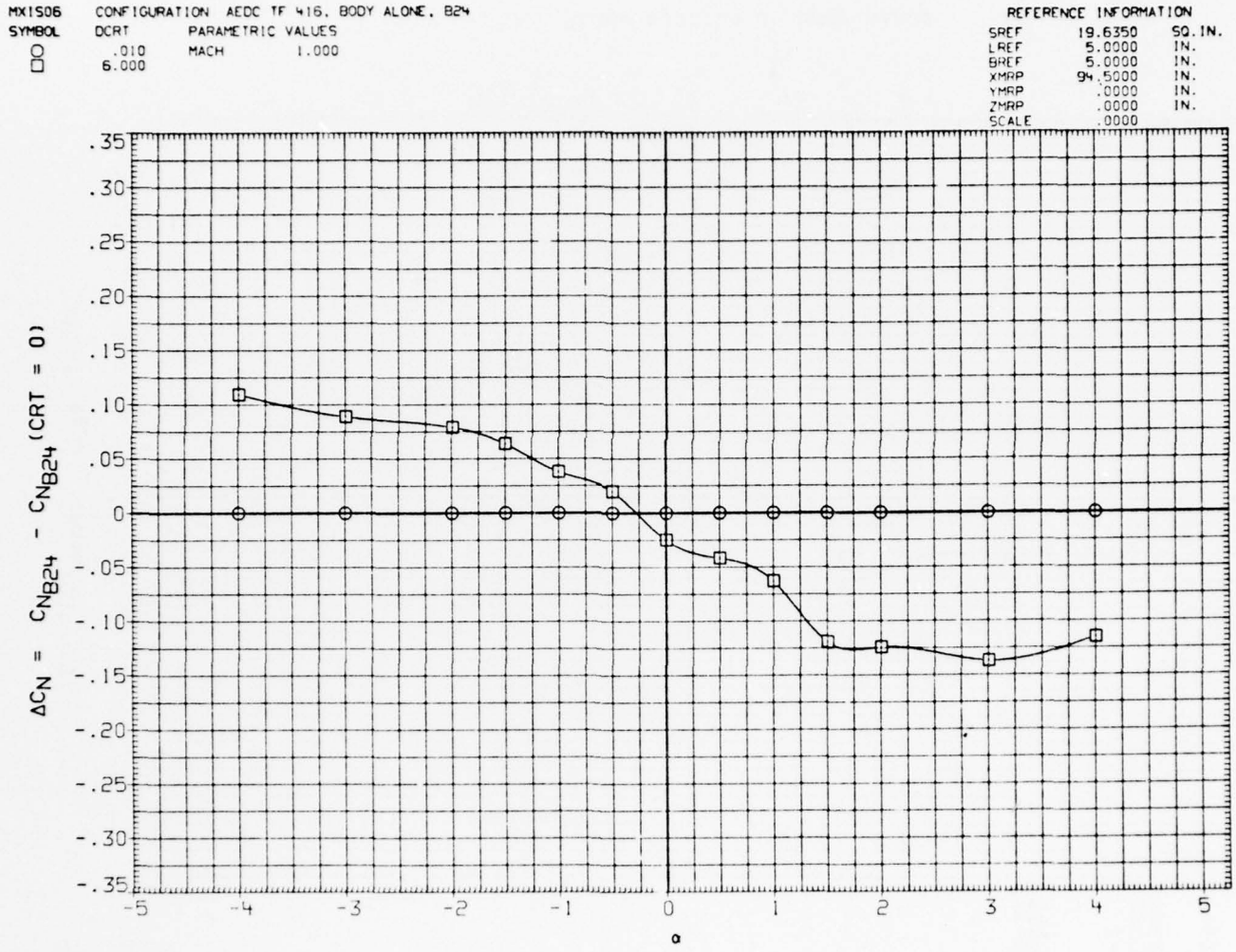

Figure A-111. Plume effects on body alone. .

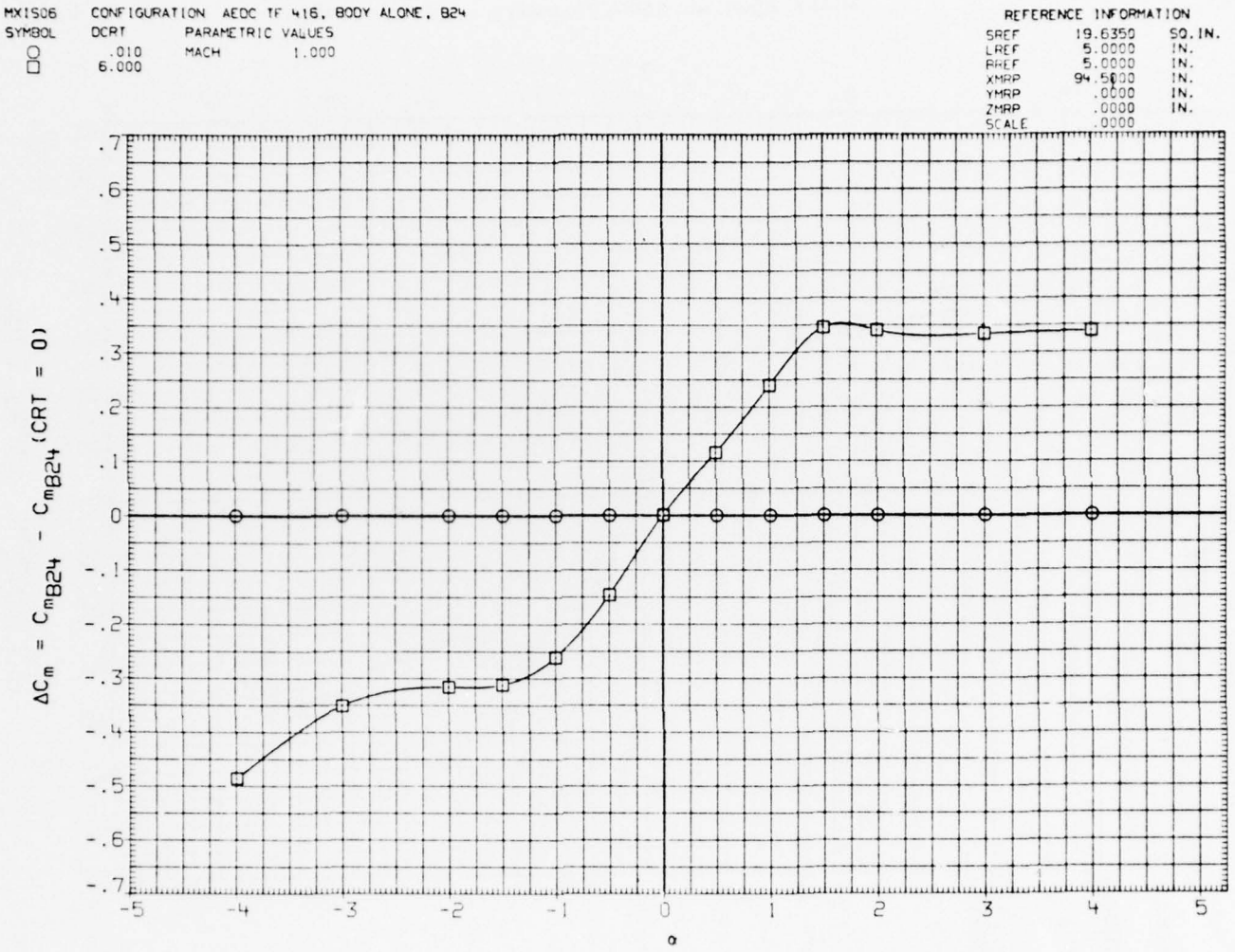

Figure A-112. Plume effects on body alone.

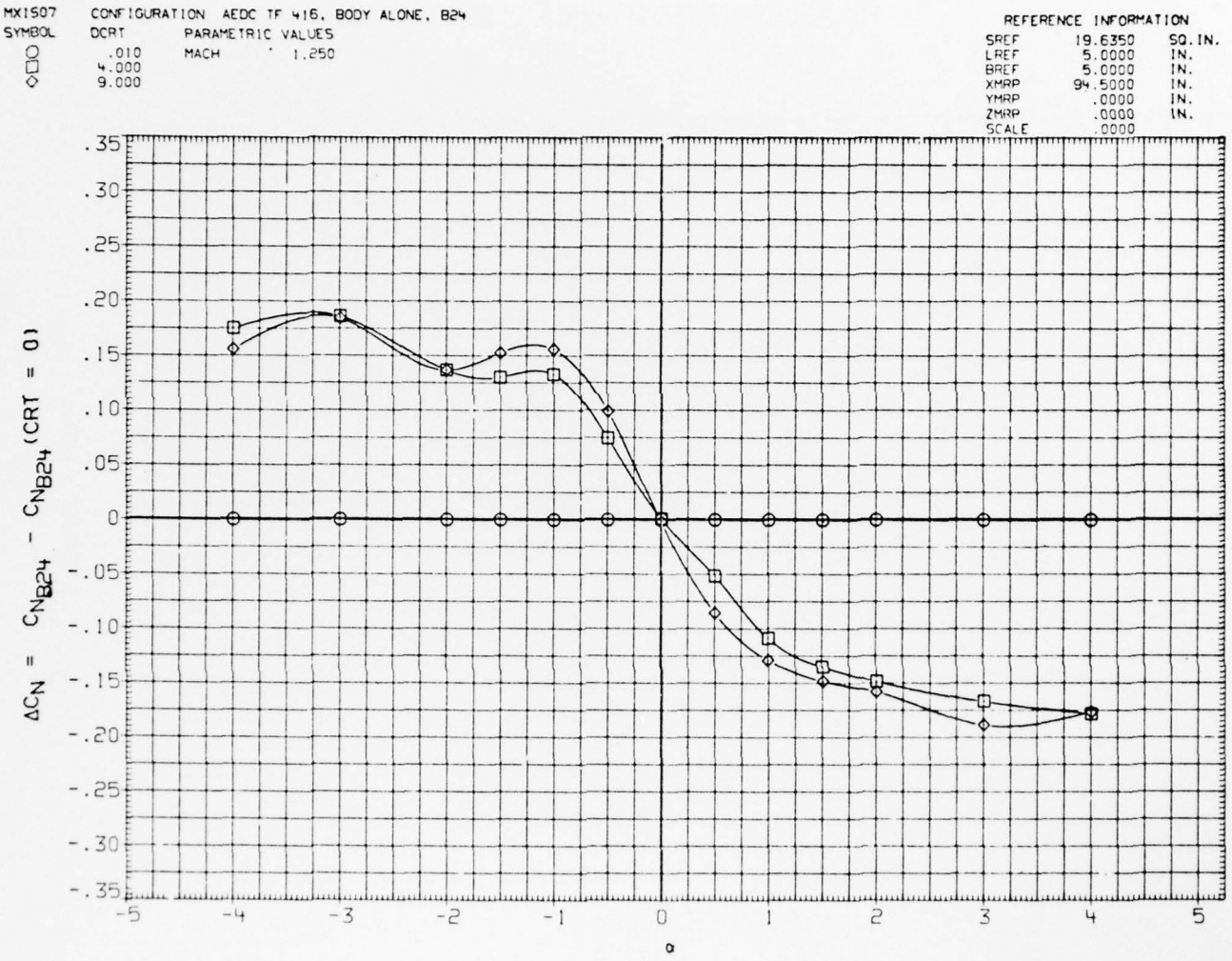

Figure A-113. Plume effects on body alone.

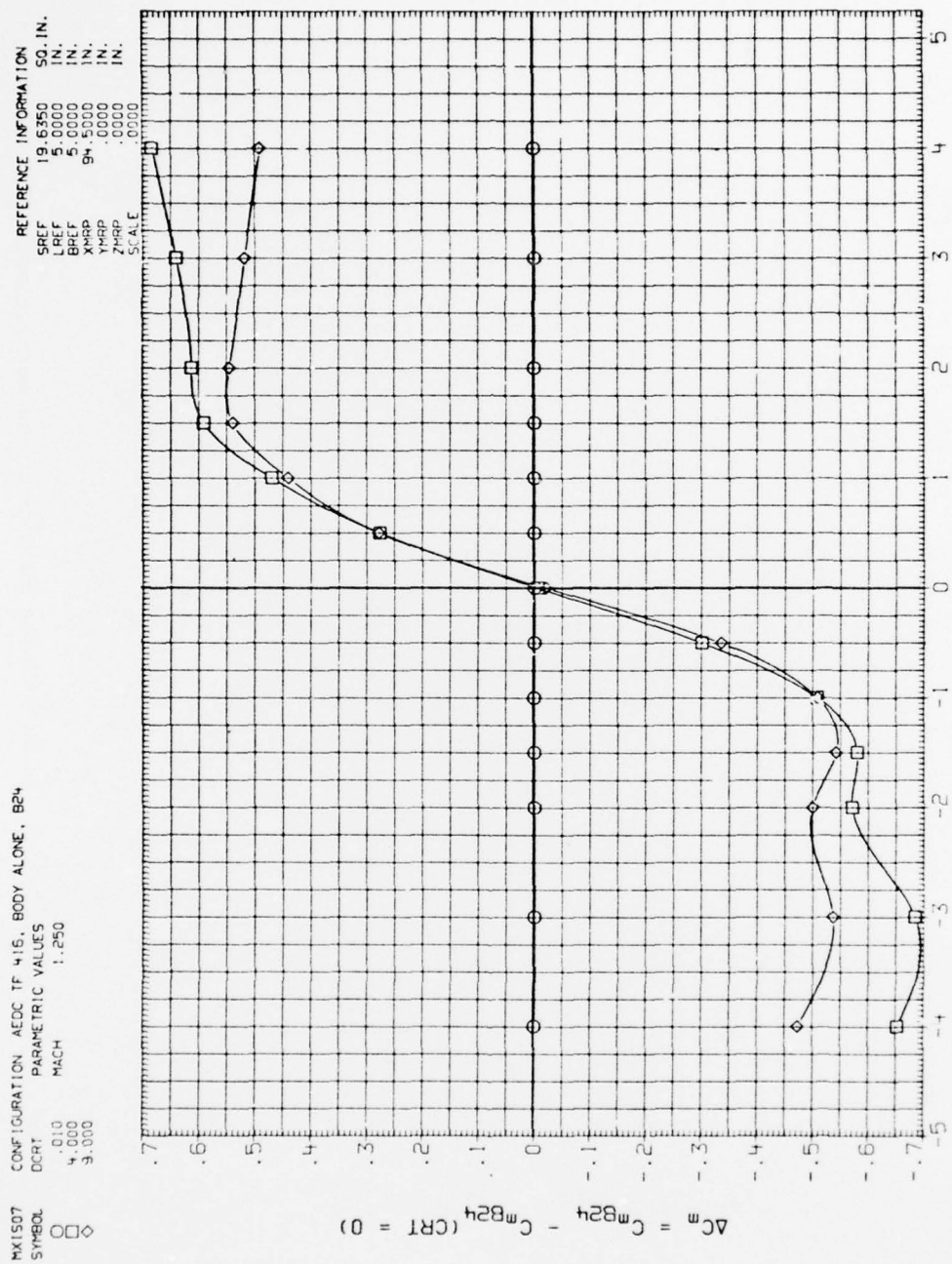

Figure A-114. Plume effects on body alone.

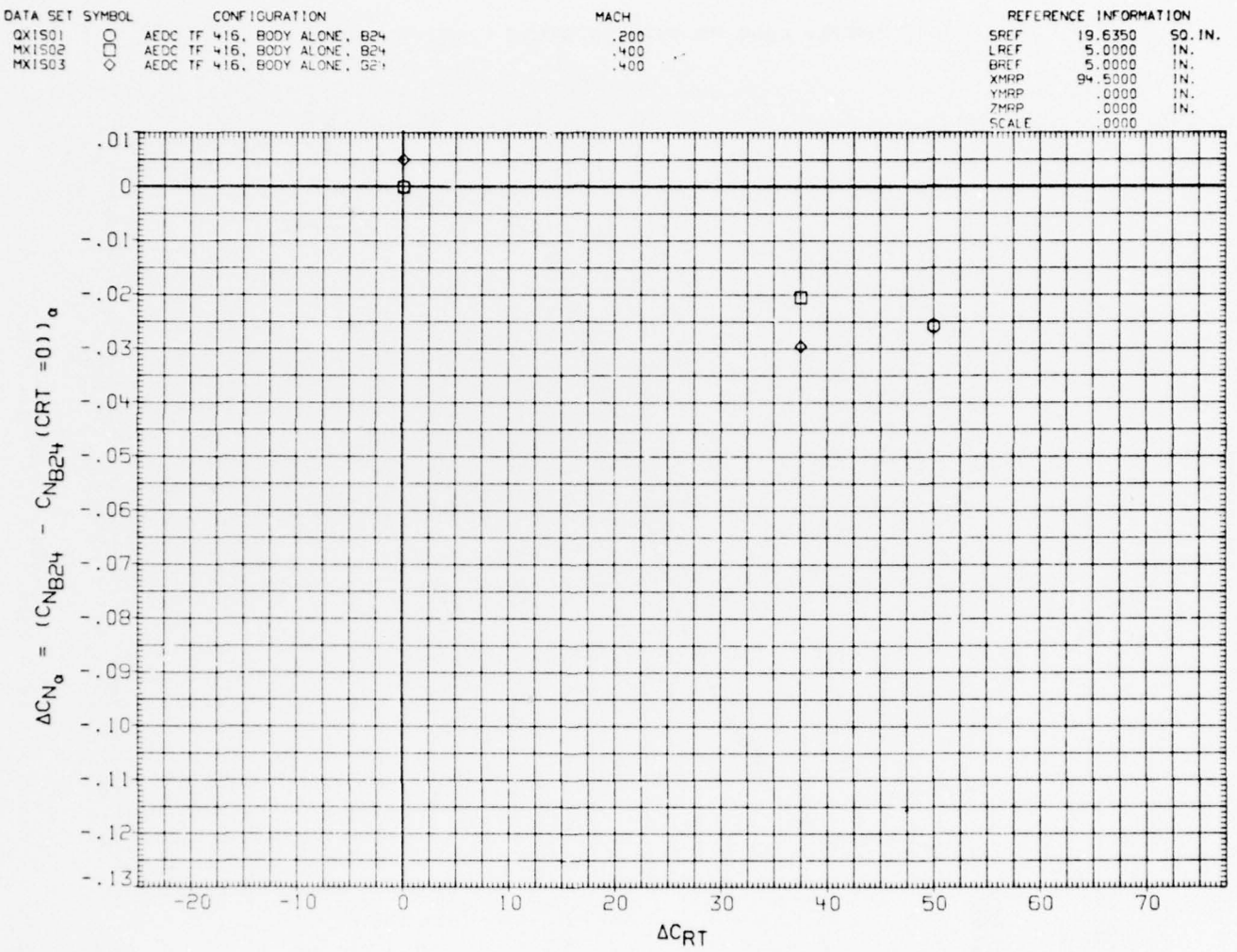

Figure A-115. Plume effects on body alone derivatives.

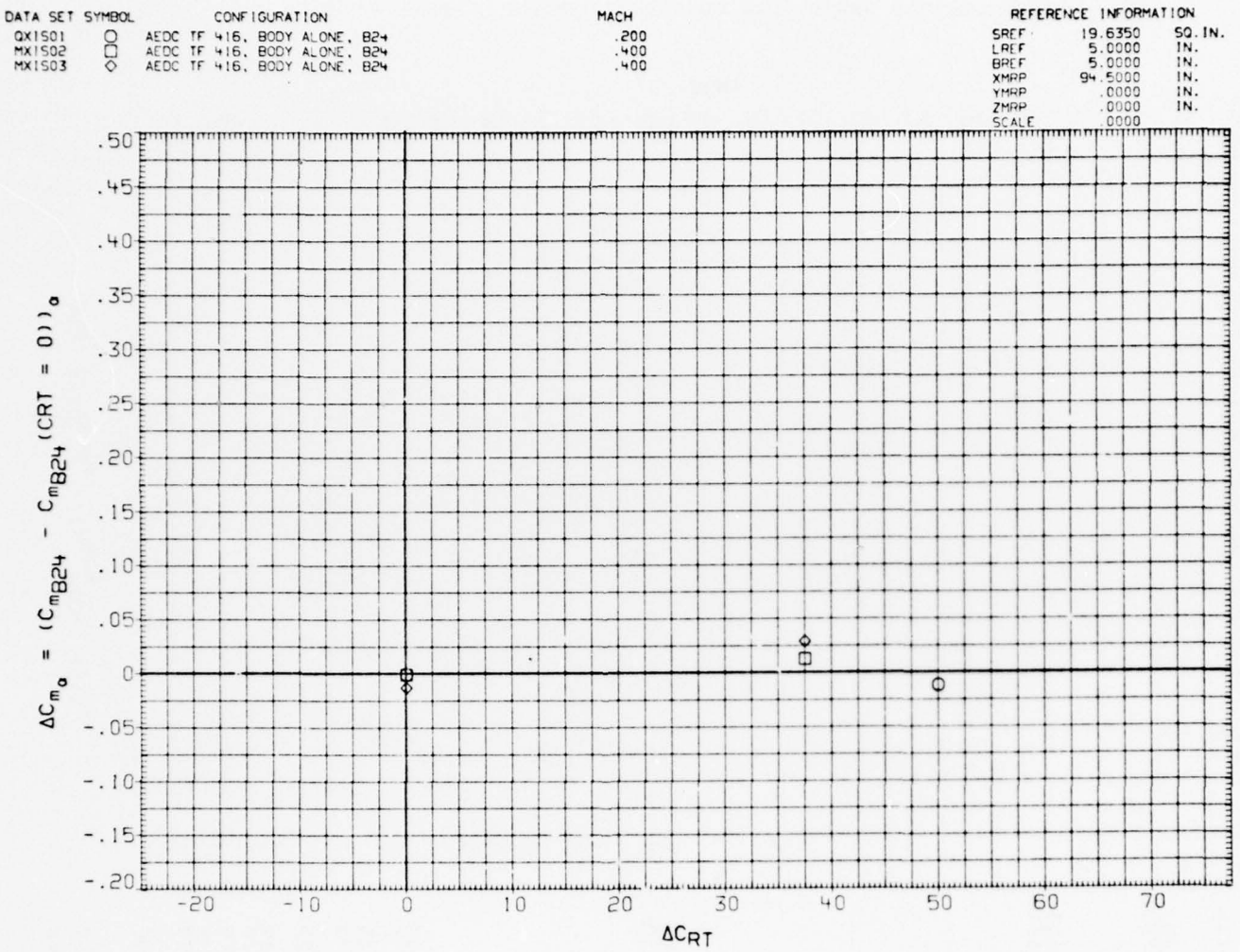

Figure A-116. Plume effects on body alone derivatives.

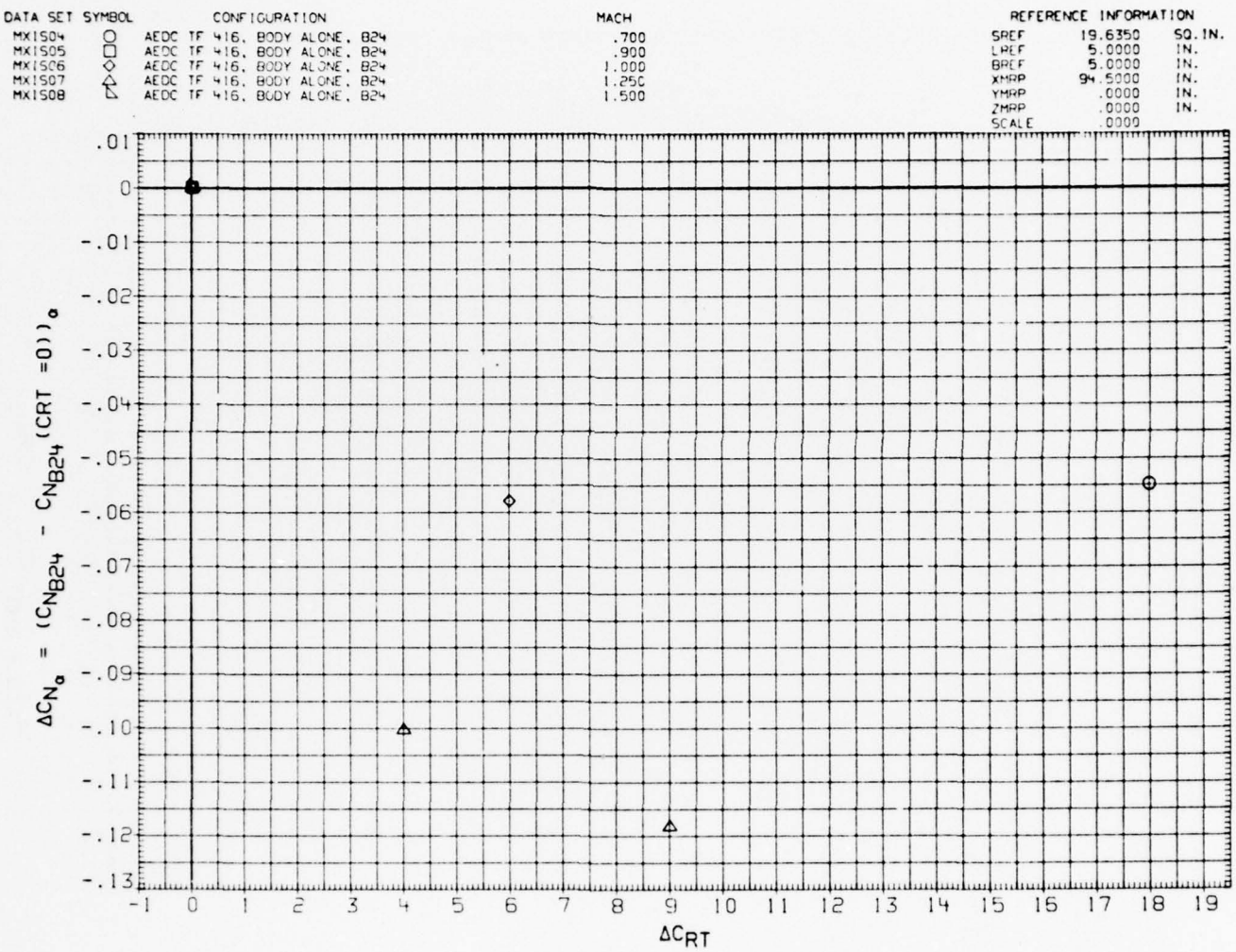

Figure A-117. Plume effects on body alone derivatives.

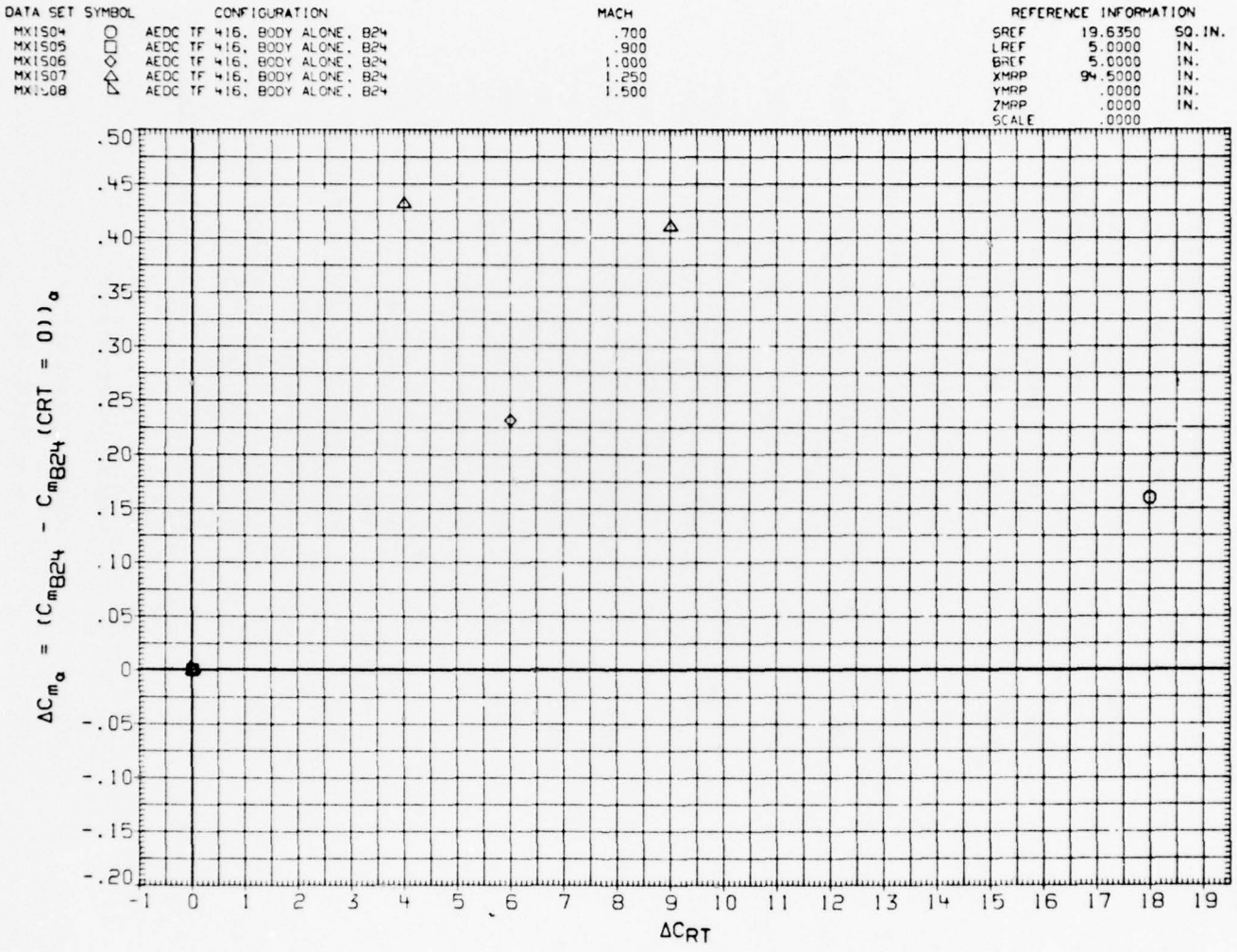

Figure A-118. Plume effects on body alone derivatives.

NOMENCLATURE

Symbol	Mnemonic	Definition
RN/L	RN/L	unit Reynolds number; per ft
V		velocity; ft/sec
α	ALPHA	angle of attack, degrees
β	BETA	angle of sideslip, degrees
ψ	PSI	angle of yaw, degrees
ϕ	PHI	angle of roll, degrees
ρ		mass density; slugs/ft^3
C_T	CT	thrust coefficient, axial thrust/qS
C_{RT}	CRT	radial thrust coefficient, defined in text
ΔC_{RT}	DCRT	differential radial thrust coefficient
$P_{b_{AVG}}/P_\infty$	PB/P1 (PBX/P)	ratio of average base pressure to tunnel freestream static pressure
a		speed of sound; ft/sec
C_p	CP	pressure coefficient; $(p_1 - p_\infty)/q$
M	MACH	Mach number; V/a
q	Q(PSF)	dynamic pressure; $1/2\rho V^2$
p_b/p_∞		base pressure ratio
A_b		base area; m^2, in^2
b	BREF	wing span or reference span; m, in
c.g.		center of gravity
ℓ_{REF}, $\bar{c}$	LREF	reference length or wing mean aerodynamic chord; m, in
S, S_{ref}, A_{ref}	SREF	reference area based on body diameter, in^2
	MRP	moment reference point
	XMRP	moment reference point on X axis
	YMRP	moment reference point on Y axis
	ZMRP	moment reference point on Z axis

Symbol	Mnemonic	Definition
$C_{N_{FX}}$ ($C_{N_{TX}}$)	CNFX	fin normal force coefficient, $\frac{\text{fin normal force}}{qS_{ref}}$
$C_{HM_{FX}}$ ($C_{HM_{TX}}$)	CLMHX	fin hinge moment coefficient, $\frac{\text{fin hinge moment}}{qS_{ref}\,\ell_{ref}}$
$C_{BM_{FX}}$ ($C_{BM_{TX}}$)	CLMRX	fin root bending moment coefficient, $\frac{\text{fin root bending moment}}{qS_{ref}\,\ell_{ref}}$
$Y_{CP_{FX}}$ (CPY_{TX})	YCPFX	fin spanwise center of pressure, YCPFX = $2b_T$(CLMRX/CNFX), inches
$X_{CP_{FX}}$ (CPX_{TX})	XCPFX	fin chordwise center of pressure location relative to fin hinge line, positive toward the leading edge, XCPFX = C_R(CLMHX/CNFX), inches
$C_{N_{\alpha FX}}$	CNAFX	fin normal force coefficient derivative with alpha, per degree
	Body Axis (Main Balance)	
C_N	CN	normal-force coefficient; $\frac{\text{normal force}}{qS}$
C_A	CA	axial-force coefficient; $\frac{\text{axial force}}{qS}$
C_Y	CY	side-force coefficient; $\frac{\text{side force}}{qS}$
C_m	CLM	pitching-moment coefficient; $\frac{\text{ptiching moment}}{qS\ell_{REF}}$
C_n	CYN	yawing-moment coefficient; $\frac{\text{yawing moment}}{qSb}$
C_ℓ	CBL	rolling-moment coefficient; $\frac{\text{rolling moment}}{qSb}$

Symbol	Mnemonic	Definition
C_{m_α}	CLMALF	pitching moment coefficient derivative with alpha, per degree
C_{N_α}	CNALFA	normal force coefficient derivative with respect to angle of attack, per degree
F_1	F1	cruciform fins of 5 inches chord length and half span of 2.5 inches
B_{24}	B24	rocket body
C_R		fin root chord length, 5 inches
b_T		fin semispan, 2.5 inches
L/D		fineness ratio, model length divided by diameter, L/D = 24
A_{NJ}	tot	total exit area, normal jet, square inches
P_t	PT	tunnel stagnation pressure, psf
P_s		tunnel static pressure, psf
P_c		normal jet simulator chamber pressure, psi
M_J		normal jet Mach number = 1.0 (sonic nozzles)
$C_{N_{B(F)}}$	CNBF	normal force coefficient of body plus fins minus the normal forces of fins 2 and 4
$C_{N_{\alpha B(F)}}$		gradient of CNBF with respect to angle of attack, per degree
$C_{m_{B(F)}}$	CMBF	pitching moment coefficient of the body plus fin minus the hinge moment coefficients of fins 2 and 4
$C_{m_{\alpha B(F)}}$		gradient of CMBF with respect to angle of attack, per degree
$\Delta C_{N_{B(F)}}$	DCNBF	normal force coefficient (CNBF) at various CRT levels minus the normal force coefficient of the body alone at CRT = 0
ΔC_N	DCN	normal force coefficient of body alone at CRT values greater than zero minus the normal force coefficient of the body alone at CRT = 0

Symbol	Mnemonic	Definition
$\Delta C_{N_{\alpha B(F)}}$		gradient of DCNBF with respect to angle of attack, per degree
$\Delta C_{N_{\alpha}}$		gradient of DCN with respect to angle of attack, per degree
$\Delta C_{m_{B(F)}}$	DCMBF	pitching moment coefficient (CMBF) at various CRT levels minus the normal force coefficient of the body alone at CRT = 0
$\Delta C_{m_{\alpha B(F)}}$		gradient of DCMBF with respect to angle of attack, per degree
ΔC_{m}	DCLM	pitching moment coefficient of body alone at CRT values greater than zero minus the pitching moment coefficient of the body alone at CRT = 0
$\Delta C_{m_{\alpha}}$		gradient of DCLM with respect to angle of attack, per degree
$d\alpha$		incremental change in angle of attack, degrees
d		denotes incremental change

Subscripts

b	base
l	local
s	static conditions
t	total conditions
∞	free stream
1,2,3,4	fin radial position about body

DISTRIBUTION

	No. of Copies
Defense Documentation Center Cameron Station Alexandria, Virginia 22314	6
Commanding General US Army Materiel Command Research and Development Directorate Attn: DRCRD Washington, D. C. 20315	1
Commanding Officer US Army Picatinny Arsenal Attn: SMUPA-VC3, Mr. A. Loeb Dover, New Jersey 07801	1
Director US Army Mobility Research and Development Laboratory Attn: SAVDL-AS Ames Research Center Moffett Field, California 94035	1
Commanding Officer Research Laboratories Attn: SMUEA-RA, Mr. Abraham Flatau Edgewood Arsenal, Maryland 21010	1
Commanding Officer Air Force Armament Laboratory Attn: Mr. C. Butler Mr. F. Howard Dr. F. Findley Eglin Air Force Base, Florida 32542	1 1 1
Arnold Engineering and Development Center Attn: Dr. McKay Library Arnold Air Force Station, Tennessee 37389	1 1
Air Force Flight Dynamics Laboratory Attn: FDMM, Mr. Gene Fleeman Wright-Patterson Air Force Base, Ohio 45433	1
Commanding Officer Ballistic Research Laboratories Attn: DRXRD-BEL, Mr. R. Krieger Aberdeen Proving Ground, Maryland 21005	1
Commanding Officer US Naval Ordnance Laboratories Attn: Mr. S. Hastings Mr. R. T. Hall Library White Oak Silver Spring, Maryland 20910	1 1 1
NASA-Langley Research Center Attn: Mr. Leroy Spearman Mr. Charles Jackson Technical Library Hampton, Virginia 23665	1 1 1
Commanding Officer and Director Naval Ship Research and Development Center Attn: Aerodynamic Laboratory Graderock, Maryland 20007	1
Naval Weapons Center Attn: Mr. R. Meeker China Lake, California 93555	1
NASA-Ames Research Center Attn: Technical Library Moffett Field, California 94035	1
NASA-Lewis Research Center Attn: Technical Library Cleveland, Ohio 44135	1
NASA-Marshall Space Flight Center Attn: Mr. K. Blackwell Mr. H. Struck Mr. J. Sims Technical Library Marshall Space Flight Center, Alabama 35812	1 1 1 1
US Air Force Academy Attn: Lt. Col. W. A. Edgington DFAN USAF Academy, Colorado 80840	1
Philco Corporation Aeronutronic Division Attn: Technical Information Services-Acquisitions Mr. L. E. Horowitz Ford Road Newport Beach, California 92663	1
Rockwell International Columbus Aircraft Division Attn: Mr. Fred Hessman 4300 East Fifth Avenue Columbus, Ohio 43216	1
Sandia Corporation Sandia Base Division 9322 Attn: Mr. W. Curry Box 5800 Albuquerque, New Mexico 87115	1
Purdue University Attn: Dr. J. Hoffman, Propulsion Center Lafayette, Indiana 47907	1
University of Tennessee Space Institute Attn: Dr. J. M. Wu Tullahoma, Tennessee 37388	1
University of Alabama Department of Aerospace Engineering Attn: Dr. Zien Dr. J. O. Doughty University, Alabama 35486	1
Jet Propulsion Laboratory California Institute of Technology Attn: Mr. R. Martin 4800 Oak Grove Drive Pasadena, California 91109	1
University of Missouri at Columbia Department of Mechanical Engineering Attn: Dr. D. E. Wollersheim Columbia, Missouri 65201	1
University of Illinois College of Engineering Attn: Dr. A. L. Addy Dr. H. H. Korst Dr. R. A. White Engineering Library Urbana, Illinois 61801	1 1 1 1

No. of Copies

John Hopkins University
Applied Physics Laboratory
Attn: Dr. L. Cronvich 1
Mr. Gordon Dugger 1
Mr. R. Walker 1
Silver Spring, Maryland 20910

University of Notre Dame
Department of Aerospace Engineering
Attn: Dr. T. J. Mueller 1
Notre Dame, Indiana 46556

Naval Air Systems Command
Attn: Mr. William Volz 6
Air 320-C, Room 778, JP-1
Washington, D. C. 20361

For Transmittal to:

TTCP

Boeing Company
Attn: Library Unit Chief 1
Mr. R. J. Dixon 1
Mr. H. L. Giles 1
P. O. Box 3707
Seattle, Washington 98124

Convair, A Division of General
Dynamics Corporation
Attn: Division Library 1
Pomona, California 91776

Nielson Engineering and Research, Inc.
Attn: Dr. Jack N. Nielson 1
850 Maude Avenue
Mountain View, California 94040

Hughes Aircraft Company
Attn: Documents Group Technical
Library 1
Florence Avenue at Teale Street
Culver City, California 90230

Ling-Temco-Vought Aerospace Corp
Attn: Mr. Dick Ellison 1
P. O. Box 404
Warren, Michigan 48090

Ling-Temco-Vought Aerospace Corp.
Vought Aeronautics Division
Attn: C. R. James, Unit 2-53330 1
Box 5907
Dallas, Texas 75222

Lockheed Missiles and Space Company
Huntsville R&E Center
Attn: Mr. J. Benefield 1
4800 Bradford Boulevard, N.W.
Huntsville, Alabama 35805

Lockheed Aircraft Corporation
Missile and Space Division
Attn: Technical Information Center 1
P. O. Box 504
Sunnyvale, California 94086

The Martin-Marietta Corporation
Orlando Division
Attn: D. Tipping 1
L. Gilbert 1
Orlando, Florida 32804

No. of Copies

McDonnel-Douglas Company-West
Attn: Library A3-328 1
5301 Bolsa Avenue
Huntington Beach, California 92646

McDonnel-Douglas Corporation
P. O. Box 516
St. Louis, Missouri 63166 1

Northrop Corporation
Electro-Mechanical Division
Attn: Mr. E. Clark 1
500 East Orangethorpe Y20
Anaheim, California 92801

Emerson Electric Company
Attn: Mr. Robert Bauman 1
8100 Florissant
St. Louis, Missouri 73136

Data Management Services
Department 2730
Chrysler Corporation Space Division
Attn: Mr. N. D. Kemp 6
P. O. Box 29200
New Orleans, Louisiana 70189

Data Management Services
Department 5807
Chrysler Corporation
Huntsville Electronics Division
Attn: Mr. J. E. Vaughn 1
102 Wynn Drive
Huntsville, Alabama 35805

DRDMI-FR 1
-X, Dr. McDaniel 1
-T, Dr. Kobler 1
-TKD, Mr. Deep 1
Mr. Henderson 20
Mr. Batiuk 10
Mr. Dahlke 4
-C, Mr. Sullivan 1
-LP, Mr. Voigt 1
-TB 3
-TI (Record Set) 1
(Reference Copy) 1